

# Axiomata sive Leges Motus

## Lex I.

corpus perseverare in statu suo  
directum, sive quiescente a  
mutare.

perseverant in motibus suis  
laetantibus et in gravitate imp  
'eccedens profectus retrahunt. His  
vix nisi qualiter a  
viam et Comitari  
reclavos in Statist  
imp.

## Lex II.

corpus motus profectum  
vix hincam reclav  
na motum quiesce  
generabit, sine fin  
imprefa fuerit. Et  
in cum in generatibus dila  
chor, motus ejus vel coefficant  
l oblique oblique adjuvitur et  
vibrationum componitur.

## Lex III.

contractionem semper et equalen  
viam actionem in se mutuo per  
vitas dirigi  
promit vel trahit alterum  
vabitur. Siquis lapidem digito  
et lapide. Si equus lapidem et  
vix et equus equaliter in le  
cedem relaxandi se corrali  
m, ac lapidem vix equus  
et quantum promovet pro  
in corpus aliud impingent.  
mutavertit, idem quoque imp  
thionem in factum contra  
(reflexionis motus) subit. His

Swantje Bargmann

Theory and numerics of  
non-classical thermo-hyperelasticity

**Bibliografische Information Der Deutschen Bibliothek**

Die Deutsche Bibliothek verzeichnet diese Publikation in der Deutschen Nationalbibliografie; detaillierte bibliografische Daten sind im Internet über <http://dnb.ddb.de> abrufbar.

**Bibliographic information published by Die Deutsche Bibliothek**

Die Deutsche Bibliothek lists this publication in the Deutsche Nationalbibliografie; detailed bibliographic data is available in the Internet at <http://dnb.ddb.de>.

Farbig erschienen auf <http://kluedo.ub.uni-kl.de>

Herausgeber: Fachbereich Maschinenbau und Verfahrenstechnik  
Lehrstuhl für Technische Mechanik  
Postfach 3049  
Technische Universität Kaiserslautern  
D-67653 Kaiserslautern

Verlag: Technische Universität Kaiserslautern

Druck: Technische Universität Kaiserslautern  
ZBT – Abteilung Foto-Repro-Druck

D-386

© by Swantje Bargmann 2008

This work is subject to copyright. All rights are reserved, whether the whole or part of the material is concerned, specifically the rights of translation, reprinting, reuse of illustrations, recitation, broadcasting, reproduction on microfilm or in any other way, and storage in data banks. Duplication of this publication or parts thereof is permitted in connection with reviews or scholarly analysis. Permission for use must always be obtained from the author.

Alle Rechte vorbehalten, auch das des auszugsweisen Nachdrucks, der auszugsweisen oder vollständigen Wiedergabe (Photographie, Mikroskopie), der Speicherung in Datenverarbeitungsanlagen und das der Übersetzung.

Als Manuskript gedruckt. Printed in Germany.

ISSN 1610-4641  
ISBN 978-3-939432-77-7

# Theory and numerics of non-classical thermo-hyperelasticity

vom Fachbereich Maschinenbau und Verfahrenstechnik  
der Technischen Universität Kaiserslautern  
zur Verleihung des akademischen Grades  
Doktor-Ingenieur (Dr.-Ing.)  
genehmigte Dissertation

von Dipl.-Math. Swantje Bargmann  
aus Kaiserslautern

Hauptreferent:	Prof. Dr.-Ing. habil. P. Steinmann
Korreferenten:	Prof. Dr. rer. nat. B. Svendsen Prof. Dr. V. Kalpakides
Vorsitzender:	Prof. Dr. techn. H.-J. Bart

Tag der Einreichung:	17.12.2007
Tag der mündl. Prüfung:	09.05.2008

Kaiserslautern, Mai 2008

D 386



# Preface

The research presented in this thesis has been carried out at the Chair of Applied Mechanics at the University of Kaiserslautern, Germany, during the period 2004 to 2007. The financial support of the DFG (Deutsche Forschungsgemeinschaft) within the project "Theory and numerics of non-classical thermoelasticity" (STE 544/23-1-2) is gratefully acknowledged.

First of all, I would like to thank Professor Paul Steinmann for giving me the opportunity to work in the fascinating field of non-classical thermoelasticity, for his support and for providing me with inspiring advice through all these years.

Moreover, I would like to express my appreciation to Professor Bob Svendsen and Professor Vassilios Kalpakides for kindly accepting to be referees of this thesis. Thanks for useful suggestions, the careful reading and the interest in my work. Also, I'm very grateful to Professor Hans-Jörg Bart for taking the chairmanship of the examination committee.

Moreover, I would like to express my gratitude to my fellow colleagues at the Chair of Applied Mechanics. The discussions I have had with them have been fruitful, inspirational and have facilitated my research. They have also helped a great deal to gain a better insight into the world of mechanics. In addition, I benefited from engineers, mathematicians and physicists who had impact on this work during research stays, conferences and personal discussions, for example.

Last but not least, I would like to thank all those who have contributed in one way or another in their very personal ways.

Kaiserslautern, May 2008

Swantje Bargmann



# Contents

<b>Nomenclature</b>	<b>VIII</b>
<b>1. Introduction</b>	<b>5</b>
1.1. The theory of Green and Naghdi . . . . .	6
1.2. Structure of the present work . . . . .	6
<b>2. State of the art</b>	<b>9</b>
<b>3. Continuum mechanics</b>	<b>13</b>
3.1. Kinematics . . . . .	13
3.1.1. Spatial motion problem . . . . .	13
3.1.2. Material motion problem . . . . .	15
3.2. Mechanical balance equations . . . . .	16
3.2.1. Spatial motion problem . . . . .	17
3.2.2. Material motion problem . . . . .	19
3.3. Material modeling . . . . .	19
<b>4. Thermodynamic principles</b>	<b>21</b>
4.1. Entropy principle of Müller and Liu . . . . .	21
4.1.1. Thermodynamical analysis of Green–Naghdi type I . . . . .	23
4.1.2. Thermodynamical analysis of Green–Naghdi type II . . . . .	28
4.1.3. Thermodynamical analysis of Green–Naghdi type III . . . . .	32
4.2. Entropy exploitation according to Green and Naghdi . . . . .	34
4.2.1. Type I . . . . .	35
4.2.2. Type II . . . . .	37
4.2.3. Type III . . . . .	38
<b>5. Theory of non-classical heat conduction</b>	<b>41</b>
5.1. Governing constitutive equations . . . . .	41
5.1.1. Type I . . . . .	41
5.1.2. Type II . . . . .	42
5.1.3. Type III . . . . .	44
5.2. Finite element discretization . . . . .	44
5.2.1. Spatial finite element discretization . . . . .	45
5.2.2. Temporal finite element discretization . . . . .	47
5.2.2.1. Discontinuous finite element method . . . . .	49

5.2.2.2. Continuous finite element method . . . . .	51
5.3. Numerical results . . . . .	53
<b>6. Theory of non-classical thermo-hyperelasticity</b>	<b>67</b>
6.1. Governing constitutive equations . . . . .	67
6.1.1. Type I . . . . .	67
6.1.2. Type II . . . . .	68
6.1.3. Type III . . . . .	69
6.2. Finite element discretization . . . . .	70
6.2.1. Spatial discretization . . . . .	70
6.2.1.1. Spatial discretization . . . . .	72
6.2.2. Temporal discretization . . . . .	74
6.2.2.1. Mixed Galerkin time finite element method . . . . .	76
6.2.2.2. Continuous Galerkin time finite element method . . . . .	76
6.3. Newton–Raphson solution method . . . . .	77
6.4. Numerical examples . . . . .	78
6.4.1. Second sound phenomenon . . . . .	78
6.4.1.1. Bismuth (Bi) . . . . .	79
6.4.1.2. Sodium Fluoride (NaF) . . . . .	84
6.4.2. Cryovolcanism on Enceladus . . . . .	88
6.4.2.1. Set-up for modeling cryovolcanism on Enceladus . . . . .	91
6.4.2.2. Results . . . . .	93
6.4.3. Material force method . . . . .	100
6.5. Energy conserving finite element discretization in time for type II . . . . .	120
6.5.1. Energy consistent algorithmic stress tensor method . . . . .	120
6.5.2. Numerical example . . . . .	123
<b>7. Incremental variational formulation</b>	<b>127</b>
7.1. Preliminaries . . . . .	127
7.1.1. Continuous setting . . . . .	127
7.1.2. Incremental setting . . . . .	128
7.1.2.1. Type I . . . . .	130
7.1.2.2. Type II . . . . .	132
7.1.3. Numerical example . . . . .	133
7.1.3.1. Type I . . . . .	133
7.1.3.2. Type II . . . . .	138
<b>8. On wave speed in Green–Naghdi heat conduction</b>	<b>141</b>
8.1. Mathematical formulation . . . . .	141
8.2. Analytical solutions . . . . .	142
8.2.1. Type III . . . . .	142
8.2.2. Type II . . . . .	145
8.2.3. Type I . . . . .	145
8.3. Results . . . . .	147



<b>9. Conclusion</b>	<b>151</b>
<b>A. Mathematics</b>	<b>153</b>
A.1. Notation . . . . .	153
A.2. Definitions . . . . .	153
A.3. Jump conditions . . . . .	155
A.4. Symmetry and skew-symmetry for two-point tensors . . . . .	155
A.5. Transformations . . . . .	156
A.6. Calculation of absolute entropy . . . . .	156
A.7. Cauchy's stress theorem . . . . .	157
A.8. Lemma on linear algebraic equations with an inequality constraint . . . . .	157
A.9. Analytical solutions . . . . .	158
<b>B. A glance at analogous fundamental laws</b>	<b>159</b>
B.1. Fourier's law . . . . .	159
B.2. Fick's law . . . . .	160
B.3. Darcy's law . . . . .	161
B.4. Hooke's law . . . . .	162
B.5. Maxwell's equations . . . . .	163
<b>C. Albert E. Green and Paul M. Naghdi</b>	<b>165</b>
C.1. Albert E. Green . . . . .	165
C.2. Paul M. Naghdi . . . . .	166

## *Nomenclature*



# Nomenclature

$\mathbf{A}_{e=1}^{n_{el}}$	assembly over all element contributions at element nodes
$A$	albedo (ratio of reflected to incident radiation)
$\mathbf{b}$	momentum source
$B$	body
$\mathcal{B}_0$	reference configuration
$\mathcal{B}_t$	current configuration
$\mathcal{B}^e$	element region
$c$	specific heat
$\mathbf{C}$	right Cauchy-Green strain tensor
$\mathbf{c}_{\rho c}$	capacity matrix
$D_t$	material time derivative
$\mathbf{D}$	rate of deformation tensor
$\mathbf{e}_x$	Cartesian basis vector in $x$ -direction
$\mathbf{e}_y$	Cartesian basis vector in $y$ -direction
$\mathbf{e}_z$	Cartesian basis vector in $z$ -direction
$\mathbf{E}$	elasticity tensor
$\mathbf{f}$	material deformation gradient
$\mathbf{F}$	spatial deformation gradient
$\mathbf{F}_1$	heat load vector due to specified nodal temperatures
$\mathbf{F}_{sc}$	heat load vector due to external heat bulk source
$\mathbf{F}_{sur}$	surface force
$\mathbf{F}_{vol}$	volume force
$h_n$	length of time element $h_n = t_n - t_{n-1}$
$\mathbf{h}$	spatial entropy flux vector
$\mathbf{H}$	material entropy flux vector
$H(\cdot)$	Heaviside unit step function
$I$	time interval
$I_n$	temporal subinterval
$\mathbf{I}$	identity matrix
$K$	bulk modulus
$K_n$	incremental kinetic energy
$\mathfrak{K}$	conductivity matrix
$L_n$	incremental Lagrangian function
$\mathbf{L}$	velocity gradient
$M_i$	temporal shape function of degree $k$
$\tilde{M}_i$	temporal shape function of degree $k - 1$
$\mathbf{M}$	mass matrix of balance of momentum
$Ma$	Mach number

$n_{\text{el}}$	number of spatial finite elements
$n_{\text{en}}$	number of local node points
$n_{\text{dof}}$	number of spatial global degrees of freedom
$\mathbf{n}$	material outward unit normal vector
$\mathbf{N}$	spatial outward unit normal vector
$n_t$	number of finite time elements
$N^i$	spatial shape function
$\mathbf{P}$	1. Piola–Kirchhoff stress tensor
$P_n$	incremental power of external loads
$\mathcal{P}^k(0, 1)$	set of polynomials on the interval $(0, 1)$ with maximal degree $k$
$\mathbf{q}$	spatial heat flux vector
$\mathbf{Q}$	material heat flux vector
$\mathcal{Q}$	orthogonal transformation $\in SO(3)$
$r$	external heat supply per unit mass
$s$	external entropy supply per unit mass
$\text{sym}(\bullet)$	symmetric part of a tensor
$\text{skw}(\bullet)$	skew-symmetric part of a tensor
$S_0$	absolute entropy density
$\mathcal{S}_0$	solar constant
$\mathbb{S}$	state space
$t$	time
$t_0$	reference time
$t$	dimensionless time
$T$	empirical temperature
$T_0$	reference empirical temperature
$[[\mathbf{T}^h]]_0$	amount of jump in dG-method
$T$	dimensionless temperature
$\mathbf{u}$	mechanical displacement vector
$\mathbf{v}$	mechanical velocity vector
$v$	wave speed
$w$	thermal expansion coefficient
$W_n$	incremental internal stress work
$\mathbf{W}$	vorticity tensor
$\mathbf{x}$	spatial position vector
$x$	dimensionless position
$\mathbf{X}$	material position vector
$\alpha$	thermal displacement
$\alpha_0$	initial value of $\alpha$ at $t_0$
$\delta\alpha$	spatial test function
$\delta\boldsymbol{\alpha}$	temporal test function
$\delta T$	spatial test function
$\delta\mathbf{T}$	temporal test function
$\delta\mathbf{x}$	spatial test function
$\delta\mathbf{x}$	temporal test function
$\epsilon$	internal energy per unit mass
$\eta$	entropy density per unit mass

## *Nomenclature*

$\kappa_1$	heat conductivity of type I
$\kappa_2$	heat conductivity of type II
$\kappa_3$	(non-classical) heat conductivity of type III
$\kappa_4$	(classical) heat conductivity of type III
$\boldsymbol{\pi}^t$	two-point stress measure of 1. Piola–Kirchhoff type
$\theta$	absolute temperature
$\theta_0$	reference value of $\theta$ at $t_0$
$\lambda$	Lamé constant
$\lambda^e$	Lagrange multiplier of balance of energy
$\boldsymbol{\lambda}^m$	Lagrange multiplier of balance of momentum
$\lambda^p$	Lagrange multiplier of balance of mass
$\mu$	Lamé constant
$\xi$	entropy production per unit mass
$\rho$	mass density
$\sigma_{\text{SB}}$	Stefan–Boltzmann constant
$\boldsymbol{\sigma}$	Cauchy stress tensor
$\boldsymbol{\Sigma}^t$	Eshelby stress tensor
$\chi$	dimensionless diffusivity
$\psi$	free energy density per unit mass

# Zusammenfassung

Diese Arbeit stellt einen Beitrag zur Theorie und Numerik nicht klassischer Thermoelastizität dar. Thermoelastizität beschäftigt sich allgemein mit der Verbindung mechanischer und thermischer Feldprobleme. Gewöhnlich ist diese Verbindung durch eine Kopplung in beide Richtungen charakterisiert. Es treten sowohl thermisch induzierte Spannungen als auch Temperaturveränderungen, die durch Deformationen hervorgerufen werden, auf.

Oft wird Wärmeleitung in Festkörpern durch das Fouriersche Gesetz beschrieben. Es nimmt an, dass der Wärmefluss proportional zum Temperaturgradienten ist. Dieser Ansatz wird in dieser Arbeit sowohl als Fouriersche als auch als klassische Theorie bezeichnet. In dieser Arbeit bezieht sich der Begriff "nicht klassisch" auf die Tatsache, dass die Konstitutivgleichung für den Wärmefluss vom Fourierschen Gesetz abweicht. Die aus dem Fourierschen Gesetz folgende parabolische Wärmeleitungsgleichung beschreibt Wärmeleitung durch Diffusion. Dabei werden, aufgrund der Parabolizität der Gleichung, Teile von lokalen Wärmeimpulsen mit einer unendlichen Ausbreitungsgeschwindigkeit simuliert. Diese Anteile werden bei Zimmertemperatur stark gedämpft, so dass die meisten ingenieurwissenschaftlichen Anwendungen ausreichend gut durch die klassische Theorie beschrieben werden. Zusätzlich zu der unphysikalischen möglichen unendlichen Ausbreitungsgeschwindigkeit versagt das Fouriersche Gesetz jedoch noch bei einigen anderen Phänomenen.

Eines dieser Phänomene existiert bei tiefen Temperaturen nahe dem absoluten Nullpunkt. Hier wurde in der Mitte des 20. Jahrhunderts das sogenannte Phänomen des Zweiten Schalls (engl. second sound phenomenon) entdeckt.

Der Zweite Schall tritt im allgemeinen in sehr reinen Kristallen bei tiefen Temperaturen auf. Bisher wurde er in kristallinen  $^3\text{He}$ ,  $^4\text{He}$ , NaF und Bi experimentell nachgewiesen<sup>1</sup>. Anstelle einer diffusiven Wärmeausbreitung breitet sich in den oben genannten Materialien Wärme in Wellenform mit der charakteristischen Ausbreitungsgeschwindigkeit des Zweiten Schalls aus. Es entstehen zwei thermische Wellen: eine schnellere mit einer kleineren Amplitude sowie eine zweite langsamere mit einer größeren Amplitude. Erstere wird durch die Kopplung mit dem mechanischen Problem induziert und breitet sich mit der Geschwindigkeit von Schall aus. Letztere, der sogenannte Zweite Schall, ist rein thermischen Ursprungs. Mit steigenden Temperaturen geht der Zweite Schall in einen diffusen Prozess über.

Aufgrund der Entdeckung des Zweiten Schalls musste eine erweiterte thermoelastische Theorie entwickelt werden, die zum einen den klassischen Fall konsistent beinhaltet und zum anderen in der Lage ist, das neu entdeckte physikalische Phänomen zu modellieren. Zur Beschreibung dieser Effekte wurden in den letzten Jahrzehnten viele nicht klassische thermoelastische Theorien entwickelt. Im Laufe dieser Forschungen wurde die parabolische Fouriersche

---

<sup>1</sup>Zweiter Schall wurde außerdem in suprafluiden  $^2\text{He}$  und  $^6\text{Li}$  entdeckt.

## Zusammenfassung

Wärmeleitungsgleichung meistens durch eine hyperbolische ersetzt. Die Kopplung letzterer mit Elastizität führt auf nicht klassische thermomechanische Theorien, die Zweiten Schall modellieren können, den klassischen Ansatz beinhalten und zusätzlich das Paradoxon der unendlichen Ausbreitungsgeschwindigkeit bewältigen.

In dieser Arbeit wird der vielversprechende Vorschlag von Green und Naghdi [51] verfolgt. Er ist in der Lage, thermische Impulse in einer sehr logischen und konsistenten Art und Weise abzubilden. Dieser Ansatz ist phänomenologisch, d.h. er beschreibt makroskopisches Materialverhalten und vernachlässigt die mikroskopische Materialstruktur. Des Weiteren ist er in das Feld der rationalen Thermodynamik eingebettet. Die Basis der Theorie von Green und Naghdi bildet die Einführung einer neuen Variablen, der sogenannten thermischen Verschiebung  $\alpha$ , die dem Zeitintegral über die empirische Temperatur  $T$  entspricht.

Zunächst wird in Kapitel 2 ein kurzer Überblick über den Zweiten Schall sowie ein Einblick in den Stand der theoretischen Forschung in der nicht klassischen Thermoelastizität gegeben. Der anschließende theoretische Teil dieser Arbeit befasst sich mit der Einbettung der Green–Naghdi Theorie in das Gebiet der rationalen Thermodynamik sowie der Aufarbeitung ihrer Grundzüge. Hierbei werden in Kapitel 3 die allgemeinen Bilanzgleichungen, die die Basis zur Beschreibung des thermodynamischen Verhaltens eines jeden Körpers bilden, zusammengefasst. Da diese per Konstruktion materialunabhängig sind, werden ergänzend individuelle, konstitutive Materialgleichungen benötigt. Die Grundzüge der Materialmodellierung werden daher in Kapitel 3.3 kurz skizziert.

Von den Bilanzgleichungen besitzt die Entropiebilanz in Verbindung mit dem 2. Hauptsatz der Thermodynamik eine besondere Bedeutung, der besagt, dass die Entropieproduktion für alle Lösungen der Bilanzgleichungen zu allen Zeiten an allen Orten nicht negativ ist. Ihre Auswertung führt zu Restriktionen an die konstitutiven Materialgleichungen. In dieser Arbeit wird die Entropiebilanz in Kapitel 4 nach dem Prinzip von Müller–Liu ausgewertet, da dieses allgemeiner als der Ansatz von Clausius–Duhem ist.

Im Anschluss daran wird in Kapitel 5 die thermische Green–Naghdi Theorie vorgestellt. Sie ist unterteilt in drei Teiltheorien, die als Typ I, II und III bezeichnet werden. Die linearisierte Theorie "Typ I" entspricht der Theorie nach Fourier, d.h. die klassische Theorie ist vollständig in der Green–Naghdi Theorie enthalten. Sowohl Typ II als auch III können thermische Wellenausbreitung abbilden und sind somit für die Modellierung des Phänomens des Zweiten Schalls geeignet. Zusätzlich ist die Ausbreitungsgeschwindigkeit von Typ II immer endlich. Die Konstitutivgleichungen für Typ II werden üblicherweise so gewählt, dass die resultierende Theorie dissipationfrei ist. Dies bedeutet, dass nun Thermoelastizität nicht mehr notwendigerweise mit Energiedissipation einhergeht. Typ III hingegen ist der allgemeinste der drei Fälle. Er beinhaltet sowohl Typ I als auch II als Grenzfälle. Damit erreicht man, dass, neben der klassischen Theorie, nun auch thermische Wellen modelliert werden können. Zusätzlich wird (bei entsprechender Parameterwahl) das Paradoxon der unendlichen Wellenausbreitungsgeschwindigkeit vermieden.

Darauf aufbauend wird in Kapitel 6 eine nicht klassische thermoelastodynamische Theorie hergeleitet, die den Deformationsprozess und das thermische Problem koppelt.

Das im theoretischen Teil dieser Arbeit vorgestellte mathematische Modell besteht aus par-



tiellen Differentialgleichungen, die neben der üblichen Raumabhängigkeit auch von der Zeit abhängig sind. Aufgrund der Komplexität der Gleichungen kann nur in den seltensten Fällen eine analytische Lösung bestimmt werden, so dass numerische Methoden diese Lösung approximieren müssen.

Basierend auf den theoretischen Grundlagen wird in den Kapiteln 5.2 und 6.2 also eine geeignete Berechnungsmethode für die Wärmeleitung bzw. die gekoppelte Thermoelastizität entwickelt. Eine Hauptaufgabe des numerischen Teils dieser Arbeit ist folglich, die Implementierung des entwickelten Ansatzes zu realisieren und diesen anhand von verschiedenen Beispielen zu verifizieren. Der in dieser Arbeit vorgestellte Ansatz verwendet sowohl im räumlichen als auch für die Zeitintegration Finite-Elemente-Methoden für die Diskretisierung der zugrunde liegenden partiellen Differentialgleichungen.

Im Rahmen von Finite-Element-Methoden bildet die schwache Form der partiellen Differentialgleichungen die Basis. Zur numerischen Lösung der schwachen Form wird in dieser Arbeit eine Semi-Diskretisierungstechnik eingesetzt. Dabei wird zunächst die Diskretisierung im Raum mit einem Standard-Bubnov–Galerkin-Verfahren realisiert. Anschließend werden für die Zeitintegration kontinuierliche und diskontinuierliche Galerkin-Verfahren verwendet.

Die Ansätze werden in den Kapiteln 5.3 und 6.4 anhand von Beispielen aus dem Bereich der Wärmeleitung sowie Problemstellungen der gekoppelten Thermomechanik diskutiert. Es wird sowohl auf eine geometrisch lineare und nichtlineare Beschreibung als auch lineares und nichtlineares Materialverhalten eingegangen. Dabei wird u.a. gezeigt, dass sich die Theorie von Green und Naghdi zur Modellierung des Zweiten Schalls hervorragend eignet. Nennenswert ist dabei die Eigenschaft des sogenannten Typs II, dass sich die thermische Welle energieerhaltend, d.h. dissipationslos, ausbreitet.

Abschließend wird in Kapitel 7 eine inkrementelle Variationsformulierung für gekoppelte Thermohyperelastizität vorgestellt. Hierbei wird sowohl auf den klassischen Typ I als auch auf den dissipationsfreien Typ II eingegangen. Motivation ist die Tatsache, dass der Entropiefluss von Typ II im Fall von Thermohyperelastizität durch das gleiche Potential, hier die freie Energiefunktion, bestimmt wird wie die mechanischen Spannungen. Dies ist für den klassischen Typ I nicht möglich. An dieser Stelle wird dann eine algorithmische Formulierung des klassischen Entropieflusses hergeleitet, die durch die freie Energie, die als Funktional fungiert, bestimmt ist.

## *Zusammenfassung*

# 1. Introduction

*Wissenschaft ist mitunter eine Reise an die Grenzen des Machbaren und des Erfassbaren. In der Tieftemperaturphysik strebt diese Reise dem absoluten Nullpunkt zu. [...] Der alltäglichen Erfahrung zum Trotz, die Kälte mit Unbehagen und Erstarren gleichsetzt, offenbart die kondensierte Materie bei tiefen Temperaturen immer neue faszinierende Eigenschaften.*  
C. Enss

Thermoelasticity represents the fusion of the fields of heat conduction and elasticity in solids and is usually characterized by a twofold coupling. Thermally induced stresses can be determined as well as temperature changes caused by deformations. Studying the mutual influence is subject of thermoelasticity. Usually, heat conduction in solids is based on Fourier's law which describes a diffusive process. It predicts unnatural infinite transmission speed for parts of local heat pulses. At room temperature, for example, these parts are strongly damped. Thus, in these cases most engineering applications are described satisfactorily by the classical theory. However, in some situations the predictions according to Fourier's law fail miserably. One of these situations occurs at temperatures near absolute zero, where the phenomenon of second sound<sup>1</sup> was discovered in the 20th century.

Consequently, non-classical theories experienced great research interest during the recent decades. Throughout this thesis, the expression "non-classical" refers to the fact that the constitutive equation of the heat flux is not based on Fourier's law. Fourier's classical theory hypothesizes that the heat flux is proportional to the temperature gradient. A new thermoelastic theory, on the one hand, needs to be consistent with classical thermoelastodynamics and, on the other hand, needs to describe second sound accurately. Hence, during the second half of the last century the traditional parabolic heat equation was replaced by a hyperbolic one. Its coupling with elasticity leads to non-classical thermomechanics which allows the modeling of second sound, provides a passage to the classical theory and additionally overcomes the paradox of infinite wave speed.

Although much effort is put into non-classical theories, the thermoelastodynamic community has not yet agreed on one approach and a systematic research is going on worldwide.

---

<sup>1</sup>Second sound refers to a wave-like heat propagation which can be found in very pure crystalline solids at cryogenic temperatures, see also Chapter 2.

## 1. Introduction

Computational methods play an important role for solving thermoelastic problems in engineering sciences. Usually this is due to the complex structure of the equations at hand. This thesis aims at establishing a basic theory and numerical treatment of non-classical thermoelasticity (rather than dealing with special cases). The finite element method is already widely accepted in the field of structural solid mechanics and enjoys a growing significance in thermal analyses. This approach resorts to a finite element method in space as well as in time.

### 1.1. The theory of Green and Naghdi

In this thesis, the very promising approach introduced in 1991 by Green and Naghdi [51] is followed because it is capable of accounting thermal pulse transmission in a very logical and consistent manner. Their approach is phenomenological - it describes the macroscopic nature and ignores the microscopic structure - and is embedded into rational thermodynamics.

The entire theory is subdivided into three types, labeled type I, II and III. A wide range of heat flow problems can be modeled and the classical theory (type I) is fully embedded. The novelty of their approach is the introduction of the so-called thermal displacement  $\alpha$ , a field whose time derivative is the empirical temperature, i.e.  $\dot{\alpha} = T$ . Three varying state spaces are skilfully defined and partly take the thermal displacement  $\alpha$  (and its gradients) directly into account. This leads to the three types of heat conduction I, II and III. The linearized version of type I is equivalent to Fourier's diffusive, parabolic heat equation.

The non-classical type II exhibits the outstanding property of being non-dissipative. In other words, heat conduction does no longer necessarily imply energy dissipation. The resulting heat equation is hyperbolic and corresponds to the well-known wave equation. In particular, thermal wave propagation at finite speed is incorporated. Furthermore, the entropy flux vector is determined in terms of the same potential as the mechanical stress and the theory does not necessarily involve energy dissipation.

Type III is a general extension and contains type I and II as limiting cases. Both, type II and III, cope with the disadvantages of classical heat conduction as they allow the transmission of heat as thermal waves and are able to overcome the paradox of infinite wave speed in Fourier's approach. Moreover, they are capable of modeling the second sound phenomenon.

### 1.2. Structure of the present work

The present work is divided into 9 chapters. Introductorily, a short state of the art is presented in Chapter 2. The second sound phenomenon and its historical detection is summarized as well as the development of non-classical thermoelastic theories.

Subsequently, in Chapter 3 the underlying framework of thermoelasticity is established. First, the basic kinematics are reiterated within the spatial as well as the material motion problem. Next, different local formats of the fundamental thermodynamic balance equations for mass, linear momentum, angular momentum, energy and entropy are stated. The chapter is closed by reviewing the basic ideas of thermo-hyperelasticity.

Chapter 4 deals with material modeling, in particular with entropy principles. There exist several forms of the second law of thermodynamics and, consequently, several forms of its exploitation. This thesis begins with the most general approach, the one of Müller [112], by introducing the entropy as a primary variable. Following the way of Müller to which later Liu [97] added the mathematical framework, further balance equations are included with the help of Lagrange multipliers. The exploitation gives rise to the so-called Liu equations being a first restriction to the structure of the constitutive equations. Then further restrictions are obtained by the subsequent application of an entropy exploitation suggested by Green and Naghdi [50].

With these general derivations at hand, the Green–Naghdi theory of non-classical heat conduction is introduced in Chapter 5. Three varying temperature equations are derived. A consequent algorithmic elaborateness and numerical implementation of their theory had not been accomplished. Therefore, the aim of this thesis is, besides a spatial finite element method, the derivation of a temporal finite element method for the modeling and computation of non-classical heat conduction and later on of the coupled thermoelastic problem. At the end of the chapter, numerical examples are presented. Among others, the original second sound experiments in which the phenomenon was first observed are modeled. Analytical findings are supported by an example and used as a benchmark.

In Chapter 6 the extension to geometrically nonlinear, coupled thermoelasticity is developed. The theoretical part is followed by the elaboration of a suitable finite element discretization. The performance of the implemented method is illustrated by means of numerical examples. Here, the original second sound experiments are used once more as a benchmark. Moreover, non-classical thermoelasticity is examined in context of the material force method. This Chapter is closed by the introduction of an energy consistent algorithmic stress tensor method which leads to an energy conserving discretization procedure. It is applied to the theory without energy dissipation of type II.

A total potential formulation cannot be established for the entire theory. Therefore, an incremental algorithmic variational formulation is derived in Chapter 7. Starting with the definition of an incremental Lagrangian function, the algorithmic balance of entropy and balance of linear momentum follow from a variational principle. On that occasion, an incremental potential for the entropy flux vector is established. Based on this considerations, the formulation of incremental material balance laws gives rise to incremental material forces in non-classical thermoelasticity.

Finally, the wave speed of Green–Naghdi heat conduction is investigated further in Chapter 8. Some analytical findings are presented in order to show that the Green–Naghdi theory of type III predicts an infinite speed of heat conduction.

Concluding, Chapter 9 summarizes and discusses this thesis and gives an outlook for possible future research work.

## *1. Introduction*

## 2. State of the art

Classical heat conduction is based on Fourier's law which leads to the well-known diffusive temperature equation. Most engineering applications are described accurately by this parabolic equation, but at cryogenic temperatures material behavior can completely differ from that at room temperature. For example, one of the properties that might change is the way heat propagates. Predictions of the classical theory may diverge conspicuously from experimental data.

In metals, thermal energy can be transmitted by free electrons, by lattice vibrations (phonons) and by electron-phonon and phonon-electron interaction, respectively. In the second case a wave like transport, the so-called second sound phenomenon, occurs, if phonons travel through crystals, interact with each other and conserve the momentum (cf. [39]). Two independent modes of wave propagation can be observed: classical first sound and the thermal second sound. The latter refers to the propagation of sound waves in phonon gas causing thermal waves and its name is due to collective excitations in the phonon gas which are similar to the propagation of sound waves in ordinary gases.

In metals, for example, heat is mainly conducted by free electrons. Until now, second sound has been observed in very pure crystals in the vicinity of the local thermal conductivity maximum at cryogenic temperatures. Outside of this temperature interval, the wave like heat propagation merges into a diffusive character. Furthermore, a wave nature of heat propagation has also been detected in superfluids, nonhomogeneous materials like sand and processed meat. The speed of second sound depends on the temperature and is smaller than that of first sound. As the temperature increases, the velocity decreases due to the increasing heat capacity.

Furthermore, experiments exhibit the existence of an additional longitudinal elastic wave which propagates at a finite speed higher than second sound. Therefore, the thermal problem has to be coupled with a deformation process.

The existence of second sound is first proposed by Tisza [163] in 1938 and supported by Landau [94] in 1941 when investigating theoretical aspects of heat propagation in suprafluid  $^4\text{He}$ . Their theories are experimentally proven by Peshkov [123] in 1944 whose results are in good agreement with Tisza's as well as Landau's theoretical predictions.

Since the theories assume the existence of phonon gas which also exists in solids, Peshkov suggests the possibility of second sound in solids in 1946. Based on his considerations various theoretical contributions are published. Ward and Wilks's investigations [170] lead to the supposition that second sound would be first observed in dielectric crystals. Although intensive effort is devoted to experiments, it lasts until 1966 when Ackermann and his research group [1] observe second sound in solids for the first time. Experiments are undertaken with  $^4\text{He}$  between 0.54 K and 0.71 K and yield a second sound velocity of 160 m/s. In 1969, Ackermann

## 2. State of the art

et al. [2] also prove second sound in solid  $^3\text{He}$  in the temperature range of  $0.42\text{ K} < T < 0.58\text{ K}$  at a velocity of  $125 \pm 7\text{ m/s}$ . Subsequently, second sound is detected in NaF by McNelly et al. [108] who also investigate NaI and LiF for which second sound is not accounted. In NaF the phenomenon is observed in a temperature range around 15 K. Jackson et al. [72], Rogers [143] and Pohl and Irniger [125] corroborate the existence of second sound in NaF and its velocity is constituted in [61] to be  $1953.1\text{ m/s}$ . Second sound waves in Bi are measured two years later in 1972 by Narayanamurti and Dynes [119] around 3 K and at a wave speed of  $78 \pm 5\text{ m/s}$ . Although Bi is elastically a very anisotropic solid, the second sound velocity is found to be independent of orientation.

Fourier's law implies the unphysical property that temperature perturbations propagate at infinite speed. In order to overcome this drawback intensive research activities lead to modified theories of heat conduction which in general are hyperbolic. The detection of second sound has intensified the development of non-classical heat conduction theories.

First approaches addressing to finite propagation speed are published by Maxwell [107], Cattaneo [24] and Vernotte [168]. The introduction of a relaxation time gives rise to finite propagation speed and results in a telegraph equation. Based on these derivations various modifications of Fourier's law and the corresponding thermal theories have been published. An extensive review of the research development and the state of the art in the field of heat transmission until 1990 is given by Joseph and Preziosi [80, 81], where an abundant number of publications are cited in chronological order. Dreyer and Struchtrup [39] narrow their excellent review to heat conduction in dielectric solids at low temperatures. In their paper, the second sound phenomenon is looked at from the theoretical and the experimental point of view. Coupled classical and non-classical thermomechanical problems are reviewed in detail by Tamma and Namburu [160]. Early and important investigations on thermodynamical aspects of non-classical thermoelasticity can be found in the works of Bogy and Naghdi [21], Müller [112], Green and Lindsay [48], Green and Laws [49] as well as Green and Naghdi [50].

Later, in 1991, Green and Naghdi develop a very promising non-classical model [51]. A similar idea to the thermal displacement introduced by Green and Naghdi is tracked by Kosinski, Cimmelli and Frischmuth [34, 47] who define a semi-empirical temperature. Contrary to the traditional Fourier case, the heat flux is related to the gradient of the semi-empirical temperature rather than to the temperature gradient.

A further attempt, published by Chandrasekharaiah [30] and Tzou [165], is based on two different time translations for the temperature gradient as well as for the heat flux. Their ideas lead to a dual-phase-lag-thermoelasticity.

Hetnarski and Ignaczak [64] present an approach in which both, an energy function and a heat flux, do not only depend on the temperature and the strain tensor but additionally on an elastic heat flow. A further paper [65] gives an overview of transient thermoelastic theories.

The Green–Naghdi theory, on which this thesis is based, enjoys great research interest as it is developed in a rational and very consistent way. The aspect of non-dissipative heat conduction is also attractive in view of a variational formulation of the balance equations. A Hamiltonian formulation for Green–Naghdi thermoelasticity is derived by Maugin and Kalpakides in [105]



and in [84, 106] they formulate the balance laws on the material manifold.

Quintanilla and co-authors present an extensive mathematical analysis of the Green–Naghdi theory in a series of papers. Uniqueness results are derived in [132], stability properties are studied in [133, 135, 136].

As mentioned above, the Green–Naghdi theory of type II does not necessarily involve energy dissipation. Consequently, several publications dealing with this part of the theory can be found in literature. Quintanilla also contributes to the analysis of type II. He investigates the thermoelastic theory for materials with microstructure in [138]. The spatial behavior of thermoelasticity without energy dissipation is subject of [131] whereas in [139] it is derived for nonsimple materials. The spatial behavior is also treated by Nappa [117] who derives spatial decay estimates for the evolution equations in linear thermoelasticity by establishing a dynamic Saint–Venant’s principle. Kumar and Deswal [92] study surface waves in a micropolar type II thermoelastic solid in a half-space. The micropolar theory is also subject of Ciarletta [33] and Svanadze et al. [156], whereas Iesan and Nappa [71] investigate micromorphic Green–Naghdi bodies. A quasi-static uncoupled thermoelastic problem is dealt with in [128] using a superposition of both the classical and the theory without energy dissipation. Sharma and Pathania’s contribution [145] about generalized thermoelastic waves in anisotropic plates includes an investigation of the type II theory. Thermoelastic waves are also subject of Verma and Hasebe [167] who investigate the propagation in an infinite homogeneous isotropic plate. Green and Naghdi themselves investigate the behavior of one-dimensional waves [52]. Their work is complemented by the studies of Chandrasekharaiah [25, 26, 28, 29, 31] and Iesan [70] who also address to the linear theory without energy dissipation. These contributions provide some of the very few analytical solutions to special non-classical thermoelastic problems. Song and Zhang [149] couple the thermoelastic theory of Green and Naghdi with a magnetic theory and investigate the effect of the magnetic field.

Using energy methods Zhang and Zuazua [174] analyze the long time behavior of type-III thermoelasticity and receive decay results in two- and three-dimensional domains. In contrast, Reissig and Wang [142] examine solution properties of linear type-III thermoelasticity problems without resorting to energy methods and the well-posedness of the Cauchy problem, the propagation of singularities as well as estimates for the decay of solutions are studied.

Puri and Jordan [130] examine the propagation of plane waves in a type-III-thermoelastic continuum. Dispersion relation solutions are determined analytically. The influence of the model parameters is examined using Mathematica<sup>®</sup>’s computational tools. The harmonic type-III thermal stress distributions for a body with a circular cylindrical hole are derived and discussed by Allam et al. [3]. Analytical solutions for thermal shock problems are presented by Li and Dhaliwal [96] applying the theory of type III.

Contrary to the extensive theoretical studies, only few papers concerning numerical simulations applying the Green–Naghdi theory have been published. Bargmann and Steinmann [7, 8, 10, 11, 12] aim at establishing a consistent and fundamental numerical implementation of the non-classical heat conduction and linear thermostatics. The discretization process is based on Galerkin finite elements in space as well as in time. The applicability of the Green–Naghdi approach for modeling second sound is shown.

Thermoelasticity in a layer, applying the theory of type II and III, is treated by Bagri et al.

## 2. *State of the art*

[6] and Taheri et al. [159]. In order to obtain the temperature, displacement and stress fields, the governing equations are Laplace transformed. In the transformed space the solutions are derived analytically and a numerical inversion of the Laplace transform method is applied subsequently.

Thermoelastic interactions are studied by Misra [110], Mukhopadhyay [115] as well as Chandrasekharaiah and Srinath [27]. Misra examines an elastic half-space applying the thermal theory of type III. Mukhopadhyay investigates the behavior of a type-II-thermoelastic body with a spherical cavity, whereas Chandrasekharaiah and Srinath devote themselves to cylindrical cavities.

The search for an all-embracing non-classical theory of thermoelasticity is not yet finished. Only a detailed investigation of the most promising approaches can judge the significance. Due to the above mentioned properties and aspects the Green–Naghdi theory possesses, it is the most promising approach, in the author's conviction, and thus it is preferred for the basis of the mathematical model in this thesis.

## 3. Continuum mechanics

This Chapter focuses on the framework of modeling thermoelasticity in solids. The underlying kinematics are introduced for the general nonlinear case and form the basis for the mechanical balance equations. Finally, the fundamental ideas of material modeling are introduced, i.e. the principles of constitutive theory of materials.

### 3.1. Kinematics

#### 3.1.1. Spatial motion problem

A body  $B$  is considered to be a collection of physical particles. Let  $\mathbf{X}$  denote the fixed position of a particular particle in the undeformed and stress-free configuration  $\mathcal{B}_0$ , the region the body  $B$  occupies at the initial time  $t_0$ .  $\mathbf{X}$  and  $\mathcal{B}_0$  are called the particle's material position and the material configuration, respectively. Then the deformation of this configuration is described by the time-dependent vector field of the nonlinear spatial deformation map

$$\varphi : \mathcal{B}_0 \times \mathbb{R}_+ \rightarrow \mathcal{B}_t \quad \text{with} \quad \varphi(\mathbf{X}, t) := \mathbf{x}, \quad (3.1.1)$$

where  $\mathbf{x}$  denotes the spatial position of the particle  $\mathbf{X}$  in the deformed (spatial) configuration  $\mathcal{B}_t$  at time  $t$ . This is also referred to as the Lagrangian viewpoint. The vector field  $\varphi$  is assumed to be unique, continuously differentiable and to have a continuous inverse. Mathematically speaking,  $\varphi$  is required to be a diffeomorphism. The motion of a body is characterized by the displacement  $\mathbf{u}$ , a time-dependent vector field,

$$\mathbf{u} : \mathcal{B}_0 \times \mathbb{R}_+ \rightarrow \mathbb{R}^n \quad \text{with} \quad \mathbf{u}(\mathbf{X}, t) := \varphi(\mathbf{X}, t) - \mathbf{X}. \quad (3.1.2)$$

Furthermore,  $n$  denotes the spatial dimension of the body and typically  $n \in \{1, 2, 3\}$ .

The deformation gradient  $\mathbf{F}$  of the spatial deformation map, i.e. the linear tangent map from the material tangent space  $\mathcal{T}\mathcal{B}_0$  to the spatial tangent space  $\mathcal{T}\mathcal{B}_t$ , is defined by

$$\mathbf{F} : \mathcal{T}\mathcal{B}_0 \rightarrow \mathcal{T}\mathcal{B}_t \quad \text{with} \quad \mathbf{F} := \nabla_{\mathbf{X}}\varphi(\mathbf{X}, t), \quad \text{i.e.} \quad F_{iA} = \frac{\partial \varphi_i}{\partial X_A}. \quad (3.1.3)$$

The small index  $i$  and the capital index  $A$  indicate the spatial and the material configuration, respectively. Thus,  $\mathbf{F}$  is a second order two-field tensor and (in general) non-symmetric. In continuum mechanics,  $\mathbf{F}$  is the most important measure of deformation and basis for strain measures. One strain measure used throughout this thesis is the right Cauchy–Green strain

### 3. Continuum mechanics

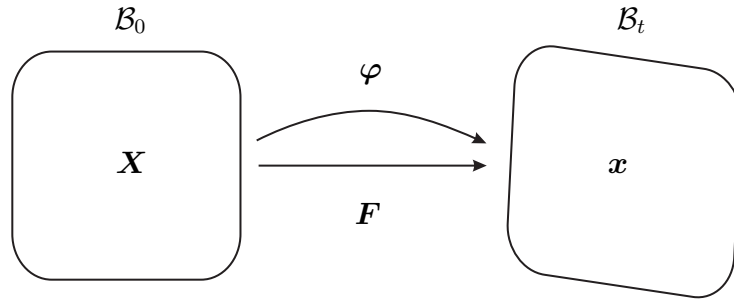


Figure 3.1.: Spatial motion problem: Kinematics

tensor. It is defined by  $\mathbf{C} := \mathbf{F}^t \cdot \mathbf{F}$ , with  $C_{AB} = F_{Ai}F_{iB}$ , where  $(F_{iA})^t = F_{Ai}$  denotes transposition.  $\mathbf{C}$  is symmetric and positive definite.

The Jacobian  $J$  of the deformation gradient  $\mathbf{F}$  is given by

$$J := \det \mathbf{F} > 0, \quad (3.1.4)$$

where the claim of a positive Jacobian  $J$  prevents the body from self-penetration. Moreover, the spatial velocity  $\mathbf{v}$  is introduced as the material time derivative of the spatial motion map

$$\mathbf{v} := D_t \varphi(\mathbf{X}, t) = \partial_t \varphi|_{\mathbf{X} \text{ fixed}} = \dot{\mathbf{x}}. \quad (3.1.5)$$

A particle's velocity is the time rate of change of the particle's position.

The thermal state in the current configuration  $\mathcal{B}_t$  is defined by the empirical temperature  $T$  and the thermal displacement  $\alpha$  which is first introduced by Green and Naghdi [51]<sup>1</sup>

$$\begin{aligned} T : \mathcal{B}_0 \times \mathbb{R}_+ &\rightarrow \mathbb{R} & \text{with } T &:= T(\mathbf{X}, t), \\ \alpha : \mathcal{B}_0 \times \mathbb{R}_+ &\rightarrow \mathbb{R} & \text{with } \alpha &:= \alpha(\mathbf{X}, t) = \int_{t_0}^t T(\mathbf{X}, \tau) \, d\tau + \alpha_0. \end{aligned} \quad (3.1.6)$$

Here,  $\alpha_0$  denotes the initial value of  $\alpha$  at the reference time  $t_0$ .  $\alpha$  is assumed to be at least twice continuously differentiable in  $\mathbf{X}$  and  $t$  and, obviously,

$$\dot{\alpha} = T \quad (3.1.7)$$

holds. The empirical temperature is a parameter  $\in \mathbb{R}$  which is based on the observed behavior of some arbitrary material. Thus, as opposed to the later introduced terminology of the absolute temperature, the value assigned to the empirical temperature is dependent of the characteristics of the chosen comparative material.

<sup>1</sup>The definition of the thermal displacement  $\alpha$  is motivated by the definition of the empirical temperature  $T$  in statistical and molecular dynamics [51]. There,  $T$  is regarded as a macroscopic measure for a mean kinetic energy or a mean velocity of the atoms. Thus, Green and Naghdi define a thermal variable which is related to the temperature in the same way the mechanical displacement  $\mathbf{u}$  is related to the mechanical velocity  $\mathbf{v}$  and can consequently be regarded as the macroscopic measure of a mean displacement magnitude on the microscale: the thermal displacement  $\alpha$ .

### 3.1.2. Material motion problem

The material deformation map  $\Phi$ , within which physical particles are followed through the material at fixed spatial coordinates  $\boldsymbol{x}$ , is given by

$$\Phi : \mathcal{B}_t \rightarrow \mathcal{B}_0 \quad \text{with } \Phi(\boldsymbol{x}, t) := \boldsymbol{X} \quad (3.1.8)$$

which is also referred to as the Eulerian viewpoint [90, 153]. Both motion problems are related via the identity maps in  $\mathcal{B}_0$  and  $\mathcal{B}_t$ :

$$id_{\mathcal{B}_0} = \Phi \circ \varphi(\boldsymbol{X}, t), \quad id_{\mathcal{B}_t} = \varphi \circ \Phi(\boldsymbol{x}, t). \quad (3.1.9)$$

In complete analogy to the spatial motion case, the deformation gradient of the material motion map  $\boldsymbol{f}$  and its Jacobian  $j$  are defined by

$$\boldsymbol{f} : \mathcal{TB}_t \rightarrow \mathcal{TB}_0 \quad \text{with } \boldsymbol{f} := \nabla_{\boldsymbol{x}} \Phi(\boldsymbol{x}, t) \quad \text{and } j := \det \boldsymbol{f} > 0 \quad (3.1.10)$$

and, consequently, are related to the spatial quantities via inversion:

$$\boldsymbol{F}^{-1} = \boldsymbol{f}, \quad J^{-1} = j. \quad (3.1.11)$$

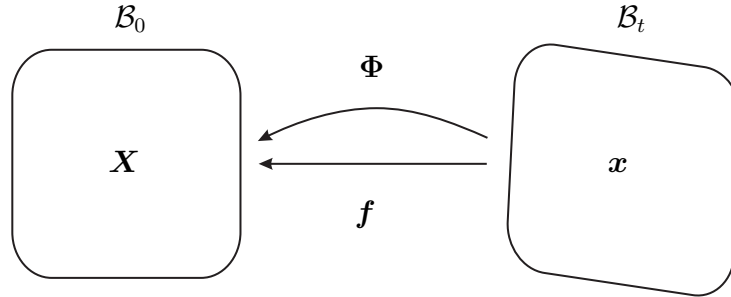


Figure 3.2.: Material motion problem: Kinematics

Furthermore, the material analogues of the thermal displacement and the empirical temperature, i.e.  $\bar{\alpha}$  and  $\bar{T}$ , are related to their spatial counterparts via

$$\begin{aligned} \alpha &= \bar{\alpha} \circ \varphi, & \bar{\alpha} &= \alpha \circ \Phi, \\ T &= \bar{T} \circ \varphi, & \bar{T} &= T \circ \Phi. \end{aligned} \quad (3.1.12)$$

The spatial and the material time derivative, i.e.  $D_t$  and  $d_t\{\bullet\} = \partial_t\{\bullet\}|_{\boldsymbol{x} \text{ fixed}}$ , of a scalar- or vector-valued function  $\{\bullet\}$  are related by

$$D_t\{\bullet\} = d_t\{\bullet\} + \nabla_{\boldsymbol{x}}\{\bullet\} \cdot \boldsymbol{v}, \quad d_t\{\bullet\} = D_t\{\bullet\} + \nabla_{\boldsymbol{X}}\{\bullet\} \cdot \boldsymbol{V}. \quad (3.1.13)$$

This relationship is also known as the Euler theorem [90]. The material velocity  $\boldsymbol{V}$  is calculated via

$$\boldsymbol{V} := d_t \Phi(\boldsymbol{x}, t) = \partial_t \Phi|_{\boldsymbol{x} \text{ fixed}}. \quad (3.1.14)$$

### 3. Continuum mechanics

Following the way of Steinmann [153, 154] and Kuhl et al. [89, 90], the terminology of description, parametrization and reference is introduced:

A tensor-valued quantity in spatial (material) description is an element of the tangent or cotangent space of  $\mathcal{B}_t$  ( $\mathcal{B}_0$ ). If a tensor-valued quantity is in two-point description, it has basic vectors in both, a tangent or cotangent space of  $\mathcal{B}_t$  and  $\mathcal{B}_0$ .

The spatial parametrization of a quantity  $\{\bullet\}$  is given, if  $\{\bullet\}$  is formulated in terms of the spatial coordinates  $\boldsymbol{x}$  as  $\{\bullet\}(\boldsymbol{x}, t)$ . Analogously, the material parametrization is formulated in terms of the material coordinates  $\boldsymbol{X}$  as  $\{\bullet\}(\boldsymbol{X}, t)$ .

Furthermore, the spatial reference  $\{\bullet\}_t$  of a volume specific quantity  $\{\bullet\}$  relating the quantity to the spatial domain  $\mathcal{B}_t$  is introduced, while the material reference is denoted by  $\{\bullet\}_0$ .

## 3.2. Mechanical balance equations

Thermodynamics is concerned with the determination of the object of interest's mechanical and thermal quantities. The unknown fields, such as e.g. the material's density  $\rho$ , the velocity  $\boldsymbol{v}$  or the temperature  $T$ , are usually described by differential equations. These so-called balance equations form a system of equations characterizing the cause of motion of any body and are independent of the material properties. A balance equation is called conservation law if it has vanishing sources.

A general integral balance equation for a closed system (for definition see Appendix A.2) in the spatial motion problem describes the evolution of a physical quantity  $\Gamma$  in a body  $\mathcal{B}_0$ . The physical properties of  $\mathcal{B}_0$  are defined by densities per unit mass of the physical variable. These densities are assumed to be additive, i.e. their values are determined by integration over the volume of its values over the infinitesimal volume elements. It reads

$$D_t \int_{\mathcal{B}_0} \Gamma \, dV = - \int_{\partial\mathcal{B}_0} \phi_b \, dA + \int_{\mathcal{B}_0} \varsigma \, dV + \int_{\mathcal{B}_0} \gamma \, dV, \quad (3.2.1)$$

where  $\varsigma$  denotes the corresponding source density,  $\gamma$  the production in the body. The non-convective flux density vector  $\phi_b$  through the surface  $\partial\mathcal{B}_0$  into  $\mathcal{B}_0$  is usually assumed to depend on the position  $\boldsymbol{x}$ , the outward unit normal vector  $\boldsymbol{n}$  (being normal to the surface element  $dA$ ) and the time  $t$ :  $\phi_b = \phi_b(\boldsymbol{x}, t, \boldsymbol{n})$ . This relation is also known as the Cauchy postulate and leads to the Cauchy fundamental theorem which states that if the Cauchy postulate holds, then there exists a unique tensor  $\phi$  such that

$$\phi_b(\boldsymbol{x}, t, \boldsymbol{n}) = \phi(\boldsymbol{x}, t) \cdot \boldsymbol{n}. \quad (3.2.2)$$

In other words, the dependence on the outward unit normal  $\boldsymbol{n}$  of the flux density vector  $\phi_b$  is linear. The proof of this theorem can be found in [55], for example.

Thus, Eq. (3.2.1) can be written in the following form:

$$D_t \int_{\mathcal{B}_0} \Gamma \, dV = - \int_{\partial\mathcal{B}_0} \phi \cdot \boldsymbol{n} \, dA + \int_{\mathcal{B}_0} \varsigma \, dV + \int_{\mathcal{B}_0} \gamma \, dV. \quad (3.2.3)$$

The integral form has to hold for all volume elements  $\mathcal{B}_0$ , even for infinitesimal small ones. Moreover, the assumption of sufficient smoothness of the flux density vector enables the application of the divergence theorem (A.5.2) relating a surface integral to a volume integral. Consequently, one obtains the local form

$$D_t \Gamma = -\operatorname{div} \phi + \varsigma + \gamma. \quad (3.2.4)$$

Thermoelasticity according to the Green–Naghdi approach [8, 51] is based on the balance of entropy and the conservation laws for mass, linear momentum, angular momentum and total energy, being introduced in the following for the spatial as well as for the material motion problem. A detailed description of classical thermoelasticity with many varying formulations in both settings can be found in [153] underlining the duality between the spatial and the material motion problem and containing a large number of relations between them.

A complete and clearly arranged list of the balance equations for open systems with respect to both motion problems, both references and both parameterizations can be found in [90]. The restriction to closed systems can easily be derived. The following section focuses on those playing a role in this work's further considerations and those providing the transition from one to the other.

### 3.2.1. Spatial motion problem

The balance of mass states that if there exist no mass sources within the body and no mass exchange through the surface occurs, i.e. mass is neither produced nor supplied, then the mass of the body is conserved. Thus, if the density  $\rho_0$  is substituted into Eq. (3.2.4) for the balanced quantity  $\Gamma$  and the flux, the production and the source densities  $\phi$ ,  $\gamma$  and  $\varsigma$  are set equal to zero, one obtains:

$$D_t \rho_0 = 0. \quad (3.2.5)$$

The spatial material's density is related to the material one via the Jacobian  $J$ :  $\rho_0 = J \rho_t$ . The continuum version of Newton's second law for particle mechanics renders the balance of momentum expressing that the change of the total momentum  $\rho_0 \mathbf{v}$  equals the sum over all forces acting on the body, i.e. the sum of the surface forces  $\mathbf{T}_C$  and the volume forces  $\mathbf{b}$ . Application of Cauchy's stress theorem (A.7) stating that  $\mathbf{T}_C = \mathbf{P} \cdot \mathbf{N}$  and of the divergence theorem (A.5.2) leads to

$$\begin{aligned} D_t (\rho_0 \mathbf{v}) &= \operatorname{Div} \mathbf{P} + \rho_0 \mathbf{b} \\ \Rightarrow \rho_0 D_t \mathbf{v} &= \operatorname{Div} \mathbf{P} + \rho_0 \mathbf{b}, \end{aligned} \quad (3.2.6)$$

as the balance of mass holds. Here,  $\mathbf{P}$  denotes the first Piola–Kirchhoff stress tensor relating spatial forces to material area elements. It is related to the well-known Cauchy stress tensor  $\boldsymbol{\sigma}$  via a push forward to the spatial configuration

$$\mathbf{P} = J \boldsymbol{\sigma} \cdot \mathbf{F}^{-t}. \quad (3.2.7)$$

### 3. Continuum mechanics

In continuum mechanics, relating spatial quantities via the Jacobian  $J$  and tensorial quantities via  $J$  and subsequent multiplication of  $\mathbf{F}^t$  is referred to as Piola transform.

The spatial balance of angular momentum is only given for the sake of completeness at this point as for a Boltzmann continuum it merely implies symmetry conditions for the stress tensors, rather than yielding further differential equations, cf. [55]. It can be reduced to

$$\mathbf{P} \cdot \mathbf{F}^t = [\mathbf{P} \cdot \mathbf{F}^t]^t \quad (3.2.8)$$

revealing that the first Piola–Kirchhoff stress tensor  $\mathbf{P}$  is not symmetric, but, its counterpart, the Cauchy stress tensor  $\boldsymbol{\sigma}$ , is symmetric:

$$\boldsymbol{\sigma}^t = \boldsymbol{\sigma}. \quad (3.2.9)$$

The first law of thermodynamics states the conservation of total energy, in terms of balance equations this is also referred to as the balance of energy. The balance of energy does not provide any information about the direction of a thermodynamic process. It reduces to the balance of internal energy in its conservative form

$$\rho_0 D_t \epsilon = -\text{Div} \mathbf{Q} + \mathbf{S} : \frac{1}{2} \dot{\mathbf{C}} + \rho_0 r, \quad (3.2.10)$$

see e.g. [55, 66]. The mass specific internal energy density is denoted by  $\epsilon$ , whereas  $\mathbf{Q}$  is the material heat flux vector and  $r$  is the external heat supply per unit mass. The symmetric second Piola–Kirchhoff stress tensor  $\mathbf{S}$  is related to the first Piola–Kirchhoff stress tensor  $\mathbf{P}$  via

$$\mathbf{S} = \mathbf{F}^{-1} \cdot \mathbf{P}. \quad (3.2.11)$$

Containing mechanical and thermal quantities, the balance of internal energy represents the interconvertibility of heat and mechanical work. The internal energy is not conserved as it possesses a production term, the internal mechanical energy  $\mathbf{S} : \frac{1}{2} \dot{\mathbf{C}}$ , which it exchanges with the kinetic energy.

The second law of thermodynamics states that the internal entropy production per unit mass  $\xi$  is non-negative implying the direction of a thermodynamical process, meaning that heat can only flow from a warmer to a cooler region and not vice versa.  $\xi$  equals the change of the entropy density  $\eta$  plus the divergence of the entropy flux  $\mathbf{h}$  minus the external entropy supply  $s$ . This can be represented as the balance of entropy

$$\rho_0 D_t \eta = -\text{Div} \mathbf{H} + \rho_0 [s + \xi]. \quad (3.2.12)$$

The spatial counterparts of the material heat and entropy flux vectors, i.e. the spatial heat flux  $\mathbf{q}$  and the spatial entropy flux  $\mathbf{h}$ , are derived via the Piola transform  $\mathbf{Q} = J \mathbf{q} \cdot \mathbf{F}^{-t}$  and  $\mathbf{H} = J \mathbf{h} \cdot \mathbf{F}^{-t}$ .



### 3.2.2. Material motion problem

The counterpart of the spatial balance of mass in the material motion problem reads

$$d_t \rho_t = 0. \quad (3.2.13)$$

The material motion problem's balance of linear momentum is often called balance of pseudomomentum [102] and establishes the so-called material (or configurational) forces. It is defined as a projection of the spatial balance of linear momentum onto the material manifold, i.e. by a premultiplication of  $-j\mathbf{F}^t$ :

$$\rho_t D_t (\mathbf{C} \cdot \mathbf{V}) = \operatorname{div} \mathbf{p} + \rho_t \mathbf{B}. \quad (3.2.14)$$

Thus, the balance of pseudomomentum is postulated analogously to (3.2.6). For information on the relation between the material two-point stress measure of first Piola–Kirchhoff type  $\mathbf{p}$  and the two-point stress tensor  $\mathbf{P}$  as well as for a more detailed definition of the material volume force  $\rho_t \mathbf{B}$  the reader is referred to the remark at the end of Section 4.2.3.

The scalar-valued material balance of internal energy with respect to a spatial reference is obtained via the Piola transform, i.e. by multiplying Eq. (3.2.10) with the material Jacobian  $j$

$$\rho_t D_t \epsilon = -j \operatorname{Div} \mathbf{Q} + j \mathbf{S} : \frac{1}{2} \dot{\mathbf{C}} + \rho_t r. \quad (3.2.15)$$

Analogously, the material balance of entropy yields

$$\rho_t D_t \eta = -j \operatorname{Div} \mathbf{H} + \rho_t [s + \xi]. \quad (3.2.16)$$

## 3.3. Material modeling

The fundamental ideas of material modeling are introduced in the following. The kinematics (cf. Section 3.1) and the balance equations (cf. Section 3.2) form a general basis for characterizing the thermomechanical behavior of a continuum body. So far, no distinction between different materials is made and therefore, they are complemented by the so-called constitutive equations in order to describe the thermodynamic behavior of the material of interest. Mathematically, they are necessitated by the fact that the balance equations are under-determined as there are more unknowns than equations.

Furthermore, the constitutive equations, which are regarded as the mathematical description of the body's physical behavior, have to fulfill principles of the constitutive theory of materials in order not to contradict general physical observations. In the following, these principles are summarized, for further details see e.g. [35, 55, 66, 99, 164]:

- Equipresence: Every constitutive equation is a priori a function of all independent variables.

### 3. Continuum mechanics

- Determinism: The present state at a particle is determined by the present and the past states (and not by any state in the future).
- Local action: The present state at a particle is determined by a small neighborhood of that particle. Distant particles do not have any influence.
- Material frame-indifference (also: material objectivity): The response of a material is independent of the observer. This means that a constitutive function must be invariant with respect to frame changes.
- Material symmetry (also: material invariance): Constitutive equations are consistent with the forms of isotropy that can exist in materials. If a material's configuration  $\mathcal{B}_1$  cannot be distinguished from another configuration  $\mathcal{B}_2$  (e.g. at a later moment) due to symmetry properties, the response of the material with respect to the first configuration must be the same as with respect to the second configuration.
- Admissibility: The constitutive equations do not contradict the balance equations and the second law of thermodynamics.

In thermo-hyperelasticity, the material modeling (i.e. the choice of the constitutive equations) is based on a potential. The existence of a scalar-valued, positive, polyconvex, objective, material specific and path independent free energy density  $\psi$  is postulated [66]. Moreover, thermo-hyperelasticity has a conservative structure implying that  $\psi$  plays the role of a potential for some of the constitutive equations, e.g. for the stress.  $\psi$  describes the amount of energy being required to achieve a particular deformation. Per convention, the free energy density  $\psi$  vanishes in the stress-free reference configuration (where  $\mathbf{F} = \mathbf{I}$ ) at thermodynamic equilibrium for elastic materials, i.e. it attains its global minimum at this stage. Additionally,  $\psi$  has to satisfy that an infinite amount of strain energy is needed in case of infinite expansion or compression, i.e.

$$\begin{aligned} \psi &\rightarrow \infty & \text{as } J &\rightarrow \infty, \\ \psi &\rightarrow \infty & \text{as } J &\rightarrow 0. \end{aligned} \tag{3.3.1}$$

## 4. Thermodynamic principles

Engineering simulations of thermodynamic processes aim at determining unknown quantities such as velocity, stress and temperature, for example. These simulations are based on the balance equations complemented by the constitutive equations and possibly others like evolution or constraining equations, for example. Constitutive equations have to be established obeying the rules listed in Section 3.3. In rational thermodynamics the second law imposes restrictions on constitutive equations and not on a body's processes, cf. [35, 116, 164]. Although thermodynamic processes have to satisfy all balance equations, the entropy balance (3.2.12) plays a special role as its exploitation reveals the restrictions on the material's constitutive relations. In the following, this is done with respect to the spatial balance laws. Whereas there exists a unified opinion about the balance laws, this is not the case for the second law of thermodynamics. Exploitations of the entropy inequality are based on distinctive mathematical procedures with the help of which conditions for a given class of constitutive material behaviors are derived in order to be compatible with the entropy inequality. Probably the best-known principle is that of Clausius and Duhem in the framework established by Coleman and Noll [35], which unfortunately can be inappropriate for complex theories such as gradient theories or mixtures, for example. Green and Naghdi [51] establish a theory based on, among others, the gradient of the history variable  $\alpha$  and take over the Clausius–Duhem approach nevertheless. The possible inappropriateness of the Clausius–Duhem approach in the case of mixtures, polar continua, structured continua and coupled field gradient theories is mentioned in the works of e.g. Hutter and Wang [69], Kirchner [87] and Svendsen [157] who suggest exploiting the entropy principle according to Müller and Liu [97, 112] as it is the most general approach.

Thus, in the following the thermodynamic analysis is done applying the entropy principle of Müller and Liu. Usually, it is applied to balance laws formulated with respect to the spatial reference (cf. [87, 157, 158]). However, as this thesis considers solid bodies, it is more reasonable to exploit Müller–Liu's entropy principle with respect to the material description.

### 4.1. Entropy principle of Müller and Liu

Müller [112] suggests to regard the balances of mass, linear momentum, angular momentum and internal energy as side conditions to the entropy balance. He multiplies the four balance equations with Lagrange multipliers, subtracts them from the entropy balance and takes the non-negativity of the entropy density  $\eta$  into account. His ideas are improved by Liu [97] who embeds Müller's ideas in a mathematical framework by reformulating the so-called Farka's Lemma (cf. Appendix A.8 and [62]).

#### 4. Thermodynamic principles

Müller's theory postulates the existence of a scalar, additive and objective quantity called entropy density  $\eta$  and introduces the following quantities as additional constitutive quantities: the free energy density  $\psi$ , the second Piola–Kirchhoff stress  $\mathbf{S}$ , the material entropy flux  $\mathbf{H}$ , the material heat flux  $\mathbf{Q}$  and the internal entropy production  $\xi$ . As opposed to the Clausius–Duhem approach, a relationship is neither stated between the entropy flux vector  $\mathbf{H}$  and the heat flux vector  $\mathbf{Q}$  nor between the entropy supply  $s$  and the heat supply  $r$ . For a long time, the a priori assumption  $\theta\mathbf{H} = \mathbf{Q}$  (made by Clausius and Duhem),  $\theta$  denoting the absolute temperature, was used for all thermodynamic theories. In the course of time, it became apparent that this relationship is simply wrong for some materials as shown in e.g. [87, 113]. Moreover, if theories including internal variables are considered as in [87], the use of  $\theta\mathbf{H} = \mathbf{Q}$  must be verified as it might be inappropriate. Green and Naghdi are aware of this fact [51], but apply the assumption nevertheless without further calculations.

In the Müller–Liu approach, the absolute temperature and the relation between the entropy flux and the heat flux vector are derived statements for isotropic solids - as opposed to the postulations of Coleman and Noll.

The constitutive quantities are functions of a state space  $\mathbb{S}$ , consisting of the independent variables, and are assumed to be smooth and at least once differentiable in  $\mathcal{B}_0$  with respect to all elements of  $\mathbb{S}$ . Following the way of Green and Naghdi [51], three state spaces  $\mathbb{S}_{i=I, II, III}$  are specified

$$\begin{aligned}\mathbb{S}_I &:= \{\dot{\alpha}, \nabla_{\mathbf{X}}\dot{\alpha}, \mathbf{C}\}, \\ \mathbb{S}_{II} &:= \{\alpha, \dot{\alpha}, \nabla_{\mathbf{X}}\alpha, \mathbf{C}\}, \\ \mathbb{S}_{III} &:= \{\alpha, \dot{\alpha}, \nabla_{\mathbf{X}}\alpha, \nabla_{\mathbf{X}}\dot{\alpha}, \mathbf{C}\}.\end{aligned}$$

Note that compared to Green and Naghdi the material (instead of the spatial) temperature gradient is taken. This choice makes Green and Naghdi's theory more consistent since now only material gradients appear in the state spaces. Furthermore,  $\mathbf{C}$  rather than  $\mathbf{F}$  is included into the state spaces because the principle of material frame indifference (cf. Section 3.3) has to be obeyed. The three different state spaces give rise to three varying theories, labeled type I, II and III.

Due to the principle of equipresence the independent variables a priori appear in each of the constitutive relationships, but these dependences are restricted by the entropy principle. All solutions of the balances of mass (3.2.5), linear momentum (3.2.6), angular momentum (3.2.9) and internal energy (3.2.10) have to satisfy the second law of thermodynamics. One possibility of ensuring this is suggested by Liu [97] who multiplies these balances with Lagrange multipliers and subtracts them from the entropy balance (3.2.12), see also Section (A.8). Thus, the exploitation of the thermodynamic problem is treated as an algebraic one<sup>1</sup>. Consequently,

---

<sup>1</sup>The aim of this thesis is to develop a theory modeling existing physical processes. Therefore it is reasonable to assume that the problem at hand, i.e. the balance equations combined with the constitutive equations, is well-posed. This implies that for finite time  $t \in [t_0, t_e]$  and for appropriate initial and boundary conditions there exist unique solutions. Inequality (4.1.1) is not an algebraic equation, but a finite system of partial differential equations (PDEs). Furthermore, it changes its class depending on the constitutive equations' nature and can be elliptic, parabolic or hyperbolic. PDEs do not always possess solutions in  $\mathbb{R}^n$ . Therefore, the turning of the thermodynamic problem into an algebraic one

one obtains

$$\begin{aligned}
 \rho_0 \dot{\xi} &= \rho_0 \dot{\eta} + \text{Div} \mathbf{H} - \rho_0 s \\
 &\quad - \boldsymbol{\lambda}^m \cdot [\rho_0 \dot{\mathbf{v}} - \text{Div} \mathbf{P} - \rho_0 \mathbf{b}] \\
 &\quad - \lambda^e \left[ \rho_0 \dot{\epsilon} + \text{Div} \mathbf{Q} - \mathbf{S} : \frac{1}{2} \dot{\mathbf{C}} - \rho_0 r \right] \\
 &\quad - \lambda^p \dot{\rho}_0 \\
 &\geq 0.
 \end{aligned} \tag{4.1.1}$$

Mathematically speaking, the four mentioned balance equations are considered as constraints<sup>2</sup> by using the vector-valued Lagrange multiplier  $\boldsymbol{\lambda}^m$  as well as the scalar-valued  $\lambda^e$  and  $\lambda^p$ . Lemma (A.8) states that at least one of the Lagrange multipliers does not vanish. In general, all multipliers depend on  $\mathbb{S}_i$  as well as on  $\mathbf{v}$ ,  $\mathbf{b}$ ,  $r$  and  $s$  [97]. Hence, the additionally introduced unknowns  $\boldsymbol{\lambda}^m$ ,  $\lambda^e$  and  $\lambda^p$  add an inconvenient complexity to the elaboration because they are functionals and not constants. Note that no relationship is stated between the entropy flux  $\mathbf{H}$  and the heat flux  $\mathbf{Q}$ .

Moreover, contrary to Coleman and Noll and thus to Green and Naghdi, no a priori known relationship between the entropy supply  $s$  and the heat supply  $r$  is assumed. Instead, a postulate from Müller [112], stating that the entropy supply  $s$  is caused by the momentum source  $\mathbf{b}$  and the heat supply  $r$ ,

$$s = \boldsymbol{\lambda}^m \cdot \mathbf{b} + \lambda^e r, \tag{4.1.2}$$

is assumed to hold in order to facilitate the evaluation of (4.1.1). Note that Eq. (4.1.2) is weaker than any other supposition commonly used in thermodynamic theories and is motivated by the assumption that the material's constitutive behavior does not depend on external sources.

### 4.1.1. Thermodynamical analysis of Green–Naghdi type I

The analysis starts with carrying out the differentiations in Eq. (4.1.1) with respect to the state space  $\mathbb{S}_I = \{\dot{\alpha}, \nabla_{\mathbf{X}} \dot{\alpha}, \mathbf{C}\}$  and applying the chain rule of differentiation. Then the terms are sorted into those depending on state space variables and those depending on higher gradients

---

and the existence of a solution has to be justified. For certain (but not for all) PDEs this can be done by using the Theorem of Cauchy–Kowalevski (also Cauchy–Kovalevskaya), cf. [68, 87]. From the physical point of view, one can argue that if such a solution does not exist, no thermodynamical process fulfills the second law and thus the entropy balance would be an empty statement.

<sup>2</sup>The balance of angular momentum needs not to be included due to the assumption of a Boltzmann continuum.

#### 4. Thermodynamic principles

which leads to

$$\begin{aligned}
\rho_0 \xi &= \rho_0 \left[ \frac{\partial \eta}{\partial \dot{\alpha}} \ddot{\alpha} + \frac{\partial \eta}{\partial \nabla_{\mathbf{X}} \dot{\alpha}} \cdot \nabla_{\mathbf{X}} \ddot{\alpha} + \frac{\partial \eta}{\partial \mathbf{C}} : \dot{\mathbf{C}} \right] \\
&+ \left[ \frac{\partial \mathbf{H}}{\partial \dot{\alpha}} \cdot \nabla_{\mathbf{X}} \dot{\alpha} + \frac{\partial \mathbf{H}}{\partial \nabla_{\mathbf{X}} \dot{\alpha}} : \nabla_{\mathbf{X}} (\nabla_{\mathbf{X}} \dot{\alpha}) + \frac{\partial \mathbf{H}}{\partial \mathbf{C}} : \nabla_{\mathbf{X}} \mathbf{C} \right] \\
&- \rho_0 \boldsymbol{\lambda}^m \cdot \dot{\mathbf{v}} + \boldsymbol{\lambda}^m \cdot \left[ \frac{\partial \mathbf{P}}{\partial \dot{\alpha}} \cdot \nabla_{\mathbf{X}} \dot{\alpha} + \frac{\partial \mathbf{P}}{\partial \nabla_{\mathbf{X}} \dot{\alpha}} : \nabla_{\mathbf{X}} (\nabla_{\mathbf{X}} \dot{\alpha}) + \frac{\partial \mathbf{P}}{\partial \mathbf{C}} : \nabla_{\mathbf{X}} \mathbf{C} \right] \\
&- \rho_0 \lambda^e \left[ \frac{\partial \epsilon}{\partial \dot{\alpha}} \ddot{\alpha} + \frac{\partial \epsilon}{\partial \nabla_{\mathbf{X}} \dot{\alpha}} \cdot \nabla_{\mathbf{X}} \ddot{\alpha} + \frac{\partial \epsilon}{\partial \mathbf{C}} : \dot{\mathbf{C}} \right] \\
&- \lambda^e \left[ \frac{\partial \mathbf{Q}}{\partial \dot{\alpha}} \cdot \nabla_{\mathbf{X}} \dot{\alpha} + \frac{\partial \mathbf{Q}}{\partial \nabla_{\mathbf{X}} \dot{\alpha}} : \nabla_{\mathbf{X}} (\nabla_{\mathbf{X}} \dot{\alpha}) + \frac{\partial \mathbf{Q}}{\partial \mathbf{C}} : \nabla_{\mathbf{X}} \mathbf{C} \right] \\
&+ \lambda^e \mathbf{S} : \frac{1}{2} \dot{\mathbf{C}} \\
&= \rho_0 \left[ \frac{\partial \eta}{\partial \dot{\alpha}} - \lambda^e \frac{\partial \epsilon}{\partial \dot{\alpha}} \right] \ddot{\alpha} + \left[ \frac{\partial \mathbf{H}}{\partial \dot{\alpha}} + \boldsymbol{\lambda}^m \cdot \frac{\partial \mathbf{P}}{\partial \dot{\alpha}} - \lambda^e \frac{\partial \mathbf{Q}}{\partial \dot{\alpha}} \right] \cdot \nabla_{\mathbf{X}} \dot{\alpha} \\
&+ \rho_0 \left[ \frac{\partial \eta}{\partial \nabla_{\mathbf{X}} \dot{\alpha}} - \lambda^e \frac{\partial \epsilon}{\partial \nabla_{\mathbf{X}} \dot{\alpha}} \right] \cdot \nabla_{\mathbf{X}} \ddot{\alpha} + \left[ \frac{\partial \mathbf{H}}{\partial \nabla_{\mathbf{X}} \dot{\alpha}} + \boldsymbol{\lambda}^m \cdot \frac{\partial \mathbf{P}}{\partial \nabla_{\mathbf{X}} \dot{\alpha}} - \lambda^e \frac{\partial \mathbf{Q}}{\partial \nabla_{\mathbf{X}} \dot{\alpha}} \right] : \nabla_{\mathbf{X}} (\nabla_{\mathbf{X}} \dot{\alpha}) \\
&+ \left[ \frac{\partial \mathbf{H}}{\partial \mathbf{C}} + \boldsymbol{\lambda}^m \cdot \frac{\partial \mathbf{P}}{\partial \mathbf{C}} - \lambda^e \frac{\partial \mathbf{Q}}{\partial \mathbf{C}} \right] : \nabla_{\mathbf{X}} \mathbf{C} + \left[ \rho_0 \frac{\partial \eta}{\partial \mathbf{C}} - \lambda^e \rho_0 \frac{\partial \epsilon}{\partial \mathbf{C}} + \lambda^e \frac{1}{2} \mathbf{S} \right] : \dot{\mathbf{C}} \\
&\geq 0. \tag{4.1.3}
\end{aligned}$$

Thereby  $\cdot$  denotes a triple contraction (cf. Appendix A.1). The term  $\lambda^e \rho_0$  vanishes due to the mass balance (3.2.5). This inequality holds for all thermodynamic processes and thus for all higher derivatives of the variables of the state space, i.e. for all values of  $\ddot{\alpha}$ ,  $\nabla_{\mathbf{X}} \ddot{\alpha}$ ,  $\nabla_{\mathbf{X}} (\nabla_{\mathbf{X}} \dot{\alpha})$ ,  $\nabla_{\mathbf{X}} \mathbf{C}$ ,  $\dot{\mathbf{C}}$  and  $\dot{\mathbf{v}}$ . Additionally, inequality (4.1.3) is linear in this list of higher derivatives and, consequently, their preceding coefficients have to vanish, as otherwise the inequality could be violated. This demand leads to the so-called Liu-equations (the terminology is adopted from Muschik and Ehrentraut [116]):

1.  $\boldsymbol{\lambda}^m = \mathbf{0}$ ,
2.  $\frac{\partial \eta}{\partial \dot{\alpha}} - \lambda^e \frac{\partial \epsilon}{\partial \dot{\alpha}} = 0$ ,
3.  $\frac{\partial \eta}{\partial \nabla_{\mathbf{X}} \dot{\alpha}} - \lambda^e \frac{\partial \epsilon}{\partial \nabla_{\mathbf{X}} \dot{\alpha}} = \mathbf{0}$ ,

$$\begin{aligned}
 4. \quad & \rho_0 \left[ \frac{\partial \eta}{\partial \mathbf{C}} - \lambda^e \frac{\partial \epsilon}{\partial \mathbf{C}} \right] + \lambda^e \frac{1}{2} \mathbf{S} = \mathbf{0}, \\
 5. \quad & \text{sym} \left( \frac{\partial \mathbf{H}}{\partial \nabla_{\mathbf{X}} \dot{\alpha}} - \lambda^e \frac{\partial \mathbf{Q}}{\partial \nabla_{\mathbf{X}} \dot{\alpha}} \right) = \mathbf{0}, \\
 6. \quad & \text{sym}_{(ij)} \left( \frac{\partial \mathbf{H}}{\partial \mathbf{C}} - \lambda^e \frac{\partial \mathbf{Q}}{\partial \mathbf{C}} \right) = \mathbf{0}. \tag{4.1.4}
 \end{aligned}$$

Here,  $\text{sym}_{(ij)}$  refers to symmetry with respect to the first two indices of the third order tensor  $\left( \frac{\partial \mathbf{H}}{\partial \mathbf{C}} - \lambda^e \frac{\partial \mathbf{Q}}{\partial \mathbf{C}} \right)_{ijk}$ . Hence, equation (4.1.3) reduces to the residual inequality

$$\rho_0 \xi = \left[ \frac{\partial \mathbf{H}}{\partial \dot{\alpha}} - \lambda^e \frac{\partial \mathbf{Q}}{\partial \dot{\alpha}} \right] \cdot \nabla_{\mathbf{X}} \dot{\alpha} \geq 0. \tag{4.1.5}$$

Due to the symmetry of the right Cauchy–Green tensor  $\mathbf{C}$ ,  $\nabla_{\mathbf{X}} \mathbf{C}$  is symmetric with respect to the last two indices. Therefore, Liu Eq. (4.1.4)<sub>6</sub> implies that the part of  $\partial \mathbf{H} / \partial \mathbf{C} - \lambda^e \partial \mathbf{Q} / \partial \mathbf{C}$  which is symmetric with respect to the first two indices vanishes. Due to the symmetry of  $\mathbf{C}$ , the skew-symmetric part with respect to those two indices equals zero, thus

$$\frac{\partial \mathbf{H}}{\partial \mathbf{C}} - \lambda^e \frac{\partial \mathbf{Q}}{\partial \mathbf{C}} = \mathbf{0}. \tag{4.1.6}$$

Further information in order to constrain the Lagrange multiplier  $\lambda^e$  and thus to state the relation between the entropy flux  $\mathbf{H}$  and the heat flux  $\mathbf{Q}$  is received by examining another principle of material modeling: the principle of material symmetry (cf. Section 3.3). This states that the constitutive equations have to be consistent with the forms of isotropy that exist in materials. Mathematically speaking, symmetry-group properties are explored.

As stated in Section 3.3, the constitutive equations have to obey material invariance properties. Mathematically speaking, material symmetries are described by the set of orthogonal transformations  $SO(3)$ .  $SO(3)$  is called the material's symmetry group and  $\mathbf{Q} \cdot \mathbf{Q}^t = \mathbf{Q}^t \cdot \mathbf{Q} = \mathbf{I}$  as well as  $\det \mathbf{Q} = 1$  holds for all  $\mathbf{Q} \in SO(3)$ . Thus, a vector-valued quantity  $\mathbf{j}$  has to fulfill  $\mathbf{j}(\mathbf{a}) = \mathbf{j}(\mathbf{Q} \cdot \mathbf{a})$  for all  $\mathbf{a} \in \mathbb{S}_I$  and for all  $\mathbf{Q} \in SO(3)$ .

Multiplying a vector-valued quantity  $\mathbf{j}$  by a rotation  $\mathbf{Q}(\tau) \in SO(3)$ , where  $\tau \in \mathbb{R}^{\geq 0}$  can be interpreted as an observer time, leads to

$$\begin{aligned}
 \mathbf{Q}(\tau) \cdot \mathbf{j}(\mathbb{S}_I) &= \mathbf{j}(\dot{\alpha}(\mathbf{X}, t), \mathbf{Q}(\tau) \cdot \nabla_{\mathbf{X}} \dot{\alpha}(\mathbf{X}, t), \mathbf{Q}(\tau) \cdot \mathbf{C}(\mathbf{X}, t) \cdot \mathbf{Q}^t(\tau)) \\
 &\quad \forall \mathbf{Q}(\tau) \in SO(3). \tag{4.1.7}
 \end{aligned}$$

Differentiating (4.1.7) with respect to  $\tau$  (denoted by  $'$ ) yields

$$\begin{aligned}
 \mathbf{Q}' \cdot \mathbf{j} &= \frac{\partial \mathbf{j}}{\partial (\mathbf{Q} \cdot \nabla_{\mathbf{X}} \dot{\alpha})} \cdot (\mathbf{Q}' \cdot \nabla_{\mathbf{X}} \dot{\alpha})' + \frac{\partial \mathbf{j}}{\partial (\mathbf{Q} \cdot \mathbf{C} \cdot \mathbf{Q}^t)} : (\mathbf{Q}' \cdot \mathbf{C} \cdot \mathbf{Q}^t)' \\
 &= \frac{\partial \mathbf{j}}{\partial (\mathbf{Q} \cdot \nabla_{\mathbf{X}} \dot{\alpha})} \cdot \mathbf{Q}' \cdot \nabla_{\mathbf{X}} \dot{\alpha} + \frac{\partial \mathbf{j}}{\partial (\mathbf{Q} \cdot \mathbf{C} \cdot \mathbf{Q}^t)} : [\mathbf{Q}' \cdot \mathbf{C} \cdot \mathbf{Q}^t] + \frac{\partial \mathbf{j}}{\partial (\mathbf{Q} \cdot \mathbf{C} \cdot \mathbf{Q}^t)} : [\mathbf{Q} \cdot \mathbf{C} \cdot \mathbf{Q}^t']. \tag{4.1.8}
 \end{aligned}$$

#### 4. Thermodynamic principles

Furthermore,  $\mathcal{Q}'$  can be replaced by  $\mathcal{Q}' = \mathcal{S} \cdot \mathcal{Q}$  due to the orthogonality of  $\mathcal{Q}$  where  $\mathcal{S}$  denotes the skew-symmetric matrix defined by  $\mathcal{S} = \mathcal{Q}' \cdot \mathcal{Q}^t$ . Thus, one obtains

$$\begin{aligned} \mathcal{S} \cdot \mathcal{Q} \cdot \mathbf{j} &= \frac{\partial \mathbf{j}}{\partial (\mathcal{Q} \cdot \nabla_{\mathbf{X}} \dot{\alpha})} \cdot \mathcal{S} \cdot \mathcal{Q} \cdot \nabla_{\mathbf{X}} \dot{\alpha} + \frac{\partial \mathbf{j}}{\partial (\mathcal{Q} \cdot \mathbf{C} \cdot \mathcal{Q}^t)} : [\mathcal{S} \cdot \mathcal{Q} \cdot \mathbf{C} \cdot \mathcal{Q}^t] \\ &+ \frac{\partial \mathbf{j}}{\partial (\mathcal{Q} \cdot \mathbf{C} \cdot \mathcal{Q}^t)} : [\mathcal{Q} \cdot \mathbf{C} \cdot \mathcal{Q}^t \cdot \mathcal{S}^t] \end{aligned} \quad (4.1.9)$$

which holds for all  $\mathcal{Q}$  and for all vector-valued quantities  $\mathbf{j}$ . Thus, if one chooses  $\mathcal{Q} = \mathbf{I}$  and successively  $\mathbf{j} = \mathbf{H}$  and  $\mathbf{j} = \mathbf{Q}$ , the consideration of material symmetry of the expression<sup>3</sup>  $\mathbf{H} - \lambda^e \mathbf{Q}$  leads to

$$\begin{aligned} \mathcal{S} \cdot \mathbf{H} - \lambda^e \mathcal{S} \cdot \mathbf{Q} &= \underbrace{\left[ \frac{\partial \mathbf{H}}{\partial \nabla_{\mathbf{X}} \dot{\alpha}} - \lambda^e \frac{\partial \mathbf{Q}}{\partial \nabla_{\mathbf{X}} \dot{\alpha}} \right]}_{=: P_{\nabla_{\mathbf{X}} \dot{\alpha}}} \cdot \mathcal{S} \cdot \nabla_{\mathbf{X}} \dot{\alpha} + \underbrace{\left[ \frac{\partial \mathbf{H}}{\partial \mathbf{C}} - \lambda^e \frac{\partial \mathbf{Q}}{\partial \mathbf{C}} \right]}_{=0 \text{ due to (4.1.6)}} : \mathcal{S} \cdot \mathbf{C} \\ &- \underbrace{\left[ \frac{\partial \mathbf{H}}{\partial \mathbf{C}} - \lambda^e \frac{\partial \mathbf{Q}}{\partial \mathbf{C}} \right]}_{=0 \text{ due to (4.1.6)}} : \mathbf{C} \cdot \mathcal{S} \\ &= P_{\nabla_{\mathbf{X}} \dot{\alpha}} \cdot \mathcal{S} \cdot \nabla_{\mathbf{X}} \dot{\alpha} \end{aligned} \quad (4.1.10)$$

due to the skew-symmetry of  $\mathcal{S}$ .

Moreover, the skew-symmetric tensor  $\mathcal{S}$  can be uniquely expressed in terms of an axial vector  $\boldsymbol{\omega}$ , see (A.4). Consequently, Eq. (4.1.10) can be rewritten in the following way

$$\boldsymbol{\omega} \times \mathbf{H} - \lambda^e \boldsymbol{\omega} \times \mathbf{Q} = P_{\nabla_{\mathbf{X}} \dot{\alpha}} \cdot [\boldsymbol{\omega} \times \nabla_{\mathbf{X}} \dot{\alpha}] \quad (4.1.11)$$

which holds for all  $\boldsymbol{\omega}$  as Eq. (4.1.10) holds for all  $\mathcal{S}$ . First choosing  $\boldsymbol{\omega} = \mathbf{e}_x$ , then  $\boldsymbol{\omega} = \mathbf{e}_y$  and  $\boldsymbol{\omega} = \mathbf{e}_z$  ( $\mathbf{e}_x, \mathbf{e}_y, \mathbf{e}_z$  being the Cartesian basis vectors) and finally comparing the coefficients of both sides in Eq. (4.1.11) leads to

$$\underbrace{\begin{pmatrix} 0 & P_{\nabla_{\mathbf{X}} \dot{\alpha} 13} & P_{\nabla_{\mathbf{X}} \dot{\alpha} 21} \\ P_{\nabla_{\mathbf{X}} \dot{\alpha} 32} & 0 & P_{\nabla_{\mathbf{X}} \dot{\alpha} 21} \\ P_{\nabla_{\mathbf{X}} \dot{\alpha} 32} & P_{\nabla_{\mathbf{X}} \dot{\alpha} 13} & 0 \end{pmatrix}}_{=: \mathbf{A}_1} \cdot \begin{pmatrix} \nabla_{\mathbf{X}} \dot{\alpha}_1 \\ \nabla_{\mathbf{X}} \dot{\alpha}_2 \\ \nabla_{\mathbf{X}} \dot{\alpha}_3 \end{pmatrix} = \begin{pmatrix} 0 \\ 0 \\ 0 \end{pmatrix}. \quad (4.1.12)$$

Thereby, the subscripts 13, 21 and 32 denote the indices of the corresponding tensor  $P_{\nabla_{\mathbf{X}} \dot{\alpha}}$ . Eq. (4.1.12) has to hold for every  $\nabla_{\mathbf{X}} \dot{\alpha}$ , also for those in which each component is non-zero. Thus,  $\mathbf{A}_1 = \mathbf{0}$  - a result which is not trivial because  $\mathbf{A}_1$  might depend on  $\nabla_{\mathbf{X}} \dot{\alpha}$  and needs to be proven as done in a similar case in [87, 158]. Turning back to Eq. (4.1.10) this implies

$$\mathcal{S} \cdot \mathbf{H} - \lambda^e \mathcal{S} \cdot \mathbf{Q} = \mathbf{0}. \quad (4.1.13)$$

<sup>3</sup>The expression  $\mathbf{H} - \lambda^e \mathbf{Q}$  is often referred to as the extra entropy flux, cf. e.g. [69, 87, 90, 157, 158].



As a consequence,  $\mathbf{H} - \lambda^e \mathbf{Q} = \mathbf{0}$  due to  $\mathbf{S} \neq \mathbf{0}$ . Thus, the entropy flux  $\mathbf{H}$  is proportional to the heat flux  $\mathbf{Q}$  - remember that this was not assumed in advance! In order to determine the factor of proportionality  $\lambda^e$ , the differential of the entropy flux vector is related to that of the heat flux vector which yields

$$\begin{aligned}
 d\mathbf{H} &= \frac{\partial \mathbf{H}}{\partial \dot{\alpha}} d\dot{\alpha} + \frac{\partial \mathbf{H}}{\partial \nabla_{\mathbf{X}} \dot{\alpha}} \cdot d\nabla_{\mathbf{X}} \dot{\alpha} + \frac{\partial \mathbf{H}}{\partial \mathbf{C}} : d\mathbf{C} \\
 &= \frac{\partial \mathbf{H}}{\partial \dot{\alpha}} d\dot{\alpha} + \lambda^e \frac{\partial \mathbf{Q}}{\partial \nabla_{\mathbf{X}} \dot{\alpha}} \cdot d\nabla_{\mathbf{X}} \dot{\alpha} + \lambda^e \frac{\partial \mathbf{Q}}{\partial \mathbf{C}} : d\mathbf{C} \\
 &= \lambda^e d\mathbf{Q} + \left[ \frac{\partial \mathbf{H}}{\partial \dot{\alpha}} - \lambda^e \frac{\partial \mathbf{Q}}{\partial \dot{\alpha}} \right] d\dot{\alpha} \\
 &=: \lambda^e d\mathbf{Q} + \mathbf{R},
 \end{aligned} \tag{4.1.14}$$

where the second transformation is due to Liu equations (4.1.4)<sub>5</sub>, (4.1.4)<sub>6</sub> and Eq. (4.1.13). The one-form  $\mathbf{R}$  from Eq. (4.1.14) (see Appendix A.2 for definition) can apparently also be written as

$$\begin{aligned}
 \mathbf{R} &= d\mathbf{H} - \lambda^e d\mathbf{Q} \\
 &= d\mathbf{H} - \lambda^e d\mathbf{Q} - [d\lambda^e] \mathbf{Q} + [d\lambda^e] \mathbf{Q} \\
 &= d[\mathbf{H} - \lambda^e \mathbf{Q}] + [d\lambda^e] \mathbf{Q} \\
 &= [d\lambda^e] \mathbf{Q}.
 \end{aligned} \tag{4.1.15}$$

Recall that

$$\mathbf{R} = \left[ \frac{\partial \mathbf{H}}{\partial \dot{\alpha}} - \lambda^e \frac{\partial \mathbf{Q}}{\partial \dot{\alpha}} \right] d\dot{\alpha}. \tag{4.1.16}$$

Comparing the coefficients of (4.1.15) and (4.1.16) leads to the fundamental result

$$\lambda^e = \bar{\lambda}^e(\dot{\alpha}), \tag{4.1.17}$$

stating that the Lagrange multiplier  $\lambda^e$  depends only on the empirical temperature  $T = \dot{\alpha}$ . Thus, the entropy flux vector  $\mathbf{H}$  and the heat flux vector  $\mathbf{Q}$  are related via the empirical temperature only. Moreover, the differential of the entropy is related to that of the internal energy which yields the so-called Gibbs relation

$$\begin{aligned}
 d\eta &= \frac{\partial \eta}{\partial \dot{\alpha}} d\dot{\alpha} + \frac{\partial \eta}{\partial \nabla_{\mathbf{X}} \dot{\alpha}} \cdot d\nabla_{\mathbf{X}} \dot{\alpha} + \frac{\partial \eta}{\partial \mathbf{C}} : d\mathbf{C} \\
 &= \lambda^e \frac{\partial \epsilon}{\partial \dot{\alpha}} d\dot{\alpha} + \lambda^e \frac{\partial \epsilon}{\partial \nabla_{\mathbf{X}} \dot{\alpha}} \cdot d\nabla_{\mathbf{X}} \dot{\alpha} + \lambda^e \frac{\partial \epsilon}{\partial \mathbf{C}} : d\mathbf{C} - \lambda^e \frac{1}{2\rho_0} \mathbf{S} \\
 &= \lambda^e d\epsilon - \lambda^e \frac{1}{2\rho_0} \mathbf{S},
 \end{aligned} \tag{4.1.18}$$

where the Liu equations (4.1.4)<sub>2</sub>, (4.1.4)<sub>3</sub> and (4.1.4)<sub>4</sub> are inserted.

Further restrictions on  $\lambda^e$  are obtained by applying a so-called ideal-wall argument which is introduced by Müller [112]. It is based on the following postulate: There exists a material

#### 4. Thermodynamic principles

singular surface (cf. Appendix A.2 for a definition), called ideal wall, between a thermoelastic continuum of Green–Naghdi type (denoted by +) and another continuum (that will later be specified as an ideal gas and is denoted by -) across which the empirical temperature is continuous, i.e. the jump vanishes (cf. Appendix A.2 for a definition).

The continuity of the heat flux vector on the ideal wall in direction  $\mathbf{N}_s$  is postulated (cf. also A.3), where  $\mathbf{N}_s$  is the unit normal vector on the material's wall pointing into the volume occupied by the Green–Naghdi continuum,

$$[[\mathbf{Q} \cdot \mathbf{N}_s]] = 0. \quad (4.1.19)$$

Here,  $[[\mathbf{Q} \cdot \mathbf{N}_s]] = 0$  denotes the vanishing of the jump of  $\mathbf{Q} \cdot \mathbf{N}_s$  (cf. Appendix A.2). Moreover, the jump of entropy flux in normal direction is postulated to vanish and  $\mathbf{H} = \lambda^e \mathbf{Q}$  and  $\mathbf{Q} \neq \mathbf{0}$  hold, one obtains

$$[[\mathbf{H} \cdot \mathbf{N}_s]] = [[\lambda^e \mathbf{Q} \cdot \mathbf{N}_s]] = [[\lambda^e]] \mathbf{Q} \cdot \mathbf{N}_s = 0 \quad (4.1.20)$$

at the ideal wall, implying

$$[[\lambda^e(\dot{\alpha})]] = 0 \quad \implies \quad \lambda^e(\dot{\alpha}) = \lambda^{e+}(\dot{\alpha}). \quad (4.1.21)$$

Müller [114] shows that if the Gibbs relation (4.1.18) holds as in this case, one can identify  $\lambda^e$  as the coldness function  $\Theta = 1/\theta$  (cf. e.g. [112]). Furthermore,  $\lambda^e$  is determined to be a universal function meaning that it is independent of material and its inverse value is the absolute temperature  $\theta$  [112]

$$\frac{1}{\lambda^e(\dot{\alpha})} = \theta \Leftrightarrow \lambda^e(\dot{\alpha}) = \frac{1}{\theta}. \quad (4.1.22)$$

Thus,

$$\theta \mathbf{H} = \mathbf{Q} \quad (4.1.23)$$

holds for type I, i.e. the heat flux vector  $\mathbf{Q}$  and the entropy flux vector  $\mathbf{H}$  are collinear. The absolute temperature  $\theta$  is the absolute measure of temperature (as opposed to the empirical temperature  $T$ , cf. Definition 3.1.6). It is an absolute scale since its zero point, absolute zero, is the lowest possible temperature, i.e.  $\theta \in \mathbb{R}^{\geq 0}$ .<sup>4</sup> Whereas the approach of Clausius and Duhem postulates the existence of the absolute temperature, this is a derived result in the theory of Müller and Liu. Furthermore, this implies that the classical relationship  $\theta s = r$  is also a derived statement by applying the Müller–Liu approach (as opposed to an a priori assumption in the Clausius–Duhem theory).

#### 4.1.2. Thermodynamical analysis of Green–Naghdi type II

Analogously to type I, the differentiations in (4.1.1) are carried out with respect to the corresponding state space, i.e.  $\mathbb{S}_H = \{\alpha, \dot{\alpha}, \nabla_{\mathbf{X}} \alpha, \mathbf{C}\}$ . Application of the chain rule yields

<sup>4</sup>In an ideal gas, statistical mechanics tells us that  $k_B \theta \propto v^2$ , where  $k_B$  is the Boltzmann constant. Since  $v^2 \geq 0$ , the absolute temperature has to be non-negative.

$$\begin{aligned}
 \rho_0 \xi &= \rho_0 \left[ \frac{\partial \eta}{\partial \alpha} - \lambda^e \frac{\partial \epsilon}{\partial \alpha} \right] \dot{\alpha} + \rho_0 \left[ \frac{\partial \eta}{\partial \dot{\alpha}} - \lambda^e \frac{\partial \epsilon}{\partial \dot{\alpha}} \right] \ddot{\alpha} + \left[ \frac{\partial \mathbf{H}}{\partial \alpha} + \boldsymbol{\lambda}^m \cdot \frac{\partial \mathbf{P}}{\partial \alpha} - \lambda^e \frac{\partial \mathbf{Q}}{\partial \alpha} \right] \cdot \nabla_{\mathbf{X}} \alpha \\
 &+ \left[ \frac{\partial \mathbf{H}}{\partial \dot{\alpha}} + \boldsymbol{\lambda}^m \cdot \frac{\partial \mathbf{P}}{\partial \dot{\alpha}} - \lambda^e \frac{\partial \mathbf{Q}}{\partial \dot{\alpha}} + \rho_0 \frac{\partial \eta}{\partial \nabla_{\mathbf{X}} \alpha} - \rho_0 \lambda^e \frac{\partial \epsilon}{\partial \nabla_{\mathbf{X}} \alpha} \right] \cdot \nabla_{\mathbf{X}} \dot{\alpha} \\
 &+ \left[ \frac{\partial \mathbf{H}}{\partial \nabla_{\mathbf{X}} \alpha} + \boldsymbol{\lambda}^m \cdot \frac{\partial \mathbf{P}}{\partial \nabla_{\mathbf{X}} \alpha} - \lambda^e \frac{\partial \mathbf{Q}}{\partial \nabla_{\mathbf{X}} \alpha} \right] : \nabla_{\mathbf{X}} (\nabla_{\mathbf{X}} \alpha) - \rho_0 \boldsymbol{\lambda}^m \cdot \dot{\mathbf{v}} \\
 &+ \left[ \frac{\partial \mathbf{H}}{\partial \mathbf{C}} + \boldsymbol{\lambda}^m \cdot \frac{\partial \mathbf{P}}{\partial \mathbf{C}} - \lambda^e \frac{\partial \mathbf{Q}}{\partial \mathbf{C}} \right] : \nabla_{\mathbf{X}} \mathbf{C} + \left[ \rho_0 \frac{\partial \eta}{\partial \mathbf{C}} - \lambda^e \rho_0 \frac{\partial \epsilon}{\partial \mathbf{C}} + \lambda^e \frac{1}{2} \mathbf{S} \right] : \dot{\mathbf{C}} \\
 &\geq 0.
 \end{aligned} \tag{4.1.24}$$

Again, the inequality has to hold for all thermodynamic processes and thus coefficients which precede the higher gradients, i.e. in case of type II:  $\ddot{\alpha}$ ,  $\nabla_{\mathbf{X}} \dot{\alpha}$ ,  $\nabla_{\mathbf{X}} (\nabla_{\mathbf{X}} \alpha)$ ,  $\nabla_{\mathbf{X}} \mathbf{C}$ ,  $\dot{\mathbf{C}}$  and  $\dot{\mathbf{v}}$ , have to vanish. The Liu-equations for type II read:

1.  $\boldsymbol{\lambda}^m = \mathbf{0}$ ,
2.  $\frac{\partial \eta}{\partial \dot{\alpha}} - \lambda^e \frac{\partial \epsilon}{\partial \dot{\alpha}} = 0$ ,
3.  $\rho_0 \left[ \frac{\partial \eta}{\partial \mathbf{C}} - \lambda^e \frac{\partial \epsilon}{\partial \mathbf{C}} \right] + \lambda^e \frac{1}{2} \mathbf{S} = \mathbf{0}$ ,
4.  $\text{sym} \left( \frac{\partial \mathbf{H}}{\partial \nabla_{\mathbf{X}} \alpha} - \lambda^e \frac{\partial \mathbf{Q}}{\partial \nabla_{\mathbf{X}} \alpha} \right) = \mathbf{0}$ ,
5.  $\text{sym}_{(ij)} \left( \frac{\partial \mathbf{H}}{\partial \mathbf{C}} - \lambda^e \frac{\partial \mathbf{Q}}{\partial \mathbf{C}} \right) = \mathbf{0}$ ,
6.  $\frac{\partial \mathbf{H}}{\partial \dot{\alpha}} - \lambda^e \frac{\partial \mathbf{Q}}{\partial \dot{\alpha}} + \rho_0 \frac{\partial \eta}{\partial \nabla_{\mathbf{X}} \alpha} - \rho_0 \lambda^e \frac{\partial \epsilon}{\partial \nabla_{\mathbf{X}} \alpha} = \mathbf{0}$ . (4.1.25)

Analogously to type I, symmetry-group properties are considered by multiplying a vector-valued quantity  $\mathbf{j}$  by a rotation  $\mathbf{Q}(\tau) \in SO(3)$ . Due to isotropy one obtains

$$\begin{aligned}
 \mathbf{Q}(\tau) \cdot \mathbf{j}(\mathbb{S}_{II}) &= \mathbf{j}(\alpha(\mathbf{X}, t), \dot{\alpha}(\mathbf{X}, t), \mathbf{Q}(\tau) \cdot \nabla_{\mathbf{X}} \alpha(\mathbf{X}, t), \mathbf{Q}(\tau) \cdot \mathbf{C}(\mathbf{X}, t) \cdot \mathbf{Q}^T(\tau)) \\
 &\quad \forall \mathbf{Q}(\tau) \in SO(3), \tag{4.1.26}
 \end{aligned}$$

and differentiating (4.1.26) with respect to  $\tau$  yields

$$\begin{aligned}
 \mathbf{S} \cdot \mathbf{Q} \cdot \mathbf{j} &= \frac{\partial \mathbf{j}}{\partial (\mathbf{Q} \cdot \nabla_{\mathbf{X}} \alpha)} \cdot \mathbf{S} \cdot \mathbf{Q} \cdot \nabla_{\mathbf{X}} \alpha + \frac{\partial \mathbf{j}}{\partial (\mathbf{Q} \cdot \mathbf{C} \cdot \mathbf{Q}^t)} : [\mathbf{S} \cdot \mathbf{Q} \cdot \mathbf{C} \cdot \mathbf{Q}^t] \\
 &\quad + \frac{\partial \mathbf{j}}{\partial (\mathbf{Q} \cdot \mathbf{C} \cdot \mathbf{Q}^t)} : [\mathbf{Q} \cdot \mathbf{C} \cdot \mathbf{Q}^t \cdot \mathbf{S}^t] \tag{4.1.27}
 \end{aligned}$$

#### 4. Thermodynamic principles

where  $\mathcal{S}$  again denotes the skew-symmetric matrix defined by  $\mathcal{S} = \mathcal{Q}' \cdot \mathcal{Q}^t$ . This is valid for all  $\mathcal{Q} \in SO(3)$  and for all vector-valued quantities  $j$ . Analogously to type I,  $\mathcal{Q} = I$  and successively  $j = H$  and  $j = Q$  are chosen, revealing that

$$\begin{aligned} \mathcal{S} \cdot H - \lambda^e \mathcal{S} \cdot Q &= \underbrace{\left[ \frac{\partial H}{\partial \nabla_X \alpha} - \lambda^e \frac{\partial Q}{\partial \nabla_X \alpha} \right]}_{=: P_{\nabla_X \alpha}} \cdot \mathcal{S} \cdot \nabla_X \alpha + \underbrace{\left[ \frac{\partial H}{\partial C} - \lambda^e \frac{\partial Q}{\partial C} \right]}_{=0 \text{ due to (4.1.25)}_5} : \mathcal{S} \cdot C \\ &\quad - \underbrace{\left[ \frac{\partial H}{\partial C} - \lambda^e \frac{\partial Q}{\partial C} \right]}_{=0 \text{ due to (4.1.25)}_5} : C \cdot \mathcal{S} \\ &= P_{\nabla_X \alpha} \cdot \mathcal{S} \cdot \nabla_X \alpha. \end{aligned} \quad (4.1.28)$$

Once more, Liu Eq. (4.1.25)<sub>5</sub> requires the symmetric part of  $\frac{\partial H}{\partial C} - \lambda^e \frac{\partial Q}{\partial C}$  to vanish and the symmetry of  $C$  forces the skew-symmetric part to also do so.

As mentioned above, the skew-symmetric tensor  $\mathcal{S}$  can be uniquely expressed in terms of an axial vector  $\omega$ , see (A.4). Consequently, we can rewrite Eq. (4.1.28) in the following way

$$\omega \times H - \lambda^e \omega \times Q = P_{\nabla_X \alpha} \cdot [\omega \times \nabla_X \alpha] \quad (4.1.29)$$

which holds for all  $\omega$ . By first choosing  $\omega = e_x$ , then  $\omega = e_y$  and  $\omega = e_z$  and comparing the coefficients of both sides in Eq. (4.1.29), one finally obtains

$$\underbrace{\begin{pmatrix} 0 & P_{\nabla_X \alpha 13} & P_{\nabla_X \alpha 21} \\ P_{\nabla_X \alpha 32} & 0 & P_{\nabla_X \alpha 21} \\ P_{\nabla_X \alpha 32} & P_{\nabla_X \alpha 13} & 0 \end{pmatrix}}_{=: A_2} \cdot \begin{pmatrix} \nabla_X \alpha_1 \\ \nabla_X \alpha_2 \\ \nabla_X \alpha_3 \end{pmatrix} = \begin{pmatrix} 0 \\ 0 \\ 0 \end{pmatrix}. \quad (4.1.30)$$

As Eq. (4.1.30) holds for every  $\nabla_X \alpha$ ,  $A_2 = 0$  is implied. Thus, Eq. (4.1.28) turns to

$$\mathcal{S} \cdot H - \lambda^e \mathcal{S} \cdot Q = 0. \quad (4.1.31)$$

As apparently  $\mathcal{S} \neq 0$ ,  $H - \lambda^e Q$  has to vanish. Thus the entropy flux  $H$  is proportional to the heat flux  $Q$  with the factor of proportionality  $\lambda^e$ . Following the line of argumentation of type I, the differential of the entropy flux  $H$  is equivalent to

$$\begin{aligned} dH &= \frac{\partial H}{\partial \alpha} d\alpha + \frac{\partial H}{\partial \dot{\alpha}} d\dot{\alpha} + \frac{\partial H}{\partial \nabla_X \alpha} \cdot d\nabla_X \alpha + \frac{\partial H}{\partial C} : dC \\ &= \frac{\partial H}{\partial \alpha} d\alpha + \frac{\partial H}{\partial \dot{\alpha}} d\dot{\alpha} + \lambda^e \frac{\partial Q}{\partial \nabla_X \alpha} \cdot d\nabla_X \alpha + \lambda^e \frac{\partial Q}{\partial C} : dC \\ &= \lambda^e dQ + \left[ \frac{\partial H}{\partial \alpha} - \lambda^e \frac{\partial Q}{\partial \alpha} \right] d\alpha + \left[ \frac{\partial H}{\partial \dot{\alpha}} - \lambda^e \frac{\partial Q}{\partial \dot{\alpha}} \right] d\dot{\alpha} \\ &=: \lambda^e dQ + R, \end{aligned} \quad (4.1.32)$$

inserting Liu equations (4.1.25)<sub>5</sub>, (4.1.25)<sub>6</sub> and Eq. (4.1.31). The one-form  $\mathbf{R}$  is also equivalent to

$$\begin{aligned}
 \mathbf{R} &= d\mathbf{H} - \lambda^e d\mathbf{Q} \\
 &= d\mathbf{H} - \lambda^e d\mathbf{Q} - [d\lambda^e] \mathbf{Q} + [d\lambda^e] \mathbf{Q} \\
 &= d[\mathbf{H} - \lambda^e \mathbf{Q}] + [d\lambda^e] \mathbf{Q} \\
 &= [d\lambda^e] \mathbf{Q}.
 \end{aligned} \tag{4.1.33}$$

Thus, in case of type II one obtains

$$\lambda^e = \bar{\lambda}^e(\alpha, \dot{\alpha}) \tag{4.1.34}$$

which follows from the comparison of the coefficients of Eq. (4.1.32) and Eq. (4.1.33). At this point, the Lagrange multiplier  $\lambda^e$  does not only depend on the empirical temperature  $T = \dot{\alpha}$  but also on the thermal displacement  $\alpha$ .

The generalized Gibbs relation of type II read

$$\begin{aligned}
 d\eta &= \frac{\partial \eta}{\partial \alpha} d\alpha + \frac{\partial \eta}{\partial \dot{\alpha}} d\dot{\alpha} + \frac{\partial \eta}{\partial \nabla_{\mathbf{X}} \alpha} \cdot d\nabla_{\mathbf{X}} \alpha + \frac{\partial \eta}{\partial \mathbf{C}} : d\mathbf{C} \\
 &= \frac{\partial \eta}{\partial \alpha} d\alpha + \lambda^e \frac{\partial \epsilon}{\partial \dot{\alpha}} d\dot{\alpha} + \frac{\partial \eta}{\partial \nabla_{\mathbf{X}} \alpha} \cdot d\nabla_{\mathbf{X}} \alpha + \lambda^e \frac{\partial \epsilon}{\partial \mathbf{C}} : d\mathbf{C} - \lambda^e \frac{1}{2\rho_0} \mathbf{S} \\
 &= \lambda^e d\epsilon + \left[ \frac{\partial \eta}{\partial \alpha} - \lambda^e \frac{\partial \epsilon}{\partial \alpha} \right] d\alpha + \left[ \frac{\partial \eta}{\partial \nabla_{\mathbf{X}} \alpha} - \lambda^e \frac{\partial \epsilon}{\partial \nabla_{\mathbf{X}} \alpha} \right] \cdot d\nabla_{\mathbf{X}} \alpha - \lambda^e \frac{1}{2\rho_0} \mathbf{S},
 \end{aligned} \tag{4.1.35}$$

where Liu equations (4.1.25)<sub>2</sub> and (4.1.25)<sub>3</sub> are inserted<sup>5</sup>.

Analogously to type I, the ideal-wall argument leads to

$$[[\lambda^e(\alpha, \dot{\alpha})]] = 0 \implies \lambda^{e-}(\alpha, \dot{\alpha}) = \lambda^{e+}(\alpha, \dot{\alpha}). \tag{4.1.36}$$

Once more, the material on the positive side is a Green–Naghdi continuum while it is an ideal gas on the negative side. This implies

$$\lambda^{e+}(\alpha, T = \dot{\alpha}) = \lambda^{e-}(\alpha, T) = \lambda^{e-}(T) \implies \lambda^{e+} = \lambda^{e+}(T), \tag{4.1.37}$$

because  $\lambda^e = \lambda^e(T)$  for an ideal gas [112]. Hence, also the proportionality factor of type II  $\lambda^e$  is only a function of the empirical temperature  $T$  and the generalized Gibbs relation (4.1.35) holds. As a consequence,  $\lambda^e$  can be identified as the coldness function [112] which is independent of the material

$$\lambda^e(\dot{\alpha}) = \frac{1}{\theta}. \tag{4.1.38}$$

Consequently,  $\theta \mathbf{H} = \mathbf{Q}$  and  $\theta s = r$  also hold for a Green–Naghdi continuum of type II and  $\theta$  is the absolute temperature [112].

<sup>5</sup>  $d\eta$  is an exact differential implying that the entropy density  $\eta$  is path-independent - a necessary condition in order not to contradict the basic assumptions of thermodynamics. The fact that  $d\mathbf{H}$  and  $d\eta$  are exact differentials is not a priori clear (as it is not clear whether  $d\alpha$  and  $d\nabla_{\mathbf{X}} \alpha$  are exact differentials) and has to be proven which can be done by straightforward, but long winded calculation, cf. e.g. [87].

### 4.1.3. Thermodynamical analysis of Green–Naghdi type III

Parts of this section are published by Bargmann and Steinmann in [9].

The same strategy as in the previous cases is applied to type III, meaning that the differentiations in (4.1.1) are carried out with respect to the state space  $\mathbb{S}_{III} = \{\alpha, \dot{\alpha}, \nabla_{\mathbf{X}}\alpha, \nabla_{\mathbf{X}}\dot{\alpha}, \mathbf{C}\}$

$$\begin{aligned}
 \rho_0 \xi = & \rho_0 \left[ \frac{\partial \eta}{\partial \alpha} - \lambda^e \frac{\partial \epsilon}{\partial \alpha} \right] \dot{\alpha} + \rho_0 \left[ \frac{\partial \eta}{\partial \dot{\alpha}} - \lambda^e \frac{\partial \epsilon}{\partial \dot{\alpha}} \right] \ddot{\alpha} + \left[ \frac{\partial \mathbf{H}}{\partial \alpha} + \boldsymbol{\lambda}^m \cdot \frac{\partial \mathbf{P}}{\partial \alpha} - \lambda^e \frac{\partial \mathbf{Q}}{\partial \alpha} \right] \cdot \nabla_{\mathbf{X}} \alpha \\
 & + \left[ \frac{\partial \mathbf{H}}{\partial \dot{\alpha}} + \boldsymbol{\lambda}^m \cdot \frac{\partial \mathbf{P}}{\partial \dot{\alpha}} - \lambda^e \frac{\partial \mathbf{Q}}{\partial \dot{\alpha}} + \rho_0 \frac{\partial \eta}{\partial \nabla_{\mathbf{X}} \alpha} - \rho_0 \lambda^e \frac{\partial \epsilon}{\partial \nabla_{\mathbf{X}} \alpha} \right] \cdot \nabla_{\mathbf{X}} \dot{\alpha} \\
 & + \rho_0 \left[ \frac{\partial \eta}{\partial \nabla_{\mathbf{X}} \dot{\alpha}} - \lambda^e \frac{\partial \epsilon}{\partial \nabla_{\mathbf{X}} \dot{\alpha}} \right] \cdot \nabla_{\mathbf{X}} \ddot{\alpha} + \left[ \frac{\partial \mathbf{H}}{\partial \nabla_{\mathbf{X}} \alpha} + \boldsymbol{\lambda}^m \cdot \frac{\partial \mathbf{P}}{\partial \nabla_{\mathbf{X}} \alpha} - \lambda^e \frac{\partial \mathbf{Q}}{\partial \nabla_{\mathbf{X}} \alpha} \right] : \nabla_{\mathbf{X}} (\nabla_{\mathbf{X}} \alpha) \\
 & + \left[ \frac{\partial \mathbf{H}}{\partial \nabla_{\mathbf{X}} \dot{\alpha}} + \boldsymbol{\lambda}^m \cdot \frac{\partial \mathbf{P}}{\partial \nabla_{\mathbf{X}} \dot{\alpha}} - \lambda^e \frac{\partial \mathbf{Q}}{\partial \nabla_{\mathbf{X}} \dot{\alpha}} \right] : \nabla_{\mathbf{X}} (\nabla_{\mathbf{X}} \dot{\alpha}) \\
 & + \left[ \frac{\partial \mathbf{H}}{\partial \mathbf{C}} + \boldsymbol{\lambda}^m \cdot \frac{\partial \mathbf{P}}{\partial \mathbf{C}} - \lambda^e \frac{\partial \mathbf{Q}}{\partial \mathbf{C}} \right] : \nabla_{\mathbf{X}} \mathbf{C} + \left[ \rho_0 \frac{\partial \eta}{\partial \mathbf{C}} - \lambda^e \rho_0 \frac{\partial \epsilon}{\partial \mathbf{C}} + \lambda^e \frac{1}{2} \mathbf{S} \right] : \dot{\mathbf{C}} \\
 & - \rho_0 \boldsymbol{\lambda}^m \cdot \dot{\mathbf{v}} \\
 \geq & 0.
 \end{aligned} \tag{4.1.39}$$

Inequality (4.1.39) has to hold for all values of  $\ddot{\alpha}$ ,  $\nabla_{\mathbf{X}} \ddot{\alpha}$ ,  $\nabla_{\mathbf{X}} (\nabla_{\mathbf{X}} \alpha)$ ,  $\nabla_{\mathbf{X}} (\nabla_{\mathbf{X}} \dot{\alpha})$ ,  $\nabla_{\mathbf{X}} \mathbf{C}$ ,  $\dot{\mathbf{C}}$  and  $\dot{\mathbf{v}}$ , giving rise to the Liu-equations for type III:

1.  $\boldsymbol{\lambda}^m = \mathbf{0}$ ,
2.  $\frac{\partial \eta}{\partial \dot{\alpha}} - \lambda^e \frac{\partial \epsilon}{\partial \dot{\alpha}} = 0$ ,
3.  $\frac{\partial \eta}{\partial \nabla_{\mathbf{X}} \dot{\alpha}} - \lambda^e \frac{\partial \epsilon}{\partial \nabla_{\mathbf{X}} \dot{\alpha}} = \mathbf{0}$ ,
4.  $\rho_0 \left[ \frac{\partial \eta}{\partial \mathbf{C}} - \lambda^e \frac{\partial \epsilon}{\partial \mathbf{C}} \right] + \lambda^e \frac{1}{2} \mathbf{S} = \mathbf{0}$ ,
5.  $\text{sym} \left( \frac{\partial \mathbf{H}}{\partial \nabla_{\mathbf{X}} \alpha} - \lambda^e \frac{\partial \mathbf{Q}}{\partial \nabla_{\mathbf{X}} \alpha} \right) = \mathbf{0}$ ,
6.  $\text{sym} \left( \frac{\partial \mathbf{H}}{\partial \nabla_{\mathbf{X}} \dot{\alpha}} - \lambda^e \frac{\partial \mathbf{Q}}{\partial \nabla_{\mathbf{X}} \dot{\alpha}} \right) = \mathbf{0}$ ,
7.  $\text{sym}_{(ij)} \left( \frac{\partial \mathbf{H}}{\partial \mathbf{C}} - \lambda^e \frac{\partial \mathbf{Q}}{\partial \mathbf{C}} \right) = \mathbf{0}$ .

(4.1.40)

Subsequently, symmetry-group properties are exploited. Following the line of argumentation as in the previous cases I and II, one obtains

$$\mathbf{S} \cdot \mathbf{H} - \lambda^e \mathbf{S} \cdot \mathbf{Q} = P_{\nabla_{\mathbf{X}} \alpha} \cdot \mathbf{S} \cdot \nabla_{\mathbf{X}} \alpha + P_{\nabla_{\mathbf{X}} \dot{\alpha}} \cdot \mathbf{S} \cdot \nabla_{\mathbf{X}} \dot{\alpha}. \tag{4.1.41}$$

Expressing the skew-symmetric tensor  $\mathcal{S}$  in terms of its axial vector  $\boldsymbol{\omega}$  leads to

$$\boldsymbol{\omega} \times \mathbf{H} - \lambda^e \boldsymbol{\omega} \times \mathbf{Q} = \mathbf{P}_{\nabla_{\mathbf{X}}\alpha} \cdot [\boldsymbol{\omega} \times \nabla_{\mathbf{X}}\alpha] + \mathbf{P}_{\nabla_{\mathbf{X}}\dot{\alpha}} \cdot [\boldsymbol{\omega} \times \nabla_{\mathbf{X}}\dot{\alpha}] \quad \forall \boldsymbol{\omega} \quad (4.1.42)$$

implying

$$\begin{aligned} & \begin{pmatrix} 0 & P_{\nabla_{\mathbf{X}}\alpha_{13}} & P_{\nabla_{\mathbf{X}}\alpha_{21}} \\ P_{\nabla_{\mathbf{X}}\alpha_{32}} & 0 & P_{\nabla_{\mathbf{X}}\alpha_{21}} \\ P_{\nabla_{\mathbf{X}}\alpha_{32}} & P_{\nabla_{\mathbf{X}}\alpha_{13}} & 0 \end{pmatrix} \cdot \begin{pmatrix} \nabla_{\mathbf{X}}\alpha_1 \\ \nabla_{\mathbf{X}}\alpha_2 \\ \nabla_{\mathbf{X}}\alpha_3 \end{pmatrix} + \begin{pmatrix} 0 & P_{\nabla_{\mathbf{X}}\dot{\alpha}_{13}} & P_{\nabla_{\mathbf{X}}\dot{\alpha}_{21}} \\ P_{\nabla_{\mathbf{X}}\dot{\alpha}_{32}} & 0 & P_{\nabla_{\mathbf{X}}\dot{\alpha}_{21}} \\ P_{\nabla_{\mathbf{X}}\dot{\alpha}_{32}} & P_{\nabla_{\mathbf{X}}\dot{\alpha}_{13}} & 0 \end{pmatrix} \cdot \begin{pmatrix} \nabla_{\mathbf{X}}\dot{\alpha}_1 \\ \nabla_{\mathbf{X}}\dot{\alpha}_2 \\ \nabla_{\mathbf{X}}\dot{\alpha}_3 \end{pmatrix} \\ &= \mathbf{A}_2 \cdot \begin{pmatrix} \nabla_{\mathbf{X}}\alpha_1 \\ \nabla_{\mathbf{X}}\alpha_2 \\ \nabla_{\mathbf{X}}\alpha_3 \end{pmatrix} + \mathbf{A}_1 \cdot \begin{pmatrix} \nabla_{\mathbf{X}}\dot{\alpha}_1 \\ \nabla_{\mathbf{X}}\dot{\alpha}_2 \\ \nabla_{\mathbf{X}}\dot{\alpha}_3 \end{pmatrix} = \begin{pmatrix} 0 \\ 0 \\ 0 \end{pmatrix}. \end{aligned} \quad (4.1.43)$$

Eq. (4.1.43) has to hold for every  $\nabla_{\mathbf{X}}\alpha$  and every  $\nabla_{\mathbf{X}}\dot{\alpha}$ . At this point, a result like for type I and II, i.e. that both matrices have to vanish, can unfortunately not be proven. Nevertheless, it is reasonable to assume that  $\mathbf{A}_2 = \mathbf{0}$  and  $\mathbf{A}_1 = \mathbf{0}$  because (i) the disappearance of one implies that of the other and (ii) if at least one of the matrices is independent of  $\nabla_{\mathbf{X}}\alpha$  and  $\nabla_{\mathbf{X}}\dot{\alpha}$  the other one vanishes, too (cf. [87]).<sup>6</sup> Thus Eq. (4.1.41) becomes

$$\mathcal{S} \cdot \mathbf{H} - \lambda^e \mathcal{S} \cdot \mathbf{Q} = \mathbf{0}. \quad (4.1.44)$$

Due to  $\mathcal{S} \neq \mathbf{0}$ ,  $\mathbf{H} - \lambda^e \mathbf{Q}$  has to vanish. Consequently, the entropy flux  $\mathbf{H}$  is proportional to the heat flux  $\mathbf{Q}$  for type III as well. The differential of the entropy flux  $\mathbf{H}$  is equivalent to

$$\begin{aligned} d\mathbf{H} &= \frac{\partial \mathbf{H}}{\partial \alpha} d\alpha + \frac{\partial \mathbf{H}}{\partial \dot{\alpha}} d\dot{\alpha} + \frac{\partial \mathbf{H}}{\partial \nabla_{\mathbf{X}}\alpha} \cdot d\nabla_{\mathbf{X}}\alpha + \frac{\partial \mathbf{H}}{\partial \nabla_{\mathbf{X}}\dot{\alpha}} \cdot d\nabla_{\mathbf{X}}\dot{\alpha} + \frac{\partial \mathbf{H}}{\partial \mathbf{C}} : d\mathbf{C} \\ &= \frac{\partial \mathbf{H}}{\partial \alpha} d\alpha + \frac{\partial \mathbf{H}}{\partial \dot{\alpha}} d\dot{\alpha} + \lambda^e \frac{\partial \mathbf{Q}}{\partial \nabla_{\mathbf{X}}\alpha} \cdot d\nabla_{\mathbf{X}}\alpha + \lambda^e \frac{\partial \mathbf{Q}}{\partial \nabla_{\mathbf{X}}\dot{\alpha}} \cdot d\nabla_{\mathbf{X}}\dot{\alpha} + \lambda^e \frac{\partial \mathbf{Q}}{\partial \mathbf{C}} : d\mathbf{C} \\ &= \lambda^e d\mathbf{Q} + \left[ \frac{\partial \mathbf{H}}{\partial \alpha} - \lambda^e \frac{\partial \mathbf{Q}}{\partial \alpha} \right] d\alpha + \left[ \frac{\partial \mathbf{H}}{\partial \dot{\alpha}} - \lambda^e \frac{\partial \mathbf{Q}}{\partial \dot{\alpha}} \right] d\dot{\alpha} \\ &=: \lambda^e d\mathbf{Q} + \mathbf{R}, \end{aligned} \quad (4.1.45)$$

where the second transformation is due to Liu equations (4.1.40)<sub>5</sub>, (4.1.40)<sub>6</sub>, (4.1.40)<sub>7</sub> and Eq. (4.1.44). The one-form  $\mathbf{R}$  can also be written as

$$\begin{aligned} \mathbf{R} &= d\mathbf{H} - \lambda^e d\mathbf{Q} \\ &= d\mathbf{H} - \lambda^e d\mathbf{Q} - [d\lambda^e] \mathbf{Q} + [d\lambda^e] \mathbf{Q} \\ &= d[\mathbf{H} - \lambda^e \mathbf{Q}] + [d\lambda^e] \mathbf{Q} \\ &= [d\lambda^e] \mathbf{Q}. \end{aligned} \quad (4.1.46)$$

<sup>6</sup>In case of the Green–Naghdi theory of type I, only  $\mathbf{A}_1$  appears in Eq. (4.1.43) for which it is easily proven in [158] that  $\mathbf{A}_1 = \mathbf{0}$  has to hold. Moreover, in case of type II, only  $\mathbf{A}_2$  exists in Eq. (4.1.43) for which it can be proven analogously to the proofs in [87, 158] that  $\mathbf{A}_2 = \mathbf{0}$  has to hold. A similar case like the one which arises for type III is dealt with in [87]. As mentioned above, it cannot be proven for the entire constitutive class that  $\mathbf{A}_1 = \mathbf{A}_2 = \mathbf{0}$ . Recalling that  $\mathbf{A}_1 = \mathbf{A}_2 = \mathbf{0}$  for some cases, this will from now on be assumed as also done in [87]. Physically, this assumption means that the dependence of the entropy flux and the heat flux on the thermal displacement and on the temperature gradient are related via the Lagrange multiplier  $\lambda^e$ . For all materials obeying the classical Fourier law of heat conduction, this is inevitably the case. For materials obeying a non-classical law of heat conduction, a final statement cannot be made. Thus, at the moment, the assumption  $\mathbf{A}_1 = \mathbf{A}_2 = \mathbf{0}$  is a restriction of the constitutive class of type III.

#### 4. Thermodynamic principles

Comparing the coefficients of (4.1.45) and (4.1.46) reveals

$$\lambda^e = \bar{\lambda}^e(\alpha, \dot{\alpha}). \quad (4.1.47)$$

Thus, the Lagrange multiplier  $\lambda^e$  can only depend on the thermal displacement  $\alpha$  and on the empirical temperature  $T = \dot{\alpha}$ .

The generalized Gibbs relations of type III are given by

$$\begin{aligned} d\eta &= \frac{\partial\eta}{\partial\alpha} d\alpha + \frac{\partial\eta}{\partial\dot{\alpha}} d\dot{\alpha} + \frac{\partial\eta}{\partial\nabla_{\mathbf{X}}\alpha} \cdot d\nabla_{\mathbf{X}}\alpha + \frac{\partial\eta}{\partial\nabla_{\mathbf{X}}\dot{\alpha}} \cdot d\nabla_{\mathbf{X}}\dot{\alpha} + \frac{\partial\eta}{\partial\mathbf{C}} d\mathbf{C} \\ &= \frac{\partial\eta}{\partial\alpha} d\alpha + \lambda^e \frac{\partial\epsilon}{\partial\dot{\alpha}} d\dot{\alpha} + \frac{\partial\eta}{\partial\nabla_{\mathbf{X}}\alpha} \cdot d\nabla_{\mathbf{X}}\alpha + \lambda^e \frac{\partial\epsilon}{\partial\nabla_{\mathbf{X}}\dot{\alpha}} \cdot d\nabla_{\mathbf{X}}\dot{\alpha} \\ &\quad + \lambda^e \frac{\partial\epsilon}{\partial\mathbf{C}} : d\mathbf{C} - \lambda^e \frac{1}{2\rho_0} \mathbf{S} \\ &= \lambda^e d\epsilon + \left[ \frac{\partial\eta}{\partial\alpha} - \lambda^e \frac{\partial\epsilon}{\partial\alpha} \right] d\alpha + \left[ \frac{\partial\eta}{\partial\nabla_{\mathbf{X}}\alpha} - \lambda^e \frac{\partial\epsilon}{\partial\nabla_{\mathbf{X}}\alpha} \right] \cdot d\nabla_{\mathbf{X}}\alpha - \lambda^e \frac{1}{2\rho_0} \mathbf{S}, \end{aligned} \quad (4.1.48)$$

applying Liu equations (4.1.40)<sub>2</sub>, (4.1.40)<sub>3</sub> and (4.1.40)<sub>4</sub><sup>7</sup>.

The application of the ideal-wall argument implies

$$\lambda^{e+}(\alpha, T = \dot{\alpha}) = \lambda^{e-}(\alpha, T) = \lambda^{e-}(T) \quad \implies \quad \lambda^{e+} = \lambda^{e-}(T), \quad (4.1.49)$$

where the Green–Naghdi continuum is denoted by + and the ideal gas by –. As the generalized Gibbs relation (4.1.48) holds,  $\lambda^e$  is the universal function called the coldness function [112]

$$\lambda^e = \frac{1}{\theta}. \quad (4.1.50)$$

Thus,  $\theta\mathbf{H} = \mathbf{Q}$  and  $\theta s = r$  hold and  $\theta$  is the absolute temperature for all three types.

## 4.2. Entropy exploitation according to Green and Naghdi

In the preceding Section 4.1 a relation between the heat flux vector  $\mathbf{Q}$  and the entropy flux vector  $\mathbf{H}$  is derived. Therefore, the set of constitutive quantities reduces to  $\psi$ ,  $\eta$ ,  $\mathbf{S}$ ,  $\mathbf{Q}$  and  $\xi$  and is extended by the absolute temperature  $\theta$ . The reduction  $\theta = \theta(\dot{\alpha})$ , compared to  $\theta = \theta(\mathbb{S}_i)$ , is not contradictory to the principle of equipresence as  $\theta$  arises from the Lagrange multiplier  $\lambda^e$  which, in the beginning, depends on  $\mathbb{S}_i$ .

In the following, further restrictions to the dependences of the constitutive equations are obtained by applying the entropy exploitation approach introduced by Green and Naghdi in [50].

The entropy balance (3.2.12) is multiplied by the absolute temperature  $\theta$ , leading to

$$\rho_0\theta\dot{\eta} = -\text{Div}(\theta\mathbf{H}) + \mathbf{H} \cdot \nabla_{\mathbf{X}}\theta + \rho_0\theta[s + \xi]. \quad (4.2.1)$$

<sup>7</sup>  $d\eta$  is an exact differential, cf. type II.



## 4.2. Entropy exploitation according to Green and Naghdi

Subsequently, the well-known definition of the internal energy  $\epsilon$ , i.e.  $\epsilon = \psi + \eta\theta$ , is inserted into Eq. (4.2.1), viz

$$\rho_0\dot{\epsilon} - \rho_0\dot{\psi} - \rho_0\eta\dot{\theta} + \text{Div}(\theta\mathbf{H}) - \mathbf{H} \cdot \nabla_{\mathbf{X}}\theta - \rho_0\theta [s + \xi] = 0. \quad (4.2.2)$$

In a next step, the balance of energy (3.2.10) is substituted into Eq. (4.2.2):

$$\mathbf{S} : \frac{1}{2}\dot{\mathbf{C}} - \rho_0\dot{\psi} - \rho_0\eta\dot{\theta} + \text{Div}(\theta\mathbf{H}) - \text{Div}\mathbf{Q} - \mathbf{H} \cdot \nabla_{\mathbf{X}}\theta + \rho_0r - \rho_0\theta [s + \xi] = 0. \quad (4.2.3)$$

Finally, relations (4.1.50) and  $\theta_s = r$  are exploited which yields

$$\mathbf{S} : \frac{1}{2}\dot{\mathbf{C}} - \rho_0\dot{\psi} - \rho_0\eta\dot{\theta} - \mathbf{H} \cdot \nabla_{\mathbf{X}}\theta - \rho_0\theta\xi = 0. \quad (4.2.4)$$

All thermodynamic processes have to fulfill Eq. (4.2.4) and, of course, the non-negativity of the entropy production  $\xi$  has to be taken into account.

**Remark:** The line of argumentation is changed compared to [50] for the following reason: In [50] Green and Naghdi state that “no assumption has been made which involves an entropy inequality”, a similar statement is repeated in [53]. This is not true. They regard Eq. (4.2.4) as written above and then argue that it has to hold for every choice of the appearing higher gradients. Subsequently, they conclude that, therefore, the coefficients which precede the higher gradients have to vanish. At this point, they hypothesize that the internal rate of entropy production  $\xi$  is non-negative: If no restriction is placed on  $\xi$ , one could identify a  $\xi$  for every combination of the higher gradients such that Eq. (4.2.4) would still be fulfilled - but  $\xi$  might be negative then. By assuming a non-negative entropy production  $\xi$ , Green and Naghdi apply the second law of thermodynamics, i.e. an entropy inequality.

A difference also arises concerning the existence of an absolute temperature  $\theta$ . Clausius and Duhem postulate the existence, whereas Müller and therefore also in this approach the existence is derived through the exploitation of the entropy principle. Green and Naghdi [51] choose a third way: They introduce, i.e. postulate the existence of  $\theta$  as a positive, monotonously increasing scalar-valued function of a hotness measure  $T^*$ .  $T^*$  itself depends on the empirical temperature  $T$  and variables characterizing material properties. At that stage,  $\theta$  cannot be identified as the absolute temperature since it is defined to only be positive and monotonously increasing but not to be unique. In the course of their considerations, the constitutive equations are chosen in such a way that  $\theta$  is an absolute temperature, but not necessarily for all materials.

### 4.2.1. Type I

The following dependences characterize the constitutive quantities for type I

$$\begin{aligned} \psi &= \psi(\dot{\alpha}, \nabla_{\mathbf{X}}\dot{\alpha}, \mathbf{C}), & \eta &= \eta(\dot{\alpha}, \nabla_{\mathbf{X}}\dot{\alpha}, \mathbf{C}), \\ \mathbf{Q} &= \mathbf{Q}(\dot{\alpha}, \nabla_{\mathbf{X}}\dot{\alpha}, \mathbf{C}), & \xi &= \xi(\dot{\alpha}, \nabla_{\mathbf{X}}\dot{\alpha}, \mathbf{C}), \\ \mathbf{S} &= \mathbf{S}(\dot{\alpha}, \nabla_{\mathbf{X}}\dot{\alpha}, \mathbf{C}), & \theta &= \theta(\dot{\alpha}). \end{aligned} \quad (4.2.5)$$

#### 4. Thermodynamic principles

Substituting the dependences (4.2.5) into Eq. (4.2.4) and applying the chain rule yields

$$\begin{aligned}
 0 &= \mathbf{S} : \frac{1}{2} \dot{\mathbf{C}} - \rho_0 \left[ \frac{\partial \psi}{\partial \dot{\alpha}} \ddot{\alpha} + \frac{\partial \psi}{\partial \nabla_{\mathbf{X}} \dot{\alpha}} \cdot \nabla_{\mathbf{X}} \ddot{\alpha} + \frac{\partial \psi}{\partial \mathbf{C}} : \dot{\mathbf{C}} \right] - \rho_0 \eta \left[ \frac{\partial \theta}{\partial \dot{\alpha}} \ddot{\alpha} \right] \\
 &\quad - \mathbf{H} \cdot \left[ \frac{\partial \theta}{\partial \dot{\alpha}} \nabla_{\mathbf{X}} \dot{\alpha} \right] - \rho_0 \theta \xi \\
 &= -\rho_0 \left[ \frac{\partial \psi}{\partial \dot{\alpha}} + \eta \frac{\partial \theta}{\partial \dot{\alpha}} \right] \ddot{\alpha} - \mathbf{H} \cdot \left[ \frac{\partial \theta}{\partial \dot{\alpha}} \nabla_{\mathbf{X}} \dot{\alpha} \right] - \rho_0 \frac{\partial \psi}{\partial \nabla_{\mathbf{X}} \dot{\alpha}} \cdot \nabla_{\mathbf{X}} \ddot{\alpha} \\
 &\quad + \left[ \frac{1}{2} \mathbf{S} - \rho_0 \frac{\partial \psi}{\partial \mathbf{C}} \right] : \dot{\mathbf{C}} - \rho_0 \theta \xi.
 \end{aligned} \tag{4.2.6}$$

Utilizing the argument that Eq. (4.2.6) has to hold for all thermodynamic processes, thus for all values of  $\ddot{\alpha}$ ,  $\nabla_{\mathbf{X}} \ddot{\alpha}$  and  $\dot{\mathbf{C}}$ , implies once more that the preceding coefficients have to vanish as  $\xi$  is non-negative due to the second law of thermodynamics.

Looking at the coefficient of  $\nabla_{\mathbf{X}} \ddot{\alpha}$ ,

$$\rho_0 \frac{\partial \psi}{\partial \nabla_{\mathbf{X}} \dot{\alpha}} = \mathbf{0}, \tag{4.2.7}$$

leads to the conclusion that the free energy density  $\psi$  can not depend on the temperature gradient  $\nabla_{\mathbf{X}} \dot{\alpha} = \nabla_{\mathbf{X}} T$  - a result also implied by Liu Eq. (4.1.4)<sub>3</sub>. Furthermore,

$$\rho_0 \left[ \frac{\partial \psi}{\partial \dot{\alpha}} + \eta \frac{\partial \theta}{\partial \dot{\alpha}} \right] = 0 \tag{4.2.8}$$

has to hold which is equivalent to Liu Eq. (4.1.4)<sub>2</sub>. Therefore, the relationship between the free energy density  $\psi$  and the entropy density  $\eta$  is given by

$$\eta = -\frac{1}{\frac{\partial \theta}{\partial \dot{\alpha}}} \frac{\partial \psi}{\partial \dot{\alpha}} = -\frac{1}{\frac{\partial \theta}{\partial \dot{\alpha}}} \frac{\partial \psi}{\partial T}. \tag{4.2.9}$$

If the absolute temperature  $\theta$  is chosen to be equal to the empirical temperature  $T$ , i.e.  $\theta = T$ , this relation agrees with the classical case in which  $\eta = -\partial \psi / \partial T$ .

The examination of the coefficient preceding the rate of the deformation gradient leads to the conclusion that

$$\mathbf{S} = 2\rho_0 \frac{\partial \psi}{\partial \mathbf{C}}. \tag{4.2.10}$$

Thus the classical relationship that the second Piola–Kirchhoff stress  $\mathbf{S}$  is energetically conjugated to the right Cauchy–Green tensor  $\mathbf{C}$  holds also for thermoelasticity of type I.

Finally, having a look at the remaining terms of Eq. (4.2.6) reveals

$$\rho_0 \theta \xi = -\mathbf{H} \cdot \left[ \frac{\partial \theta}{\partial \dot{\alpha}} \nabla_{\mathbf{X}} \dot{\alpha} \right] = -\mathbf{H} \cdot \nabla_{\mathbf{X}} \theta \tag{4.2.11}$$

for the entropy production. Thus, the dissipation for heat conduction of type I is given by the classical relation  $-\mathbf{H} \cdot \nabla_{\mathbf{X}} \theta$ .

### 4.2.2. Type II

The same procedure is applied to type II where the dependences are given by

$$\begin{aligned}\psi &= \psi(\alpha, \dot{\alpha}, \nabla_{\mathbf{X}}\alpha, \mathbf{C}), & \eta &= \eta(\alpha, \dot{\alpha}, \nabla_{\mathbf{X}}\alpha, \mathbf{C}), \\ \mathbf{Q} &= \mathbf{Q}(\alpha, \dot{\alpha}, \nabla_{\mathbf{X}}\alpha, \mathbf{C}), & \xi &= \xi(\alpha, \dot{\alpha}, \nabla_{\mathbf{X}}\alpha, \mathbf{C}), \\ \mathbf{S} &= \mathbf{S}(\alpha, \dot{\alpha}, \nabla_{\mathbf{X}}\alpha, \mathbf{C}), & \theta &= \theta(\dot{\alpha}).\end{aligned}\quad (4.2.12)$$

Consequently, in case of type II Eq. (4.2.4) yields

$$\begin{aligned}0 &= \mathbf{S} : \frac{1}{2}\dot{\mathbf{C}} - \rho_0 \left[ \frac{\partial\psi}{\partial\alpha}\dot{\alpha} + \frac{\partial\psi}{\partial\dot{\alpha}}\ddot{\alpha} + \frac{\partial\psi}{\partial\nabla_{\mathbf{X}}\alpha} \cdot \nabla_{\mathbf{X}}\dot{\alpha} + \frac{\partial\psi}{\partial\mathbf{C}} : \dot{\mathbf{C}} \right] - \rho_0\eta \left[ \frac{\partial\theta}{\partial\dot{\alpha}}\ddot{\alpha} \right] \\ &\quad - \mathbf{H} \cdot \left[ \frac{\partial\theta}{\partial\dot{\alpha}}\nabla_{\mathbf{X}}\dot{\alpha} \right] - \rho_0\theta\xi \\ &= -\rho_0\frac{\partial\psi}{\partial\alpha}\dot{\alpha} - \rho_0 \left[ \frac{\partial\psi}{\partial\dot{\alpha}} + \eta\frac{\partial\theta}{\partial\dot{\alpha}} \right] \ddot{\alpha} - \left[ \rho_0\frac{\partial\psi}{\partial\nabla_{\mathbf{X}}\alpha} + \mathbf{H}\frac{\partial\theta}{\partial\dot{\alpha}} \right] \cdot \nabla_{\mathbf{X}}\dot{\alpha} \\ &\quad + \left[ \frac{1}{2}\mathbf{S} - \rho_0\frac{\partial\psi}{\partial\mathbf{C}} \right] : \dot{\mathbf{C}} - \rho_0\theta\xi\end{aligned}\quad (4.2.13)$$

which has to hold for all values of  $\ddot{\alpha}$ ,  $\nabla_{\mathbf{X}}\dot{\alpha}$  and  $\dot{\mathbf{C}}$ .

As for type I, the free energy density  $\psi$  and the entropy density  $\eta$  are related via

$$\eta = -\frac{1}{\frac{\partial\theta}{\partial\dot{\alpha}}}\frac{\partial\psi}{\partial\dot{\alpha}}\quad (4.2.14)$$

as the coefficient of  $\ddot{\alpha}$  has to vanish. The investigation of the coefficient preceding  $\dot{\mathbf{C}}$  reveals that the classical relation for the second Piola–Kirchhoff stress holds:

$$\mathbf{S} = 2\rho_0\frac{\partial\psi}{\partial\mathbf{C}}.\quad (4.2.15)$$

Taking a look at the coefficient of  $\nabla_{\mathbf{X}}\dot{\alpha}$  leads to the astonishing characteristic of type II that the entropy flux vector is determined by means of the potential  $\psi$

$$\mathbf{H} = -\frac{\rho_0}{\frac{\partial\theta}{\partial\dot{\alpha}}}\frac{\partial\psi}{\partial\nabla_{\mathbf{X}}\alpha}.\quad (4.2.16)$$

The residual equality of type II, leading to the relationship for  $\xi$ , reads

$$\rho_0\theta\xi = -\rho_0\frac{\partial\psi}{\partial\alpha}\dot{\alpha}.\quad (4.2.17)$$

Thus, the entropy production  $\xi$ , the entropy flux vector  $\mathbf{H}$  and the second Piola–Kirchhoff stresses  $\mathbf{S}$  are determined by means of the same potential, the free energy density  $\psi$ . This leads to the outstanding property that by defining the free energy density  $\psi$  and the absolute temperature  $\theta$  all other constitutive relations follow immediately. The potential  $\psi$  is a scalar-valued isotropic function which only depends on the arguments of the state space  $\mathbb{S}_{II}$  and on the scalar invariants generated by combinations of elements of  $\mathbb{S}_{II}$ . A list of isotropic scalar invariants for some general state spaces can be found in [99, 171], for example.

#### 4. Thermodynamic principles

### 4.2.3. Type III

Inserting the dependences

$$\begin{aligned}
 \psi &= \psi(\alpha, \dot{\alpha}, \nabla_{\mathbf{X}}\alpha, \nabla_{\mathbf{X}}\dot{\alpha}, \mathbf{C}), & \eta &= \eta(\alpha, \dot{\alpha}, \nabla_{\mathbf{X}}\alpha, \nabla_{\mathbf{X}}\dot{\alpha}, \mathbf{C}), \\
 \mathbf{Q} &= \mathbf{Q}(\alpha, \dot{\alpha}, \nabla_{\mathbf{X}}\alpha, \nabla_{\mathbf{X}}\dot{\alpha}, \mathbf{C}), & \xi &= \xi(\alpha, \dot{\alpha}, \nabla_{\mathbf{X}}\alpha, \nabla_{\mathbf{X}}\dot{\alpha}, \mathbf{C}), \\
 \mathbf{S} &= \mathbf{S}(\alpha, \dot{\alpha}, \nabla_{\mathbf{X}}\alpha, \nabla_{\mathbf{X}}\dot{\alpha}, \mathbf{C}), & \theta &= \theta(\dot{\alpha})
 \end{aligned} \tag{4.2.18}$$

into Eq. (4.2.4) and straightforward calculation yields

$$\begin{aligned}
 0 &= \mathbf{S} : \frac{1}{2}\dot{\mathbf{C}} - \rho_0 \left[ \frac{\partial\psi}{\partial\alpha}\dot{\alpha} + \frac{\partial\psi}{\partial\nabla_{\mathbf{X}}\alpha} \cdot \nabla_{\mathbf{X}}\dot{\alpha} + \frac{\partial\psi}{\partial\dot{\alpha}}\ddot{\alpha} + \frac{\partial\psi}{\partial\nabla_{\mathbf{X}}\dot{\alpha}} \cdot \nabla_{\mathbf{X}}\ddot{\alpha} + \frac{\partial\psi}{\partial\mathbf{C}} : \dot{\mathbf{C}} \right] \\
 &\quad - \rho_0\eta \left[ \frac{\partial\theta}{\partial\dot{\alpha}}\ddot{\alpha} \right] - \mathbf{H} \cdot \left[ \frac{\partial\theta}{\partial\dot{\alpha}}\nabla_{\mathbf{X}}\dot{\alpha} \right] - \rho_0\theta\xi \\
 &= -\rho_0 \frac{\partial\psi}{\partial\alpha}\dot{\alpha} - \rho_0 \left[ \frac{\partial\psi}{\partial\alpha} + \eta \frac{\partial\theta}{\partial\dot{\alpha}} \right] \ddot{\alpha} - \left[ \rho_0 \frac{\partial\psi}{\partial\nabla_{\mathbf{X}}\alpha} + \mathbf{H} \frac{\partial\theta}{\partial\dot{\alpha}} \right] \cdot \nabla_{\mathbf{X}}\dot{\alpha} \\
 &\quad - \rho_0 \frac{\partial\psi}{\partial\nabla_{\mathbf{X}}\dot{\alpha}} \cdot \nabla_{\mathbf{X}}\ddot{\alpha} + \left[ \frac{1}{2}\mathbf{S} - \rho_0 \frac{\partial\psi}{\partial\mathbf{C}} \right] \cdot \dot{\mathbf{C}} - \rho_0\theta\xi
 \end{aligned} \tag{4.2.19}$$

which has to hold for all values of  $\ddot{\alpha}$ ,  $\nabla_{\mathbf{X}}\ddot{\alpha}$  and  $\dot{\mathbf{C}}$ . Therefore, the coefficients which precede the higher gradients have to vanish once more.

In a first step, looking at the coefficient preceding  $\nabla_{\mathbf{X}}\ddot{\alpha}$ ,

$$\rho_0 \frac{\partial\psi}{\partial\nabla_{\mathbf{X}}\dot{\alpha}} = \mathbf{0}, \tag{4.2.20}$$

leads to the conclusion that the free energy density  $\psi$  is not depending on the temperature gradient  $\nabla_{\mathbf{X}}\dot{\alpha}$ . Once more, the consideration of  $\ddot{\alpha}$  yields the following relationship between the free energy density  $\psi$  and the entropy density  $\eta$  which thus holds for all three types

$$\eta = -\frac{1}{\dot{\alpha}} \frac{\partial\psi}{\partial\dot{\alpha}}. \tag{4.2.21}$$

Analogously to type II, the investigation of the coefficient preceding the rate of the deformation gradient leads to

$$\mathbf{S} = 2\rho_0 \frac{\partial\psi}{\partial\mathbf{C}}. \tag{4.2.22}$$

Finally, the residual equation reads

$$\rho_0\theta\xi = - \left[ \mathbf{H} \frac{\partial\theta}{\partial\dot{\alpha}} + \rho_0 \frac{\partial\psi}{\partial\nabla_{\mathbf{X}}\alpha} \right] \cdot \nabla_{\mathbf{X}}\dot{\alpha} - \rho_0 \frac{\partial\psi}{\partial\alpha}\dot{\alpha}, \tag{4.2.23}$$

giving the relation for the entropy production  $\xi$  and thus for the dissipation.

**Remark (First Piola–Kirchhoff stress tensor):**

The first and the second Piola–Kirchhoff stress tensors  $\mathbf{P}$  and  $\mathbf{S}$  are related via Eq. (3.2.11). Since the classical relation  $\mathbf{S} = 2\rho_0\partial\psi/\partial\mathbf{C}$  holds for all three cases, one obtains (cf. e.g. [66])

$$\mathbf{P} = \rho_0 2\mathbf{F} \frac{\partial\psi}{\partial\mathbf{C}} = \rho_0 \frac{\partial\psi(\mathbf{F})}{\partial\mathbf{F}} \quad (4.2.24)$$

for type I, II and III.

**Remark (spatial versus material quantities):**

After having derived the possible dependences of the primary variables on the thermodynamic potential  $\psi$ , relations between the material and the spatial quantities introduced in Section 3.1 can be stated at this point.

Due to the vector-valued nature of the balance of linear momentum, its material formulation differs more from the spatial one than in case of the scalar-valued balance of mass. The two-point stress measure of first Piola–Kirchhoff type  $\mathbf{p}$  can be divided into a classical statical stress measure and an additional contribution originating from the kinetic energy density (see [89] for the classical case). In case of type I and III this reads

$$\mathbf{p} = [-j\mathbf{F}^t \cdot \mathbf{P} \cdot \mathbf{F}^t + j\rho_0\psi\mathbf{F}^t] + [\rho_0\mathbf{V} \cdot \mathbf{C} \cdot \mathbf{V}\mathbf{F}^t/2] \quad (4.2.25)$$

whereas for type II  $\mathbf{p}$  yields

$$\mathbf{p} = [-j\mathbf{F}^t \cdot \mathbf{P} \cdot \mathbf{F}^t + j\rho_0\psi\mathbf{F}^t - j\nabla_{\mathbf{X}}\alpha \otimes \mathbf{H} \cdot \mathbf{F}^t] + [\rho_0\mathbf{V} \cdot \mathbf{C} \cdot \mathbf{V}\mathbf{F}^t/2] \quad (4.2.26)$$

since the entropy flux vector  $\mathbf{H}$  and the thermal displacement gradient  $\nabla_{\mathbf{X}}\alpha$  are additionally thermodynamically conjugated (cf. Eq. (4.2.16)).

The Eshelby stress tensor  $\Sigma$  is obtained from the statical stress measure which leads to

$$\Sigma = J [-j\mathbf{F}^t \cdot \mathbf{P} \cdot \mathbf{F}^t + j\rho_0\psi\mathbf{F}^t] \cdot \mathbf{f}^t = \rho_0\psi\mathbf{I} - \mathbf{F}^t \cdot \mathbf{P} \quad (4.2.27)$$

for type I and III and to

$$\Sigma^t = \rho_0\psi\mathbf{I} - \mathbf{F}^t \cdot \mathbf{P} - \nabla_{\mathbf{X}}\alpha \otimes \mathbf{H} \quad (4.2.28)$$

for type II.

The classical spatial volume force  $\mathbf{b}$  only consists of an external part and, furthermore, does not contain any contribution from the kinetic energy. Contrarily, the material volume force  $\rho_0\mathbf{B}$  can be expressed as

$$\rho_0\mathbf{B} = \rho_0\mathbf{B}_{\text{ext}} + \rho_0\mathbf{B}_{\text{int}} + \partial_{\mathbf{X}} (\rho_0\mathbf{V} \cdot \mathbf{C} \cdot \mathbf{V}\mathbf{F}^t/2), \quad (4.2.29)$$

where the internal force  $\rho_0\mathbf{B}_{\text{int}}$  can be interpreted as a measure of the material's inhomogeneity in the material motion context [89] and reads for all three types

$$\rho_0\mathbf{B}_{\text{int}} = -\rho_0\mathbf{F}^t \cdot \mathbf{b} + \rho_0 \frac{\partial_{\theta} T}{\partial_T \theta} \eta \nabla_{\mathbf{X}} T - \rho_0 \partial_{\mathbf{X}} \psi. \quad (4.2.30)$$

#### 4. *Thermodynamic principles*

# 5. Theory of non-classical heat conduction

This section is restricted to the thermal aspect of the Green-Naghdi theory in order to investigate and compare the three types of heat conduction based on the Green–Naghdi approach [51]. Constitutive equations are introduced for each type. The linearized theory of type I corresponds to Fourier’s law, consequently, the classical theory is fully embedded. Both, type II and III, allow heat transmission at finite wave speed and therefore are able to overcome the paradox of infinite wave speed in Fourier’s approach. Furthermore, the applicability of type II and III for modeling the second sound phenomenon is shown. First, the basic ideas and equations of [51] are reiterated. Then, for the numerical treatment, a solution method fully based on finite elements is suggested and evaluated by means of numerical examples. First results are published by Bargmann and Steinmann in [7].

## 5.1. Governing constitutive equations

Heat conduction in an isotropic, stationary rigid solid  $\mathcal{B}_t = \mathcal{B}_0 =: \mathcal{B} \subset \mathbb{R}^n$ ,  $n \in \{1, 2, 3\}$ , is considered. In a rigid body, the distance between any two particles remains unchanged. Thus,  $\mathbf{X} = \mathbf{x}$  and no distinction is made between the spatial and the material motion problem in this section. This implies  $\rho_0 = \rho_t =: \rho$  for the material’s mass density. In a first step, appropriate constitutive laws are suggested for each of the three types. This process is referred to as constitutive modeling.

### 5.1.1. Type I

As mentioned above, the linearized theory of type I corresponds to the classical theory based on Fourier’s law of heat conduction. For the theory of type I the following constitutive assumptions are suggested

$$\begin{aligned}\theta &:= T, \\ \rho\psi &:= -\frac{\rho c}{T_0} \frac{[T - T_0]^2}{2} - [T - T_0] S_0, \\ \mathbf{q} &:= -\kappa_1 \nabla T.\end{aligned}\tag{5.1.1}$$

Thereby,  $c$ ,  $T_0$  and  $\kappa_1$  denote the non-negative specific heat, the reference temperature and the thermal conductivity, respectively. The absolute entropy density  $S_0$  is introduced into the

## 5. Theory of non-classical heat conduction

free energy density  $\psi$  in order to scale the entropy  $\eta$  (cf. Appendix A.6). Otherwise  $\eta$  would represent the change of entropy and not the entropy itself.

Regarding relations (4.2.9) and (4.2.11) this leads to

$$\begin{aligned}\rho\theta\xi &= -\mathbf{h} \cdot \nabla T = -\frac{\mathbf{q}}{T} \cdot \nabla T, \\ \rho\eta &= \frac{\rho c}{T_0} [T - T_0] + S_0.\end{aligned}\quad (5.1.2)$$

Note that the introduced constitutive equations are mainly in agreement with Green and Naghdi's ideas, but not fully. This is the case for all three types and for the thermal as well as for the coupled thermoelastic theory. Deviations are due to (i) consistency reasons and (ii) the different treatment of the absolute temperature  $\theta$  (cf. Section 4.1).

Inserting these assumptions into the entropy equation multiplied by the absolute temperature  $\theta$ , cf. Eq. (4.2.1), yields the following linearized temperature equation:

$$\rho c \dot{T} = \operatorname{div}(\kappa_1 \nabla T) + \rho r. \quad (5.1.3)$$

Since its discriminant equals zero, Eq. (5.1.3) is parabolic for all points  $\mathbf{x}$  and all time instances  $t$ , cf. also Appendix A.2 for the classification of second-order partial differential equations. The temperature Eq. (5.1.3) describes classical Fourier, i.e. diffusive, heat conduction.

One drawback of the classical temperature equation is the unphysical behavior of perturbations propagating at infinite wave speed. Herrera and Pavón [63], for example, calculate the temperature profile for an infinite one-dimensional bar which is initially set at equilibrium, i.e. the temperature  $T$  is zero for  $t < 0$  and for all  $x > x_0$ . A perturbation is initiated by a heat source at  $x = x_0$  and  $t = 0$ . Then, for constant  $\kappa_1$ , the temperature profile reads

$$T = \frac{1}{\sqrt{t}} \exp\left(-\frac{\rho c [x - x_0]^2}{4\kappa_1 t}\right).$$

One can easily see that  $T > 0$  for all  $x > x_0$  for  $t > 0$ . Figure 5.1 depicts the temperature profile for the bar very shortly after the temperature perturbation was initiated at  $x_0$ .

### 5.1.2. Type II

Now, let's take a look at type II which distinguishes from the classical theory by the introduction of the thermal displacement and allows thermal waves to propagate at finite speed.

The following constitutive equations relate the absolute temperature  $\theta$  and the free energy density  $\psi$  to the independent variables  $\dot{\alpha}$  and  $\nabla_{\mathbf{x}}\alpha$ :

$$\begin{aligned}\theta &:= T, \\ \rho\psi &:= -\frac{\rho c [T - T_0]^2}{2} - [T - T_0] S_0 + \frac{\kappa_2}{2} \nabla\alpha \cdot \nabla\alpha.\end{aligned}\quad (5.1.4)$$



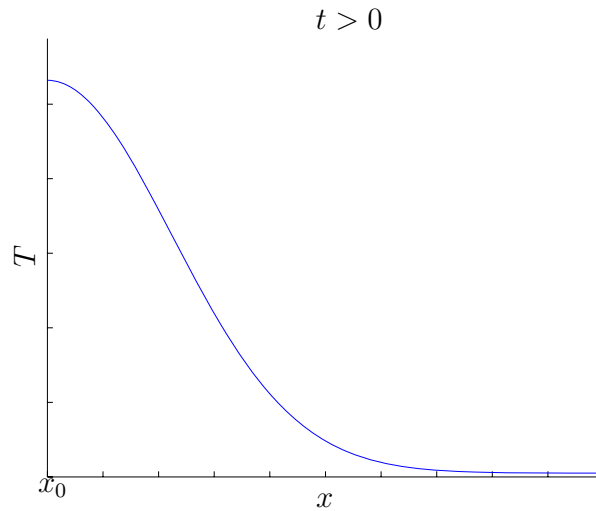


Figure 5.1.: Qualitative temperature profile according to [63]. The heat flux vector  $\mathbf{q}$  responds immediately to the temperature gradient  $\nabla T$ , thus a perturbation is instantly felt everywhere in the infinite one dimensional medium leading to a global temperature rise.

The dependent material quantities follow from equations (4.2.14), (4.2.16) and (4.2.17):

$$\begin{aligned} \mathbf{h} &= -\kappa_2 \nabla \alpha, \\ \xi &= 0, \\ \rho \eta &= \frac{\rho c}{T_0} [T - T_0] + S_0. \end{aligned} \quad (5.1.5)$$

Here,  $\xi = 0$  stems from the choice of  $\psi$  being independent of  $\alpha$ . This signifies that the theory of type II does not involve any energy dissipation which is the only known non-diffusive thermal theory so far. In literature, type II is referred to as the theory without energy dissipation and usually it is overseen that this is not intrinsically the case as the right hand side of Eq. (4.2.17) is not zero. Thus one has to choose the free energy density  $\psi$  independent of the thermal displacement  $\alpha$  in order to receive a non-dissipative theory.

The constitutive assumptions of type II are substituted into Eq. (4.2.1) (multiplied by the absolute temperature  $\theta$ ) and subsequent linearization yields

$$\rho c \dot{T} = \text{div} (\kappa_2 \nabla \alpha) + \rho r. \quad (5.1.6)$$

The discriminant  $\delta = -\rho c \kappa_2$  of the temperature equation of type II is negative<sup>1</sup>, thus the heat equation of type II (5.1.6) is hyperbolic for all points  $\mathbf{x}$  and all times  $t$ , cf. Appendix A.2.

Differentiating it with respect to time reveals that, if  $\dot{r} = 0$  and constant  $\kappa_2 > 0$ , the hyperbolic temperature equation is a standard wave equation describing heat propagating undamped at

<sup>1</sup>The material's density  $\rho$ , the specific heat  $c$  and the thermal conductivity  $\kappa_2$  are always defined positive in physics.

## 5. Theory of non-classical heat conduction

a finite wave speed of

$$v = \sqrt{\frac{\kappa_2}{\rho c}}. \quad (5.1.7)$$

### 5.1.3. Type III

The main feature of the theory of type III is that a dissipative heat flux of the Fourier type is added to type II. Type III is the most general of the three approaches as contains type I and II as special cases. A heat conductor of type III is described by

$$\begin{aligned} \theta &:= T, \\ \rho\psi &:= -\frac{\rho c}{T_0} \frac{[T - T_0]^2}{2} - [T - T_0] S_0, \\ \mathbf{q} &:= -[\kappa_3 \nabla \alpha + \kappa_4 \nabla T], \end{aligned} \quad (5.1.8)$$

leading to

$$\begin{aligned} \rho\theta\xi &= -\mathbf{h} \cdot \nabla T, \\ \rho\eta &= \frac{\rho c}{T_0} [T - T_0] + S_0. \end{aligned} \quad (5.1.9)$$

The non-negative thermal conductivities  $\kappa_3$  and  $\kappa_4$  are allowed to become 0, in order to obtain both, type I and II, as limiting cases of type III. Nevertheless,  $\kappa_3$  and  $\kappa_4$  are restricted such that for all positions  $\mathbf{x}$  and all time instances  $t$  at least one of them must be positive, i.e.  $\kappa_3 > 0 \vee \kappa_4 > 0 \forall \mathbf{x}, t$ . The constitutive assumptions (5.1.8) are inserted into Eq. (4.2.1). Subsequent linearization results in

$$\rho c \dot{T} = \operatorname{div} (\kappa_3 \nabla \alpha + \kappa_4 \nabla T) + \rho r. \quad (5.1.10)$$

Depending on the values of the thermal conductivities  $\kappa_3$  and  $\kappa_4$ , the heat equation of type III (5.1.10) might, but does not necessarily, involve energy dissipation. Only in case that  $\kappa_3 = 0$  or  $\kappa_4 = 0$ , Eq. (5.1.10) can be classified as parabolic ( $\kappa_3 = 0$ ) or hyperbolic ( $\kappa_4 = 0$ ). If both parameters,  $\kappa_3$  and  $\kappa_4$ , are positive, Eq. (5.1.10) is a third order partial differential equation. Thus, such a classification can no longer be made.

## 5.2. Finite element discretization

The solution of the temperature equations of a particular process can usually only be calculated by using numerical methods. One powerful approach is the finite element method of which the first roots go back to the 1940s and which earned triumphant progress started in the 1950s. It is based on the idea that the domain under consideration can be decomposed into a finite number of disjoint subsets. Today, the finite element method is one of the most powerful numerical methods for solving mathematical models describing engineering problems.

In thermoelasticity, the governing partial differential equations are often first discretized in space applying the finite element method (cf. e.g. [160]). This is referred to as a semi-discretization technique because it reduces the partial differential equations to a system of ordinary differential equations in time. Second, the resulting semi-discrete equations are integrated in time in order to obtain the transient temperature response. Often, this time integration is realized with finite difference schemes.

In this contribution, the finite element method is applied for the spatial as well as the temporal discretization to numerically solve the temperature equations in order to transfer the consistency of the theory to the numerical framework. It is resorted to a semi-discretization technique based on spatial and temporal Galerkin finite element methods.

For general literature on the spatial finite element method, the reader is referred to the textbooks of Hughes [67] or Zienkiewicz and Taylor [175], for example. General information on the temporal finite element methods used in this thesis can be found in the book of Eriksson et al. [42].

### 5.2.1. Spatial finite element discretization

The weak form of the temperature equations (5.1.3), (5.1.6) and (5.1.10) forms the prerequisite for the standard Bubnov–Galerkin finite element method. Therefore, the mentioned equations are weighted by a test function  $\delta T \in C_0^\infty(\mathcal{B})$  and integrated over the domain  $\mathcal{B}$ :

Type I

$$\int_{\mathcal{B}} \delta T \rho c \dot{T} \, dV + \int_{\mathcal{B}} \nabla \delta T \cdot [\kappa_1 \nabla T] \, dV = \int_{\mathcal{B}} \delta T \rho r \, dV - \int_{\partial \mathcal{B}} \delta T \mathbf{q} \cdot \mathbf{n} \, dA, \quad (5.2.1)$$

Type II

$$\int_{\mathcal{B}} \delta T \rho c \dot{T} \, dV + \int_{\mathcal{B}} \nabla \delta T \cdot [\kappa_2 \nabla \alpha] \, dV = \int_{\mathcal{B}} \delta T \rho r \, dV - \int_{\partial \mathcal{B}} \delta T \mathbf{q} \cdot \mathbf{n} \, dA, \quad (5.2.2)$$

Type III

$$\int_{\mathcal{B}} \delta T \rho c \dot{T} \, dV + \int_{\mathcal{B}} \nabla \delta T \cdot [\kappa_3 \nabla \alpha + \kappa_4 \nabla T] \, dV = \int_{\mathcal{B}} \delta T \rho r \, dV - \int_{\partial \mathcal{B}} \delta T \mathbf{q} \cdot \mathbf{n} \, dA, \quad (5.2.3)$$

where  $\mathbf{n}$  denotes the outward normal vector on the boundary  $\partial \mathcal{B}$  and the divergence theorem (A.5.2) is applied. Furthermore, the relation (3.1.7) between the thermal displacement  $\alpha$  and the empirical temperature  $T$  is weighted by a test function  $\delta \alpha$  and also integrated over the domain  $\mathcal{B}$ :

$$\int_{\mathcal{B}} \delta \alpha \dot{\alpha} \, dV - \int_{\mathcal{B}} \delta \alpha T \, dV = 0. \quad (5.2.4)$$

Subsequently, the domain  $\mathcal{B}$  is discretized into  $n_{el}$  disjoint spatial elements  $\mathcal{B}^e$ , cf. Figure 5.2, and the geometry  $\mathbf{X}$  is interpolated elementwise by shape functions  $N^i$  at the  $i = 1, \dots, n_{en}$  local node point positions:

$$\mathcal{B} = \bigcup_{e=1}^{n_{el}} \mathcal{B}^e, \quad \mathcal{B}^i \cap \mathcal{B}^j = \emptyset \text{ for } i \neq j, \quad \mathbf{X}^h|_{\mathcal{B}^e} = \sum_{i=1}^{n_{en}} N^i \mathbf{X}_i. \quad (5.2.5)$$

## 5. Theory of non-classical heat conduction

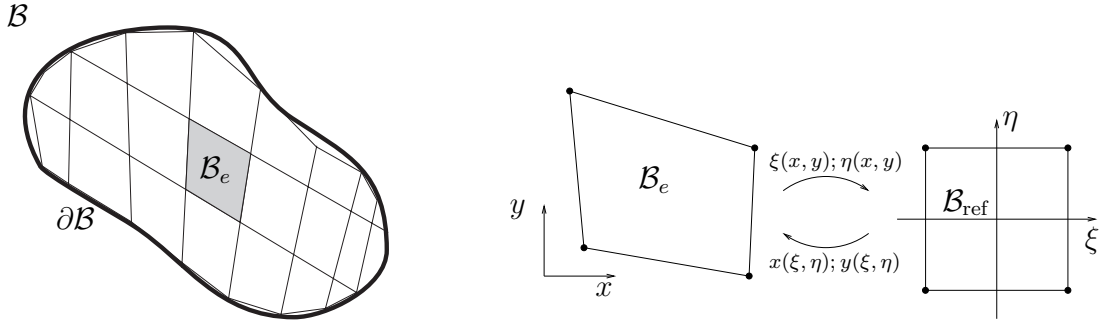


Figure 5.2.: Spatial discretization of a body  $\mathcal{B}$ : The domain  $\mathcal{B}$  is subdivided into a finite number of subdomains  $\mathcal{B}_e$ . Each element  $\mathcal{B}_e$  is transferred onto the spatial reference element  $\mathcal{B}_{\text{ref}}$ .

Following the isoparametric concept, the unknowns, i.e. the thermal displacement  $\alpha$  and the temperature  $T$ , are interpolated with the same shape functions  $N^i$  as the element geometry  $\mathbf{X}$ . Moreover, according to the Bubnov–Galerkin method, the test functions  $\delta\alpha$  and  $\delta T$  are discretized with the same shape functions  $N^i$ , i.e.:

$$\begin{aligned} \alpha^h|_{\mathcal{B}^e} &= \sum_{i=1}^{n_{\text{en}}} N^i \alpha_i, & T^h|_{\mathcal{B}^e} &= \sum_{i=1}^{n_{\text{en}}} N^i T_i \quad \in \mathbf{H}^1(\mathcal{B}) \\ \delta\alpha^h|_{\mathcal{B}^e} &= \sum_{i=1}^{n_{\text{en}}} N^i \delta\alpha_i, & \delta T^h|_{\mathcal{B}^e} &= \sum_{i=1}^{n_{\text{en}}} N^i \delta T_i \quad \in \mathbf{H}_0^1(\mathcal{B}). \end{aligned} \quad (5.2.6)$$

Thus, in each spatial finite element  $\mathcal{B}^e$  the unknowns  $\alpha$  and  $T$  are approximated by a linear combination of algebraic polynomials and the unknown nodal values.<sup>2</sup> The discrete gradients of the unknowns  $\nabla\alpha$ ,  $\nabla T$  and of the test functions  $\nabla\delta\alpha$  and  $\nabla\delta T$  can, therefore, be written as

$$\begin{aligned} \nabla\alpha^h|_{\mathcal{B}^e} &= \sum_{i=1}^{n_{\text{en}}} \alpha_i \nabla N^i, & \nabla T^h|_{\mathcal{B}^e} &= \sum_{i=1}^{n_{\text{en}}} T_i \nabla N^i, \\ \nabla\delta\alpha^h|_{\mathcal{B}^e} &= \sum_{i=1}^{n_{\text{en}}} \delta\alpha_i \nabla N^i, & \nabla\delta T^h|_{\mathcal{B}^e} &= \sum_{i=1}^{n_{\text{en}}} \delta T_i \nabla N^i. \end{aligned} \quad (5.2.7)$$

Consequently, the following semi-discretized temperature equations are obtained:

Type I

$$\mathfrak{C} \cdot \dot{\mathbf{T}}(t) + \mathfrak{K}_{\kappa_1} \cdot \mathbf{T}(t) = \mathbf{f}_{\text{vol}} - \mathbf{f}_{\text{surI}}, \quad (5.2.8)$$

Type II

$$\mathfrak{C} \cdot \dot{\mathbf{T}}(t) + \mathfrak{K}_{\kappa_2} \cdot \boldsymbol{\alpha}(t) = \mathbf{f}_{\text{vol}} - \mathbf{f}_{\text{surII}}, \quad (5.2.9)$$

<sup>2</sup> $\mathbf{H}^1(\mathcal{B}) = \{f : Df \in L^2(\mathcal{B})\} = \{f \text{ and the first weak derivative } Df \text{ belong to } L^2(\mathcal{B})\}$  and  $\mathbf{H}_0^1(\mathcal{B}) = \{f : Df \in L^2(\mathcal{B}) \text{ and } f(\partial\mathcal{B}) = 0\}$  are called Sobolev spaces. Both are Hilbert spaces, i.e. complete inner product spaces.

Type III

$$\mathbf{c} \cdot \dot{\mathbf{T}}(t) + \mathfrak{K}_{\kappa_3} \cdot \boldsymbol{\alpha}(t) + \mathfrak{K}_{\kappa_4} \cdot \mathbf{T}(t) = \mathbf{f}_{\text{vol}} - \mathbf{f}_{\text{surIII}}, \quad (5.2.10)$$

The semi-discretized relation between  $\boldsymbol{\alpha}$  and  $\mathbf{T}$  reads

$$\dot{\boldsymbol{\alpha}} - \mathbf{T} = \mathbf{0}. \quad (5.2.11)$$

Here,  $\boldsymbol{\alpha} = \{\alpha_i\}$  and  $\mathbf{T} = \{T_i\}$  denote the global node vectors of the thermal displacement and the temperature, respectively.  $\boldsymbol{\alpha}, \mathbf{T} \in \mathbb{R}^{n_{\text{dof}}}$ ,  $n_{\text{dof}}$  denoting the number of spatial global degrees of freedom.

Furthermore, the capacitance and conductance matrices take the format

$$\mathbf{c} = \mathbf{A} \sum_{e=1}^{n_{\text{el}}} \sum_{i,j=1}^{n_{\text{en}}} \int_{B^e} N^i \rho c N^j \, dV, \quad \mathfrak{K} = \mathbf{A} \sum_{e=1}^{n_{\text{el}}} \sum_{i,j=1}^{n_{\text{en}}} \int_{B^e} \nabla N^i \cdot \nabla N^j \, dV \quad (5.2.12)$$

in the sense that e.g.

$$\mathfrak{K}_{\kappa_1} := \mathbf{A} \sum_{e=1}^{n_{\text{el}}} \sum_{i,j=1}^{n_{\text{en}}} \int_{B^e} N^i \kappa_1 N^j \, dV. \quad (5.2.13)$$

The operator  $\mathbf{A}_{e=1}^{n_{\text{el}}}$  denotes the assembly over all element contributions at the element nodes.

On the right-hand side of Eqs. (5.2.8)-(5.2.10), the heat load vector due to external heat bulk source  $\mathbf{f}_{\text{vol}}$  and those due to specified nodal temperatures  $\mathbf{f}_{\text{sur}}$

$$\begin{aligned} \mathbf{f}_{\text{vol}} &= \mathbf{A} \sum_{e=1}^{n_{\text{el}}} \sum_{i=1}^{n_{\text{en}}} \int_{B^e} N^i \rho r_e \, dV, & \mathbf{f}_{\text{surI}} &= \mathbf{A} \sum_{e=1}^{n_{\text{el}}} \sum_{i=1}^{n_{\text{en}}} \int_{\partial B^e} N^i \mathbf{q}_e \cdot \mathbf{n}_e \, dA, \\ \mathbf{f}_{\text{surII}} &= \mathbf{A} \sum_{e=1}^{n_{\text{el}}} \sum_{i=1}^{n_{\text{en}}} \int_{\partial B^e} N^i \mathbf{q}_e \cdot \mathbf{n}_e \, dA, & \mathbf{f}_{\text{surIII}} &= \mathbf{A} \sum_{e=1}^{n_{\text{el}}} \sum_{i=1}^{n_{\text{en}}} \int_{\partial B^e} N^i \mathbf{q}_e \cdot \mathbf{n}_e \, dA \end{aligned} \quad (5.2.14)$$

are obtained.

### 5.2.2. Temporal finite element discretization

The temporal discretization is done with Galerkin finite element time integration schemes. Analogous to spatial finite element methods, the time interval under consideration  $I = [t_0, t_e]$  is divided into a finite number  $n_t$  of elements such that

$$\int_{t_0}^{t_e} [\dots] \, dt = \sum_{i=1}^{n_t} \int_{t_{i-1}}^{t_i} [\dots] \, dt \quad (5.2.15)$$

and  $t_0 < t_1 < \dots < t_{n_t} = t_e$ . Each  $t \in I_n = [t_{n-1}, t_n]$  is transformed to  $\tau \in I_\tau = [0, 1]$  via the mapping  $\tau(t) = \frac{t-t_{n-1}}{t_n-t_{n-1}}$ , cf. Figure 5.3.

## 5. Theory of non-classical heat conduction

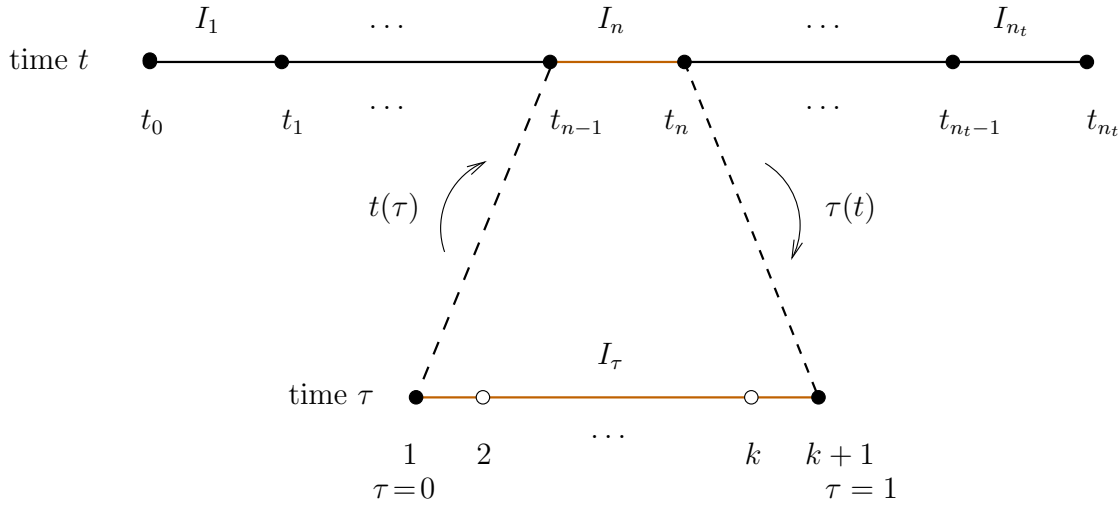


Figure 5.3.: Temporal discretization: Each time interval  $I_n = [t_{n-1}; t_n]$  is transferred onto the reference time interval  $I_\tau = [0; 1]$  via the transformation map  $\tau(t)$ .

The length of a time interval is denoted by  $h_n = t_n - t_{n-1}$ . Contrary to the spatial procedure, the weak form is formed for each subinterval and the discrete system of equations is subsequently solved for one subinterval after the other.

At each timestep, the primary variables (in this case:  $\alpha$  and  $\mathbf{T}$ ) are calculated at time  $t_n$  for given values at time  $t_{n-1}$ . The primary variables have to be continuous across the time element boundaries, i.e.  $[[\mathbf{T}_n]] = \mathbf{T}_n^+ - \mathbf{T}_n^- = \mathbf{0}$ .

One distinguishes between discontinuous and continuous Galerkin methods. Retaining the terminology of Eriksson in [42] the expression “dG( $k$ ) method” refers to the discontinuous method of degree  $k$ , whereas the continuous method of degree  $k$  is called “cG( $k$ ) method” throughout this thesis. The temporal polynomial degree  $k \geq 1$  can, of course, be arbitrarily chosen. Therefore, the order of accuracy is not restricted: cG( $k$ ) is of the order  $2k$  and dG( $k$ ) of the order  $2k + 1$  accurate (cf. [57]). Thus, the local temporal error can be controlled by the user which is especially important in long-term simulations.

The dG( $k$ ) and the cG( $k$ ) methods differ in the treatment of the assumption that the primary variables have to be continuous across the time element boundaries. cG( $k$ ) methods meet the continuity condition strong, whereas it is taken into account weakly in dG( $k$ ) methods, cf. Figure 5.4.

Moreover, the discontinuous Galerkin time integration leads to numerical dissipation in the time discretization, see for instance [14, 57, 76]. On the contrary, the continuous Galerkin time integration can be energy conserving. Betsch and Steinmann [17, 18, 19, 20] publish a series of papers addressing the conservation properties of the cG( $k$ ) method. Therefore, the cG( $k$ ) method is of particular interest for heat conduction without energy dissipation (type II).

In the following, both approaches are introduced and applied. The dG( $k$ ) method has proven

to suit well for parabolic problems, consequently, it is applied to the semi-discrete temperature equation of type I (5.2.8). Those of type II and III, i.e. (5.2.9) and (5.2.10), are discretized with a  $cG(k)$  method which works well for hyperbolic equations. Note that the temperature equation of type III (5.1.10) is a third order partial differential equation and therefore cannot be classified as hyperbolic. Nevertheless, since  $\kappa_3 \gg \kappa_4$  is chosen in all numerical examples presented in this thesis, the  $cG(k)$  method has proven to be the better choice for the temporal discretization of Eq. (5.1.10), see [7].

Both approaches are based on formulating the temporal weak form of the ordinary differential equations and the subsequent finite element approximations

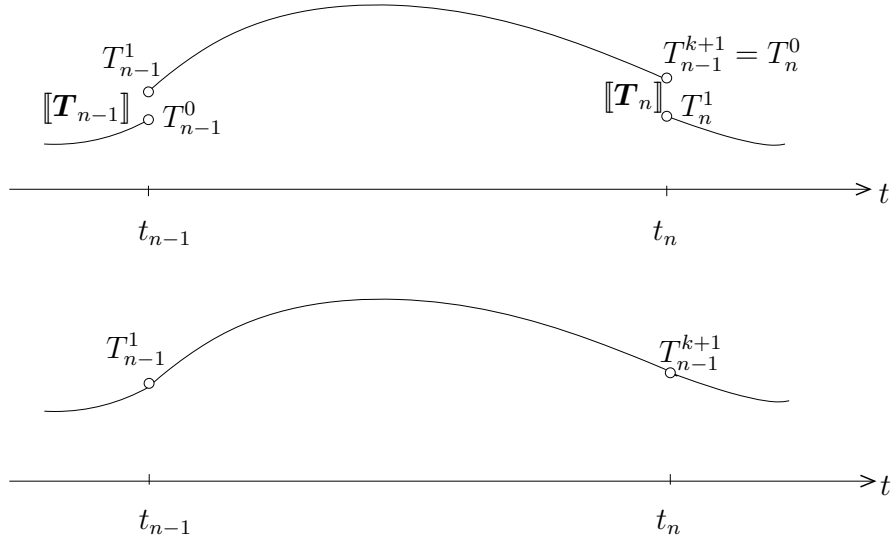


Figure 5.4.: The approximation of the primary variables differs in the  $dG(k)$ - and the  $cG(k)$ -method, here the approximation of the temperature  $T$  is exemplarily illustrated in the time subinterval  $I_n = [t_{n-1}; t_n]$ . The  $dG(k)$ -method (upper) fulfills the continuity assumption weakly and allows for a jump  $[[\mathbf{T}_n]]$ . The  $cG(k)$ -method (lower) fulfills the continuity assumption strongly, thus  $[[\mathbf{T}_n]] = \mathbf{0}$ .

### 5.2.2.1. Discontinuous finite element method

The trial function  $\mathbf{T}(\tau)$  and the test function  $\delta^t \mathbf{T}(\tau)$  are elements of the same space, i.e. the set of  $n_{\text{dof}}$ -dimensional polynomials of degree at most  $k$  on the interval  $(0, 1)$ :  $\mathcal{P}^k(0, 1)^{n_{\text{dof}}}$ . They are approximated on each subinterval  $I_n$  by smooth Lagrange polynomials of degree  $k$

$$\mathbf{T}^h(\tau)|_{I_n} = \sum_{i=1}^{k+1} M_i(\tau) \mathbf{T}^i, \quad \delta^t \mathbf{T}^h(\tau)|_{I_n} = \sum_{i=1}^{k+1} M_i(\tau) \delta^t \mathbf{T}^i \quad (5.2.16)$$

## 5. Theory of non-classical heat conduction

which are discontinuous across the time element boundaries and given by

$$M_i(\tau) = \prod_{j=1; j \neq i}^{k+1} \frac{\tau - \tau_j}{\tau_i - \tau_j}, \quad 1 \leq i \leq k+1. \quad (5.2.17)$$

As the trial and the test functions are approximated identically, the dG( $k$ ) method belongs to the Bubnov–Galerkin methods. The identical function spaces are advantageous in the error analysis and yield improved stability properties for parabolic problems [42].

The time derivatives take the format

$$\dot{\mathbf{T}}^h(\tau)|_{I_n} = \frac{1}{h_n} \sum_{i=1}^{k+1} M'_i(\tau) \mathbf{T}^i, \quad (5.2.18)$$

where the prime ' denotes the derivation with respect to  $\tau$  and the superimposed dot  $\dot{\phantom{x}}$  is the derivation with respect to  $t$ , i.e.  $M'_i(\tau) = dM_i/d\tau$  and  $\dot{\mathbf{T}}^h(\tau) = d\mathbf{T}^h(\tau)/dt$ . As mentioned above, a discontinuity in the master element  $I_\tau$  has to be admitted in order to prevent that the trial functions are over-determined at the boundary nodal values, cf. Figure 5.5.  $[[\mathbf{T}^h]] = \mathbf{T}^1 - \mathbf{T}^0$  denotes the jump of  $\mathbf{T}$  at  $\tau = 0$ .  $\mathbf{T}^0$  is the known value at the local node  $\tau = 0$  from the previous time step.

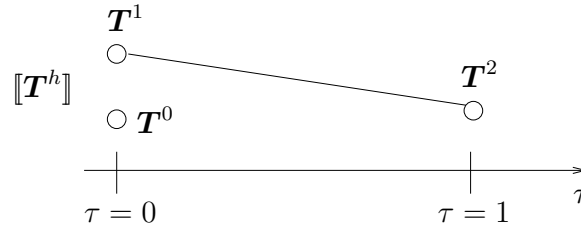


Figure 5.5.: A discontinuity  $[[\mathbf{T}^h]] = \mathbf{T}^1 - \mathbf{T}^0$  is admitted. The picture shows the discontinuity on a linear master element  $I_\tau$ .  $\mathbf{T}^0$  denotes the value at the local node  $\tau = 0$  which is known from the previous time step.  $\mathbf{T}^1$  and  $\mathbf{T}^2$  have to be calculated.

This discontinuity is added to the temporal element weak form of (5.2.8) as follows

$$h_n \int_0^1 \delta^t \mathbf{T}^h \cdot \left[ \mathbf{c} \cdot \dot{\mathbf{T}}(t) + \mathbf{r}_{\kappa_1} \cdot \mathbf{T}(t) - \mathbf{f}_{\text{vol}} + \mathbf{f}_{\text{sur}I} \right] d\tau + \delta \mathbf{T}_1 \cdot [[\mathbf{T}^h]] = 0. \quad (5.2.19)$$

The discrete algebraic set of equations is obtained by substituting the finite element approximation (5.2.16) into (5.2.19) and exploiting the arbitrariness of the test function:

$$\sum_{j=1}^{k+1} \int_0^1 M_i \mathbf{c} M'_j d\tau \mathbf{T}^j + h_n \int_0^1 M_i \mathbf{r}_{\kappa_1} M_j d\tau \mathbf{T}^j + \delta_{i1} [[\mathbf{T}^h]] = h_n \sum_{j=1}^{k+1} \int_0^1 M_i [\mathbf{f}_{\text{vol}} - \mathbf{f}_{\text{sur}I}] d\tau \quad (5.2.20)$$



for  $i = 1, \dots, k + 1$ .  $\delta_{i1}$  denotes Kronecker's Delta.

### 5.2.2.2. Continuous finite element method

The cG( $k$ ) method suits well for hyperbolic equations, therefore it is applied to discretize the temperature equations of type II, Eq. (5.2.9). It is also applied to the temperature equation of type III, Eq. (5.2.10). It approximates trial functions piecewise and continuously with polynomials of degree  $k$  and test functions piecewise and discontinuously across the element boundaries with polynomials of degree  $k - 1$ . Consequently, it belongs to the Petrov–Galerkin methods.

The approximations of the test functions  $\delta^t \boldsymbol{\alpha}$  and  $\delta^t \mathbf{T}$  are elements of  $\mathcal{P}^{k-1}(0, 1)^{n_{\text{dof}}}$  and fulfill

$$\delta^t \boldsymbol{\alpha}^h(\tau) |_{I_n} = \sum_{j=1}^k \tilde{M}_j \delta^t \boldsymbol{\alpha}^j, \quad \delta^t \mathbf{T}^h(\tau) |_{I_n} = \sum_{j=1}^k \tilde{M}_j \delta^t \mathbf{T}^j, \quad (5.2.21)$$

whereas those of the trial functions  $\boldsymbol{\alpha}^h$  and  $\mathbf{T}^h$  are elements of  $\mathcal{P}^k(0, 1)^{n_{\text{dof}}}$  and take the form

$$\boldsymbol{\alpha}^h(\tau) |_{I_n} = \sum_{j=1}^{k+1} M_j \boldsymbol{\alpha}^j, \quad \mathbf{T}^h(\tau) |_{I_n} = \sum_{j=1}^{k+1} M_j \mathbf{T}^j. \quad (5.2.22)$$

The reduced nodal shape functions  $\tilde{M}_j$  of order  $k - 1$  are defined by

$$\tilde{M}_i(\tau) = \prod_{j=1; j \neq i}^k \frac{\tau - \tau_j}{\tau_i - \tau_j}, \quad 1 \leq i \leq k \quad (5.2.23)$$

and related to the shape functions  $M_i$  via

$$\dot{\boldsymbol{\alpha}}^h(\tau) = \frac{1}{h_n} \sum_{i=1}^{k+1} M_i'(\tau) \boldsymbol{\alpha}^i = \frac{1}{h_n} \sum_{i=1}^k \tilde{M}_i(\tau) \tilde{\boldsymbol{\alpha}}^i, \quad (5.2.24)$$

where the  $\tilde{\boldsymbol{\alpha}}^i$ 's are linear combinations of the  $\boldsymbol{\alpha}^i$ 's (see also Tab. 5.1).

Eventually, the cG( $k$ ) approximation of type-II heat conduction is obtained by multiplication with the temporal test functions and integration over the time interval of interest

$$\begin{aligned} & h_n \int_0^1 \delta^t \mathbf{T}^h \cdot \left[ \boldsymbol{\epsilon} \cdot \dot{\mathbf{T}}^h + \boldsymbol{\kappa}_{\kappa_2} \cdot \boldsymbol{\alpha}^h - \mathbf{f}_{\text{vol}} + \mathbf{f}_{\text{surII}} \right] d\tau = 0 \\ \text{and } & h_n \int_0^1 \delta^t \boldsymbol{\alpha}^h \cdot [\dot{\boldsymbol{\alpha}}^h - \mathbf{T}^h] d\tau = 0. \end{aligned} \quad (5.2.25)$$

Table 5.1.: Nodal shape functions  $M_i(\tau)$  and  $\tilde{M}_i(\tau)$  for polynomial approximations of degrees  $k = 1, 2, 3$  along with associated values  $\tilde{\alpha}^i$

	$M_i(\tau)$	$\tilde{M}_i(\tau)$	$\tilde{\alpha}^i$
$k = 1$	$M_1 = 1 - \tau$	$\tilde{M}_1 = 1$	$\tilde{\alpha}_1 = \alpha_2 - \alpha_1$
	$M_2 = \tau$		
$k = 2$	$M_1 = [2\tau - 1][\tau - 1]$	$\tilde{M}_1 = 1 - \tau$	$\tilde{\alpha}_1 = -3\alpha_1 + 4\alpha_2 - \alpha_3$
	$M_2 = -4[\tau^2 - \tau]$	$\tilde{M}_2 = \tau$	$\tilde{\alpha}_2 = \alpha_1 - 4\alpha_2 + 3\alpha_3$
	$M_3 = [2\tau - 1]\tau$		
$k = 3$	$M_1 = -\frac{9}{2}[\tau - \frac{1}{3}][\tau - \frac{2}{3}][\tau - 1]$	$\tilde{M}_1 = [2\tau - 1][\tau - 1]$	$\tilde{\alpha}_1 = -\frac{11}{2}\alpha_1 + 9\alpha_2 - \frac{9}{2}\alpha_3 + \alpha_4$
	$M_2 = \frac{27}{2}[\tau - \frac{2}{3}][\tau - 1]\tau$	$\tilde{M}_2 = -4[\tau^2 - \tau]$	$\tilde{\alpha}_2 = \frac{1}{8}\alpha_1 - \frac{27}{8}\alpha_2 + \frac{27}{8}\alpha_3 - \frac{1}{8}\alpha_4$
	$M_3 = -\frac{27}{2}[\tau - \frac{1}{3}][\tau - 1]\tau$	$\tilde{M}_3 = [2\tau - 1]\tau$	$\tilde{\alpha}_3 = -\alpha_1 + \frac{9}{2}\alpha_3 + \frac{11}{2}\alpha_4$

The fully discrete system of equations of type II can be expressed as

$$\sum_{j=1}^{k+1} \int_0^1 \tilde{M}_i \mathbf{e} M_j' d\tau \mathbf{T}^j + h_n \int_0^1 \tilde{M}_i \mathbf{K}_{\kappa_2} M_j d\tau \boldsymbol{\alpha}^j = h_n \int_0^1 \tilde{M}_i [\mathbf{f}_{\text{vol}} - \mathbf{f}_{\text{surII}}] d\tau$$

and

$$\sum_{j=1}^{k+1} \int_0^1 \tilde{M}_i M_j' d\tau \boldsymbol{\alpha}^j - h_n \int_0^1 \tilde{M}_i M_j d\tau \mathbf{T}^j = \mathbf{0}. \quad (5.2.26)$$

Analogously, the cG( $k$ ) approximation of type III can be written as

$$h_n \int_0^1 \delta^t \mathbf{T}^h \cdot [\mathbf{e} \cdot \dot{\mathbf{T}}^h + \mathbf{K}_{\kappa_3} \cdot \boldsymbol{\alpha}^h + \mathbf{K}_{\kappa_4} \cdot \mathbf{T}^h - \mathbf{f}_{\text{vol}} + \mathbf{f}_{\text{surIII}}] d\tau = 0$$

and

$$h_n \int_0^1 \delta^t \boldsymbol{\alpha}^h \cdot [\dot{\boldsymbol{\alpha}}^h - \mathbf{T}^h] d\tau = 0. \quad (5.2.27)$$

The fully discrete system of equations of type III reads

$$\sum_{j=1}^{k+1} \int_0^1 \tilde{M}_i \mathbf{e} M_j' d\tau \mathbf{T}^j + h_n \int_0^1 \tilde{M}_i \mathbf{K}_{\kappa_3} M_j d\tau \boldsymbol{\alpha}^j + h_n \int_0^1 \tilde{M}_i \mathbf{K}_{\kappa_4} M_j d\tau \mathbf{T}^j$$

$$= h_n \int_0^1 \tilde{M}_i [\mathbf{f}_{\text{vol}} - \mathbf{f}_{\text{surIII}}] d\tau$$

and

$$\sum_{j=1}^{k+1} \int_0^1 \tilde{M}_i M_j' d\tau \boldsymbol{\alpha}^j - h_n \int_0^1 \tilde{M}_i M_j d\tau \mathbf{T}^j = \mathbf{0}. \quad (5.2.28)$$

## 5.3. Numerical results

In the following, numerical examples are presented to underline the performance of the method. Isotropic and homogeneous rigid heat conductors of sodium fluoride (NaF) and bismuth (Bi) are studied.

Bismuth is a silver-white metal with a pinkish tinge and a multi-colored iridescent tarnish, see Figure 5.6. In the periodic system, the symbol “Bi” is used and its atomic number is 83. This brittle metal is one of the few non-toxic heavy metals and possesses a rhombohedral crystal structure. Bismuth has many outstanding properties. It is the metal with the highest natural diamagnetism, the strongest Hall effect and the second lowest thermal conductivity. Moreover, it is very slightly radioactive with an exceptional long half-life of  $1.9 \cdot 10^{19}$  years [101] and one of the few substances which is denser in its liquid than in its solid phase.

At cryogenic temperatures below 3.5 K, phonons are the dominant mechanism for thermal conduction in bismuth [119]. Although it is elastically a very anisotropic solid, the second sound velocity is independent of the orientation and stated to be  $7.8 \cdot 10^{-4} \text{m}/\mu\text{s}$  [119].

## 5. Theory of non-classical heat conduction

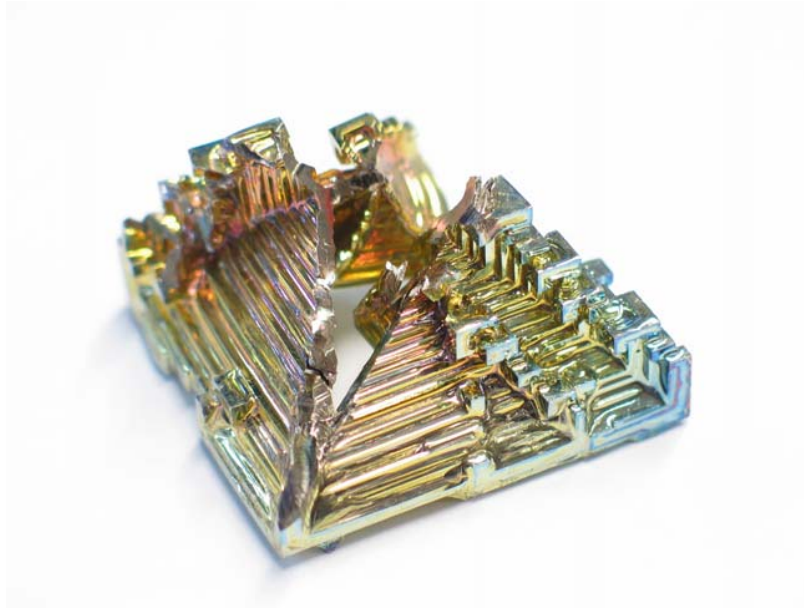


Figure 5.6.: Synthetic bismuth crystal with a multi-colored iridescent tarnish. The bottom front edge has a length of about 3.5cm. Picture credit: Wikipedia.

Sodium fluoride is a transparent-white ionic fluoride with chemical formula “NaF”. It is brittle, very toxic and possesses a face-centered cubic crystal structure, see Figure 5.7 (left). Second sound was detected in a temperature range around 15 K [108] and its velocity is stated to be  $1.9531 \cdot 10^{-3} \text{m}/\mu\text{s}$  [61].

The material parameters of NaF and Bi are listed in Table 5.2.

Table 5.2.: Material parameters for heat conduction in NaF and Bi

	NaF	Bi
material’s density $\rho$	2886 $\left[\frac{\text{kg}}{\text{m}^3}\right]$	9780 $\left[\frac{\text{kg}}{\text{m}^3}\right]$
specific heat $c$	2.774 $\left[\frac{\text{W}}{\text{kgK}}\right]$	0.052 $\left[\frac{\text{W}}{\text{kgK}}\right]$
thermal conductivity $\kappa_1$	20500 $\left[\frac{\text{W}}{\text{mK}}\right]$	875 $\left[\frac{\text{W}}{\text{mK}}\right]$
absolute entropy density $S_0$	0.9247 $\left[\frac{\text{N}}{\text{m}^2\text{K}}\right]$	0.0173 $\left[\frac{\text{N}}{\text{m}^2\text{K}}\right]$
reference temperature $T_0$	15 [K]	3 [K]
length $l$	10 [mm]	9 [mm]
external heat source $r$	0	0

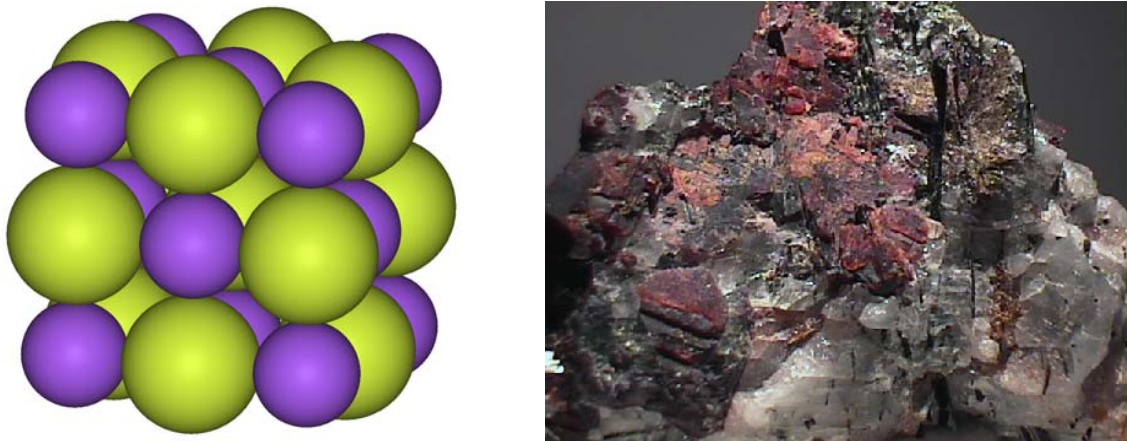


Figure 5.7.: Left: Face-centered cubic crystal structure of NaF. Na atoms are indicated in green, F atoms in purple. Picture credit: Wikipedia.

Right: In nature, NaF is found in form of the mineral villiaumite. It is often colored red, orange or pink. Villiaumite is transparent to translucent. Moreover, it is soft and soluble in water. Picture credit: Amethyst Galleries, Inc. [4].

The thermal conductivity  $\kappa_1$  is a material parameter which is determined experimentally presuming Fourier's law of heat conduction. Thus, it is reasonable to recalculate the value of the thermal conductivity at the temperatures where second sound occurs and Fourier's law fails. This leads to the following values of  $\kappa_2$ ,  $\kappa_3$  and  $\kappa_4$ : Instead of Fourier's law, the Green–Naghdi-type-II approach is used as a basis for the calculation of  $\kappa_2$ ,  $\kappa_3$  and  $\kappa_4$ . Thus, one obtains  $\kappa_2 = 20500 \frac{\text{W}}{\text{mK}} \cdot 14897 \frac{1}{\text{s}^2} = 305388500 \frac{\text{W}}{\text{s}^2 \text{mK}}$  for NaF and  $\kappa_2 = 875 \frac{\text{W}}{\text{mK}} \cdot 353609 \frac{1}{\text{s}^2} = 309407875 \frac{\text{W}}{\text{s}^2 \text{mK}}$  for Bi. Moreover,  $\kappa_3 = \kappa_2$  and  $\kappa_4 = \kappa_3/1000\text{s}^2$  are chosen. Due to only small changes in temperatures, the thermal conductivities are assumed to be constant.

First, the applicability of the Green–Naghdi approach for modeling the second sound phenomenon is investigated. Numerical results proving the suitability for modeling the NaF-second sound experiments of Jackson and Walker [72, 73] are published in the work of Bargmann and Steinmann [7].

In a first example, the thermal behavior in bismuth is studied. In 1972, Narayanamurti and Dynes [119] detected second sound in a 9 mm-long-bar of Bi. The velocity of second sound in Bi,  $7.8 \cdot 10^{-4} \frac{\text{m}}{\mu\text{s}}$ , leads to a wave front arrival at the opposed end after 11.5  $\mu\text{s}$ . Initially, the specimen (cf. Figure 5.8) has a homogeneous temperature distribution at a value of 3 K. A short heat pulse increases the temperature from 3 K to 4 K at the left end. The thermal displacement  $\alpha$  is initiated at zero everywhere in the bar.

## Type I

## 5. Theory of non-classical heat conduction

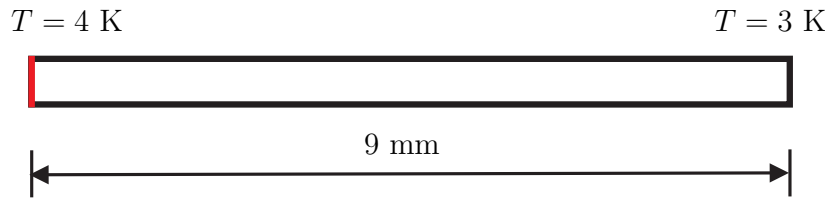


Figure 5.8.: Set-up of second sound model. A 9 mm-long one-dimensional bar of Bi with initial temperature 3 K is heated by a short heat pulse from 3 K to 4 K at the left end.

As expected, Fourier's law is inapplicable to model the second sound phenomenon. Figure 5.9 (left) shows the numerical solution according to Fourier's law, i.e. according to type I. The heat does not propagate as a thermal wave, thus type I is not applicable for modeling second sound. This result is also stated in [7]. However, the comparison of the numerical (Figure 5.9 (left)) with the analytical (Figure 5.9 (right)) solution clearly monitors that the discretization approach suggested in Section 5.2 works well for the classical theory. Furthermore, the internal energy  $\epsilon$  is studied in order to show the different behavior of type I, II and III. Figure 5.10 shows the evolution of the internal energy  $\epsilon$  in case of heat conduction of type I. The dissipation in the beginning of the simulation and the subsequent equilibration are visible.

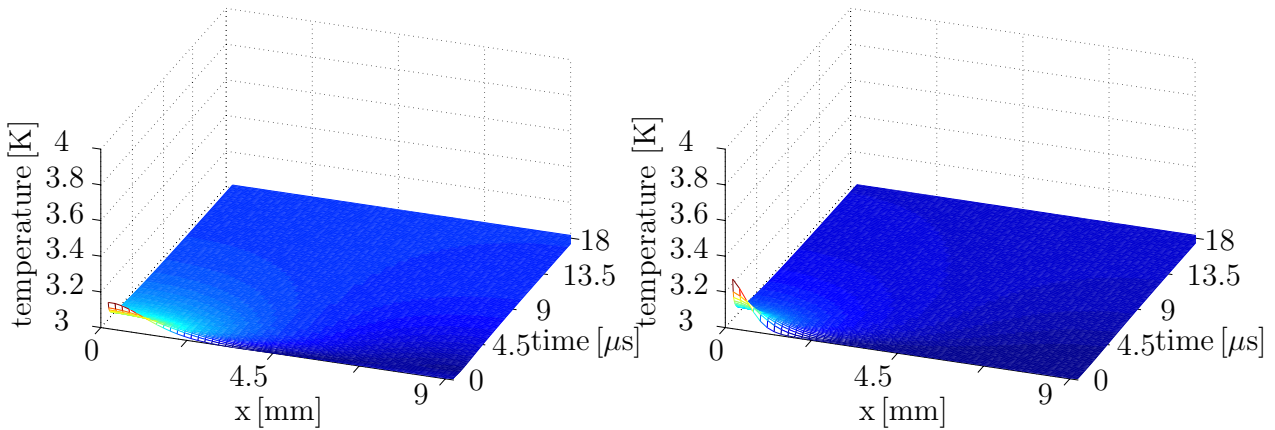


Figure 5.9.: Numerical (left) and analytical (right) solution of heat conduction in Bi according to Fourier's law, i.e. type I. The temperature is plotted versus space and time. The numerical solution corresponds to the analytical solution. However, the governing heat equation of type I (5.1.3) is not suitable for modeling heat conduction in Bi at cryogenic temperatures, i.e. where the second sound phenomenon occurs. The mathematical formulation of the analytical solution for this initial value problem is given in the appendix A.9. The analytical solution of the classical heat equation of type I in general, i.e. Eq. (5.1.3), is given by expression (5.1.4).

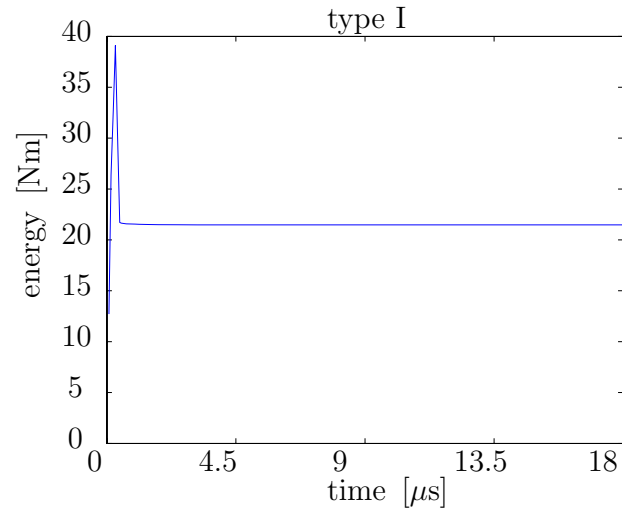


Figure 5.10.: Numerical simulation of the second sound experiments in Bi. The internal energy  $\epsilon$  is plotted in the course of time. The increase in energy at the beginning is due to fact that the heat pulse of 1 K is applied piecewise during the first  $0.5 \mu\text{s}$ . The classical Fourier case, i.e. type I, is strongly dissipative.

### Type II

Figures 5.11 and 5.12 prove the applicability of Green and Naghdi's theory of type II and the discretization approach suggested above for modeling the second sound phenomenon. Heat propagates as a thermal wave at finite speed and without energy dissipation (see also Figure 5.13 for the conservation of the internal energy  $\epsilon$ ). The wave's arrival point at the bar's right end is in very good agreement to the experimental data of Narayanamurti and Dynes [119], see Figure 5.12. Comparing the numerical and the analytical solutions (Figure 5.11 (left) respectively (right)) also reveals that the discretization method derived in Section 5.2 is suitable for heat conduction of type II.

As expected, the energy is conserved, see Figure 5.13. Whether or not second sound in solids involves energy dissipation is not resolved. However, second sound was also detected in superfluids - a state in which it is known that energy is not dissipated.

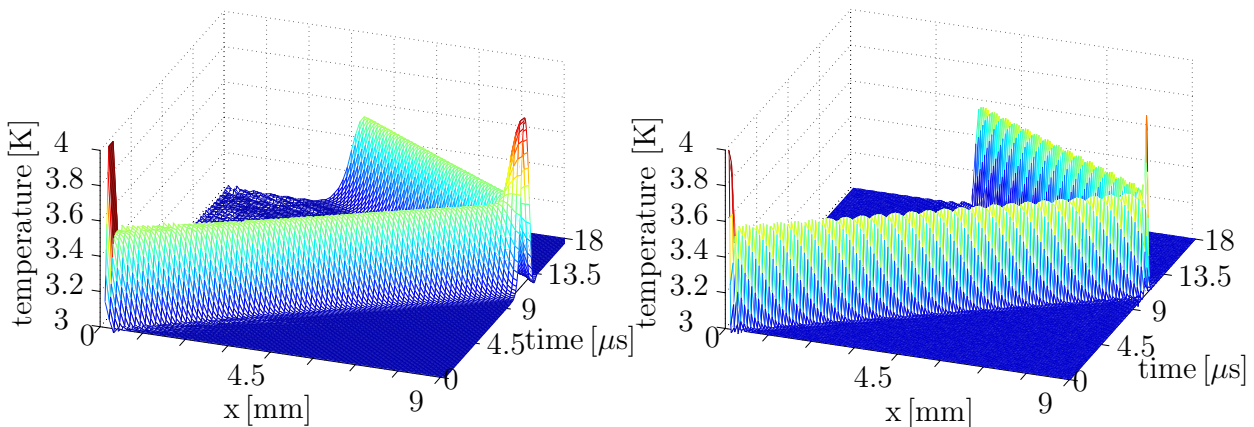


Figure 5.11.: Numerical (left) and analytical (right) solution of heat conduction in Bi according to type II. Again, temperature is plotted versus space and time. The constitutive equations (5.1.1) are chosen such that energy is not dissipated. The wave runs without stopping between the two ends of the bar. See Appendix A.9 for the mathematical formulation of the analytical solution.



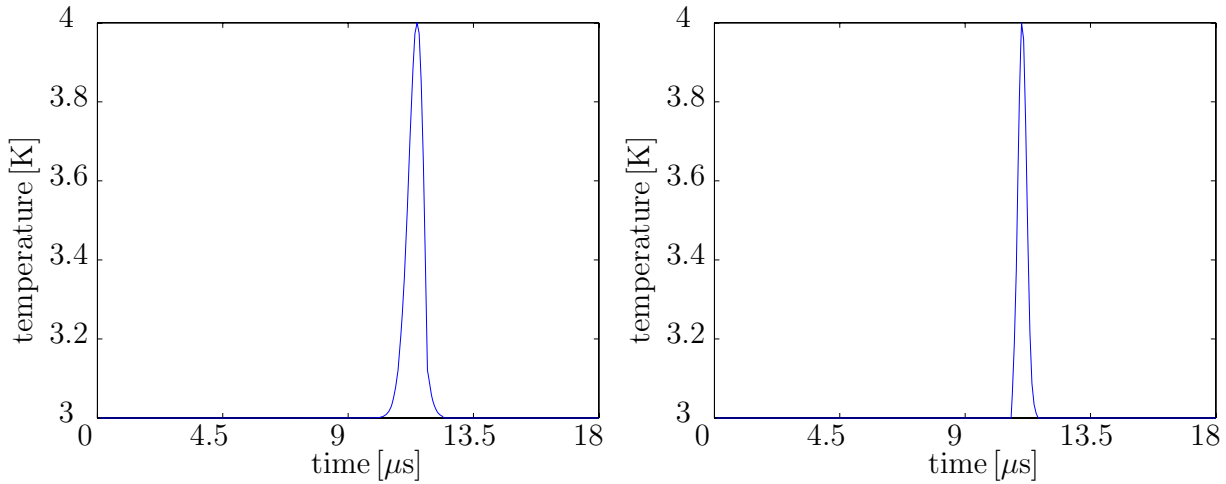


Figure 5.12.: Numerical (left) and analytical (right) solution of heat conduction in Bi according to type II. The temperature is plotted versus time at the right end of the specimen ( $x = 9$  mm). The arrival time of the thermal wave is perfectly met.

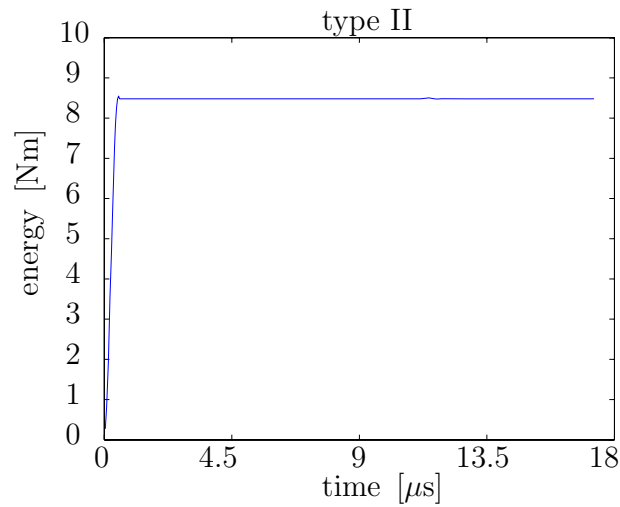


Figure 5.13.: Numerical simulation of the second sound experiments in Bi. The internal energy  $\epsilon$  is plotted in the course of time. The increase in energy at the beginning is due to fact that the heat pulse of 1 K is applied piecewise during the first  $0.5 \mu\text{s}$ . As expected, type II conserves the internal energy. Due to the continuous Galerkin temporal finite element discretization, not only the theory is energy conserving but also the numerical discretization.

## 5. Theory of non-classical heat conduction

### Type III

Also, type III is suitable for modeling the second sound phenomenon, see Figures 5.14 and 5.15. In contrast to type II, type III does involve energy dissipation due to an additional heat flux of the Fourier type. The latter adds dissipation being clearly visible because the wave's amplitude decreases with time (Figures 5.14 and 5.15). This fact is also supported by the behavior of the energy shown in Figure 5.16. Like type II, type III also allows thermal waves to propagate at finite speed. The comparison of the numerical and the analytical solution (Figure 5.12 (left) respectively (right)) underlines the suitability of the discretization method suggested in Section 5.2 for heat conduction of type III.

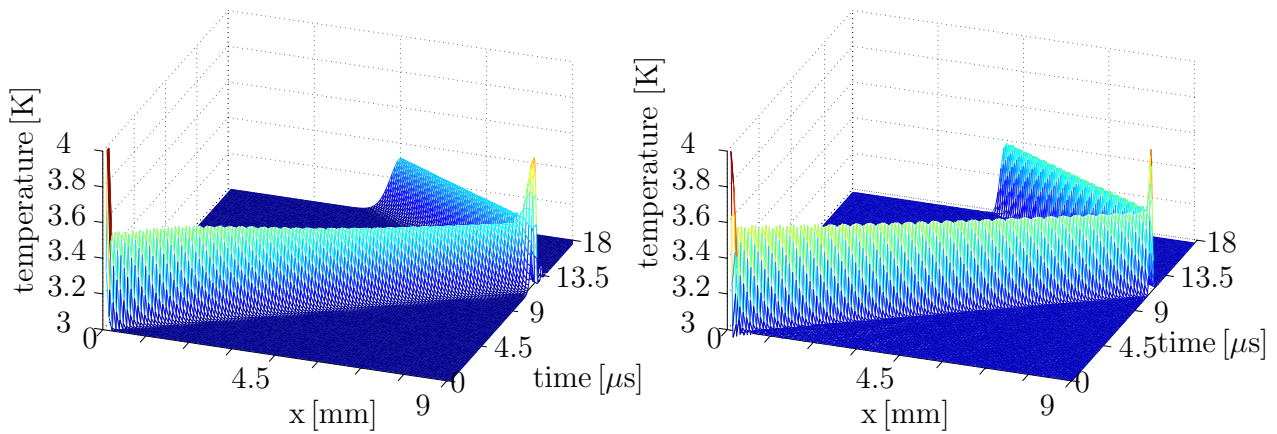


Figure 5.14.: Numerical (left) and analytical (right) solution of heat conduction in Bi according to type III. The temperature is plotted versus space and time. A dissipative heat flux of the Fourier type is added compared to type II. The amplitude of the wave decreases, thus the energy dissipation is clearly visible. See Appendix A.9 for the mathematical formulation of the analytical solution.

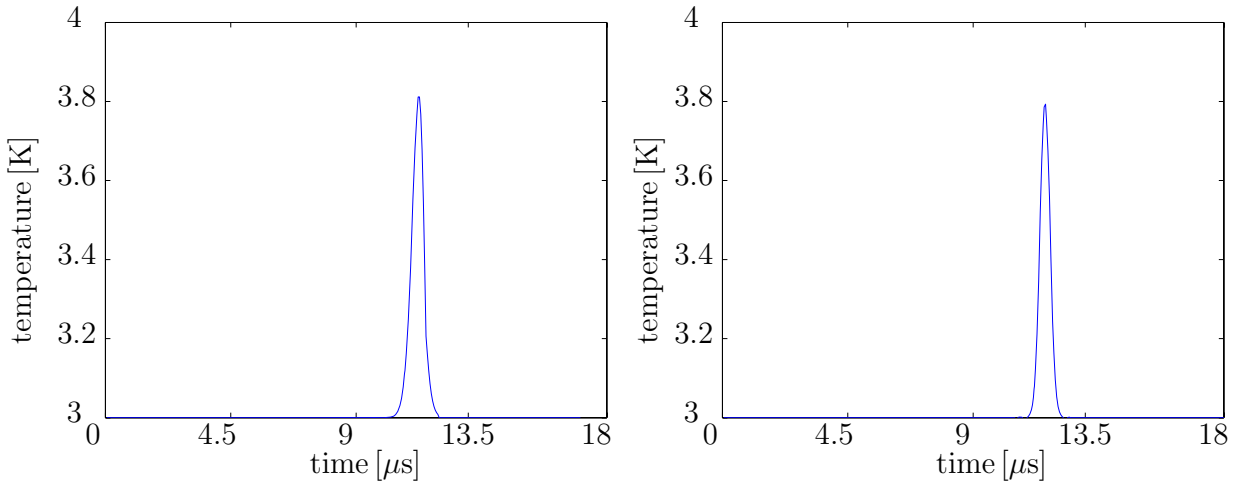


Figure 5.15.: Numerical (left) and analytical (right) solution of heat conduction in Bi according to type III. The temperature is plotted versus time at the right end of the specimen ( $x = 9$  mm). The arrival time of the thermal wave is perfectly met. Furthermore, the energy dissipation leads to a decreasing wave amplitude: the initial heat pulse of 1 K leads to an arriving heat pulse of about 0.8 K.

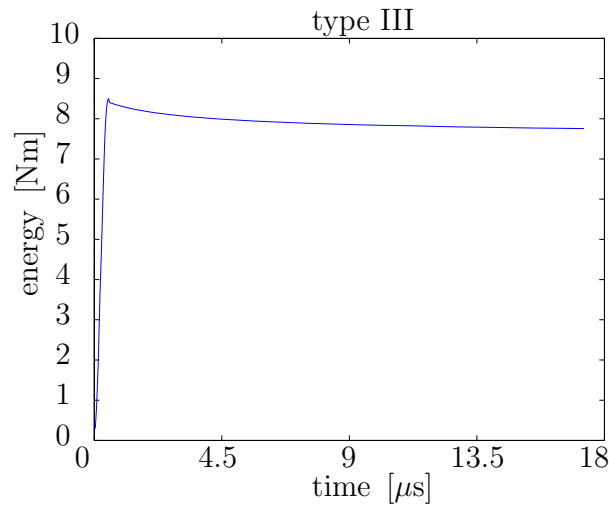


Figure 5.16.: The internal energy  $\epsilon$  is plotted versus time during the simulation of the second sound experiments in Bi. The increase in energy at the beginning is due to fact that the heat pulse of 1K is applied piecewise during the first  $0.5 \mu\text{s}$ . Type III is slightly dissipative because of the additional dissipative heat flux of the Fourier type.

## 5. Theory of non-classical heat conduction

In the second example, a disc of NaF is analyzed. The disc's radius is 10 mm, see Figure 5.17. Further material parameters are listed in Table 5.2. At the boundary, the temperature is initiated at 16 K, whereas in the inside it is set at 15 K. The specimen is observed for  $5.12 \mu\text{s}$ . Figure 5.18 depicts the temperature solution of type I and shows its strongly dissipative behavior. The corresponding temperature solutions of type II and III are illustrated in Figures 5.19 and 5.20, respectively. It is obvious that both admit a wavelike heat propagation. The influence of the additive dissipative heat flux in type III is clearly visible compared to the solution of type II.

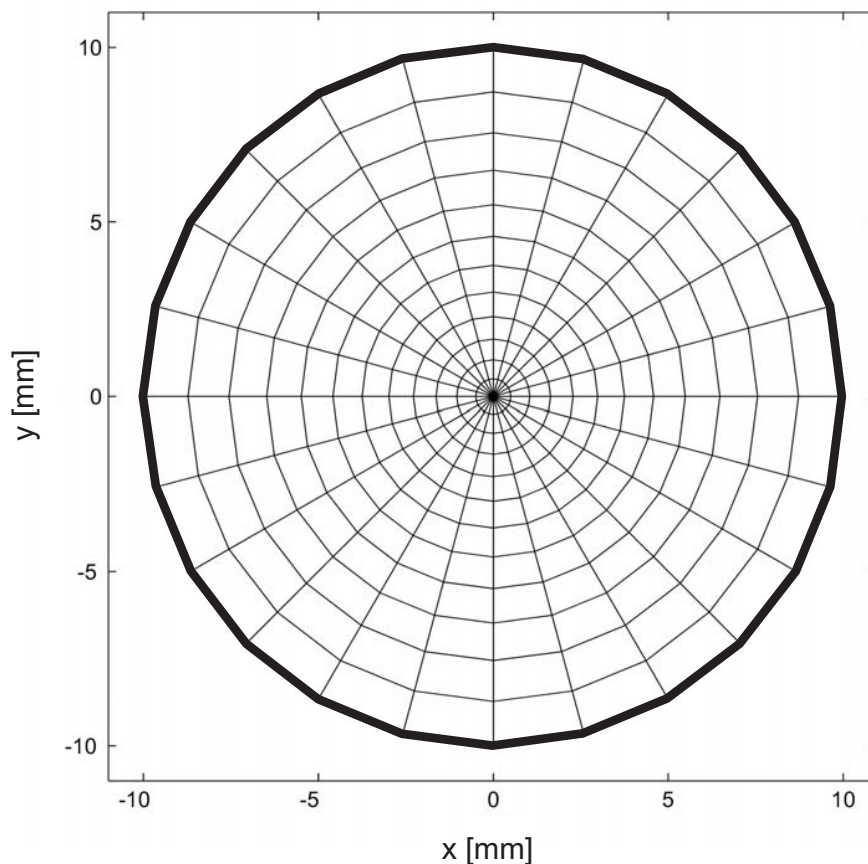


Figure 5.17.: The NaF disc has a radius of 10 mm. It is discretized in space with 24 elements along the circumference and 12 elements along the ligament. Thus, in total there are 288 spatial elements. For the temporal discretization 1000 time steps were chosen. Initially, the temperature of the circle's inside is set at 15 K. At the boundary, the temperature is initiated at 16 K.

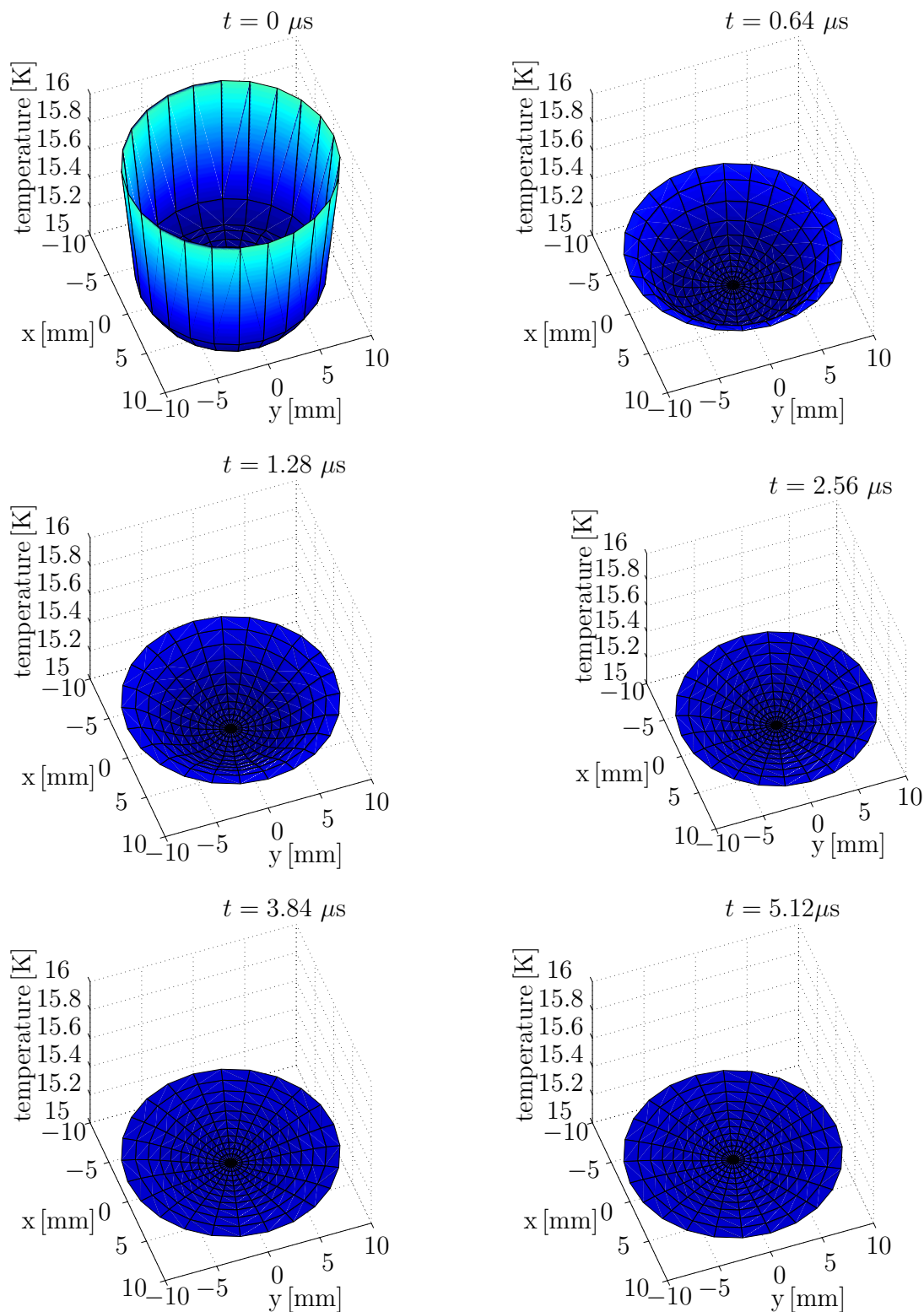


Figure 5.18.: Heat conduction in a two-dimensional disc of NaF according to type I. A heat pulse of 1 K is initiated at the circle's boundary. The temperature distribution is plotted at times  $t = 0 \mu\text{s}$ ,  $t = 0.64 \mu\text{s}$ ,  $t = 1.28 \mu\text{s}$ ,  $t = 2.56 \mu\text{s}$ ,  $t = 3.84 \mu\text{s}$  and  $t = 5.12 \mu\text{s}$ .

## 5. Theory of non-classical heat conduction

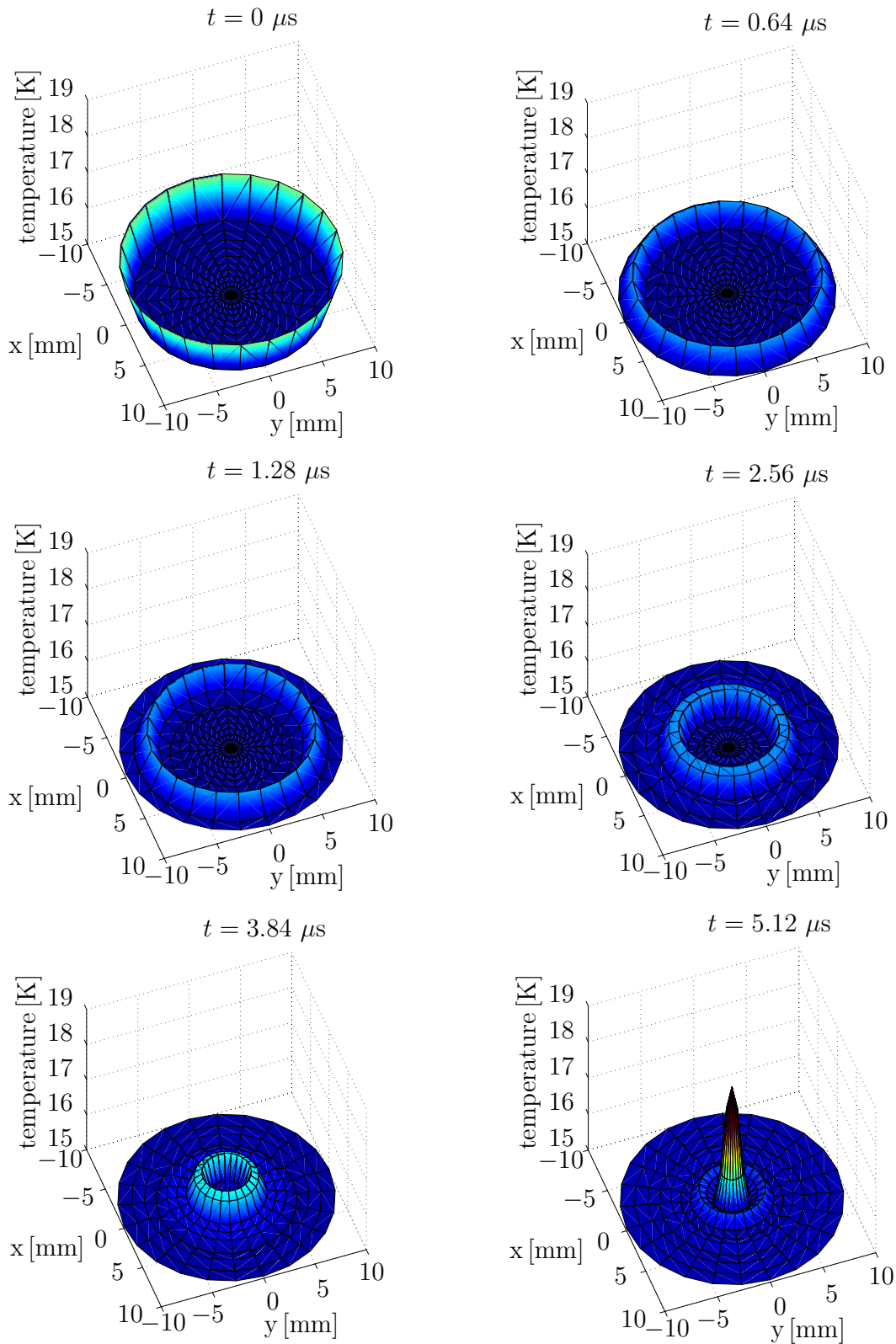


Figure 5.19.: Heat conduction in a two-dimensional disc of NaF according to type II. A heat pulse of 1 K is initiated at the circle's boundary. The temperature distribution is plotted at times  $t = 0 \mu s$ ,  $t = 0.64 \mu s$ ,  $t = 1.28 \mu s$ ,  $t = 2.56 \mu s$ ,  $t = 3.84 \mu s$  and  $t = 5.12 \mu s$ . Note that here, the temperature range is plotted from 15 K to 19 K.

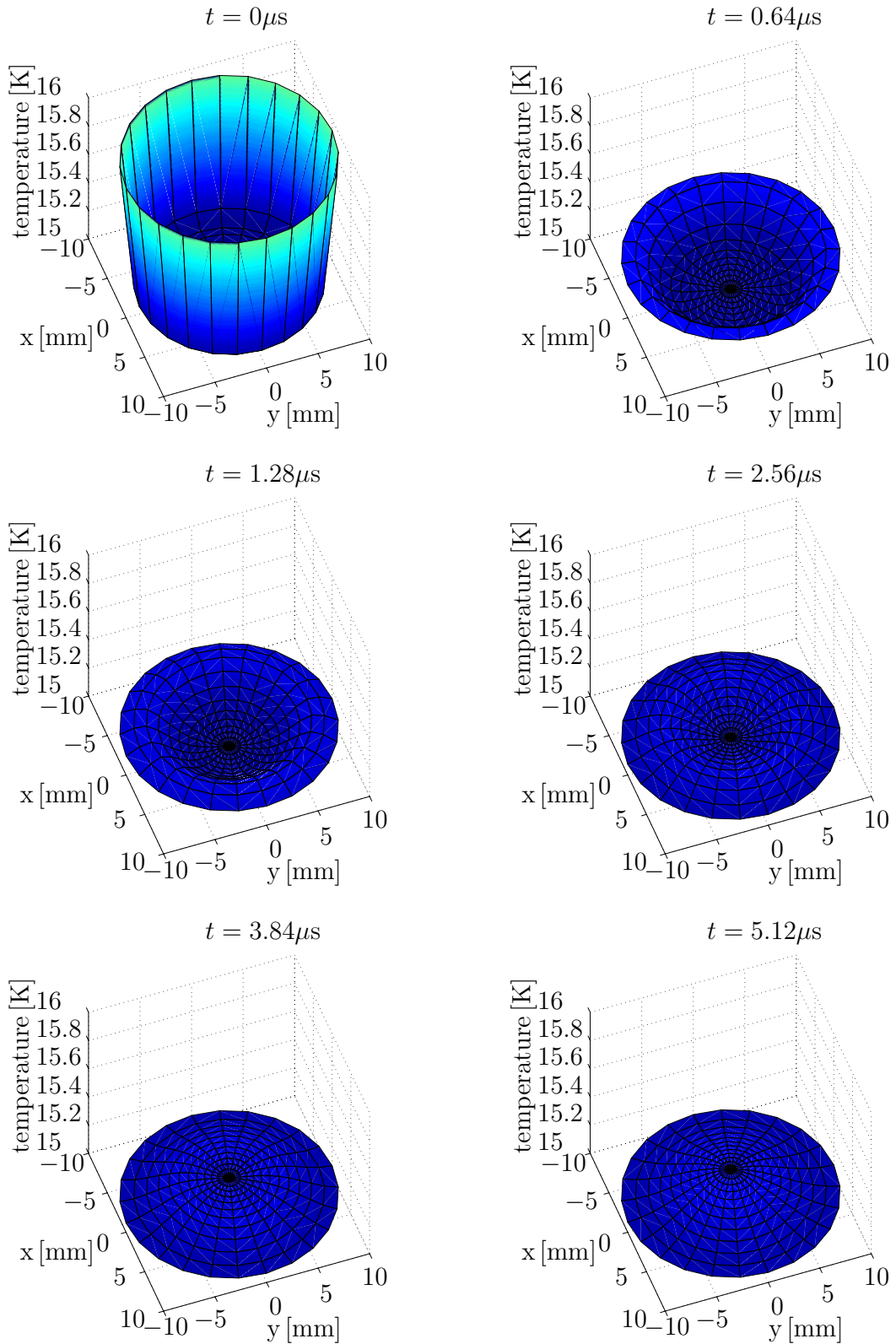


Figure 5.20.: Heat conduction in a two-dimensional disc of NaF according to type III. A heat pulse of 1 K is initiated at the circle's boundary. The temperature distribution is plotted at times  $t = 0 \mu\text{s}$ ,  $t = 0.64 \mu\text{s}$ ,  $t = 1.28 \mu\text{s}$ ,  $t = 2.56 \mu\text{s}$ ,  $t = 3.84 \mu\text{s}$  and  $t = 5.12 \mu\text{s}$ .

## 5. *Theory of non-classical heat conduction*



## 6. Theory of non-classical thermo-hyperelasticity

In the previous Chapter 5 the Green–Naghdi approach is applied to the pure thermal problem. Now the thermal problem is coupled with the deformation process since the experiments clearly revealed the existence of additional elastic waves. In detail, a longitudinal elastic, a slower transverse elastic and a separate temperature wave have been observed. The quasistatic linear and the dynamic linear coupled problems are accounted for by Bargmann and Steinmann in [8] and in [10], respectively. These achievements form the basis for the extension to non-classical, (geometrically and constitutively) nonlinear thermoelasticity being treated in this chapter. The extension to the nonlinear case is reasonable due to the fact that many real-world engineering applications need nonlinear approximations for an adequate simulation.

Each of the three types is coupled with the balance of linear momentum (3.2.6) and the inertia terms are fully taken into consideration. The discretization methods already designed for the thermal problem are extended to the coupled problem and again the comparison of the results to experimental data proves the applicability of the suggested non-classical thermoelasticity model.

### 6.1. Governing constitutive equations

In the following, a finite, isotropic, geometrically nonlinear and elastic deformable solid  $\mathcal{B} \subset \mathbb{R}^n$ ,  $n \in \{1, 2, 3\}$ , is considered. The basic ideas and equations of Chapters 3 and 4 hold.

The governing equations will be formulated within the spatial motion problem with respect to the material reference, see Section 3.2. The constitutive equations are inserted into corresponding balance of entropy (3.2.12) multiplied by the absolute temperature  $\theta$

$$\begin{aligned} \rho_0 \theta D_t \eta &= -\theta \operatorname{Div} \mathbf{H} + \rho_0 \theta [s + \xi] \\ &= -\operatorname{Div} \mathbf{Q} + \mathbf{H} \cdot \nabla_{\mathbf{X}} \theta + \rho_0 \theta [s + \xi]. \end{aligned} \quad (6.1.1)$$

#### 6.1.1. Type I

The absolute temperature  $\theta$  and the empirical temperature  $T$  are equivalent, as in the pure thermal case

$$\theta := T.$$

## 6. Theory of non-classical thermo-hyperelasticity

The free energy density  $\psi$  of the Neo–Hooke type is assumed to be

$$\begin{aligned} \rho_0\psi &:= \frac{\mu}{2} [\mathbf{C} - \mathbf{I}] : \mathbf{I} + \frac{\lambda}{2} \ln^2 J - \mu \ln J + \rho_0 c \left[ T - T_0 - T \ln \frac{T}{T_0} \right] \\ &\quad - 3wK [T - T_0] \frac{\ln J}{J} - [T - T_0] S_0, \end{aligned} \quad (6.1.2)$$

with  $\lambda$  and  $\mu$  denoting the Lamé constants and  $w$  and  $K$  are the thermal expansion coefficient and the bulk modulus. The Jacobideterminant  $J$  can be calculated via  $J = \sqrt{\det \mathbf{C}} = \det \mathbf{F}$ . The heat flux vector is assumed to be isotropic in the reference configuration  $\mathcal{B}_0$  in order to obtain a clearer analysis in the context of material forces given in Section 6.4.3, thus

$$\mathbf{Q} := -\kappa_1 \nabla_{\mathbf{X}} T. \quad (6.1.3)$$

Consequently, the spatial heat flux vector represents an anisotropic behavior  $\mathbf{q} = -j\kappa_1 \mathbf{F} \cdot \mathbf{F}^t \cdot \nabla_{\mathbf{x}} T$ . The internal dissipation  $\rho_0\theta\xi$ , the entropy density  $\eta$  and the first Piola–Kirchhoff stress tensor  $\mathbf{P}$  with respect to the material reference read

$$\begin{aligned} \rho_0\theta\xi &= -\mathbf{H} \cdot \nabla_{\mathbf{X}} T, \\ \rho_0\eta &= -\frac{1}{\frac{\partial \theta}{\partial T}} \frac{\partial(\rho_0\psi)}{\partial T} = 3wK \frac{\ln J}{J} + \rho_0 c \ln \frac{T}{T_0} + S_0 \\ \mathbf{P} &= \frac{\partial(\rho_0\psi)}{\partial \mathbf{F}} = [\lambda \ln J - \mu] \mathbf{F}^{-t} + \mu \mathbf{F} - \frac{3wK}{J} [T - T_0] [1 - \ln J] \mathbf{F}^{-t}. \end{aligned} \quad (6.1.4)$$

The time derivative of the entropy density  $\eta$  renders

$$\rho_0\dot{\eta} = \rho_0 \frac{\partial \eta}{\partial T} \dot{T} + \rho_0 \frac{\partial \eta}{\partial \mathbf{F}} : \dot{\mathbf{F}} = \rho_0 \frac{\partial \eta}{\partial T} \dot{T} - \frac{\partial \mathbf{P}}{\partial T} : \dot{\mathbf{F}} \quad (6.1.5)$$

since  $\eta$  is thermodynamically conjugated to the empirical temperature  $T$  in the same way the first Piola–Kirchhoff stress  $\mathbf{P}$  is conjugated to the deformation gradient  $\mathbf{F}$ , see Section 4.2.1. Inserting relation (6.1.5) and the constitutive equations into Eq. (6.1.1) yields

$$\rho_0 c \dot{T} = -\text{Div} \mathbf{Q} + \rho_0 r + T \frac{\partial \mathbf{P}}{\partial T} : \dot{\mathbf{F}} \quad (6.1.6)$$

The thermomechanical coupling term  $\mathcal{Q}_0^{\text{mech}} = T \frac{\partial \mathbf{P}}{\partial T} : \dot{\mathbf{F}}$  is responsible for the Gough–Joule effect, i.e. when deformations lead to structural heating. An investigation of a type I-material in the context of the material force method can be found in Kuhl et al. [89].

### 6.1.2. Type II

In the following, the constitutive laws determining the material response for a Green–Naghdi continuum of type II are suggested

$$\begin{aligned} \theta &:= T, \\ \rho_0\psi &:= \frac{\mu}{2} [\mathbf{C} - \mathbf{I}] : \mathbf{I} + \frac{\lambda}{2} \ln^2 J - \mu \ln J + \rho_0 c \left[ T - T_0 - T \ln \frac{T}{T_0} \right] \\ &\quad - 3wK [T - T_0] \frac{\ln J}{J} - [T - T_0] S_0 + \frac{\kappa_2}{2} \nabla_{\mathbf{X}} \alpha \cdot \nabla_{\mathbf{X}} \alpha. \end{aligned} \quad (6.1.7)$$

Application of the relations derived in Section 4.2.2 yields

$$\begin{aligned}
 \mathbf{H} &= -\kappa_2 \nabla_{\mathbf{X}} \alpha, \\
 \xi &= 0, \\
 \rho_0 \eta &= 3wK \frac{\ln J}{J} + c\rho_0 \ln \frac{T}{T_0} + S_0, \\
 \mathbf{P} &= \frac{\partial [\rho_0 \psi]}{\partial \mathbf{F}} \\
 &= [\lambda \ln J - \mu] \mathbf{F}^{-t} + \mu \mathbf{F} - \frac{3wK}{J} [T - T_0] [1 - \ln J] \mathbf{F}^{-t}. \quad (6.1.8)
 \end{aligned}$$

As in the thermal case (cf. Section 5.1.2), the free energy density  $\psi$  is chosen to be independent of the thermal displacement  $\alpha$  leading to a theory without energy dissipation. Furthermore, this choice of  $\psi$  leads to an entropy density  $\eta = \eta(T, \mathbf{F})$  only depending on  $T$  and  $\mathbf{F}$ . Thus, the time derivative of the entropy density  $\eta$  yields

$$\dot{\eta} = \frac{\partial \eta}{\partial T} \dot{T} + \frac{\partial \eta}{\partial \mathbf{F}} : \dot{\mathbf{F}} = \frac{\partial \eta}{\partial T} \dot{T} - \frac{\partial \mathbf{P}}{\partial T} : \dot{\mathbf{F}} = \frac{\partial \eta}{\partial T} \dot{T} - \frac{\partial \mathbf{P}}{\partial T} : \dot{\mathbf{F}}. \quad (6.1.9)$$

Analogously to type I, the constitutive equations are inserted into Eq. (3.2.12)

$$\rho_0 c \dot{T} = -T \text{Div} \mathbf{H} + \rho_0 r + T \frac{\partial \mathbf{P}}{\partial T} : \dot{\mathbf{F}}. \quad (6.1.10)$$

### 6.1.3. Type III

As mentioned before, the heat conduction theory of type III is a combination of the the classical Fourier theory (type I) and the theory without energy dissipation (type II). It contains both, type I and II, as special cases. In the following, it is coupled with the classical theory of mechanics. The free energy density  $\psi$  and the heat flux  $\mathbf{Q}$  are assumed to be functions of the thermal displacement  $\alpha$ , its gradient  $\nabla_{\mathbf{X}} \alpha$ , the temperature  $\dot{\alpha} = T$ , the right Cauchy–Green tensor  $\mathbf{C}$  and additionally on the temperature gradient  $\nabla_{\mathbf{X}} \dot{\alpha} = \nabla_{\mathbf{X}} T$ :

$$\begin{aligned}
 \theta &:= T, \\
 \rho_0 \psi &:= \frac{\mu}{2} [\mathbf{C} - \mathbf{I}] : \mathbf{I} + \frac{\lambda}{2} \ln^2 J - \mu \ln J + \rho_0 c \left[ T - T_0 - T \ln \frac{T}{T_0} \right] \\
 &\quad - 3wK [T - T_0] \frac{\ln J}{J} - [T - T_0] S_0, \\
 \mathbf{Q} &:= -\frac{1}{b} [\kappa_3 \nabla_{\mathbf{X}} \alpha + \kappa_4 \nabla_{\mathbf{X}} T]. \quad (6.1.11)
 \end{aligned}$$

Once more the absolute temperature is assumed to be equal to the empirical temperature, i.e.  $\theta = T$ . Note that, analogously to the thermal theory of type III (cf. Section 5.1.3), the thermal conductivities  $\kappa_3$  and  $\kappa_4$  are admitted to be positive or zero in order to include type

## 6. Theory of non-classical thermo-hyperelasticity

I and II as limiting cases of type III. However, for no position  $\mathbf{X}$  and no time  $t$  both,  $\kappa_3$  and  $\kappa_4$ , can be zero, i.e.  $\kappa_3 > 0 \vee \kappa_4 > 0 \forall \mathbf{X}, t$ .

Green and Naghdi [51] suggest a spatial heat flux vector based on the material thermal displacement gradient and the spatial temperature gradient. This relation is changed in this contribution for consistency reasons. Thus the spatial counterpart of  $\mathbf{Q}$  reads  $\mathbf{q} = -j/b\mathbf{F} \cdot \mathbf{F}^t \cdot [\kappa_3 \nabla_{\mathbf{x}} \alpha + \kappa_4 \nabla_{\mathbf{x}} T]$ . The remaining quantities are expressed as

$$\begin{aligned} \rho_0 \theta \xi &= -\mathbf{H} \cdot \nabla_{\mathbf{x}} T, \\ \rho_0 \eta &= 3wK \frac{\ln J}{J} + \rho_0 c \ln \frac{T}{T_0} + S_0, \\ \mathbf{P} &= [\lambda \ln J - \mu] \mathbf{F}^{-t} + \mu \mathbf{F} - \frac{3wK}{J} [T - T_0] [1 - \ln J] \mathbf{F}^{-t}. \end{aligned} \quad (6.1.12)$$

Thus, one obtains the temperature equation

$$\rho_0 c \dot{T} = -\text{Div } \mathbf{Q} + \rho_0 r + T \frac{\partial \mathbf{P}}{\partial T} : \dot{\mathbf{F}}. \quad (6.1.13)$$

## 6.2. Finite element discretization

Like in the pure thermal case (cf. Section 5.2), the numerical discretization is done with Galerkin finite element methods. Again, the equations are first discretized in space with a Bubnov–Galerkin finite element approach and subsequently the temporal discretization, applying a temporal Galerkin time finite element method, is carried out.

### 6.2.1. Spatial discretization

First, the spatial weak forms of the balance of linear momentum and the temperature equation are stated as this is a prerequisite for the classical Bubnov–Galerkin finite element method.

#### Spatial motion problem

The balance of linear momentum (3.2.6) and the temperature equations (which, for brevity, are summarized in one general temperature equation without inserting the constitutive assumptions for the heat flux) are supplemented by appropriate boundary conditions for the mechanical and the thermal fields. For the deformation problem, the boundary  $\partial \mathcal{B}_0$  is subdivided into disjoint contributions, such that  $\partial \mathcal{B}_0^\sigma \cap \partial \mathcal{B}_0^t = \emptyset$  and  $\partial \mathcal{B}_0^\sigma \cup \partial \mathcal{B}_0^t = \partial \mathcal{B}_0$ . Correspondingly, for the thermal problem, the boundary  $\partial \mathcal{B}_0$  is decomposed into disjoint parts, such that  $\partial \mathcal{B}_0^\alpha \cap \partial \mathcal{B}_0^\theta = \emptyset$ ,  $\partial \mathcal{B}_0^\alpha \cap \partial \mathcal{B}_0^Q = \emptyset$ ,  $\partial \mathcal{B}_0^\theta \cap \partial \mathcal{B}_0^Q = \emptyset$  and  $\partial \mathcal{B}_0^\alpha \cup \partial \mathcal{B}_0^\theta \cup \partial \mathcal{B}_0^Q = \partial \mathcal{B}_0$ .

After integrating both equations and relation (3.1.7) over the material configuration  $\mathcal{B}_0$ , they are weighted with the vector- and scalar-valued test functions  $\delta \boldsymbol{\varphi} \in H_0^1(\mathcal{B}_0)$ ,  $\delta \alpha \in H_0^1(\mathcal{B}_0)$

and  $\delta T \in H_0^1(\mathcal{B}_0)$  and the divergence theorem is applied. Thus, the weak form of the spatial balance of momentum reads

$$\int_{\mathcal{B}_0} \delta \boldsymbol{\varphi} \cdot \rho_0 \dot{\boldsymbol{v}} \, dV + \int_{\mathcal{B}_0} \nabla_{\mathbf{x}} \delta \boldsymbol{\varphi} : \mathbf{P} \, dV - \int_{\mathcal{B}_0} \delta \boldsymbol{\varphi} \cdot [\rho_0 \mathbf{b}] \, dV - \int_{\partial \mathcal{B}_0^\varphi} \delta \boldsymbol{\varphi} \cdot \mathbf{P} \cdot \mathbf{N} \, dA = 0, \quad (6.2.1)$$

Moreover, the weak form of the temperature equation and the relation between the thermal displacement  $\alpha$  and the temperature  $T$  yield

$$\begin{aligned} \int_{\mathcal{B}_0} \delta T \rho_0 c \dot{T} \, dV - \int_{\mathcal{B}_0} \nabla_{\mathbf{x}} \delta T \cdot \mathbf{Q} \, dV - \int_{\mathcal{B}_0} \delta T [\mathbf{H} \cdot \nabla_{\mathbf{x}} \theta + \rho_0 \theta \xi] \, dV \\ - \int_{\mathcal{B}_0} \delta T [\rho_0 \theta s + \mathcal{Q}_0^{\text{mech}}] \, dV + \int_{\partial \mathcal{B}_0^\varphi} \delta T \mathbf{Q} \cdot \mathbf{N} \, dA = 0, \end{aligned} \quad (6.2.2)$$

and

$$\int_{\mathcal{B}_0} \delta \alpha [\dot{\alpha} - T] \, dV = 0. \quad (6.2.3)$$

### Material motion problem

Likewise, the boundary  $\partial \mathcal{B}_t$  of the current configuration  $\mathcal{B}_t$  is splitted such that  $\partial \mathcal{B}_t^\varphi \cap \partial \mathcal{B}_t^t = \emptyset$  and  $\partial \mathcal{B}_t^\varphi \cup \partial \mathcal{B}_t^t = \partial \mathcal{B}_t$  for the mechanical problem and  $\partial \mathcal{B}_t^\alpha \cap \partial \mathcal{B}_t^\theta = \emptyset$ ,  $\partial \mathcal{B}_t^\alpha \cap \partial \mathcal{B}_t^q = \emptyset$ ,  $\partial \mathcal{B}_t^\theta \cap \partial \mathcal{B}_t^t = \emptyset$  and  $\partial \mathcal{B}_t^\alpha \cup \partial \mathcal{B}_t^\theta \cup \partial \mathcal{B}_t^q = \partial \mathcal{B}_t$  for the thermal problem.

In complete analogy to the spatial motion problem, the balance of linear momentum, i.e. Eq. (3.2.14), and the general temperature equation of the material motion problem are integrated over the current domain  $\mathcal{B}_t$  and weighted by test functions  $\delta \Phi \in H_0^1(\mathcal{B}_t)$ ,  $\delta \alpha \in H_0^1(\mathcal{B}_t)$  and  $\delta T \in H_0^1(\mathcal{B}_t)$ . Consequently, one obtains

$$\begin{aligned} \int_{\mathcal{B}_t} \delta \Phi \cdot D_t(\rho_t \mathbf{C} \cdot \mathbf{V}) \, dv + \int_{\mathcal{B}_t} \nabla_{\mathbf{x}} \delta \Phi : \left[ \boldsymbol{\pi}^t - \frac{\rho_t \mathbf{V} \cdot \mathbf{C} \cdot \mathbf{V}}{2} \mathbf{F}^t \right] \, dv \\ - \int_{\mathcal{B}_t} \delta \Phi \cdot \left[ \rho_t \mathbf{B} + \frac{\partial \rho_t \mathbf{V} \cdot \mathbf{C} \cdot \mathbf{V}}{2 \partial \Phi} \right] \, dv - \int_{\partial \mathcal{B}_t^\Phi} \delta \Phi \cdot \left[ \boldsymbol{\pi}^t - \frac{\rho_t \mathbf{V} \cdot \mathbf{C} \cdot \mathbf{V}}{2} \right] \cdot \mathbf{n} \, da = 0. \end{aligned} \quad (6.2.4)$$

Remember,  $\boldsymbol{\pi}^t$  is the two-point static material motion flux given by  $\boldsymbol{\pi}^t = \rho_t \partial \psi / \partial \mathbf{f}$  and the material velocity  $\mathbf{V}$  is related to the spatial velocity  $\mathbf{v}$  by  $\mathbf{V} = -\mathbf{F}^{-1} \cdot \mathbf{v}$  (see Chapter 3.1). Furthermore, one gets

$$\begin{aligned} \int_{\mathcal{B}_t} \delta T \rho_t c \dot{T} \, dv - \int_{\mathcal{B}_t} \nabla_{\mathbf{x}} \delta T \cdot \mathbf{q} \, dv - \int_{\mathcal{B}_t} \delta T [\mathbf{h} \cdot \nabla_{\mathbf{x}} \theta + \rho_t \theta \xi] \, dv \\ - \int_{\mathcal{B}_t} \delta T [\rho_t \theta s + \mathcal{Q}_t^{\text{mech}}] \, dv + \int_{\partial \mathcal{B}_t^q} \delta T \mathbf{q} \cdot \mathbf{n} \, da = 0, \end{aligned} \quad (6.2.5)$$

## 6. Theory of non-classical thermo-hyperelasticity

$$\int_{\mathcal{B}_t} \delta\alpha[\dot{\alpha} - T] dv = 0. \quad (6.2.6)$$

**Remark:** Note that the scalar-valued test functions  $\delta\alpha$  and  $\delta T$  testing relation (3.1.7) and the temperature equation are identical for the spatial and the material motion problem. The mechanical test functions  $\delta\varphi$  and  $\delta\Phi$  are related via  $\delta\varphi = -\delta\Phi \cdot \mathbf{F}^t$ .

### 6.2.1.1. Spatial discretization

#### Spatial motion problem

In complete analogy to the thermal case, the reference domain  $\mathcal{B}_0$  is discretized into  $n_{el}$  finite elements  $\mathcal{B}_0^e$  with  $\mathcal{B}_0 = \bigcup_{e=1}^{n_{el}} \mathcal{B}_0^e$ . Applying the isoparametric concept, the unknowns  $\varphi$ , the thermal displacement  $\alpha$  and the temperature  $T$  as well as the test functions  $\delta\varphi$ ,  $\delta\alpha$  and  $\delta T$  are interpolated with shape functions  $N_\varphi^i$  and  $N_\theta^i$ . Thus, they are approximated as follows

$$\begin{aligned} \varphi^h|_{\mathcal{B}_0^e} &= \sum_{i=1}^{n_{en}} N_\varphi^i \varphi_i, & \delta\varphi^h|_{\mathcal{B}_0^e} &= \sum_{i=1}^{n_{en}} N_\varphi^i \delta\varphi_i, \\ \alpha^h|_{\mathcal{B}_0^e} &= \sum_{i=1}^{n_{en}} N_\theta^i \alpha_i, & \delta\alpha^h|_{\mathcal{B}_0^e} &= \sum_{i=1}^{n_{en}} N_\theta^i \delta\alpha_i, \\ T^h|_{\mathcal{B}_0^e} &= \sum_{i=1}^{n_{en}} N_\theta^i T_i, & \delta T^h|_{\mathcal{B}_0^e} &= \sum_{i=1}^{n_{en}} N_\theta^i \delta T_i. \end{aligned} \quad (6.2.7)$$

The expressions for the discrete gradients of the primary unknowns  $\nabla_{\mathbf{X}}\varphi$ ,  $\nabla_{\mathbf{X}}\alpha$ ,  $\nabla_{\mathbf{X}}T$  and those of the test functions  $\nabla_{\mathbf{X}}\delta\varphi$ ,  $\nabla_{\mathbf{X}}\delta\alpha$ ,  $\nabla_{\mathbf{X}}\delta T$  yield

$$\begin{aligned} \nabla_{\mathbf{X}}\varphi^h|_{\mathcal{B}^e} &= \sum_{i=1}^{n_{en}} \varphi_i \otimes \nabla_{\mathbf{X}}N^i, & \nabla_{\mathbf{X}}\delta\varphi^h|_{\mathcal{B}^e} &= \sum_{i=1}^{n_{en}} \delta\varphi_i \otimes \nabla_{\mathbf{X}}N^i, \\ \nabla_{\mathbf{X}}\alpha^h|_{\mathcal{B}^e} &= \sum_{i=1}^{n_{en}} \alpha_i \nabla_{\mathbf{X}}N^i, & \nabla_{\mathbf{X}}\delta\alpha^h|_{\mathcal{B}^e} &= \sum_{i=1}^{n_{en}} \delta\alpha_i \nabla_{\mathbf{X}}N^i, \\ \nabla_{\mathbf{X}}T^h|_{\mathcal{B}^e} &= \sum_{i=1}^{n_{en}} T_i \nabla_{\mathbf{X}}N^i, & \nabla_{\mathbf{X}}\delta T^h|_{\mathcal{B}^e} &= \sum_{i=1}^{n_{en}} \delta T_i \nabla_{\mathbf{X}}N^i. \end{aligned} \quad (6.2.8)$$

The discrete gradient of the spatial motion  $\nabla_{\mathbf{X}}\varphi^h|_{\mathcal{B}^e}$  corresponds to the discrete spatial deformation gradient  $\mathbf{F}^h|_{\mathcal{B}^e} = \nabla_{\mathbf{X}}\varphi^h|_{\mathcal{B}^e}$ .

Thus, the following semi-discretized system of equations is received:

$$\begin{aligned} \mathbf{f}_{\text{dyn}}^{\varphi h} + \mathbf{f}_{\text{int}}^{\varphi h} - \mathbf{f}_{\text{sur}}^{\varphi h} - \mathbf{f}_{\text{vol}}^{\varphi h} &= \mathbf{0}, \\ \mathbf{f}_{\text{dyn}}^{\theta h} + \mathbf{f}_{\text{int}}^{\theta h} + \mathbf{f}_{\text{con}}^{\theta h} - \mathbf{f}_{\text{sur}}^{\theta h} - \mathbf{f}_{\text{vol}}^{\theta h} &= \mathbf{0}, \\ \dot{\alpha} - T &= \mathbf{0}. \end{aligned} \quad (6.2.9)$$

Again,  $\alpha = \{\alpha_i\}$  and  $T = \{T_i\}$  denote the global node vectors of the thermal displacement and the temperature, respectively.

Considering the arbitrariness of the test functions  $\delta\varphi$ ,  $\delta\alpha$  and  $\delta T$ , the semi-discrete inertia forces, the internal forces, the surface forces and the volume forces of the balance of linear momentum are computed as

$$\begin{aligned} \mathbf{f}_{\text{dyn}}^{\varphi h} &= \mathbf{A} \sum_{e=1}^{n_{\text{el}}} \sum_{i=1}^{n_{\text{en}}} \int_{\mathcal{B}_0^e} N_\varphi^i \rho_0 \dot{\mathbf{v}} \, dV, & \mathbf{f}_{\text{int}}^{\varphi h} &= \mathbf{A} \sum_{e=1}^{n_{\text{el}}} \sum_{i=1}^{n_{\text{en}}} \int_{\mathcal{B}_0^e} \mathbf{P} \cdot \nabla_{\mathbf{X}} N_\varphi^i \, dV, \\ \mathbf{f}_{\text{sur}}^{\varphi h} &= \mathbf{A} \sum_{e=1}^{n_{\text{el}}} \sum_{i=1}^{n_{\text{en}}} \int_{\partial \mathcal{B}_0^{\varphi, e}} N_\varphi^i \mathbf{P} \cdot \mathbf{N} \, dA, & \mathbf{f}_{\text{vol}}^{\varphi h} &= \mathbf{A} \sum_{e=1}^{n_{\text{el}}} \sum_{i=1}^{n_{\text{en}}} \int_{\mathcal{B}_0^e} N_\varphi^i \rho_0 \mathbf{b} \, dV. \end{aligned} \quad (6.2.10)$$

The dynamic, the internal, the surface and the volume contribution of the thermal problem read

$$\begin{aligned} \mathbf{f}_{\text{dyn}}^{\theta h} &= \mathbf{A} \sum_{e=1}^{n_{\text{el}}} \sum_{i,j=1}^{n_{\text{en}}} \int_{\mathcal{B}_0^e} N_\theta^i \rho_0 c N_\theta^j \, dV \dot{T}_j, & \mathbf{f}_{\text{int}}^{\theta h} &= -\mathbf{A} \sum_{e=1}^{n_{\text{el}}} \sum_{i=1}^{n_{\text{en}}} \int_{\mathcal{B}_0^e} \nabla_{\mathbf{X}} N_\theta^i \cdot \mathbf{Q} \, dV, \\ \mathbf{f}_{\text{sur}}^{\theta h} &= -\mathbf{A} \sum_{e=1}^{n_{\text{el}}} \sum_{i=1}^{n_{\text{en}}} \int_{\partial \mathcal{B}_0^{Q, e}} N_\theta^i \mathbf{Q} \cdot \mathbf{N} \, dA, & \mathbf{f}_{\text{vol}}^{\theta h} &= \mathbf{A} \sum_{e=1}^{n_{\text{el}}} \sum_{i=1}^{n_{\text{en}}} \int_{\mathcal{B}_0^e} N_\theta^i [\rho_0 \theta_s + \rho_0 \theta \xi + \mathcal{Q}_0^{\text{mech}}] \, dV, \\ \mathbf{f}_{\text{con}}^{\theta h} &= -\mathbf{A} \sum_{e=1}^{n_{\text{el}}} \sum_{i=1}^{n_{\text{en}}} \int_{\mathcal{B}_0^e} N_\theta^i \mathbf{H} \cdot \nabla_{\mathbf{X}} \theta \, dV. \end{aligned} \quad (6.2.11)$$

### Material motion problem

The current solution domain  $\mathcal{B}_t$  is likewise discretized into  $n_{\text{el}}$  finite elements  $\mathcal{B}_t^e$ . Again following the way of Bubnov–Galerkin methods, the unknowns  $\Phi$ , the thermal displacement  $\alpha$  and the temperature  $T$  as well as the test functions  $\delta\Phi$ ,  $\delta\alpha$  and  $\delta T$  are interpolated with shape functions  $N_\Phi^i$  and  $N_\theta^i$ .

$$\begin{aligned} \Phi^h|_{\mathcal{B}_t^e} &= \sum_{i=1}^{n_{\text{en}}} N_\Phi^i \Phi_i, & \delta\Phi^h|_{\mathcal{B}_t^e} &= \sum_{i=1}^{n_{\text{en}}} N_\Phi^i \delta\Phi_i, \\ \alpha^h|_{\mathcal{B}_t^e} &= \sum_{i=1}^{n_{\text{en}}} N_\theta^i \alpha_i, & \delta\alpha^h|_{\mathcal{B}_t^e} &= \sum_{i=1}^{n_{\text{en}}} N_\theta^i \delta\alpha_i, \\ T^h|_{\mathcal{B}_t^e} &= \sum_{i=1}^{n_{\text{en}}} N_\theta^i T_i, & \delta T^h|_{\mathcal{B}_t^e} &= \sum_{i=1}^{n_{\text{en}}} N_\theta^i \delta T_i. \end{aligned} \quad (6.2.12)$$

The semi-discrete balance of pseudomomentum and the semi-discrete temperature equation

## 6. Theory of non-classical thermo-hyperelasticity

of the material motion problem can be expressed as

$$\begin{aligned} \mathbf{F}_{\text{dyn}}^{\varphi h} + \mathbf{F}_{\text{int}}^{\varphi h} - \mathbf{F}_{\text{sur}}^{\varphi h} - \mathbf{F}_{\text{vol}}^{\varphi h} &= \mathbf{0}, \\ \mathbf{F}_{\text{dyn}}^{\theta h} + \mathbf{F}_{\text{int}}^{\theta h} + \mathbf{F}_{\text{con}}^{\theta h} - \mathbf{F}_{\text{sur}}^{\theta h} - \mathbf{F}_{\text{vol}}^{\theta h} &= \mathbf{0}, \\ \dot{\boldsymbol{\alpha}} - \mathbf{T} &= \mathbf{0}. \end{aligned} \quad (6.2.13)$$

Herein, the semi-discrete inertia forces, the internal forces, the surface forces and the volume forces of the balance of linear momentum take the expression

$$\begin{aligned} \mathbf{F}_{\text{dyn}}^{\Phi h} &= \mathbf{A} \sum_{e=1}^{n_{\text{el}}} \sum_{i=1}^{n_{\text{en}}} \int_{\mathcal{B}_t^e} N_{\Phi}^i \rho_t D_t(\mathbf{C} \cdot \mathbf{V}) \, dv, \\ \mathbf{F}_{\text{int}}^{\Phi h} &= \mathbf{A} \sum_{e=1}^{n_{\text{el}}} \sum_{i=1}^{n_{\text{en}}} \int_{\mathcal{B}_t^e} \left[ \boldsymbol{\pi}^t - \frac{\rho_t \mathbf{V} \cdot \mathbf{C} \cdot \mathbf{V}}{2} \mathbf{F}^t \right] \cdot \nabla_{\mathbf{x}} N_{\Phi}^i \, dv, \\ \mathbf{F}_{\text{sur}}^{\Phi h} &= \mathbf{A} \sum_{e=1}^{n_{\text{el}}} \sum_{i=1}^{n_{\text{en}}} \int_{\partial \mathcal{B}_t^{\Phi, e}} N_{\Phi}^i \left[ \boldsymbol{\pi}^t - \frac{\rho_t \mathbf{V} \cdot \mathbf{C} \cdot \mathbf{V}}{2} \mathbf{F}^t \right] \cdot \mathbf{n} \, da, \\ \mathbf{F}_{\text{vol}}^{\Phi h} &= \mathbf{A} \sum_{e=1}^{n_{\text{el}}} \sum_{i=1}^{n_{\text{en}}} \int_{\mathcal{B}_t^e} N_{\Phi}^i \left[ \rho_t \mathbf{B} + \frac{\partial \rho_t \mathbf{V} \cdot \mathbf{C} \cdot \mathbf{V}}{2 \partial \Phi} \right] \, dv. \end{aligned} \quad (6.2.14)$$

whereas the dynamic, the internal, the surface and the volume contribution of the thermal problem are given by

$$\begin{aligned} \mathbf{F}_{\text{dyn}}^{\theta h} &= \mathbf{A} \sum_{e=1}^{n_{\text{el}}} \sum_{i,j=1}^{n_{\text{en}}} \int_{\mathcal{B}_t^e} N_{\theta}^i \rho_t c N_{\theta}^j \, dv \, \dot{T}_j, & \mathbf{F}_{\text{int}}^{\theta h} &= -\mathbf{A} \sum_{e=1}^{n_{\text{el}}} \sum_{i=1}^{n_{\text{en}}} \int_{\mathcal{B}_t^e} \nabla_{\mathbf{x}} N_{\theta}^i \cdot \mathbf{q} \, dv, \\ \mathbf{F}_{\text{sur}}^{\theta h} &= -\mathbf{A} \sum_{e=1}^{n_{\text{el}}} \sum_{i=1}^{n_{\text{en}}} \int_{\partial \mathcal{B}_t^{\theta, e}} N_{\theta}^i \mathbf{q} \cdot \mathbf{n} \, da, & \mathbf{F}_{\text{vol}}^{\theta h} &= \mathbf{A} \sum_{e=1}^{n_{\text{el}}} \sum_{i=1}^{n_{\text{en}}} \int_{\mathcal{B}_t^e} N_{\theta}^i \left[ \rho_t \theta s + \rho_t \theta \xi + Q_t^{\text{mech}} \right] \, dv, \\ \mathbf{F}_{\text{con}}^{\theta h} &= -\mathbf{A} \sum_{e=1}^{n_{\text{el}}} \sum_{i=1}^{n_{\text{en}}} \int_{\mathcal{B}_t^e} N_{\theta}^i \mathbf{h} \cdot \nabla_{\mathbf{x}} \theta \, dv. \end{aligned} \quad (6.2.15)$$

As opposed to the spatial motion problem, in the material motion problem the Neumann boundary conditions are usually not given as input data. Therefore, the material forces are generally computed in a postprocessing step, see Section 6.4.3.

### 6.2.2. Temporal discretization

In a next step, the governing equations are discretized in time. As in the thermal case, it is resorted to Galerkin finite element methods in time as well. For general information on and basic relations in Galerkin temporal finite element methods, the reader is referred to the Section 5.2.2.



Analogously to the spatial finite element method, the weak form is constructed by multiplying with test functions  $\delta \mathbf{T}_*$ ,  $\delta \boldsymbol{\alpha}_*$ ,  $\delta \Phi_*$  and  $\delta \boldsymbol{\varphi}_*$  and integrating over the time domain  $I = [t_0, t_e]$ . Therefore, the time element weak form of the governing semi-discrete system of equations (6.2.9) and (6.2.13) can be expressed by:

$$h_n \int_0^1 \delta \boldsymbol{\varphi}_* \cdot [\mathbf{f}_{\text{dyn}}^{\varphi h} + \mathbf{f}_{\text{int}}^{\varphi h} - \mathbf{f}_{\text{sur}}^{\varphi h} - \mathbf{f}_{\text{vol}}^{\varphi h}] \, d\tau = 0, \quad (6.2.16)$$

$$h_n \int_0^1 \delta \mathbf{T}_* \cdot [\mathbf{f}_{\text{dyn}}^{\theta h} + \mathbf{f}_{\text{int}}^{\theta h} + \mathbf{f}_{\text{con}}^{\theta h} - \mathbf{f}_{\text{sur}}^{\theta h} - \mathbf{f}_{\text{vol}}^{\theta h}] \, d\tau = 0, \quad (6.2.17)$$

$$h_n \int_0^1 \delta \boldsymbol{\alpha}_* \cdot [\dot{\boldsymbol{\alpha}} - \mathbf{T}] \, d\tau = 0, \quad (6.2.18)$$

$$h_n \int_0^1 \delta \Phi_* \cdot [\mathbf{F}_{\text{dyn}}^{\Phi h} + \mathbf{F}_{\text{int}}^{\Phi h} - \mathbf{F}_{\text{sur}}^{\Phi h} - \mathbf{F}_{\text{vol}}^{\Phi h}] \, d\tau = 0, \quad (6.2.19)$$

$$h_n \int_0^1 \delta \mathbf{T}_* \cdot [\mathbf{F}_{\text{dyn}}^{\theta h} + \mathbf{F}_{\text{int}}^{\theta h} + \mathbf{F}_{\text{con}}^{\theta h} - \mathbf{F}_{\text{sur}}^{\theta h} - \mathbf{F}_{\text{vol}}^{\theta h}] \, d\tau = 0. \quad (6.2.20)$$

Each of the equations is discretized with a temporal Galerkin finite element method. The test functions are approximated piecewise by polynomial shape functions  $\tilde{M}_i$ , see Definition 5.2.23. Thus, the temporal test functions  $\delta \boldsymbol{\alpha}_*$ ,  $\delta \mathbf{T}_*$ ,  $\delta \boldsymbol{\varphi}_*$  and  $\delta \Phi_*$  are of the format:

$$\begin{aligned} \delta \boldsymbol{\alpha}_*^h(\tau) |_{I_n} &= \sum_{i=1}^k \tilde{M}_i \delta \boldsymbol{\alpha}^i, & \delta \mathbf{T}_*^h(\tau) |_{I_n} &= \sum_{i=1}^k \tilde{M}_i \delta \mathbf{T}^i, \\ \delta \boldsymbol{\varphi}_*^h(\tau) |_{I_n} &= \sum_{i=1}^k \tilde{M}_i \delta \boldsymbol{\varphi}^i, & \delta \Phi_*^h(\tau) |_{I_n} &= \sum_{i=1}^k \tilde{M}_i \delta \Phi^i. \end{aligned} \quad (6.2.21)$$

Inserting (6.2.21) into Eqs. (6.2.16)–(6.2.20) leads to the fully discretized systems of equations:

$$\mathbf{r}_i^{\varphi} = h_n \int_0^1 \tilde{M}_i [\mathbf{f}_{\text{dyn}}^{\varphi h} + \mathbf{f}_{\text{int}}^{\varphi h} - \mathbf{f}_{\text{sur}}^{\varphi h} - \mathbf{f}_{\text{vol}}^{\varphi h}] \, d\tau = \mathbf{0}, \quad (6.2.22)$$

$$\mathbf{r}_i^{\theta} = h_n \int_0^1 \tilde{M}_i [\mathbf{f}_{\text{dyn}}^{\theta h} + \mathbf{f}_{\text{int}}^{\theta h} + \mathbf{f}_{\text{con}}^{\theta h} - \mathbf{f}_{\text{sur}}^{\theta h} - \mathbf{f}_{\text{vol}}^{\theta h}] \, d\tau = \mathbf{0}, \quad (6.2.23)$$

$$\mathbf{r}_i^{\alpha} = h_n \int_0^1 \tilde{M}_i [\dot{\boldsymbol{\alpha}} - \mathbf{T}] \, d\tau = \mathbf{0}, \quad (6.2.24)$$

$$\mathbf{R}_i^{\Phi} = h_n \int_0^1 \tilde{M}_i [\mathbf{F}_{\text{dyn}}^{\Phi h} + \mathbf{F}_{\text{int}}^{\Phi h} - \mathbf{F}_{\text{sur}}^{\Phi h} - \mathbf{F}_{\text{vol}}^{\Phi h}] \, d\tau = \mathbf{0}, \quad (6.2.25)$$

$$\mathbf{R}_i^{\theta} = h_n \int_0^1 \tilde{M}_i [\mathbf{F}_{\text{dyn}}^{\theta h} + \mathbf{F}_{\text{int}}^{\theta h} + \mathbf{F}_{\text{con}}^{\theta h} - \mathbf{F}_{\text{sur}}^{\theta h} - \mathbf{F}_{\text{vol}}^{\theta h}] \, d\tau = \mathbf{0}, \quad (6.2.26)$$

for all  $i = 1, \dots, k$ . Eqs. (6.2.22), (6.2.23) and (6.2.24), resp. Eqs. (6.2.24), (6.2.25) and (6.2.26), represent fully discretized coupled nonlinear systems of equations which govern the spatial resp. the material motion problem of Green–Naghdi thermoelasticity.

Now, the constitutive assumptions for the heat fluxes of type I, II and III are inserted. As

## 6. Theory of non-classical thermo-hyperelasticity

already mentioned in Chapter 5, the resulting heat equation of type I (Eq. (6.1.6)) is parabolic, the one of type II (Eq. (6.1.10)) is hyperbolic and the mathematical property of the one of type III (Eq. (6.1.13)) depends on the values of  $\kappa_3$  and  $\kappa_4$ . For all three types, the balance of momentum is hyperbolic. Therefore, a different treatment concerning the temporal discretization is reasonable, see also Section 5.2.2. A mixed Galerkin finite element method in time for the governing equations of type I as it has proven to suit well for mixed parabolic and hyperbolic problems. The problems of type II and III are discretized with continuous Galerkin finite elements in time.

### 6.2.2.1. Mixed Galerkin time finite element method

The mixed Galerkin time finite element method of order  $k$  is based on the idea that the test functions are approximated piecewise by polynomials of degree  $k - 1$ . The trial function  $\varphi$  of the hyperbolic balance of linear momentum is approximated piecewise and continuously by polynomials of order  $k$ , whereas the trial function  $T$  of the parabolic equation is discretized piecewise with polynomials of degree  $k - 1$  which are discontinuous across the element boundaries. Consequently, the trial functions can be written in the following format:

$$\mathbf{T}^h(\tau)|_{I_n} = \sum_{i=1}^k \tilde{M}_i(\tau) \mathbf{T}^i \quad \bar{\varphi}^h(\tau)|_{I_n} = \sum_{i=1}^{k+1} M_i(\tau) \bar{\varphi}^i. \quad (6.2.27)$$

The global node vectors of the spatial placement is denoted by  $\bar{\varphi} = \{\varphi_i\}$ . In other words, the mG( $k$ )-discretization of the coupled thermoelastic problem of type I is based on the idea of a cG( $k$ )-discretized balance of momentum and a dG( $k$ )-discretized heat equation.

In order to prevent that the trial functions of the temperature are over-determined at the boundary nodal values, once more a discontinuity is admitted (cf. Figure 5.5). Again,  $[[\mathbf{T}^h]] = \mathbf{T}_1 - \mathbf{T}_0$  denotes the amount of the jump at the local time node  $\tau = 0$ .  $\mathbf{T}_0$  is the known value at local time node  $\tau = 0$  from the previous time step, whereas  $\mathbf{T}_1$  is the unknown value at  $\tau = 0$  from the present time step. Thus, those terms which are linear in the empirical temperature  $T$  and the spatial positions  $\varphi$  can be discretized further:

$$\begin{aligned} h_n \int_0^1 \tilde{M}_i \mathbf{f}_{\text{dyn}}^{\varphi h} d\tau &= h_n \sum_{j=1}^{k+1} \int_0^1 \tilde{M}_i \left[ \mathbf{A}_{e=1}^{n_{\text{el}}} \sum_{m,n=1}^{n_{\text{en}}} \int_{\mathcal{B}_0^e} N_\varphi^m \rho_0 \mathbf{I} N_\varphi^n dV \right] M_j'' d\tau \cdot \bar{\varphi}^j, \\ h_n \int_0^1 \tilde{M}_i \mathbf{f}_{\text{dyn}}^{\theta h} d\tau &= h_n \sum_{j=1}^{k+1} \int_0^1 \tilde{M}_i \left[ \mathbf{A}_{e=1}^{n_{\text{el}}} \sum_{m,n=1}^{n_{\text{en}}} \int_{\mathcal{B}_0^e} N_\theta^m \rho_0 c \mathbf{I} N_\theta^n dV \right] \tilde{M}_j' d\tau \cdot \mathbf{T}^j, \\ h_n \int_0^1 \tilde{M}_i \mathbf{f}_{\text{int}}^{\theta h} d\tau &= h_n \sum_{j=1}^{k+1} \int_0^1 \tilde{M}_i \left[ \mathbf{A}_{e=1}^{n_{\text{el}}} \sum_{m,n=1}^{n_{\text{en}}} \int_{\mathcal{B}_0^e} \nabla_{\mathbf{X}} N_\theta^m \cdot \kappa_1 \mathbf{I} \cdot \nabla_{\mathbf{X}} N_\theta^n dV \right] \tilde{M}_j d\tau \cdot \mathbf{T}^j. \end{aligned} \quad (6.2.28)$$

### 6.2.2.2. Continuous Galerkin time finite element method

As mentioned above, the continuous Galerkin method of order  $k$  is applied to the coupled thermoelastic problems of type II and III. The piecewise, continuously approximation of trial

functions consists of polynomials of degree  $k$  whereas the test functions are approximated piecewise by polynomials of degree  $k-1$  which are discontinuous across the element boundaries. The shape functions  $M_i$  are defined in Eq. (5.2.17), approximate the trial functions  $\alpha^h$ ,  $\mathbf{T}^h$  and  $\bar{\varphi}^h$  continuously across the element boundaries

$$\alpha^h(\tau)|_{I_n} = \sum_{i=1}^{k+1} M_i \alpha^i, \quad \mathbf{T}^h(\tau)|_{I_n} = \sum_{i=1}^{k+1} M_i \mathbf{T}^i, \quad \bar{\varphi}^h(\tau)|_{I_n} = \sum_{i=1}^{k+1} M_i \bar{\varphi}^i. \quad (6.2.29)$$

Again, those terms which are linear in the thermal displacement  $\alpha$ , the empirical temperature  $T$  and the spatial placement  $\varphi$  can be discretized further. For type II and III, one obtains

$$\begin{aligned} h_n \int_0^1 \tilde{M}_i \mathbf{f}_{\text{dyn}}^{\varphi h} d\tau &= h_n \sum_{j=1}^{k+1} \int_0^1 \tilde{M}_i \left[ \mathbf{A} \sum_{e=1}^{n_{\text{el}}} \sum_{m,n=1}^{n_{\text{en}}} \int_{\mathcal{B}_0^e} N_\varphi^m \rho_0 \mathbf{I} N_\varphi^n dV \right] M_j' d\tau \cdot \bar{\varphi}^j, \\ h_n \int_0^1 \tilde{M}_i \mathbf{f}_{\text{dyn}}^{\theta h} d\tau &= h_n \sum_{j=1}^{k+1} \int_0^1 \tilde{M}_i \left[ \mathbf{A} \sum_{e=1}^{n_{\text{el}}} \sum_{m,n=1}^{n_{\text{en}}} \int_{\mathcal{B}_0^e} N_\theta^m \rho_0 c \mathbf{I} N_\theta^n dV \right] M_j' d\tau \cdot \mathbf{T}^j, \\ h_n \int_0^1 \tilde{M}_i [\dot{\alpha} - \mathbf{T}] d\tau &= \sum_{j=1}^{k+1} \int_0^1 \tilde{M}_i M_j' d\tau \alpha_j + h_n \sum_{j=1}^{k+1} \int_0^1 \tilde{M}_i M_j d\tau \mathbf{T}^j, \end{aligned} \quad (6.2.30)$$

for all  $i = 1, \dots, k$ . Furthermore, for type III, one additionally has

$$\begin{aligned} h_n \int_0^1 \tilde{M}_i \mathbf{f}_{\text{int}}^{\theta h} d\tau &= h_n \sum_{j=1}^{k+1} \int_0^1 \tilde{M}_i \left[ \mathbf{A} \sum_{e=1}^{n_{\text{el}}} \sum_{m,n=1}^{n_{\text{en}}} \int_{\mathcal{B}_0^e} \nabla_{\mathbf{X}} N_\theta^m \cdot \frac{\kappa_3}{b} \mathbf{I} \cdot \nabla_{\mathbf{X}} N_\theta^n dV \right] M_j d\tau \cdot \alpha^j \\ &+ h_n \sum_{j=1}^{k+1} \int_0^1 \tilde{M}_i \left[ \mathbf{A} \sum_{e=1}^{n_{\text{el}}} \sum_{m,n=1}^{n_{\text{en}}} \int_{\mathcal{B}_0^e} \nabla_{\mathbf{X}} N_\theta^m \cdot \frac{\kappa_4}{b} \mathbf{I} \cdot \nabla_{\mathbf{X}} N_\theta^n dV \right] M_j d\tau \cdot \mathbf{T}^j, \end{aligned} \quad (6.2.31)$$

for all  $i = 1, \dots, k$ .

### 6.3. Newton–Raphson solution method

In the following, the more natural spatial motion problem is considered for the numerical simulations. In order to take the two-folded coupling fully into account, we solve the system of equations monolithically. The zeros of the residua  $\mathbf{r}^\varphi$ ,  $\mathbf{r}^\alpha$  and  $\mathbf{r}^\theta$  are found with the help of the Newton–Raphson algorithm. To find the solution at time  $t_n$ , one starts with an initial guess which is reasonable close to the supposed solution. The initial guess, resp. the  $k$ -th iterate, is then updated in an incremental iterative way, see Eq. (6.3.4). The  $k$ -th iterate of the Newton–Raphson iteration reads:

$$\begin{aligned} \mathbf{r}_n^{\varphi k} &= \mathbf{r}_n^{\varphi k-1} + d\mathbf{r}^\varphi \doteq \mathbf{0}, \\ \mathbf{r}_n^{\alpha k} &= \mathbf{r}_n^{\alpha k-1} + d\mathbf{r}^\alpha \doteq \mathbf{0}, \\ \mathbf{r}_n^{\theta k} &= \mathbf{r}_n^{\theta k-1} + d\mathbf{r}^\theta \doteq \mathbf{0}. \end{aligned} \quad (6.3.1)$$

## 6. Theory of non-classical thermo-hyperelasticity

Here,  $d\mathbf{r}^\varphi$ ,  $d\mathbf{r}^\alpha$  and  $d\mathbf{r}^\theta$  denote the iterative residua and take the following format

$$\begin{bmatrix} d\mathbf{r}^\varphi \\ d\mathbf{r}^\alpha \\ d\mathbf{r}^\theta \end{bmatrix} = \begin{bmatrix} \mathbf{K}^{\varphi\varphi} & \mathbf{K}^{\varphi\alpha} & \mathbf{K}^{\varphi T} \\ \mathbf{K}^{\alpha\varphi} & \mathbf{K}^{\alpha\alpha} & \mathbf{K}^{\alpha T} \\ \mathbf{K}^{\theta\varphi} & \mathbf{K}^{\theta\alpha} & \mathbf{K}^{\theta T} \end{bmatrix} \cdot \begin{bmatrix} d\varphi \\ d\alpha \\ dT \end{bmatrix} \quad (6.3.2)$$

$d\varphi$ ,  $d\alpha$  and  $dT$  are the incremental changes of the vectors of the unknown spatial placement, the unknown thermal displacement and the unknown temperature. The tangential stiffness matrices  $\mathbf{K}^{\varphi\varphi}$ ,  $\mathbf{K}^{\varphi\alpha}$ ,  $\mathbf{K}^{\varphi T}$ ,  $\mathbf{K}^{\alpha\varphi}$ ,  $\mathbf{K}^{\alpha\alpha}$ ,  $\mathbf{K}^{\alpha T}$ ,  $\mathbf{K}^{\theta\varphi}$ ,  $\mathbf{K}^{\theta\alpha}$  and  $\mathbf{K}^{\theta T}$  are calculated via

$$\begin{aligned} \mathbf{K}^{\varphi\varphi} &= \frac{\partial \mathbf{r}^\varphi}{\partial \varphi}, & \mathbf{K}^{\varphi\alpha} &= \frac{\partial \mathbf{r}^\varphi}{\partial \alpha}, & \mathbf{K}^{\varphi T} &= \frac{\partial \mathbf{r}^\varphi}{\partial T}, \\ \mathbf{K}^{\alpha\varphi} &= \frac{\partial \mathbf{r}^\alpha}{\partial \varphi}, & \mathbf{K}^{\alpha\alpha} &= \frac{\partial \mathbf{r}^\alpha}{\partial \alpha}, & \mathbf{K}^{\alpha T} &= \frac{\partial \mathbf{r}^\alpha}{\partial T}, \\ \mathbf{K}^{\theta\varphi} &= \frac{\partial \mathbf{r}^\theta}{\partial \varphi}, & \mathbf{K}^{\theta\alpha} &= \frac{\partial \mathbf{r}^\theta}{\partial \alpha}, & \mathbf{K}^{\theta T} &= \frac{\partial \mathbf{r}^\theta}{\partial T}. \end{aligned} \quad (6.3.3)$$

As mentioned above, the iterative update for the increments of the global unknowns  $\varphi$ ,  $\alpha$  and  $T$  is defined by the solution of the linearized system of equations (6.3.1):

$$\begin{aligned} \Delta \varphi_n^k &= \Delta \varphi_n^{k-1} + d\varphi, \\ \Delta \alpha_n^k &= \Delta \alpha_n^{k-1} + d\alpha, \\ \Delta T_n^k &= \Delta T_n^{k-1} + dT. \end{aligned} \quad (6.3.4)$$

## 6.4. Numerical examples

In the following, several numerical examples are presented. First, a closer look at the simulation of the second sound experiments is taken. Herein, the fully coupled problem is considered for the geometrically linear and nonlinear case. Bismuth as well as sodium fluoride is treated. Second, cryovolcanism, i.e. the icy counterpart of volcanism on Earth, on Saturn's moon Enceladus is simulated. It is followed by the application of the material force method with respect to an example in the field of fracture mechanics. This Section is closed by the introduction of an energy-conserving discretization scheme applied to a geometrically nonlinear example in fracture mechanics.

### 6.4.1. Second sound phenomenon

Thermal wave propagation is due to second sound (cf. Chapter 2 for further information on this phenomenon). Here, two independent modes of wave propagation can be observed: classical

first sound and the thermal second sound. The application of the Green-Naghdi theory for modeling pure second sound has already been discussed in Section 5.3. It has been evident that the classical theory of type I is inapplicable, whereas type II and III are capable of modeling thermal waves. Now, the pure thermal case is coupled with elasticity. In the first example, the second sound experiments of Narayanamurti and Dynes [119], who proved the existence of second sound in Bi for the first time, are simulated for geometrically linear behavior, i.e. only small deformations and strains are assumed. These results are published in the work of Bargmann and Steinmann [10]. Second, second sound in sodium fluoride is modeled with an underlying geometrical nonlinear theory, i.e. large deformations are allowed.

#### 6.4.1.1. Bismuth (Bi)

For information on the material Bi itself, the reader is referred to Section 5.3. In order to avoid unnecessary repetitions, only the material parameters applied during the simulations are listed:

Table 6.1.: Material parameters for coupled thermoelasticity in Bi

	Bi	
density $\rho$	9780	$\left[\frac{\text{kg}}{\text{m}^3}\right]$
specific heat $c$	0.052	$\left[\frac{\text{W}}{\text{kgK}}\right]$
thermal expansion coefficient $w$	$6.75 \cdot 10^{-6}$	$\left[\frac{1}{\text{K}}\right]$
thermal conductivities $\kappa_2, \kappa_3$	309407875	$\left[\frac{\text{W}}{\text{s}^2\text{mK}}\right]$
Young's modulus $E$	$40 \cdot 10^9$	$\left[\frac{\text{N}}{\text{m}^2}\right]$
reference temperature $T_0$	3	[K]

Moreover,  $\kappa_4 = \kappa_3 / (5000 \text{ 1/s}^2) = 61881.575 \left[\frac{\text{W}}{\text{mK}}\right]$  is set. Initially, a one-dimensional specimen of length 9 mm is set at equilibrium with reference temperature 3 K. Then, a temperature perturbation of height 1 K is added at the left end of the specimen. The thermal displacement  $\alpha$  is initiated to be zero everywhere in the bar. The specimen is fixed at both ends, cf. Figure 6.1. The external sources are assumed to be non-existing, i.e.  $r = 0$  and  $\mathbf{b} = \mathbf{0}$ . The temperature development is simulated for 11.5  $\mu\text{s}$ . A discretization of 250 spatial and 800 temporal elements is applied for type II as well as III.

Figure 6.2 depicts the temperature solution according to type II. The faster but smaller wave is driven by the mechanical problem and propagates with the speed of first sound, whereas the

6. Theory of non-classical thermo-hyperelasticity

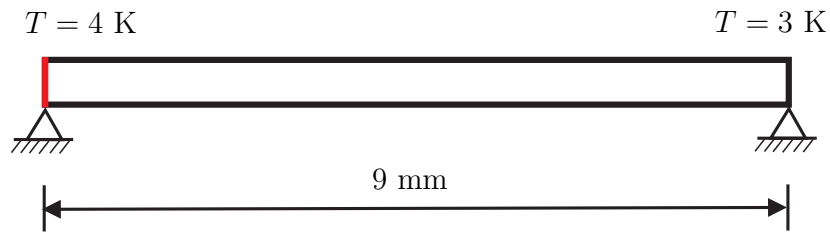


Figure 6.1.: Set-up of second sound model. A 9 mm-long one-dimensional bar of Bi with initial temperature 3 K is heated by a short heat pulse from 3 K to 4 K at the left end. The specimen is fixed at both ends.

second sound wave is slower and due to the hyperbolic nature of the temperature equation (6.1.10). There is no energy dissipation involved, thus the thermal waves propagate without damping through the bar.

Figure 6.3 depicts the temperature solution according to Green-Naghdi thermoelasticity of type III. In comparison to type II, a diffusive heat flux of the Fourier type is added to the heat equation (6.1.13). Although only 0.02% diffusion is added, the diffusive behavior of the second sound wave is clearly visible.

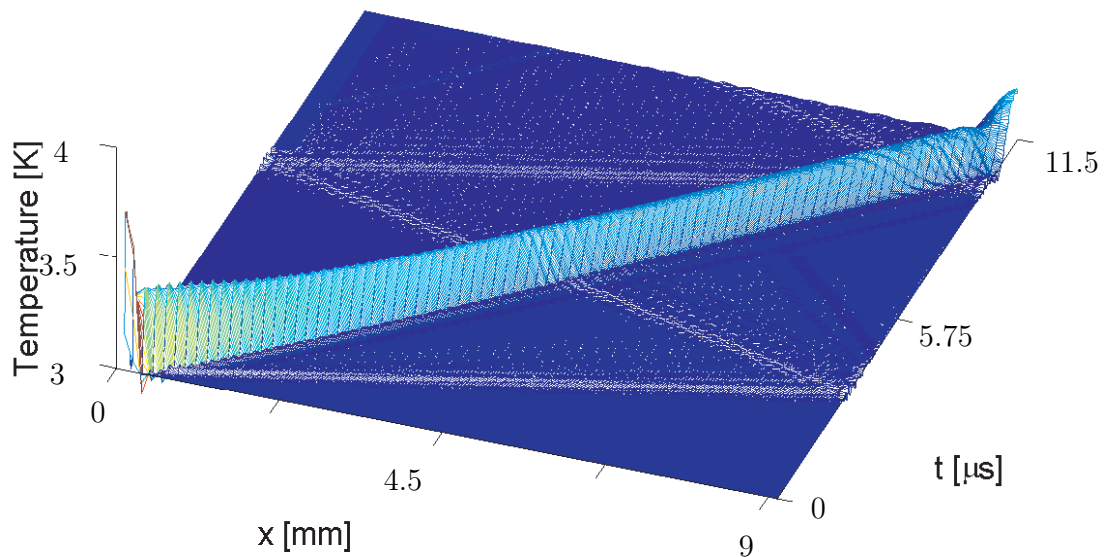


Figure 6.2.: Type II. Temperature is plotted vs. space and time. One can clearly see the existence of two temperature waves. The inertia term of the balance of linear momentum is fully considered, thus a smaller but faster first sound wave exists. The bigger but slower one is the second sound. Due to small numerical oscillations a streamline-upwind stabilization is added (cf. [7, 169]).

6. Theory of non-classical thermo-hyperelasticity

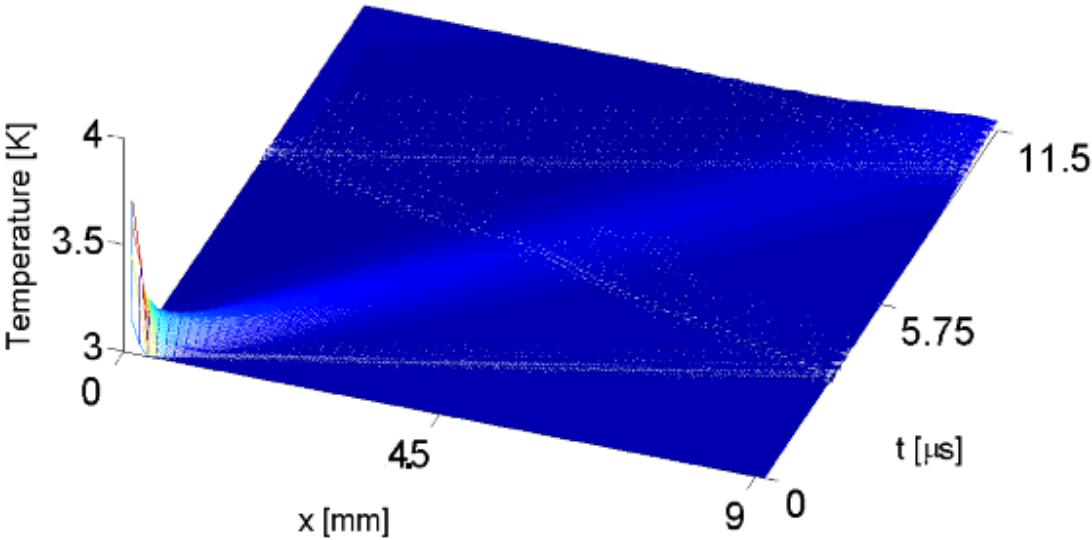


Figure 6.3.: Type III. Temperature is plotted vs. space and time. Once more, both waves are clearly visible. Compared to type II, a Fourier type heat flux is added. This induces the diffusive behavior of the second sound wave.



### Two-dimensional square

The second sound velocity of  $7.8 \cdot 10^{-4} \text{ m}/\mu\text{s}$  corresponds to an arrival time of  $11.5 \mu\text{s}$  at the right end of the 9 mm-bar. Type II as well as type III perfectly meet this arrival time. The elastic wave is smaller and faster than the thermal one. Its velocity reads  $v_{\text{mech}} = \sqrt{E/\rho} = 2.02 \cdot 10^5 \text{ cm/s}$ . In order to have a closer look at the different velocities and its impact on the temperature waves, a two-dimensional square with an edge length of 10 mm is looked at from above. The material is once more chosen to be bismuth and the material parameters are given in Table 6.1. Poisson's ratio  $\nu$  is set to zero, i.e.  $\nu = 0$ . The square possesses a homogeneous temperature distribution of 0 K which is disturbed in the middle with a short heat pulse of 10 K. The development of the temperature is observed for  $3.9 \mu\text{s}$ . The plate is discretized with  $20 \times 20$  elements, whereas 400 elements are used for the temporal discretization.

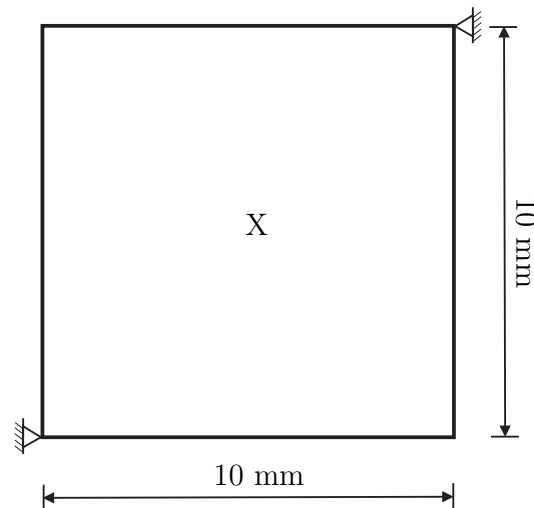


Figure 6.4.: Set-up of second sound model. A 9 mm-long one-dimensional bar of Bi with initial temperature 3 K is heated by a short heat pulse from 3 K to 4 K at the left end. The specimen is fixed at both ends.

Figure 6.5 illustrates the solution of the temperature solution according to the more general type III. Only a very small dissipation is admitted. The isolines are plotted at 0.005 K and 0.05 K in order to show the different velocities of the first and the second sound. At first, cf. Figure 6.5<sub>1</sub>, only the temperature difference in the middle can be seen. Figure 6.5<sub>2</sub> already illustrates the development of two circles. The outer circle indicates the smaller but faster thermal wave induced by the first sound. The inner circle represents the bigger but slower thermal wave, the second sound. The outer circle moves faster than the inner and, in the course of time, it detaches from the inner one.

A radiallysymmetric example is chosen in which the temperature disturbance is initiated in the middle - in only one node. Consequently, only the first sound wave (the longitudinal mechanical

## 6. Theory of non-classical thermo-hyperelasticity

wave) and the second sound wave (the temperature wave) occur. When the first sound wave meets the plate's edges a transversal wave would develop. However, this is not considered here as this example is intended to clarify the different propagation speeds of the first and second sound further.

### 6.4.1.2. Sodium Fluoride (NaF)

Another example for a solid in which the existence of second sound has been verified is NaF. Experimental data is available in the publications of Jackson and Walker [72, 73], for example. The thermal aspect and the thermoelastostatic aspect of the second sound phenomenon in NaF is investigated by Bargmann and Steinmann [7, 9]. Here, the fully coupled geometrically nonlinear theory is used for the underlying model. Thus, the inertia term of the balance of momentum is taken into account and large deformations are allowed. Exemplarily, the theory of type III is studied.

A one-dimensional bar of NaF with fixed bearings at both ends initially has a homogeneous temperature distribution of 15 K. At the beginning of the simulation, a short heat pulse of 1 K is applied. The bar is observed for 5  $\mu\text{s}$  and the set-up of the model is depicted in Figure 6.6. For the spatial discretization 50 linear finite elements are applied. Moreover, the time interval is discretized with 250 finite elements and a cG(1)-discretization is applied. The material parameters are given in Table 6.2.

Figure 6.7 depicts the temperature solution in case of geometrically nonlinear thermoelasticity of type III. Two waves are clearly seen. The bigger but slower wave is the second sound wave. Its arrival time of 4.1  $\mu\text{s}$  is perfectly met. Also the arrival time of the smaller but faster first sound wave is met. Consequently, a very good correspondence with arrival times is found and the numerical results agree well with the experimental data of [72, 73]. The model of type III involves energy dissipation. Thus the wave amplitude decreases and the second sound wave becomes diffusive.

Table 6.2.: Material parameters for coupled thermoelasticity in NaF

material's density $\rho$	2886	$\left[\frac{\text{kg}}{\text{m}^3}\right]$
specific heat $c$	2.774	$\left[\frac{\text{W}}{\text{kgK}}\right]$
thermal conductivity $\kappa_3$	20500	$\left[\frac{\text{W}}{\text{s}^2\text{mK}}\right]$
thermal conductivity $\kappa_4$	2.05	$\left[\frac{\text{W}}{\text{mK}}\right]$
absolute entropy density $S_0$	0.9247	$\left[\frac{\text{N}}{\text{m}^2\text{K}}\right]$
reference temperature $T_0$	15	[K]
thermal expansion coefficient $w$	$18.5 \cdot 10^{-6}$	$\left[\frac{1}{\text{K}}\right]$
Young's modulus $E$	$85.97 \cdot 10^9$	$\left[\frac{\text{N}}{\text{m}^2}\right]$
length $l$	8	[mm]
external heat source $r$	0	
volume force $\mathbf{b}$	0	

## 6. Theory of non-classical thermo-hyperelasticity

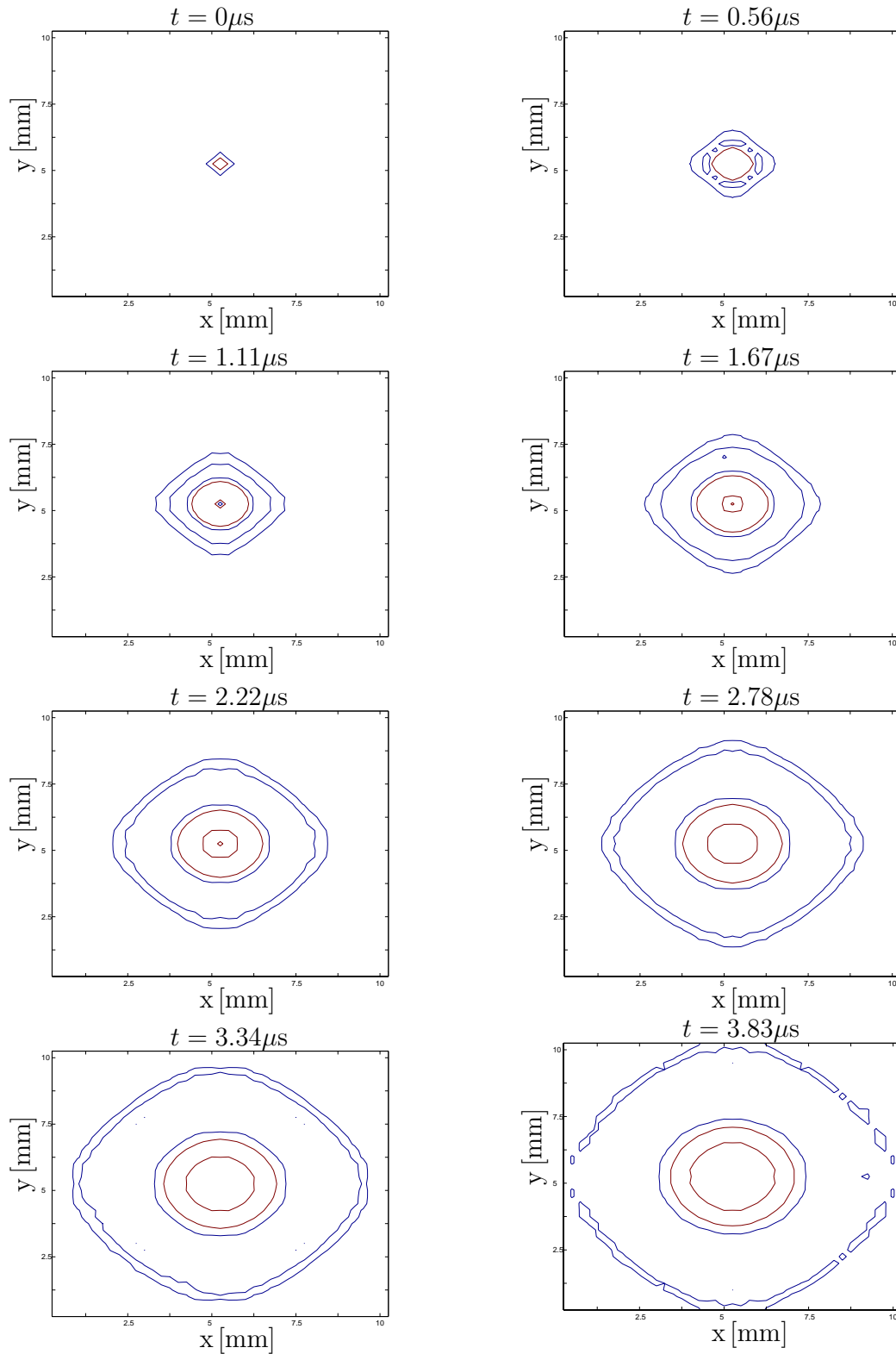


Figure 6.5.: Temperature solution according to type III. A heat pulse of 10 K is initiated at the square's middle. The temperature isolines are depicted at times  $t = 0 \mu\text{s}$ ,  $t = 0.56 \mu\text{s}$ ,  $t = 1.11 \mu\text{s}$ ,  $t = 1.67 \mu\text{s}$ ,  $t = 2.22 \mu\text{s}$ ,  $t = 2.78 \mu\text{s}$ ,  $t = 3.34 \mu\text{s}$  and  $t = 3.83 \mu\text{s}$ . The isolines are plotted at values 0.005 K and 0.05 K.

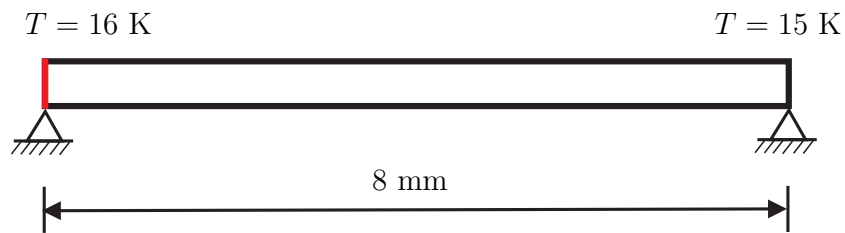


Figure 6.6.: A 8 mm-long one-dimensional bar of NaF with initial temperature 15 K is heated by a short heat pulse from 15 K to 16 K at the left end. The specimen is fixed at both ends.

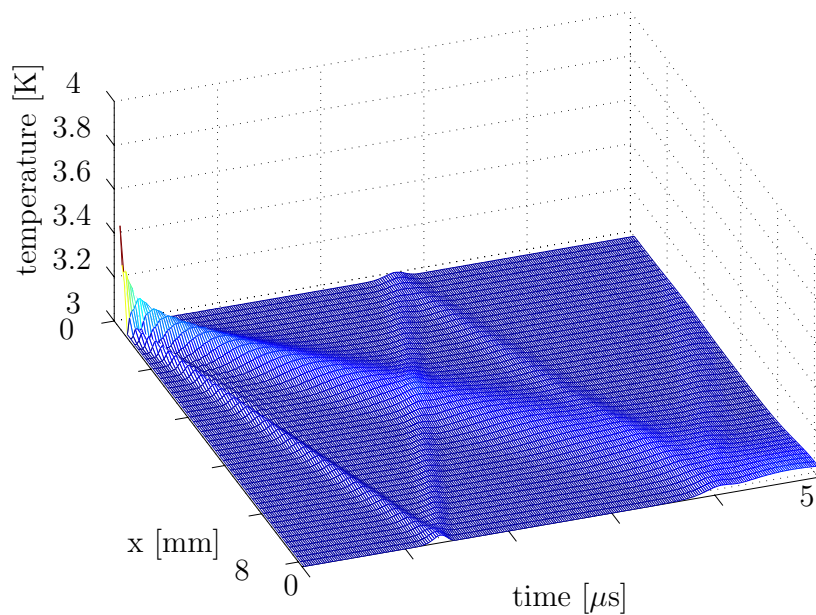


Figure 6.7.: Simulation of second sound experiments of [72, 73] in a one-dimensional bar of NaF with initial temperature 15 K. At the left end a short heat pulse of 1 K is initiated. The temperature distribution is plotted vs. time and position. Two waves are clearly seen. The bigger but slower wave is the second sound wave. Its arrival time of  $4.1 \mu\text{s}$  is perfectly met. Also the arrival time of the smaller but faster first sound wave is met.

### 6.4.2. Cryovolcanism on Enceladus

In 2005, the Cassini spacecraft proved the existence of cryovolcanism, i.e. the icy counterpart of volcanism on Earth, on Saturn's moon Enceladus during its close fly-bys. In particular, water-rich plume venting was discovered in the south polar region. Thus, Enceladus was found to be one out of three outer solar bodies being geologically active. This section is concerned with the modeling and computation of this phenomenon. For the underlying thermoelastic theory, it is resorted to the Green–Naghdi theory of type III. However, since only small deformations are expected, it is resorted to geometrically linear thermoelasticity. This section is based on the results published in [11].

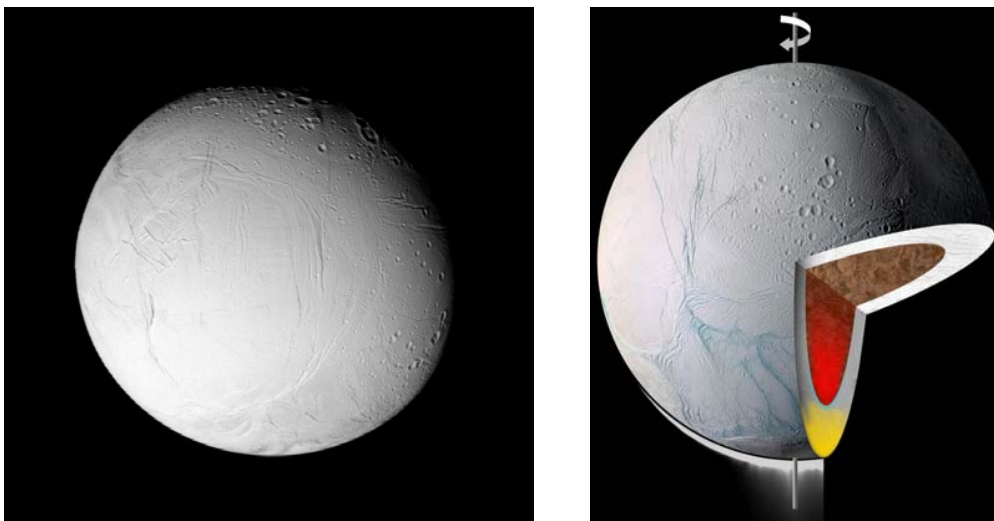


Figure 6.8.: Left: This picture of Saturn's moon Enceladus was taken by the Voyager 2 mission in the early 1980s. Enceladus has only a diameter of ca. 500 km. With an albedo of 0.99, its icy surface is the most reflecting in the solar system. Despite the cryovolcanoes existing in Enceladus south polar region, several more geologic terrains have been discovered. For example, the north polar region is heavily cratered whereas there are also terrains which are relatively smooth. Picture credit: NASA/JPL.

Right: This graphic illustrates the interior of Enceladus: a rocky core (brown, red) and an icy shell (yellow). Picture credit: NASA/JPL.

Enceladus (see Figure 6.8) is one of Saturn's inner satellites. It was discovered in 1789 and orbits Saturn in an almost circular orbit with a semi-major axis of 237,948 km and a period of 1.37 days. Enceladus has the shape of a flattened ellipsoid with a mean diameter of 504 km, which makes it the sixth largest Saturnian moon. It consists of a rocky core and an icy mantle and surface, see Figure 6.8 (right). The mean surface temperature is at a value of 77 K. In many ways, the general properties of Enceladus are very different from those of other satellites, and thus, it is a very active research topic. With an albedo of 0.99, it has the most reflective surface of any body in the solar system. Scientists assume that one explanation

for this high reflectivity is the continuous surface renovation by icy particles originating from cryovolcanoes.

Of particular interest is Enceladus' south polar region. In 2005, active cryovolcanism was found there during a close fly-by of the Cassini spacecraft [127], which makes Enceladus the fourth body in the solar system (along with the Earth, Jupiter's moon Io and Neptune's moon Triton) where volcanic eruptions have been observed, see Figure 6.9. This finding goes along with the spectrometric detection of a distinctive warm spot centered on the south pole with a temperature of approximately 85 K, which is 15 K more than expected from a simple radiation balance [150]. Figure 6.10 compares the predicted with the observed surface temperatures on Enceladus.

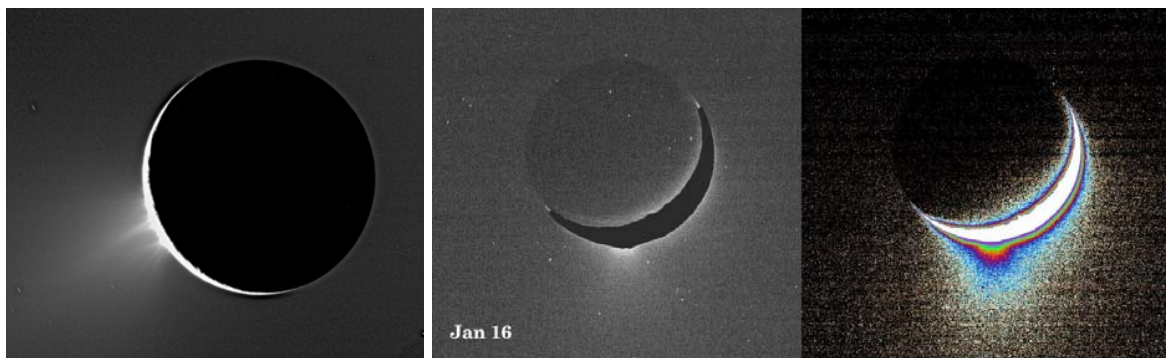


Figure 6.9.: The plumes on Enceladus' south polar region are the source of the material from Saturn's E ring. A mixture of water and water vapor is erupted from pressurized subsurface water chambers in Enceladus' interior. The left picture shows Enceladus backlit by the sun. On the right, a monochrome view of its cold geysers from January, 16th 2005 is shown along with a color-coded image. Picture credit: NASA/JPL/Space Science Institute.

Cryovolcanoes are icy equivalents of the well-known terrestrial volcanoes. Their main features are illustrated in Figure 6.11. Instead of magma Enceladus' cryovolcanoes erupt water which has its source in pressurized subsurface water chambers [127]. No ammonia (which would lower the melting point) was found [22], suggesting that the cryomagma is pure  $H_2O$ . Cryovolcanoes on other icy moons may also erupt a mixture of water and, for example, ammonia or methane. The heat source powering Enceladus cryovolcanoes is tidal heating induced by Enceladus' orbital motion around Saturn [122].

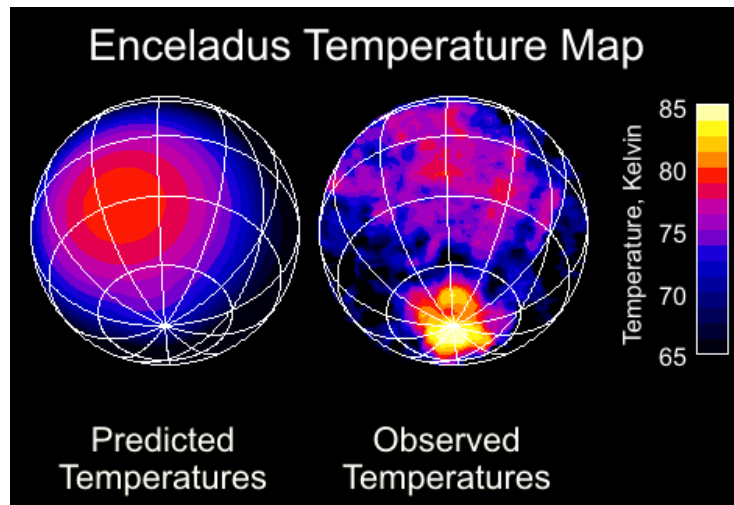


Figure 6.10.: Predicted (radiation balance) vs. observed (composite infrared spectrometer CIRS onboard the Cassini spacecraft) surface temperatures of Enceladus. The south polar region shows a warm spot due to active cryovolcanism. Picture credit: NASA/JPL/GSFC.

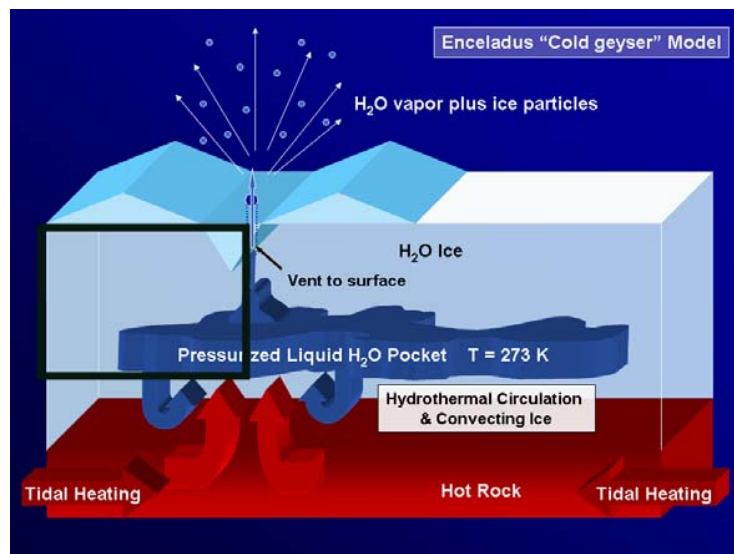


Figure 6.11.: "Cold geyser model" for cryovolcanism on Enceladus: Pressurized sub-surface water erupts through a volcanic pipe (vent) into the atmosphere. The black box on the left shows the area investigated during the numerical simulations, see Section 6.4.2.2. Picture (modified) credit: NASA/JPL/Space Science Institute/Cassini-Huygens.



### 6.4.2.1. Set-up for modeling cryovolcanism on Enceladus

#### Model parameters for cryogenic ice

According to Powell et al. [129], Slack [147] and Greve [56], the thermal conductivity  $\kappa$ , the thermal expansion coefficient  $w$  and the specific heat  $c$  of ice are

$$\begin{aligned}\kappa(T) &= \frac{615}{T} \frac{\text{W}}{\text{mK}}, \\ w(T) &= [56.5 + 0.25[T - 273]] \times 10^{-6} \frac{1}{\text{K}}, \\ c(T) &= 146.3 + 7.253 T \frac{\text{J}}{\text{kgK}},\end{aligned}\tag{6.4.1}$$

where the temperature  $T$  is taken in units of [K]. Natural ice is composed of a large number of individual crystals. Here, it is assumed that the orientation distribution is random, following the way of [56]. Thus, its macroscopic mechanical behavior is isotropic, and the elasticity tensor  $\mathbf{E}$  is fully determined by the Young's modulus,  $E_{\text{ice}} = 10$  GPa, and the Poisson's ratio,  $\nu = 0.33$ . Both quantities are assumed to be independent of temperature. For the ice density, the standard value  $\rho_{\text{ice}} = 910 \text{ kg m}^{-3}$  is employed, and the acceleration due to gravity on Enceladus is  $g = 0.079 \text{ m s}^{-2}$ .

The Green–Naghdi theory of type III includes the two thermal conductivities  $\kappa_3$  and  $\kappa_4$  of which the ratio is not narrowed. Although no experimental data exists on energy dissipation during the eruption of a cryovolcano on Enceladus, one can certainly conclude that the model should include energy dissipation due to the experiences on Earth, and due to the fact that so far a pure thermal wave propagation has only been proven below 20 K. No data on the propagation speed of heat in Enceladus' ice is available, thus, an ad hoc assumption of the values of the thermal conductivities  $\kappa_3$  and  $\kappa_4$  cannot be given. Therefore, the classical thermal conductivity  $\kappa_4$  is identified with the measured temperature-dependent thermal conductivity given in Eq. (6.4.1)<sub>1</sub>,

$$\kappa_4(T) = \frac{615}{T} \frac{\text{W}}{\text{mK}}.\tag{6.4.2}$$

For the non-classical thermal conductivity  $\kappa_3$ , it is assumed that it is proportional to  $\kappa_4$ ,

$$\kappa_3(T) = \frac{\kappa_4(T)}{t_{\text{proc}}} \times f,\tag{6.4.3}$$

where  $t_{\text{proc}}$  is a time-scale for the modeled process and  $f$  is an adjustable, dimensionless factor. It is clear that for small values of  $f$  the Fourier-type (diffusive) heat flux will be dominant, while for large values of  $f$ , heat transport will be governed mainly by the non-classical  $\nabla\alpha$ -type flux.

## 6. Theory of non-classical thermo-hyperelasticity

For materials with confirmed second sound, the velocity of the thermal waves was found to be typically about  $\sqrt{3}$  times smaller than the velocity of the elastic waves (“first sound”), cf. Section 6.4.1. If this approximation is applied to ice, an independent estimate for the value of  $\kappa_3$  can be obtained. For example, at 100 K, this yields  $\kappa_3 = 2.9 \times 10^{12} \text{ W m}^{-1} \text{ s}^{-1} \text{ K}^{-1}$ , while  $\kappa_4 = 6.15 \text{ W m}^{-1} \text{ K}^{-1}$ . If the process time-scale is chosen to be  $t_{\text{proc}} = 1 \text{ d} = 86400 \text{ s}$  (see below), a factor  $f$  as large as  $f = 4 \times 10^{16}$  is obtained. However, since it is not likely that ice shows fully developed second-sound phenomena (otherwise it would most likely have been observed already), reasonable values for  $f$  must be at least several orders of magnitude smaller.

### Computational domain, initial and boundary conditions

As a simplified representation of a cryovolcano and its environment on Enceladus, a two-dimensional domain of 50 km (approx. 10 degrees of latitude) length and 500 m thickness is considered, with the volcanic pipe at the right edge. The problem is supposed to be symmetric around the pipe and the curvature of the surface is neglected. The water chamber is 1 km long and over-pressurized by a factor of 10 compared to the hydrostatic pressure of the ice. The set-up is depicted in Figure 6.12.

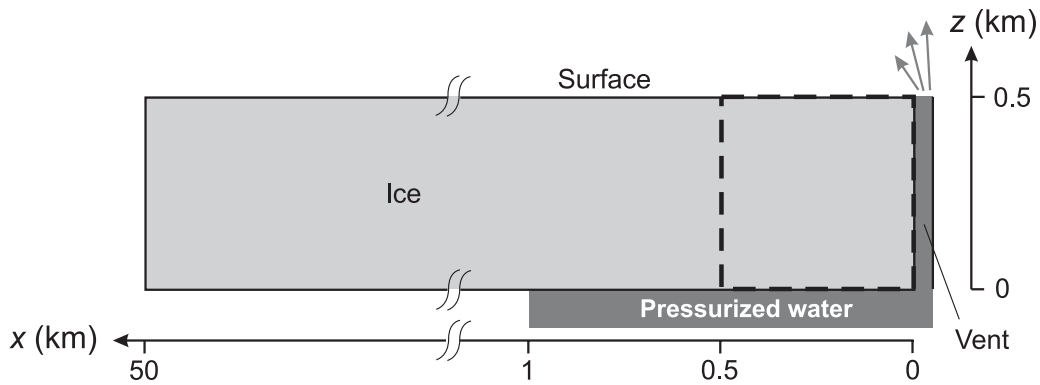


Figure 6.12.: Model of the cryovolcano. The adjacent ice layer is 50 km long and 500 m thick. The dashed square marks the 500 m  $\times$  500 m area next to the volcanic vent for which the evolution of the temperature  $T$  is plotted in Figures 6.13–6.16.

As initial conditions at the time  $t_0 = 0$ , the surface temperature is set to 85 K (see the observed surface temperatures in south polar region in Figure 6.10) and the bottom temperature to 273 K, i.e. the melting point of ice. The reference temperature  $T_0$  is set to the initial surface temperature, that is,  $T_0 = 85 \text{ K}$ . The simulated eruption starts abruptly at this time and lasts for 1 day. During the eruption period, the temperature over the entire depth of the volcanic vent is set to 273 K, and the pressure in the pipe falls linearly from the over-pressurized water chamber at the bottom to the zero value at the surface. The melting point of terrestrial ice is pressure dependent. Due to the low gravity on Enceladus, this effect is negligible for simulating its volcanic eruptions. At  $t = 1 \text{ day}$ , the eruption is “switched off”, and the computation is continued until  $t_f = 10 \text{ days}$ . For the process time-scale  $t_{\text{proc}}$  in Eq. (6.4.3) is chosen to be

the duration of the eruption, that is  $t_{\text{proc}} = 1$  day.

There is no data available on the duration of a real eruption, thus the choice of one day is arbitrary. However, the general development of the heat propagation will not be affected by the eruption time. Here, the effect of the non-classical Green–Naghdi model is discussed, and therefore, details of the temporal evolution are set aside.

Furthermore, the boundary condition at the surface has to be considered: Here, the radiation balance, which takes into account the incoming solar radiation, the black-body radiation from the ice surface and the geothermal heat flux approaching the ice surface from below. It reads

$$-S_0[1 - A] + \sigma_{\text{SB}}T_s^4 - \mathbf{q} \cdot \mathbf{n} = 0, \quad (6.4.4)$$

where  $S_0$  is the solar constant for Enceladus,  $A$  the albedo (reflexivity of the ice surface),  $\sigma_{\text{SB}}$  the Stefan–Boltzmann constant and  $T_s$  the temperature at the surface. As already mentioned above, the Enceladus' albedo is as high as 0.99, which is the highest value of any known body in our solar system [22]. The solar constant is computed from its terrestrial counterpart  $S_{0, \text{Earth}}$  via

$$S_0 = S_{0, \text{Earth}} \frac{r_{\text{SE}}}{r_{\text{SS}}} = 3.76 \frac{\text{W}}{\text{m}^2}, \quad (6.4.5)$$

where  $r_{\text{SE}}$  and  $r_{\text{SS}}$  are the distances Sun–Earth and Sun–Saturn, respectively.

#### 6.4.2.2. Results

The dimensionless factor  $f$  in Eq. (6.4.3) still needs to be specified. Since the available data on Enceladus does not give a hint on how to choose  $f$  in the first place, this parameter is varied starting with  $f = 1$  and going up to  $f = 10^8$ . As mentioned above, for small values of  $f$ , the model will be close to the classical, Fourier-type heat conduction. By increasing  $f$ , the model will become more and more non-classical because of the increasing impact of the  $\nabla\alpha$ -type flux. However, note that the maximum value  $f = 10^8$  is still eight orders of magnitude smaller than the estimate given in the discussion of a pure second sound scenario, so that in neither case fully developed second-sound properties for ice are assumed.

In the following, the solutions for  $f = 1$  (“case 1”),  $f = 10^6$  (“case 2”),  $f = 10^7$  (“case 3”) and  $f = 10^8$  (“case 4”) are discussed. All simulations have been carried out with a numerical time-step of  $\Delta t = 10^{-3}$  days = 1.44 min.

Figures 6.13–6.16 illustrate the temperature development of the  $500 \text{ m} \times 500 \text{ m}$  square next to the volcanic pipe. The solutions are plotted at four different times of the simulation for each of the four cases. First, the temperature  $T$  is depicted right after the beginning of the volcanic eruption (i.e. at time  $t = 1.44$  min). The next plot shows the temperature distribution 1 hour and 12 minutes after the beginning of the volcanic eruption – at that time the volcano is still erupting. Immediately after the end of the eruption, i.e. after 1 day, the temperature solution is looked at for the third time. Fourth, the temperature is plotted 10 days after the beginning of the eruption, that is, 9 days after its end.

## 6. Theory of non-classical thermo-hyperelasticity

In case 1, which is very close to the classical Fourier approach, no change in temperature can be seen during the entire observation time, see Figure 6.13. Neither the 1-day-lasting volcanic eruption nor the cooling down period of 9 days have any noticeable impact on the temperature distribution within the ice.

In case 2, where  $f = 10^6$ , hardly any changes in temperature can be seen during the volcanic eruption, see Figure 6.14. However, 9 days after the end of the eruption, it can be clearly seen that the temperature in the volcanic pipe is decreasing, starting at the top, i.e. at Enceladus' surface.

Figures 6.15 and 6.16 show that with an increasing impact of the non-classical  $\nabla\alpha$ -type flux (cases 3 and 4), the volcanic eruption starts to heat the interior of the ice next to the pipe, and the surface temperature rises. Also, immediately after the end of the eruption, the ice starts to cool down, which is best visible in the volcanic pipe next to the surface. Depending on the dimensionless factor  $f$ , the ice temperature equilibrates slower or faster: The higher the value of  $f$ , the faster the system equilibrates. Furthermore, due to the increasing impact of the  $\nabla\alpha$ -type heat flux, the temperature rises within the ice during the eruption. Owing to the radiation balance (6.4.4), the temperature change is most pronounced in the interior of the ice layer and smaller at the surface; however, a surface warming of the order of several degrees occurs in the vicinity of the vent during the eruption and fades away afterwards.

Spencer et al. [150] discuss the temperature on Enceladus' surface observed during the Cassini fly-bys in 2005 based on infrared spectrometry. High-resolution data reveal that the occurrence of high temperatures is spatially correlated with the geological features termed "tiger stripes" (linear troughs), which are most likely the source of the cryomagma delivered during the volcanic eruptions. With regard to the results of our simulations, it is particularly interesting that the data also indicate some increased thermal emission from regions adjacent to the warm troughs (several kilometers away). This spreading of surface warming agrees roughly with the results of our cases 3 and 4, where the non-classical,  $\nabla\alpha$ -type heat flux contributes significantly to the heat transfer in the ice. By contrast, in case 1, which is very close to the classical Fourier approach, the warming extends to only a few meters away from the volcanic pipe during the simulation time (and is therefore invisible in Figure 6.13). Of course, this depends on the assumed duration of the eruption, but the time-scale  $[t]$  for purely diffusive heat transport over a length-scale of  $[L] = 1$  km is as large as  $[t] = \rho c [L]^2 / k_2 \approx 4000$  a (computed for 100 K), and it appears unlikely that a stationary cryovolcanic eruption can be sustained over such a long time. Therefore, with all due caution arising from our simplified model and the data uncertainties, it seems that non-classical heat transport in ice at cryogenic temperatures may play a role in explaining the observed temperature distribution in the vicinity of the volcanically active troughs in Enceladus' south polar region.

Unfortunately, the analysis of cryovolcanism on Enceladus has just started and there is no data available on the temperature distribution within the ice during and after a volcanic eruption. Nevertheless, the comparisons of cases 1–4 seem to indicate that a classical Fourier model probably will not be sufficient because of the very slow impact. However, a good guess for the value of  $f$  can only be found when further observed data is known. While the approach close to the classical theory (case 1) seems unlikely, the non-classical approaches (cases 2–4) yield

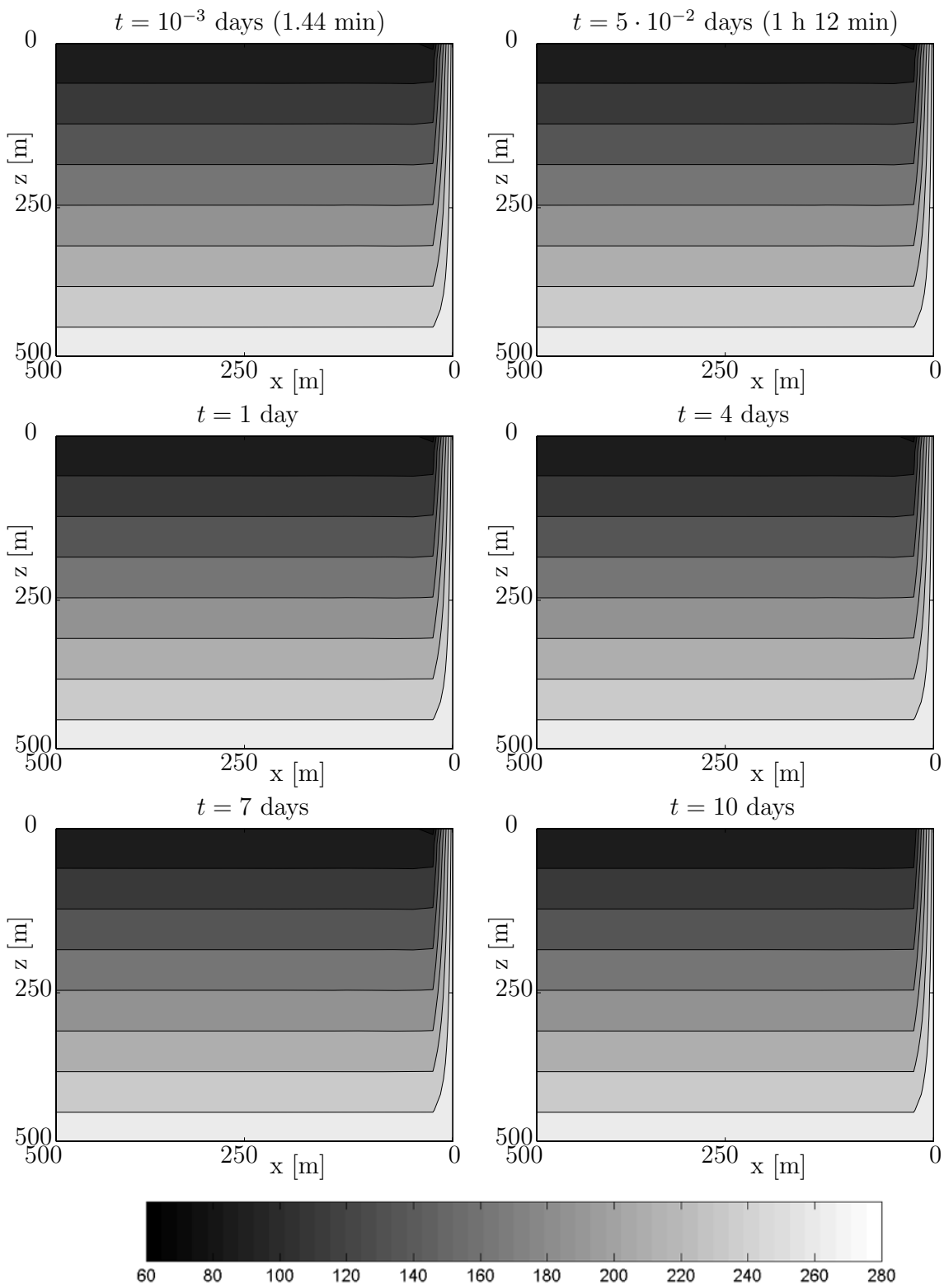


Figure 6.13.: Case 1 ( $f = 1$ ): Evolution of the temperature field (in K) in the  $500 \text{ m} \times 500 \text{ m}$  area next to the volcanic vent shown in Figure 6.12.

6. Theory of non-classical thermo-hyperelasticity

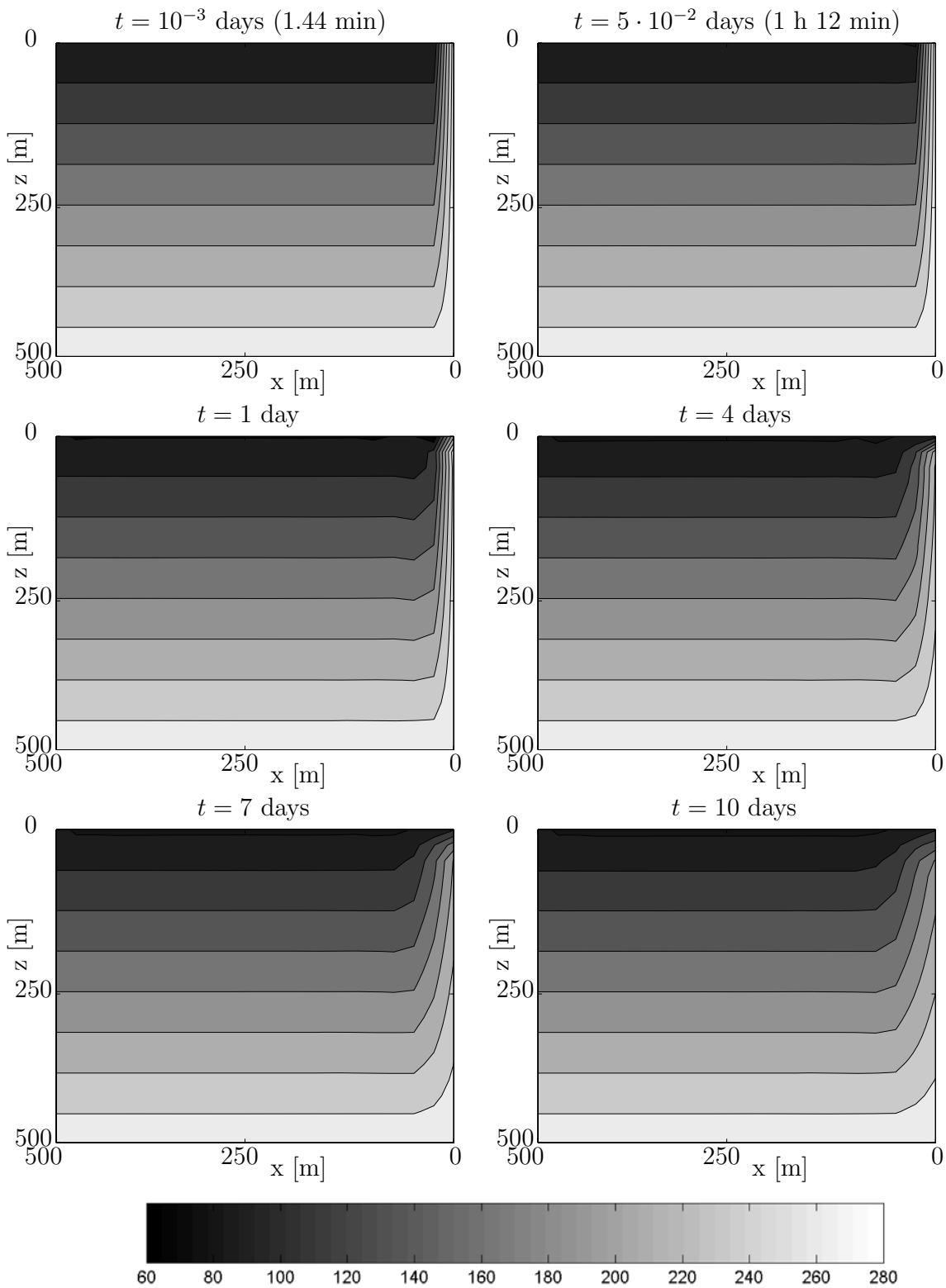


Figure 6.14.: Case 2 ( $f = 10^6$ ): Evolution of the temperature field (in K) in the 500 m × 500 m area next to the volcanic vent shown in Figure 6.12.

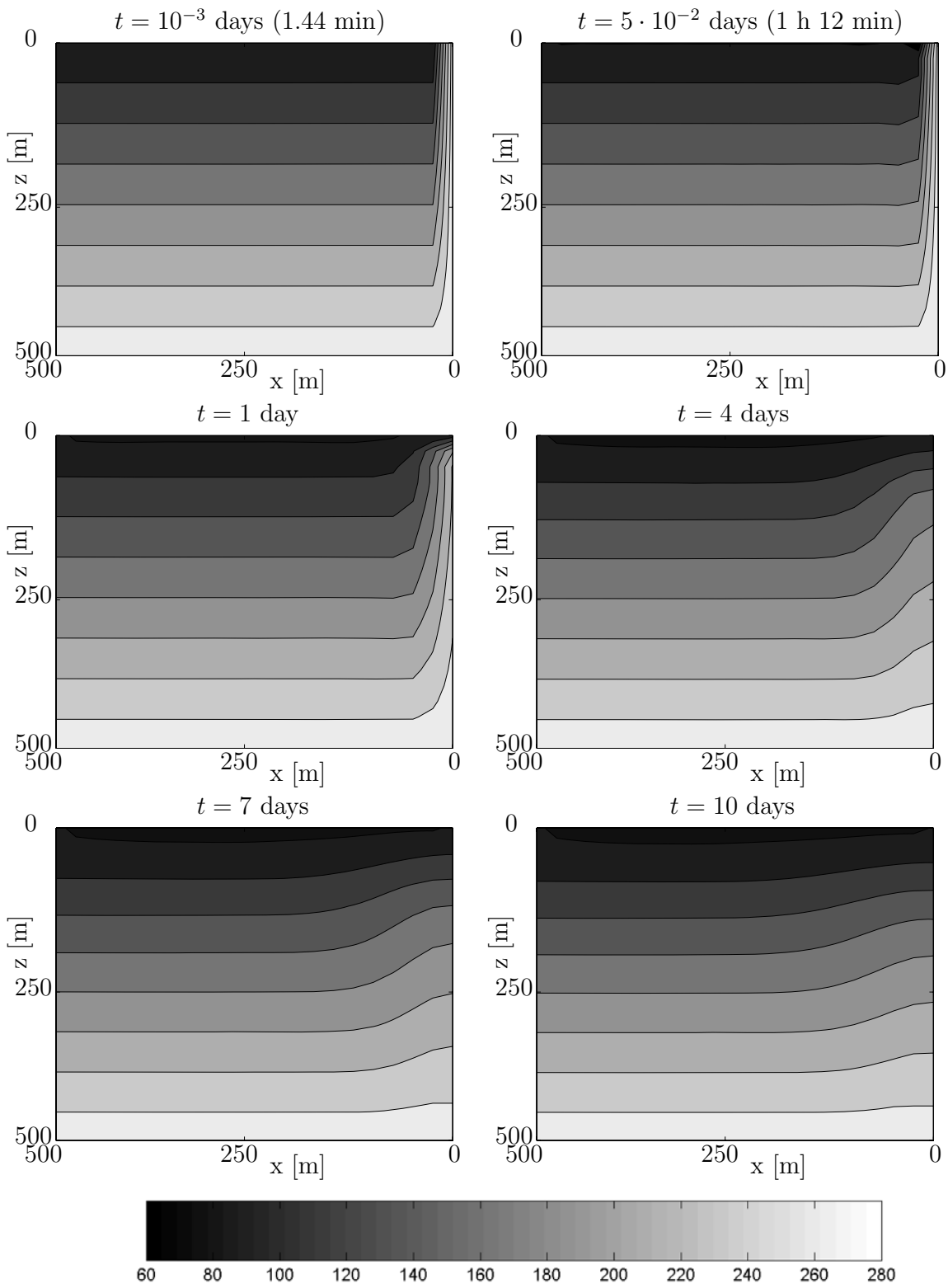


Figure 6.15.: Case 3 ( $f = 10^7$ ): Evolution of the temperature field (in K) in the 500 m × 500 m area next to the volcanic vent shown in Figure 6.12.

6. Theory of non-classical thermo-hyperelasticity

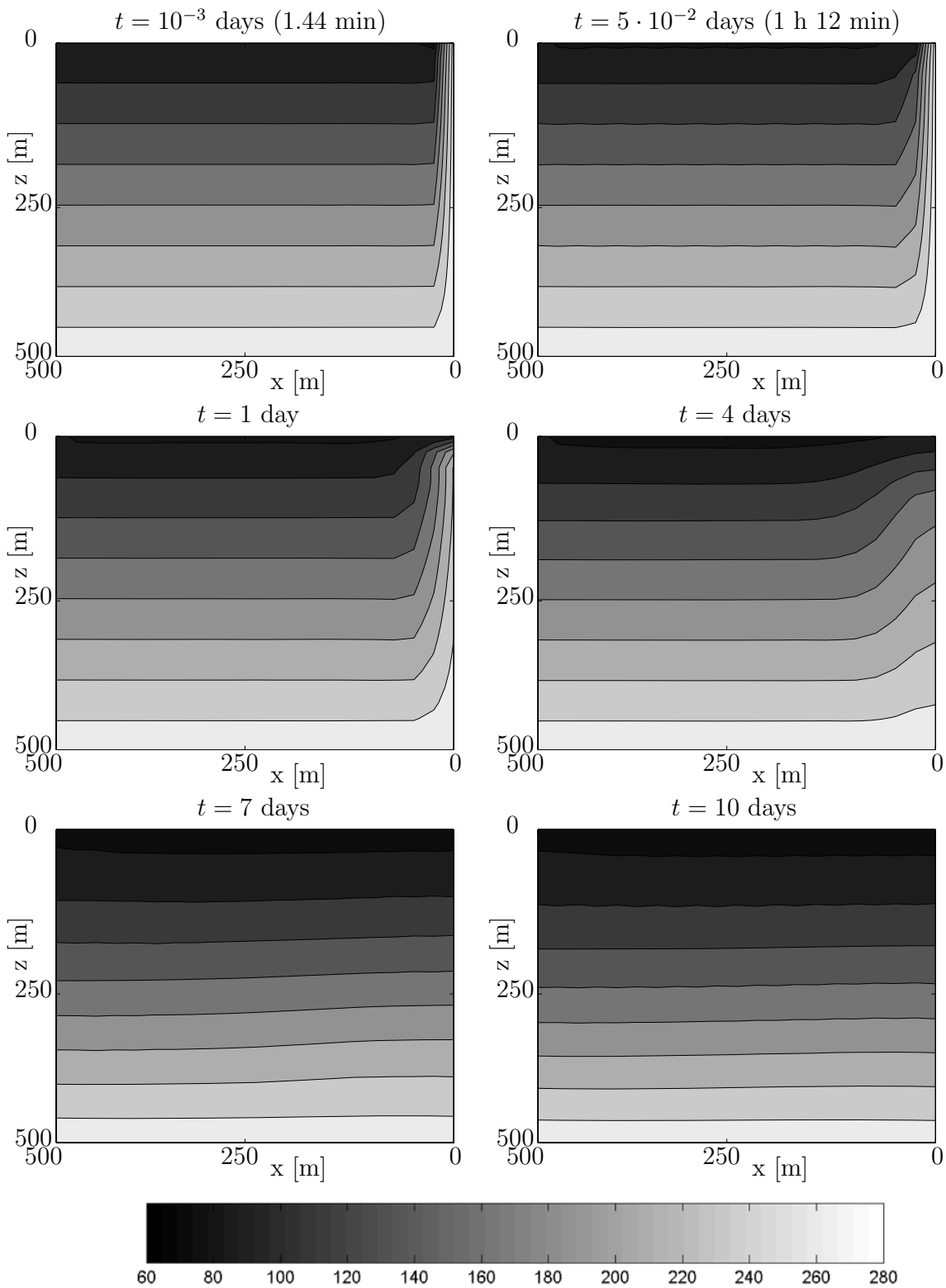


Figure 6.16.: Case 4 ( $f = 10^8$ ): Evolution of the temperature field (in K) in the 500 m × 500 m area next to the volcanic vent shown in Figure 6.12.



reasonably-looking simulations of cryovolcanism. They fit the data which are available at the moment well. However, further observational data are necessary in order to fully understand what is going on during Enceladus' eruptions. This contribution is a first successful approach to establish numerical simulations on this very peculiar and interesting phenomenon. Furthermore, it indicates that Enceladus' cryovolcanism should be simulated with a non-classical rather than a classical theory of thermoelasticity.

### 6.4.3. Material force method

The seminal ideas of Eshelby [43, 44] introduced the fundamental idea of material forces. His work is extended by the contributions of Gurtin [60], Maugin [102] and Steinmann [152] who deal with continuum mechanics of inhomogeneities. E.g. the work of Steinmann lead to the so-called material force method. Commonly, in continuum mechanics, material forces take the interpretation to be the response of variations of material placements of particles with respect to the ambient material. Consequently, material forces have proven to be well suited for the examination of defect mechanics, i.e. if dislocations, inhomogeneities, inclusions, interfaces or cracks are involved, for example. The material deformation map  $\Phi$  (Definition (3.1.8)) is governed by the material motion balance of momentum (3.2.14).

During the last decades, material forces have become a very active research topic and are successfully applied in the field of computational mechanics, see e.g. [5, 37, 60, 83, 84, 89, 90, 102, 106, 152, 153, 154]. For example, material forces occur as a result of discretization of the continuum equations, e.g. in finite element simulations. Nowadays, the most popular application of material forces is the field of fracture mechanics. However, the information gained by the material force method is used to adapt finite element meshes or structural optimization, see e.g. [5].

The main goal of this Chapter is to investigate the applicability of the material force method in the framework of non-classical thermo-hyperelasticity. A numerical example investigating material forces in the context of fracture mechanics is provided. Here, material forces represent the crack driving forces.

For the analysis of the material force method, the material forces as stated in Eq. (6.2.14) are calculated in a post-processing step.

#### Heat conduction

First, heat conduction in a two-dimensional bi-material square is considered, see Figure 6.17. The material parameters are listed in Table 6.3. Those of the lower material correspond to bismuth. The upper material's density  $\rho_1$  is three times bigger than the one of the lower material. The total observation time is  $0.1 \mu\text{s}$ . For the spatial discretization, a standard Bubnov–Galerkin finite element method is applied and the square is discretized with 900 bilinear quadrilateral spatial finite elements of equal size. For a square obeying Green–Naghdi type I, the temporal discretization is done with a discontinuous Galerkin temporal finite element method. In case of type III heat conduction, the heat conductivities  $\kappa_3$  and  $\kappa_4$  are set in such a way that the resulting heat equation is hyperbolic-like. Consequently, the continuous Galerkin temporal finite element method is chosen for its temporal discretization. In both cases, 1000 elements are applied for the temporal discretization.

The temperature  $T$  of the square is set to 10 K. Its lower edge is heated to 20 K. For type III, the thermal displacement  $\alpha$  is initialized to be zero everywhere.

The temperature development for a type I-square is depicted in Figure 6.18. The inhomogeneous temperature field induces a heat flux equalizing the temperature difference within the square over time.

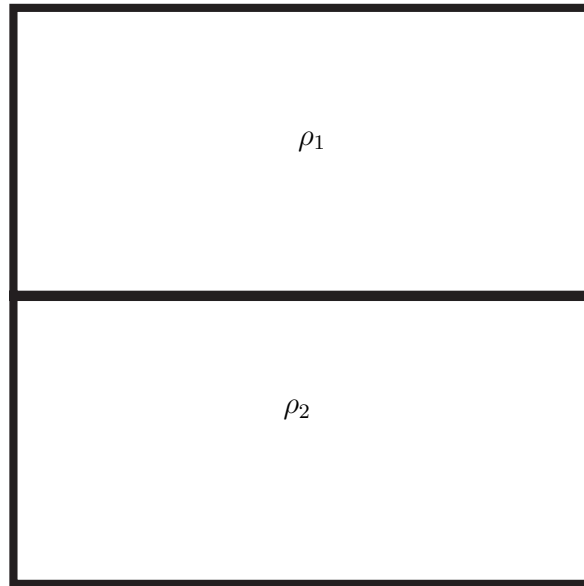


Figure 6.17.: A bi-material square with an edge length of 9 mm is considered. The upper material's density is  $\rho_1$ , whereas the one of the lower material is  $\rho_2$ . Initially, the material's temperature at the lower edge is set at 20 K. The rest of the square has a temperature distribution of 10 K. The square is discretized with 900 equidistant spatial and 1000 temporal finite elements.

Table 6.3.: Material parameters for bi-material square

density $\rho_1$	29340	$\left[\frac{\text{kg}}{\text{m}^3}\right]$
density $\rho_2$	9780	$\left[\frac{\text{kg}}{\text{m}^3}\right]$
specific heat $c$	0.052	$\left[\frac{\text{W}}{\text{kgK}}\right]$
thermal conductivity $\kappa_1$	875	$\left[\frac{\text{W}}{\text{mK}}\right]$
thermal conductivity $\kappa_3$	875	$\left[\frac{\text{W}}{\text{s}^2\text{mK}}\right]$
thermal conductivity $\kappa_4$	$875/10^5$	$\left[\frac{\text{W}}{\text{mK}}\right]$
reference temperature $T_0$	3	[K]
absolute entropy $S_0$	0.0173	$\left[\frac{\text{N}}{\text{m}^2\text{K}}\right]$
material parameter $b$	$0.354 \cdot 10^6$	$\left[\frac{1}{\text{s}^2}\right]$

## 6. Theory of non-classical thermo-hyperelasticity

The development of the material forces over time is shown in Figures 6.19 and 6.20. In particular, the material forces  $\mathbf{F}^{\Phi h} = \mathbf{F}_{\text{int}}^{\Phi h} + \mathbf{F}_{\text{vol}}^{\Phi h}$ , where  $\mathbf{F}_{\text{int}}^{\Phi h}$  and  $\mathbf{F}_{\text{vol}}^{\Phi h}$  are calculated according to Eq. (6.2.14), are plotted at times  $t = 0.0002$  s,  $t = 0.0006$  s,  $t = 0.0010$  s,  $t = 0.0014$  s,  $t = 0.0018$  s,  $t = 0.0022$  s,  $t = 0.0026$  s and  $t = 0.0030$  s. Note that in case of pure heat conduction  $\mathbf{F}_{\text{dyn}}^{\Phi h} = \mathbf{0}$ . In the beginning, large material forces can be seen at the hotter lower edge due to the relatively large temperature gradient  $\nabla T$ . As the heat approaches the upper material, the discrete node point material forces begin to develop at the interface, pointing from the material with the lower density  $\rho_1$  to the one with the higher density  $\rho_2$ . In the course of time, the temperature distribution within the square continues to equilibrate very slowly. In this stage, material forces are left at the boundary and at the interface, as expected.

Now, heat conduction in Green–Naghdi type III material is considered. The situation differs from the one of type I which has been discussed first. The temperature distribution is plotted in Figure 6.21 at times  $t = 10^{-5}$  s,  $t = 3 \cdot 10^{-4}$  s,  $t = 5.3 \cdot 10^{-4}$  s,  $t = 7.6 \cdot 10^{-4}$  s,  $t = 9.8 \cdot 10^{-4}$  s,  $t = 0.0012$  s,  $t = 0.0014$  s and  $t = 0.0017$  s. Not only the temperature development differs: especially the course of the material forces  $\mathbf{F}^{\Phi h}$  is of interest. Those are shown in Figures 6.22 and 6.23. In this model, the heat flux  $\mathbf{q} = [-\kappa_3 \nabla \alpha - \kappa_4 \nabla T] / b$  is dominated by the thermal displacement gradient  $\nabla \alpha$ . In the beginning, this leads to material forces pointing from the hot lower edge to the outside. As the heat propagates through the lower less dense material, the material forces follow. Analogously to type I, material forces can be seen at the interface from the time the heat reaches the interface. Due to the different temperature field, the state of the material forces deviates from that of type I. After 0.0017 seconds, at the material's interface and at the boundary of the upper denser material, the material forces are larger than those at the same nodes in case of type I. For both types, they point into the interior. In case of type III, the material forces are negligible at the boundary of the lower less dense material.

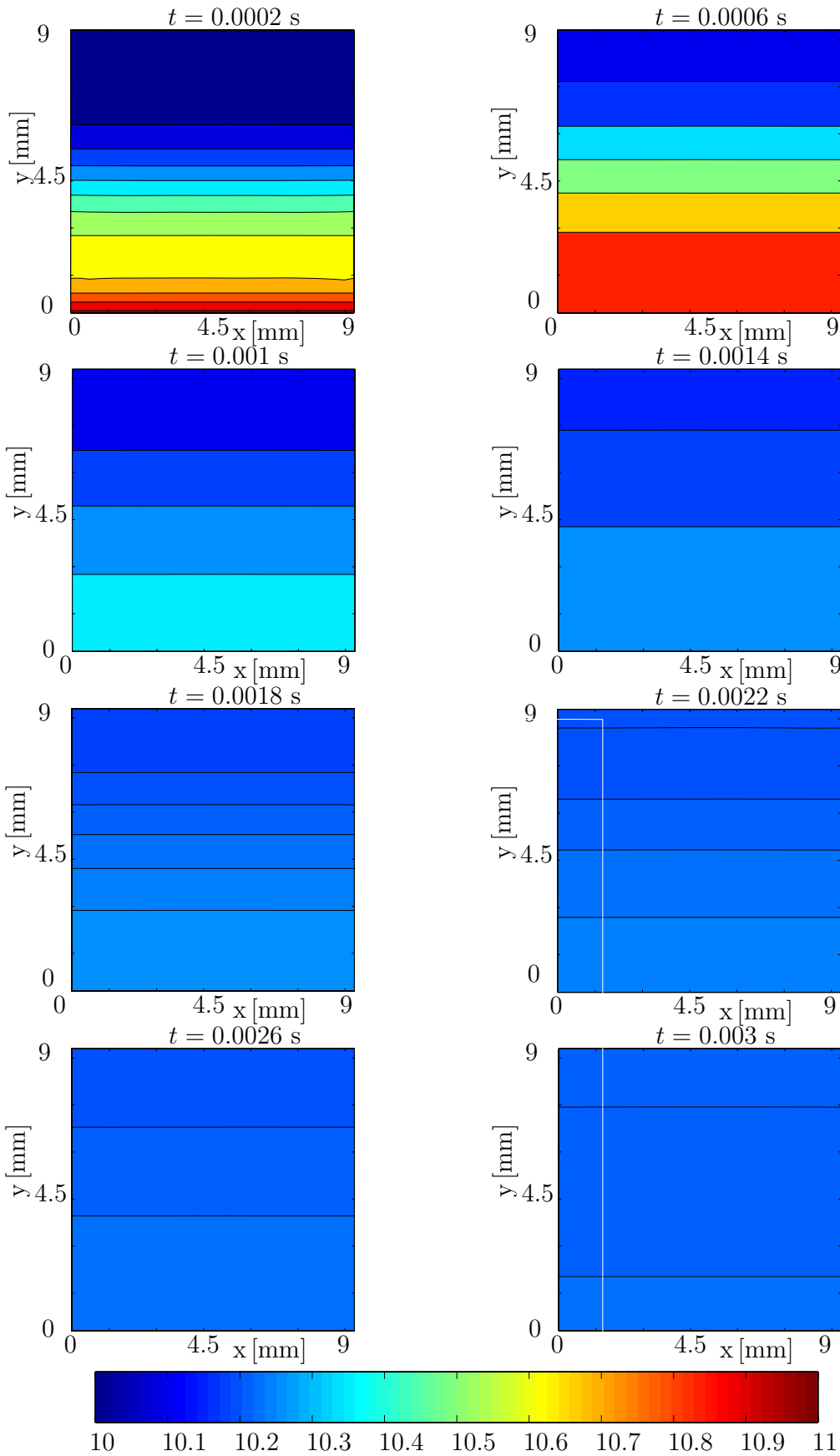


Figure 6.18.: Bimaterial square, heat conduction of type I. Temperature distribution.

6. Theory of non-classical thermo-hyperelasticity

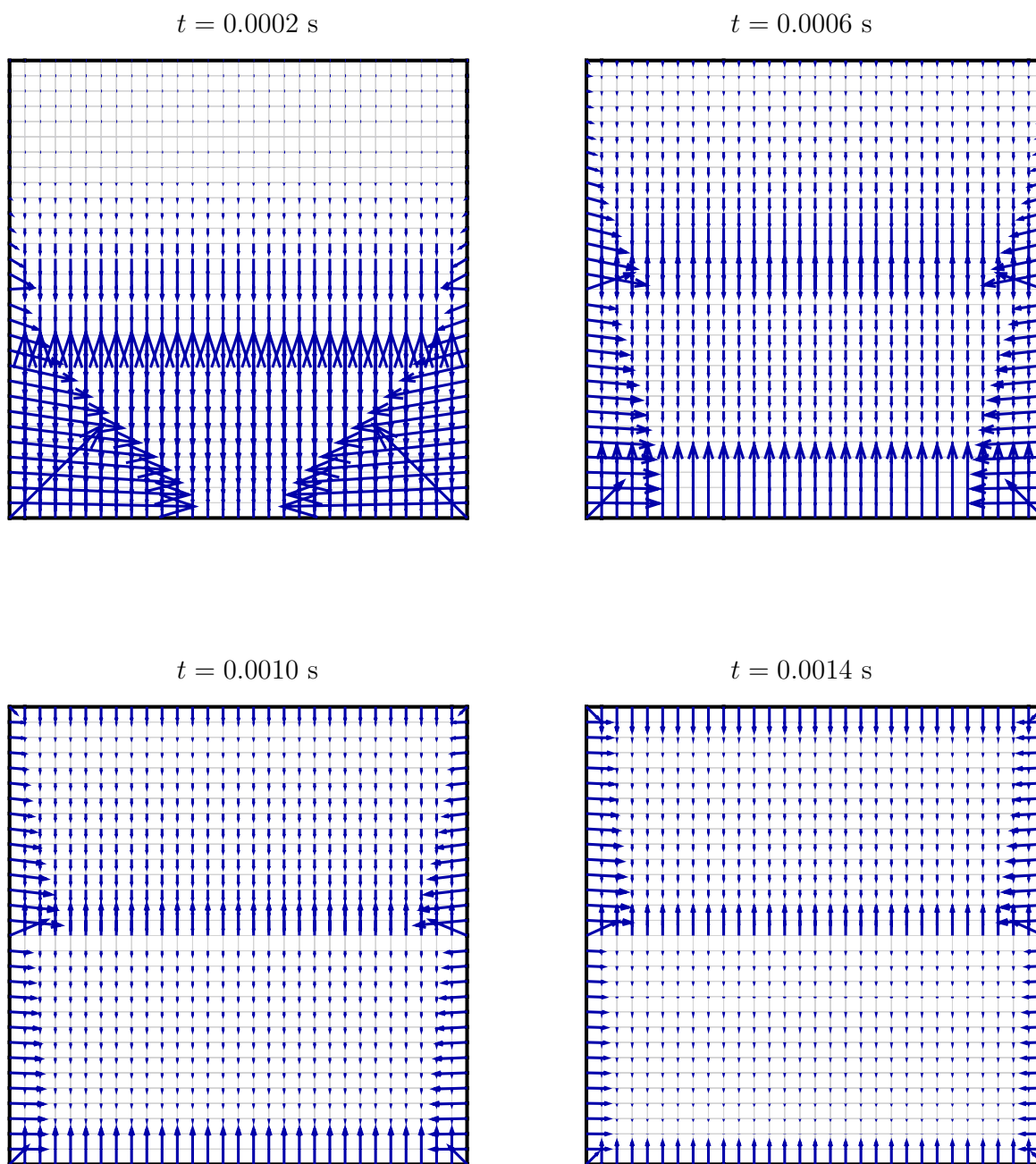


Figure 6.19.: Bimaterial square, heat conduction of type I. The discrete material node point forces  $\mathbf{F}^{\Phi h}$  are plotted at times  $t = 0.0002$  s,  $t = 0.0006$  s,  $t = 0.0010$  s and  $t = 0.0014$  s. In the first time moment taken right after the beginning of the simulation, material forces develop at the material's boundary, especially at the hot lower edge. This is caused by the relatively large heat flux induced by the temperature difference in this part of the square. When the heat reaches the interface, material forces pointing from the lower to the upper material arise.

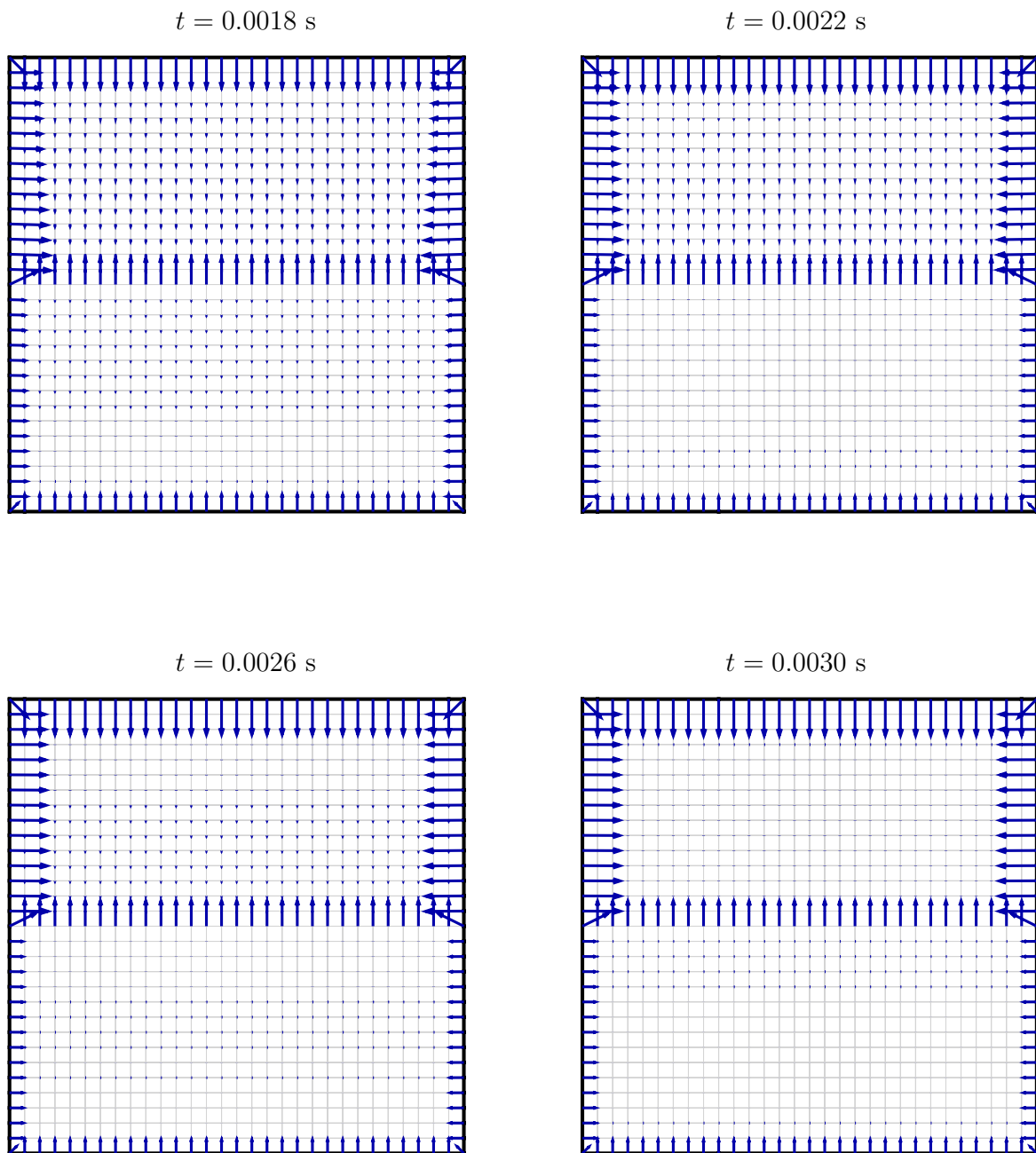


Figure 6.20.: Bimaterial square, heat conduction of type I. The discrete material node point forces  $\mathbf{F}^{\Phi^h}$  are plotted at times  $t = 0.0018$  s,  $t = 0.0022$  s,  $t = 0.0026$  s and  $t = 0.0030$  s. Due to the decreasing heat flux, the material forces vanish only very slowly over time. As expected, material forces exist on the boundary pointing to the inner part of the square as well as at the interface. Those at the boundary point from the less dense to the denser material.

6. Theory of non-classical thermo-hyperelasticity

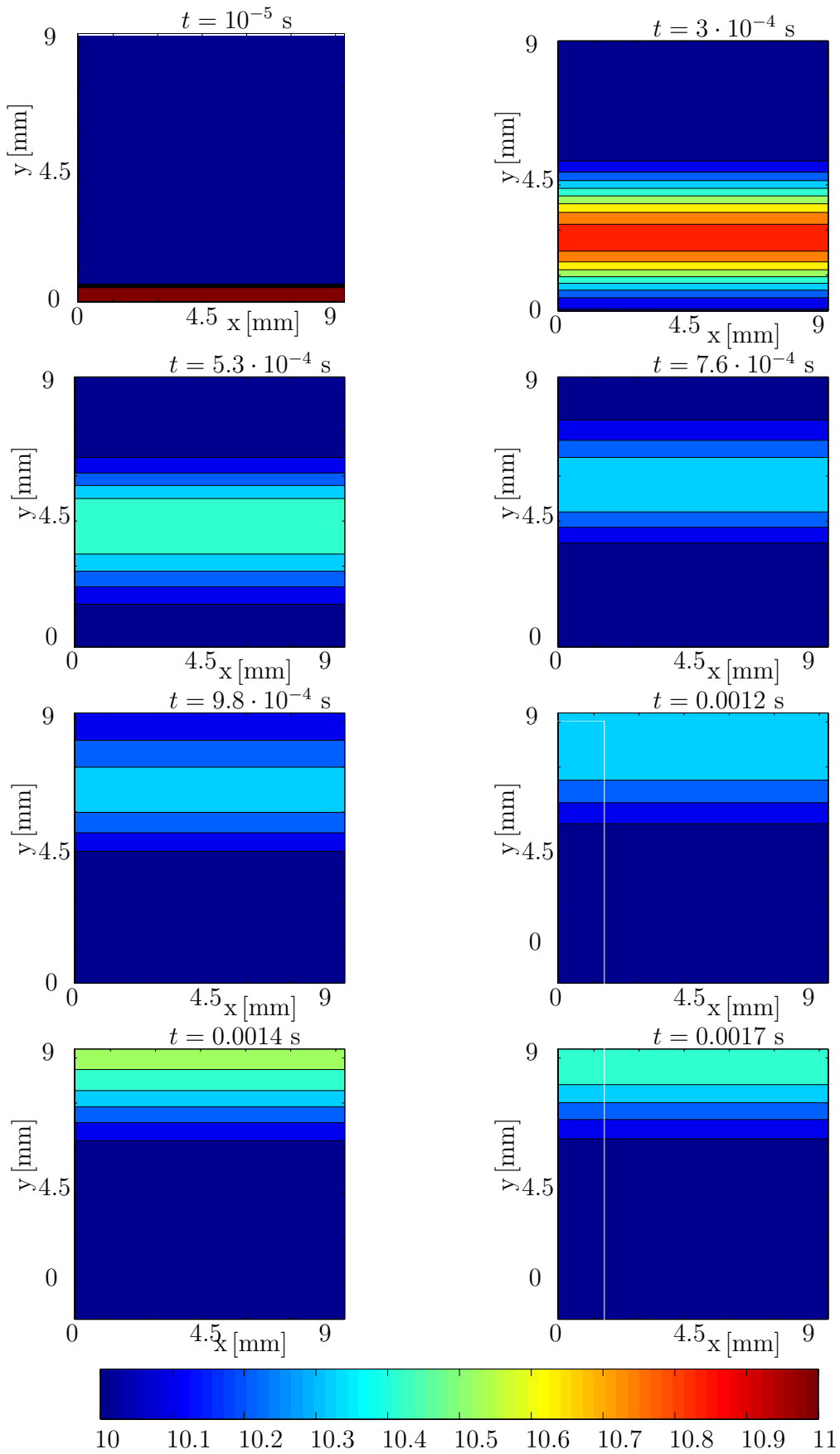


Figure 6.21.: Bimaterial square, heat conduction of type III. Temperature distribution.



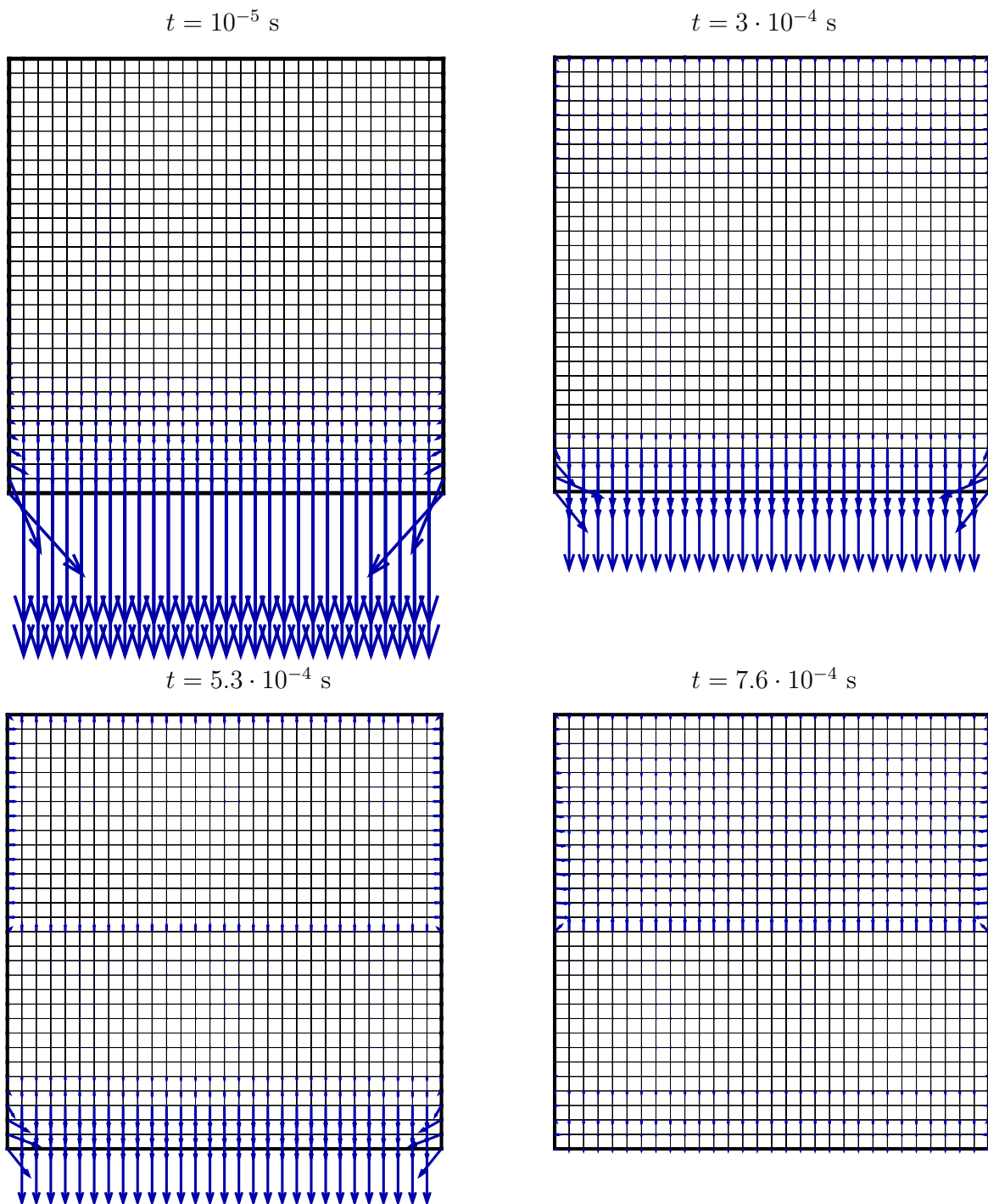


Figure 6.22.: Bimaterial square, heat conduction of type III. The discrete material node point forces  $\mathbf{F}^{\Phi h}$  are plotted at times  $t = 10^{-5} \text{ s}$ ,  $t = 3 \cdot 10^{-4} \text{ s}$ ,  $t = 5.3 \cdot 10^{-4} \text{ s}$  and  $t = 7.6 \cdot 10^{-4} \text{ s}$ . At first, the development of the material forces differs significantly from that in case of heat conduction of type I. The material forces point from the hot lower edge to the outside. This difference is due to the property that the heat flux of type III, and thus the way the heat propagates, is dominated by the thermal displacement gradient  $\nabla_{\mathbf{X}}\alpha$ . In the following, material forces develop at the material's interface similar to type I.

6. Theory of non-classical thermo-hyperelasticity

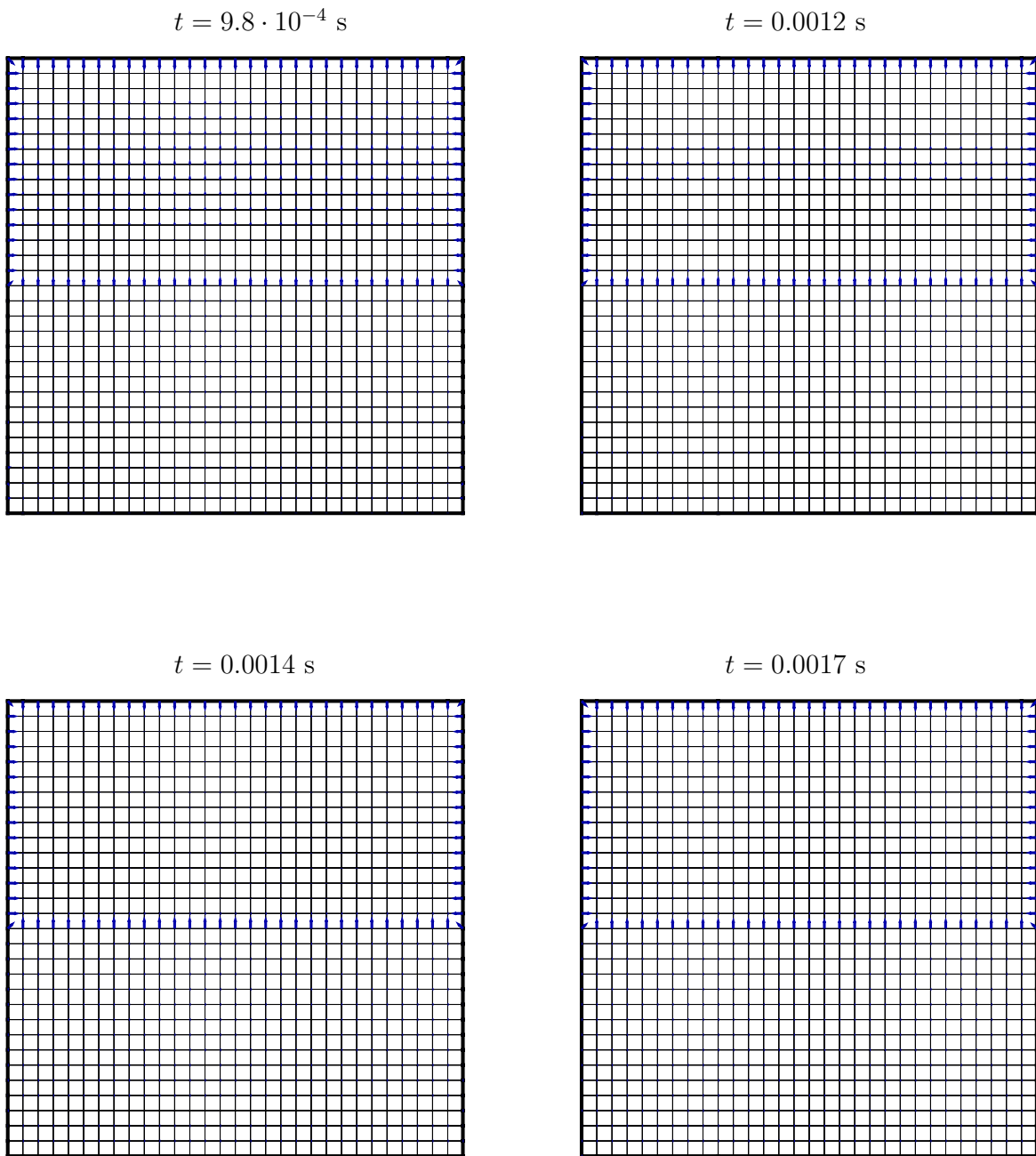


Figure 6.23.: Bimaterial square, heat conduction of type III. The discrete material node point forces  $\mathbf{F}^{\Phi h}$  are plotted at times  $t = 9.8 \cdot 10^{-4} \text{ s}$ ,  $t = 0.0012 \text{ s}$ ,  $t = 0.0014 \text{ s}$  and  $t = 0.0017 \text{ s}$ . After 0.0017 seconds, the heat flux is slowed down a lot. At this time, the state of type III differs from that of type I: the material forces are larger at the interface and at the boundary of the upper denser material. Moreover, they are negligible at the boundary of the lower less dense material. This is due to the different temperature field.

### Coupled thermoelasticity

In the second example, coupled geometrically nonlinear thermoelasticity is discussed. A disc with a crack is considered, as shown in Figure 6.24. The specimen has diameter of 10 m and is modeled with the parameters stated in Table 6.4. Figure 6.24 also illustrates the spatial discretization. In space, it is discretized with 12 constant strain triangular and 84 bilinear quadrilateral finite elements. Moreover, the spatial mesh is refined towards the crack tip. For the temporal discretization 10000 equidistant finite elements are applied. The problem of type I is discretized with a mG(1)-method, whereas for the one of type III a cG(1)-method is chosen. The specimen is fixed at nodes A, B and C (as indicated in Figure 6.24), meaning the movement of the nodes mentioned is limited in x- as well as in y-direction. The disc is observed for 10 seconds, thus the time step equals  $h_n = 0.01$  s.

The disc has a temperature distribution of 10 K with a Dirichlet boundary of 20 K. The displacements are assumed to be zero in the beginning. In case of type III, the thermal displacement  $\alpha$  is initialized to be zero at every node.

Table 6.4.: Material parameters of two-dimensional disc

density $\rho$	10	$\left[\frac{\text{kg}}{\text{m}^3}\right]$
specific heat $c$	100	$\left[\frac{\text{W}}{\text{kgK}}\right]$
thermal conductivity $\kappa_1$	100	$\left[\frac{\text{W}}{\text{mK}}\right]$
thermal conductivity $\kappa_3$	100	$\left[\frac{\text{W}}{\text{s}^2\text{mK}}\right]$
thermal conductivity $\kappa_4$	0.001	$\left[\frac{\text{W}}{\text{mK}}\right]$
thermal expansion coefficient $w$	$10^{-5}$	$\left[\frac{1}{\text{K}}\right]$
Young's modulus $E$	210000	$\left[\frac{\text{N}}{\text{m}^2}\right]$
Poisson's ratio $\nu$	0.4	
reference temperature $T_0$	10	[K]
absolute entropy $S_0$	1	$\left[\frac{\text{N}}{\text{m}^2\text{K}}\right]$
material parameter $b$	1	$\left[\frac{1}{\text{s}^2}\right]$

Figures 6.25 and 6.26 depict the temperature development in the disc in case of thermoelasticity type I at times  $t = 0.01$  s,  $t = 14$  s,  $t = 28$  s,  $t = 42$  s,  $t = 56$  s,  $t = 70$  s,

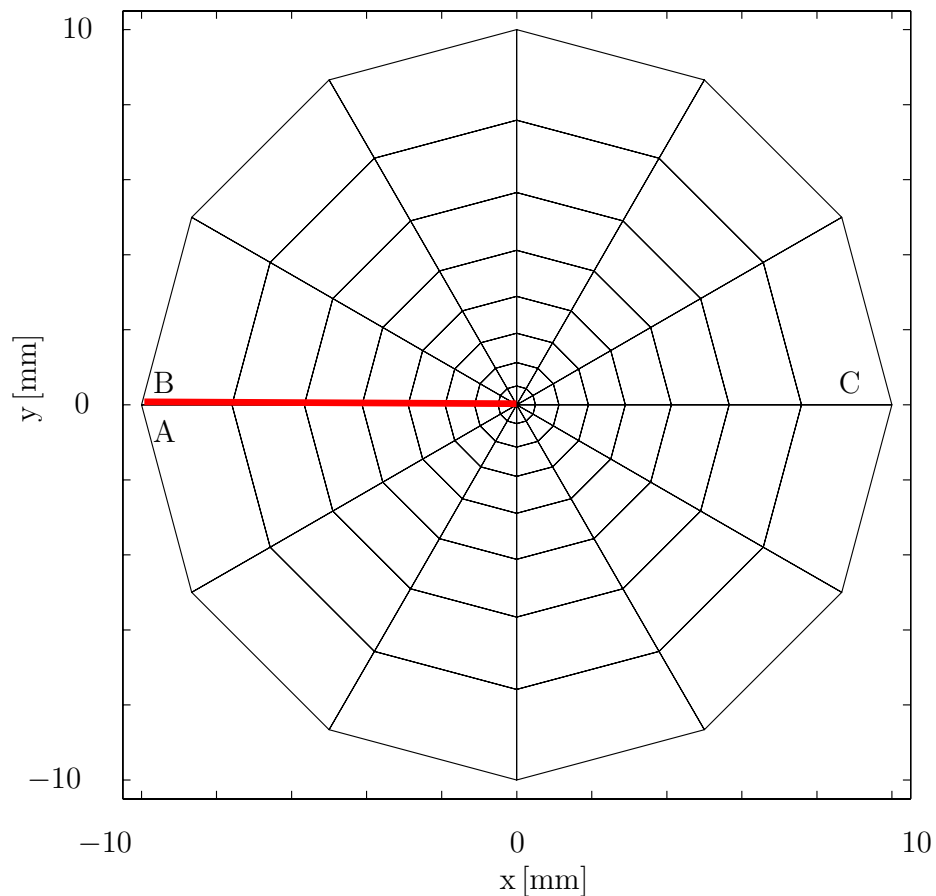


Figure 6.24.: The disc is discretized with 12 constant strain triangular and 84 bilinear quadrilateral finite elements in space. It is fixed at nodes A, B and C in both directions. The red line indicates the crack of the specimen.

$t = 84$  s and  $t = 98$  s. The heat propagates diffusively from the boundary to the interior. In Figures 6.27 and 6.28 the corresponding discrete node point forces  $\mathbf{F}^{\Phi h} = \mathbf{F}_{\text{dyn}}^{\Phi h} + \mathbf{F}_{\text{int}}^{\Phi h} + \mathbf{F}_{\text{vol}}^{\Phi h}$  are shown. As opposed to the thermal example discussed above, the dynamic material force does not vanish in case of coupled thermoelastodynamics as considered in this example, i.e.  $\mathbf{F}_{\text{dyn}}^{\Phi h} \neq \mathbf{0}$ . As the heat and the temperature gradient  $\nabla_{\mathbf{x}}T$  decrease at the boundary, the boundary discrete node point material forces become smaller, too. Moreover, as the center heats up, material forces develop in this region.

The temperature distribution according to type III is illustrated in contour plots, see Figures 6.29 and 6.30. After the boundary is heated, the heat propagates as a thermal wave towards the disc's interior. However, due to the existing diffusive part of the heat flux (remember,  $\kappa_4 \neq 0$ ), the wave's amplitude declines in the beginning. Because of the smaller diameter, it starts to increase again as it travels towards the disc's center point. Furthermore, the computed discrete material node point forces  $\mathbf{F}^{\Phi h}$  are shown in Figures 6.31 and 6.32. The material node point forces decrease over time due to the decreasing heat flux  $\mathbf{Q}$  and propagate along with the wave. Moreover, while pointing to the middle in the beginning, their direction changes when the wave detaches from the boundary.

Concluding, it has to be mentioned that due to the relatively young history of the material force method, the significance of the method itself and the physical interpretation of the discrete material node point forces  $\mathbf{F}^{\Phi h}$  is not yet fully analyzed. Consequently, it is desirable that further investigations are made in the future.

6. Theory of non-classical thermo-hyperelasticity

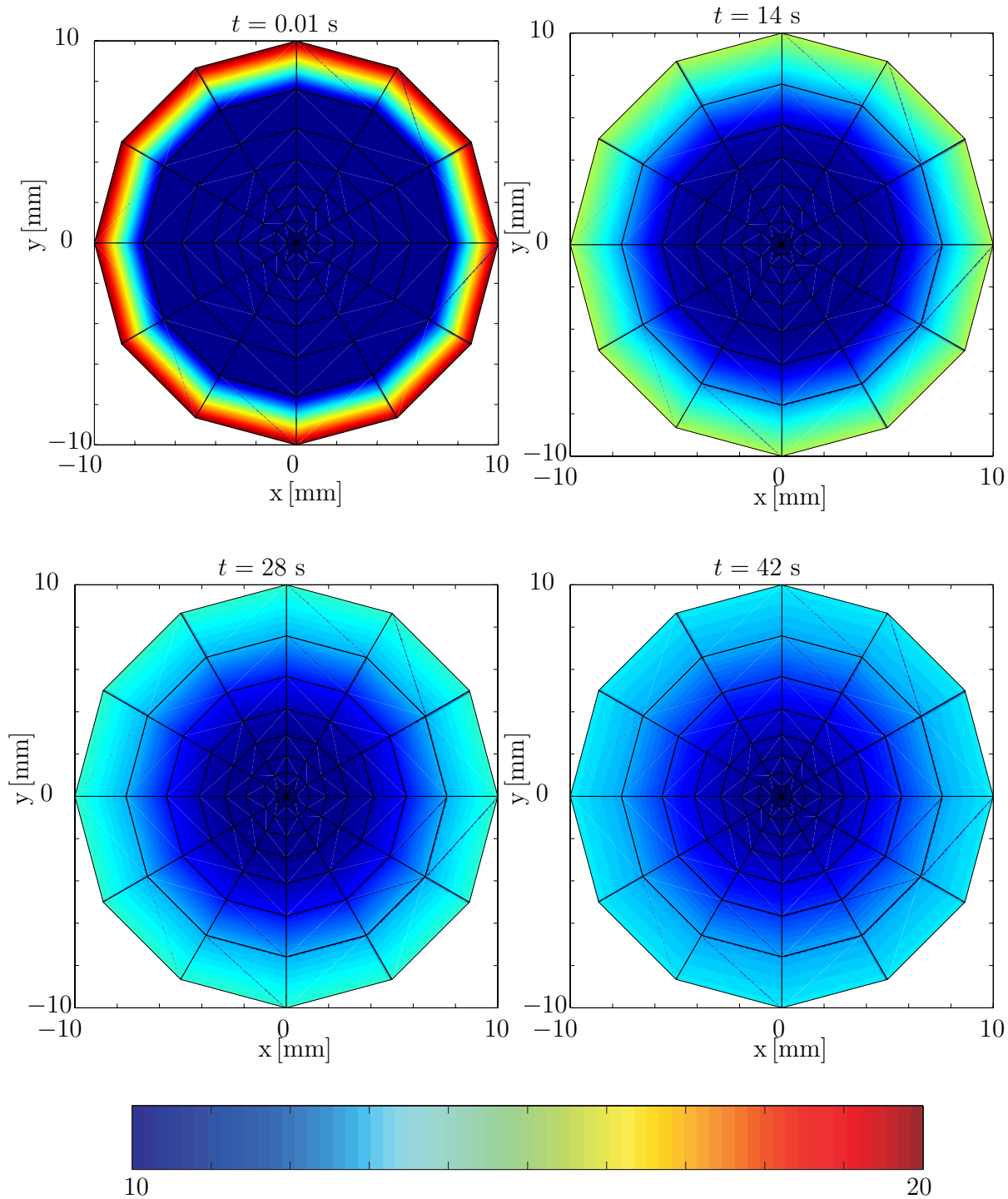


Figure 6.25.: Two dimensional disc with crack. Heat conduction of type I. The temperature distribution is plotted at times  $t = 0.01$  s,  $t = 14$  s,  $t = 28$  s and  $t = 42$  s.

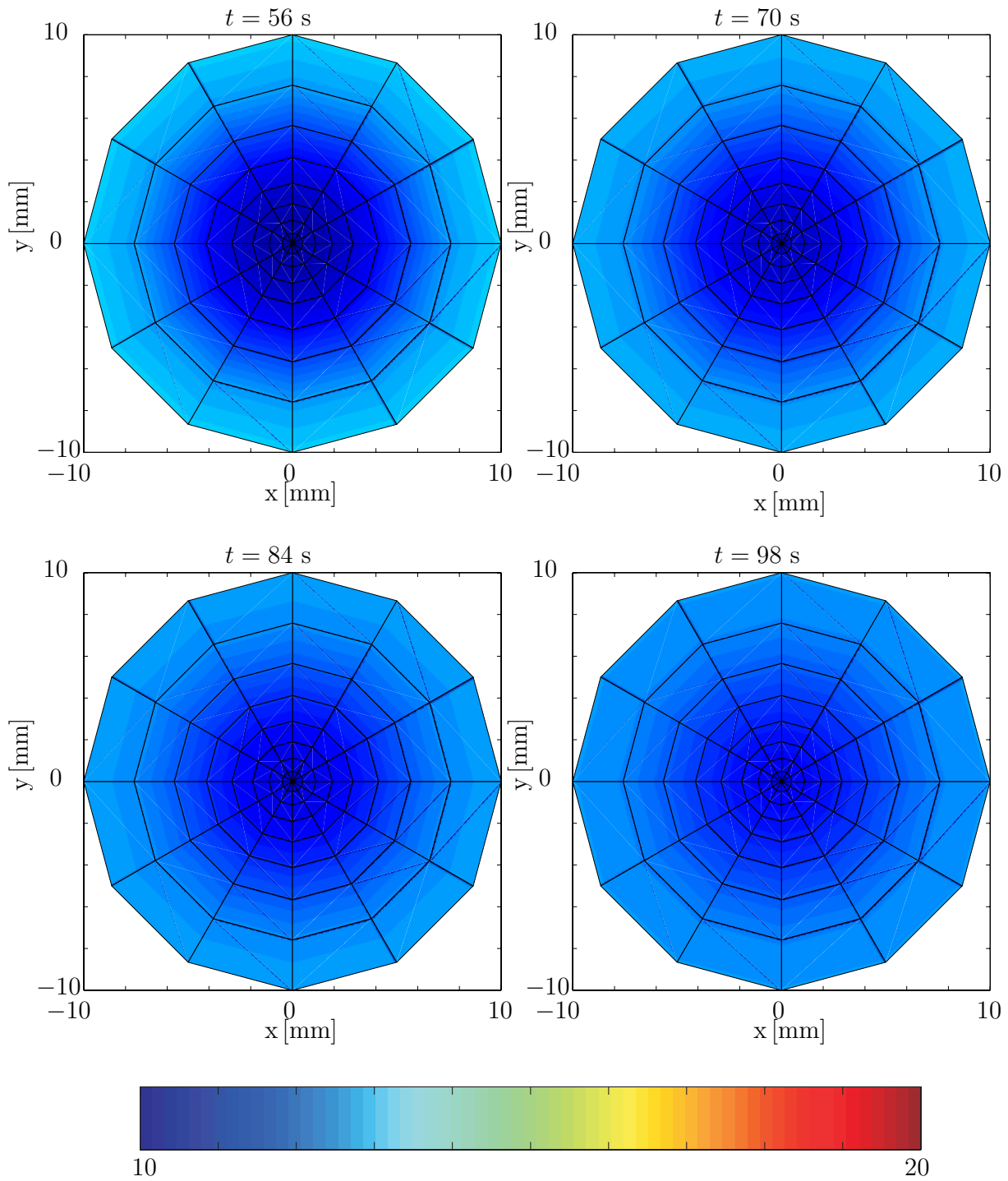


Figure 6.26.: Two dimensional disc with crack. Heat conduction of type I. The temperature distribution plotted at times  $t = 56$  s,  $t = 70$  s,  $t = 84$  s and  $t = 98$  s.

6. Theory of non-classical thermo-hyperelasticity

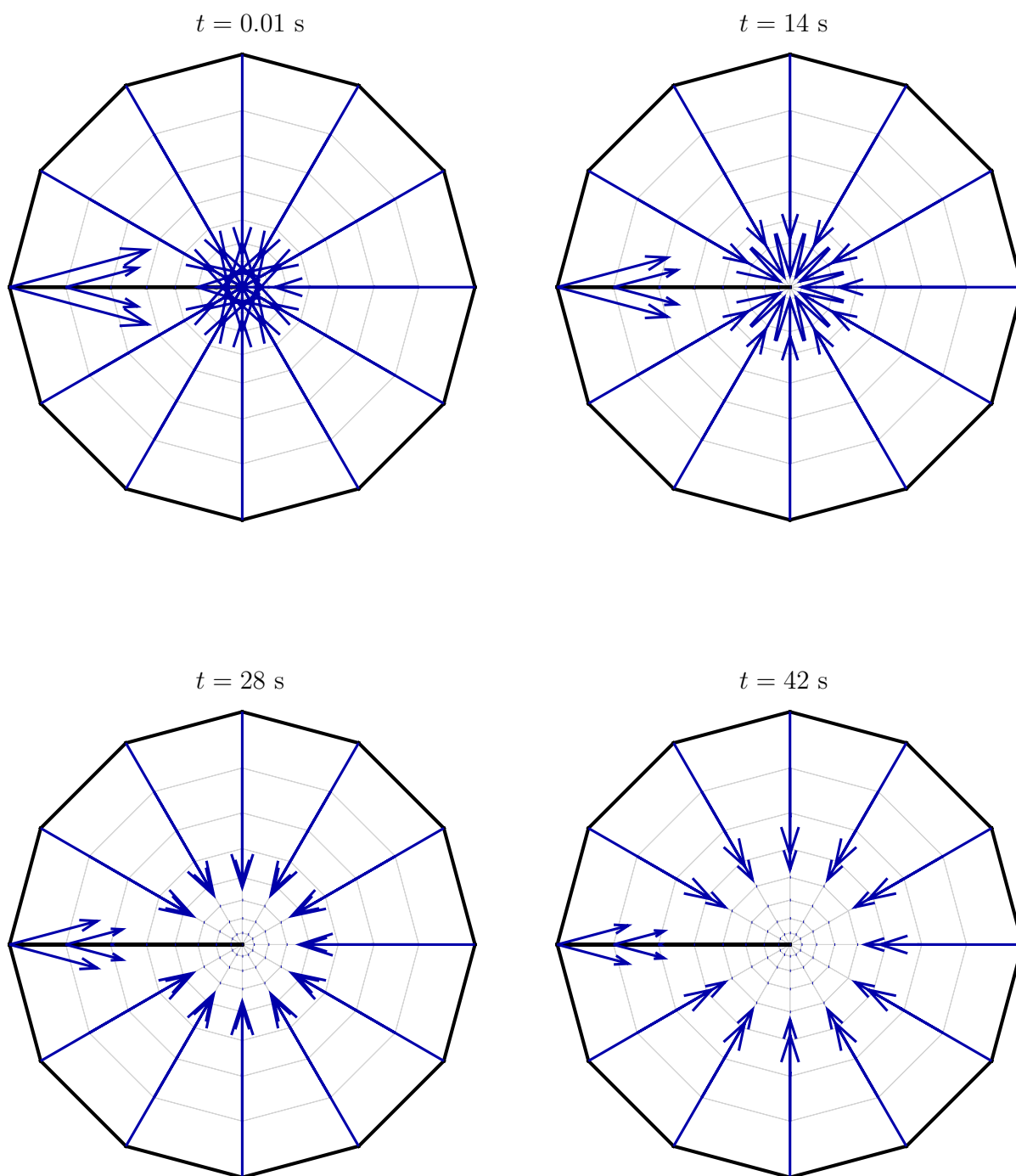


Figure 6.27.: Two dimensional disc with crack. Heat conduction of type I. The discrete material node point forces  $\mathbf{F}^{\Phi h}$  are plotted at times  $t = 0.01$  s,  $t = 14$  s,  $t = 28$  s and  $t = 42$  s.



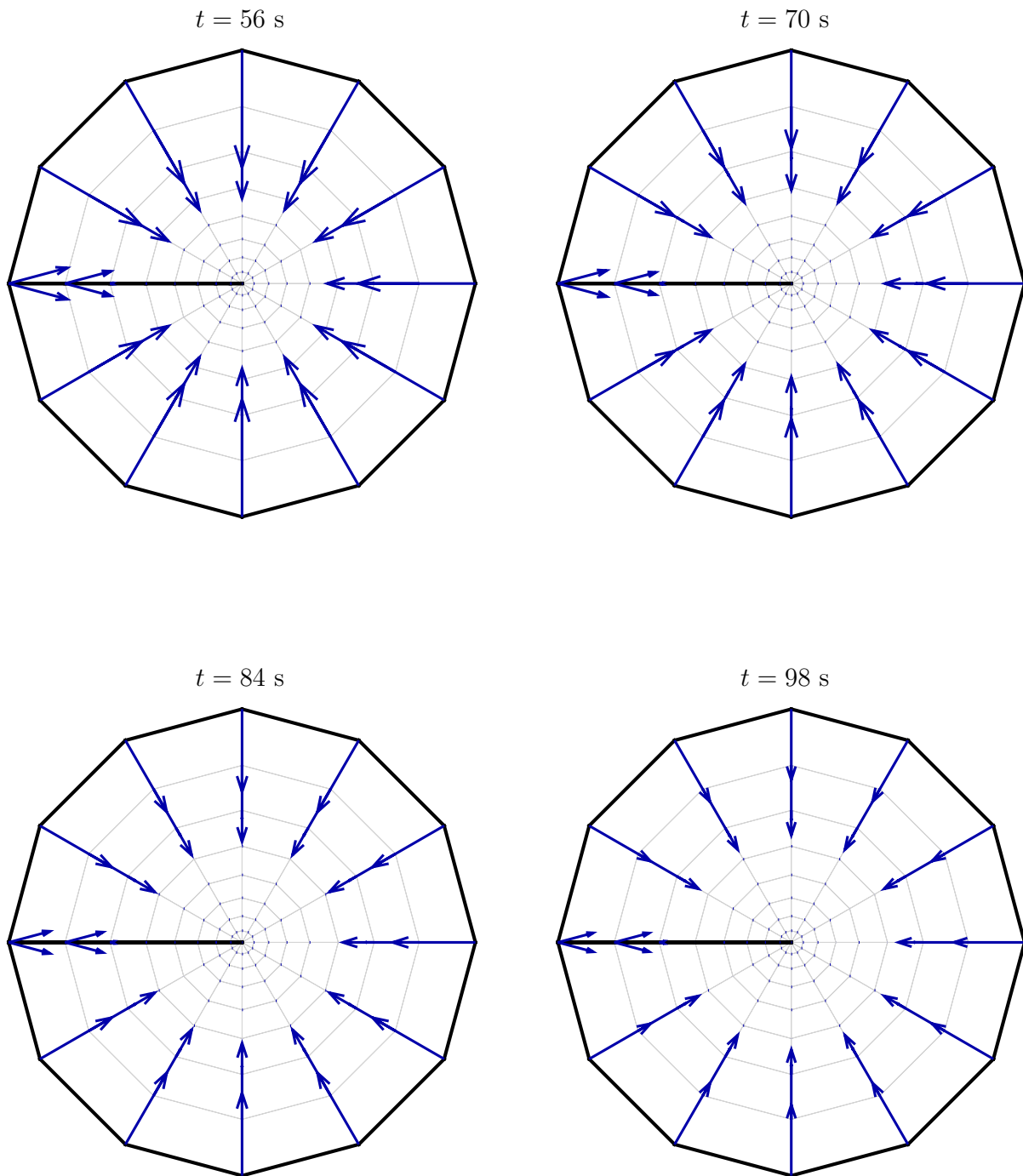


Figure 6.28.: Two dimensional disc with crack. Heat conduction of type I. The discrete material node point forces  $\mathbf{F}^{\Phi h}$  are plotted at times  $t = 56$  s,  $t = 70$  s,  $t = 84$  s and  $t = 98$  s.

6. Theory of non-classical thermo-hyperelasticity

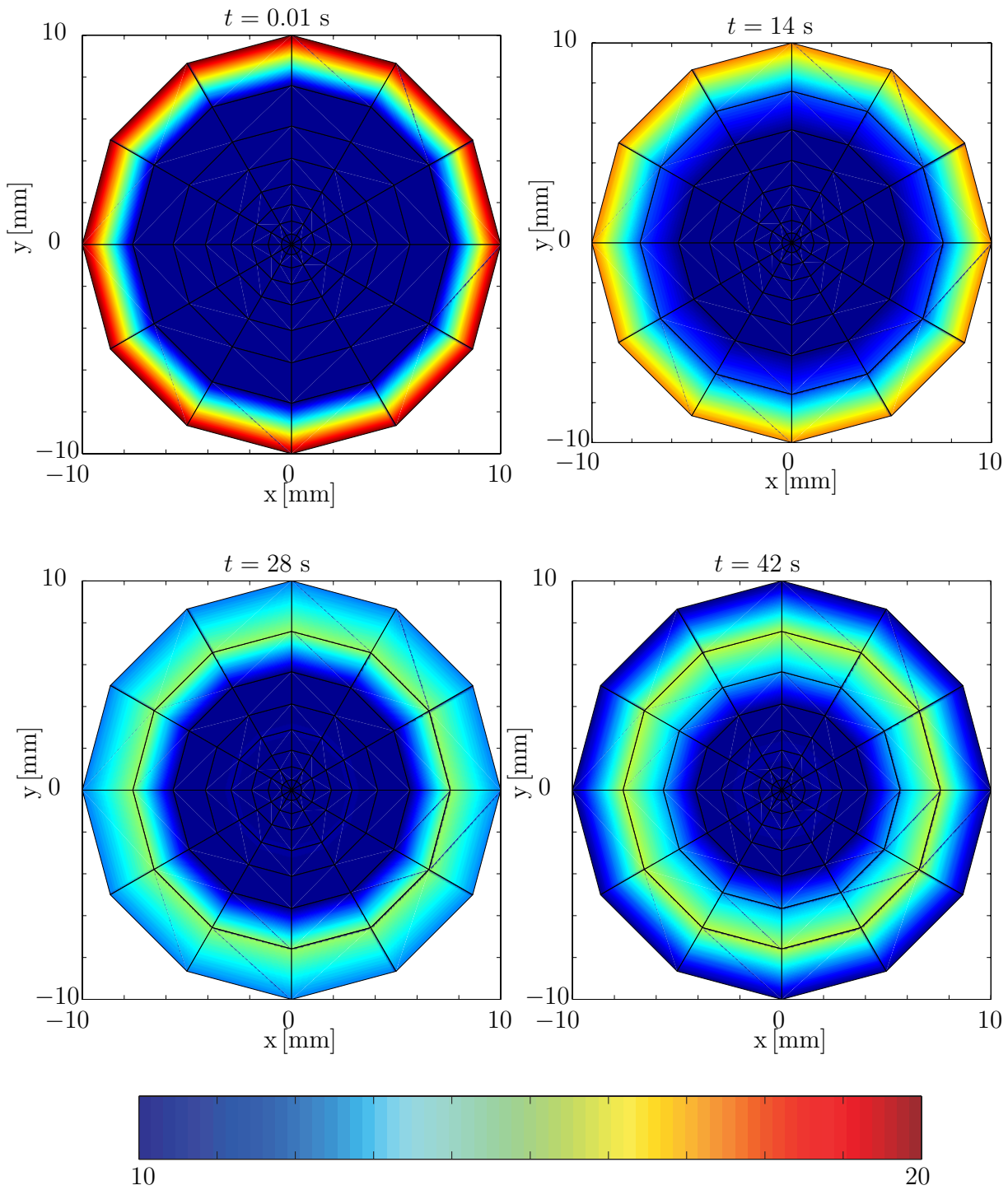


Figure 6.29.: Two dimensional disc with crack. Heat conduction of type III. The temperature distribution is plotted at times  $t = 0.01$  s,  $t = 14$  s,  $t = 28$  s and  $t = 42$  s. Heat propagates as a thermal wave from the warmer boundary to the cooler middle of the disc.

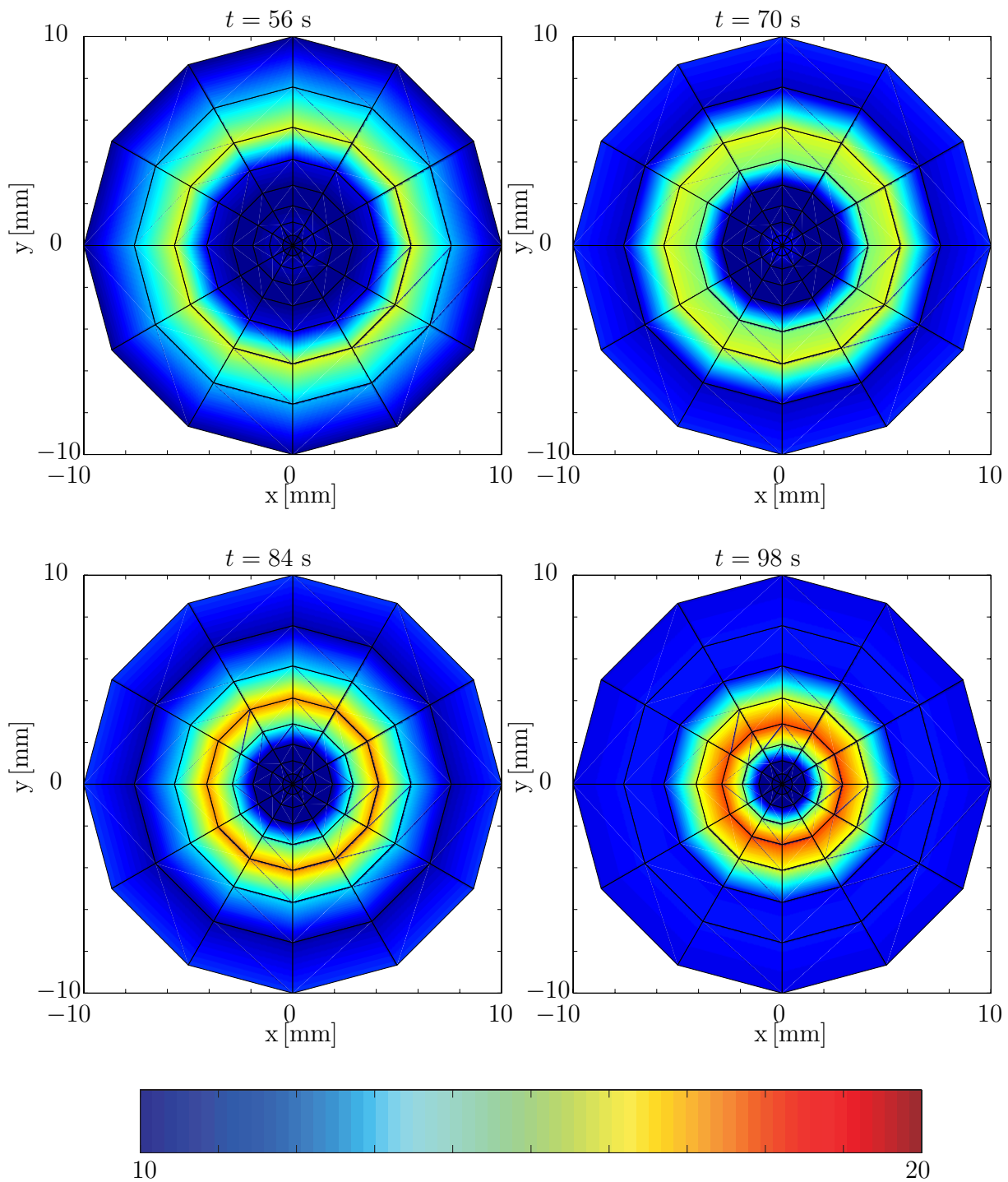


Figure 6.30.: Two dimensional disc with crack. Heat conduction of type III. The temperature distribution is plotted at times  $t = 56$  s,  $t = 70$  s,  $t = 84$  s and  $t = 98$  s. The thermal wave continues to travel towards the disc's middle.

6. Theory of non-classical thermo-hyperelasticity

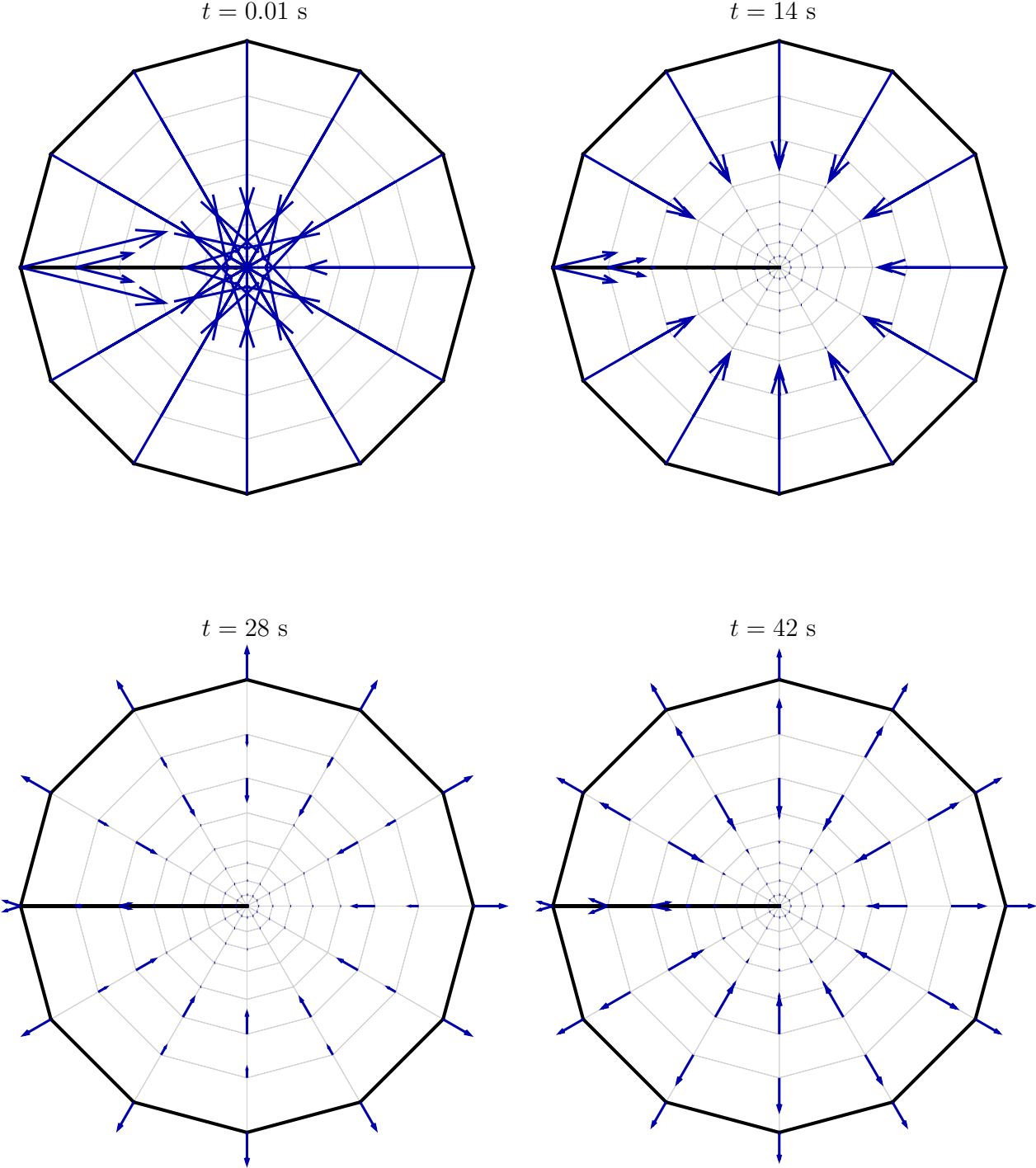


Figure 6.31.: Two dimensional disc with crack. Heat conduction of type III. The discrete material node point forces  $\mathbf{F}^{\Phi h}$  are plotted at times  $t = 0.01 \text{ s}$ ,  $t = 14 \text{ s}$ ,  $t = 28 \text{ s}$  and  $t = 42 \text{ s}$ .

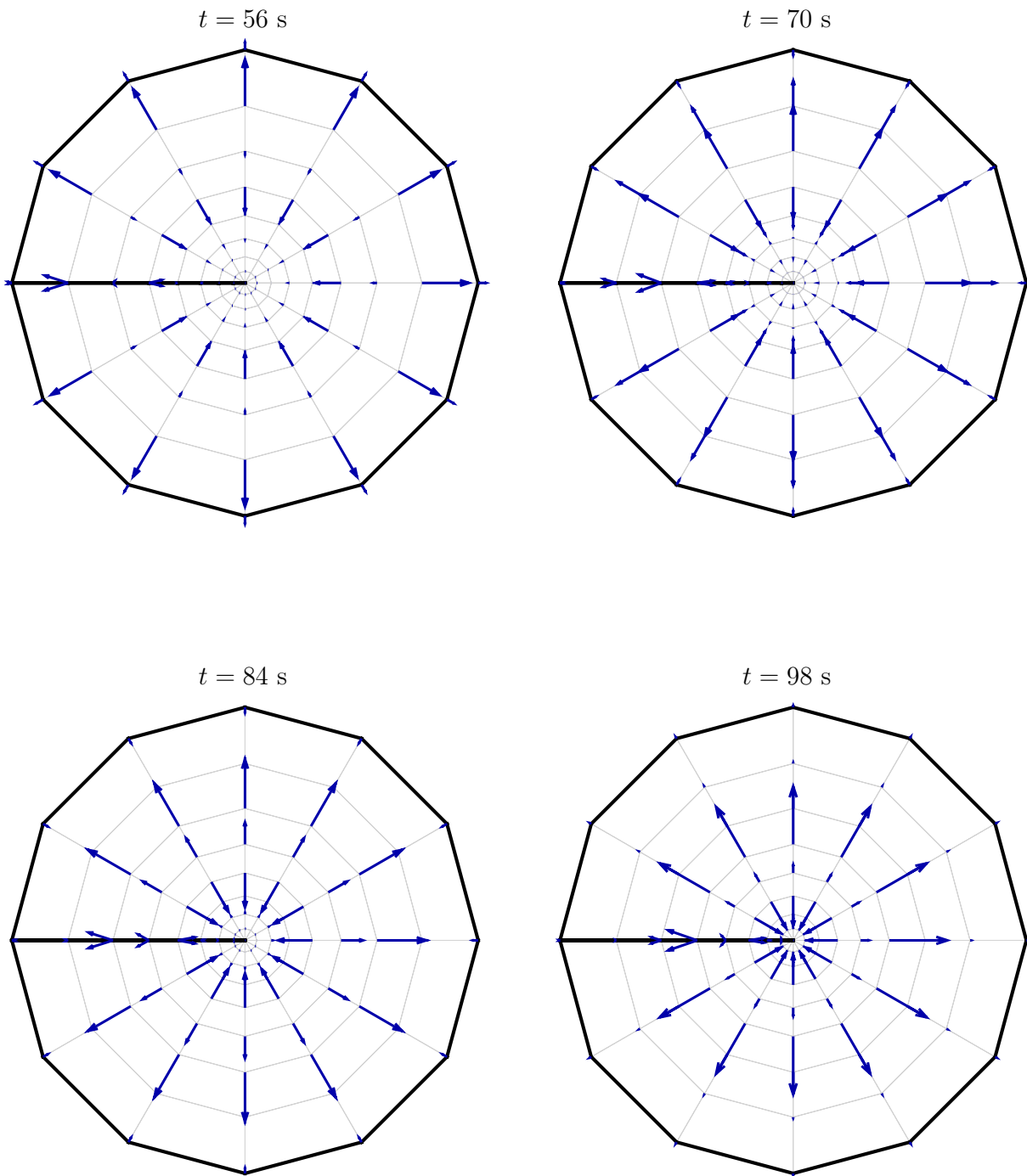


Figure 6.32.: Two dimensional disc with crack. Heat conduction of type III. The discrete material node point forces  $\mathbf{F}^{\Phi h}$  are plotted at times  $t = 56$  s,  $t = 70$  s,  $t = 84$  s and  $t = 98$  s.

## 6.5. Energy conserving finite element discretization in time for type II

Contrary to others, the Green–Naghdi approach of type II does not necessarily include energy dissipation. To complement the fully consistent derivation of Green and Naghdi, an elegant and consequent discretization process was chosen. The solution method suggested above is based on finite elements for the spatial as well as for the temporal discretization. However, due to numerical dissipation, the total energy is not conserved in case of geometrically nonlinear coupled thermoelasticity of type II - although the theory is inherently energy-conserving if  $\partial\psi/\partial\alpha = 0$ .

The works of Betsch and Steinmann [17, 18, 19, 20], Groß [57] and Groß et al. [58] show that in the nonlinear elastodynamic case the balance of momentum is conserved if the cG-method is used for the time discretization. The references also prove that additional work is necessary in order to provide the conservation of the balance of energy and the balance of angular momentum during numerical simulations, which eventually is possible. In particular, the quadrature rules applied during the numerical time integration play an important role. Mohr et al. [111] extend their work to an energy-consistent momentum-conserving finite element time stepping scheme for large strain elasto-plasto dynamics. Groß and Betsch [59] present an dissipation consistent finite element discretization for coupled thermoelasticity of type I - “dissipation consistent” meaning that no numerical, i.e. no non-physical, dissipation shall be involved. Motivated by their work, an energy conserving finite element discretization in time for type II will be derived in the following.

### 6.5.1. Energy consistent algorithmic stress tensor method

Betsch and Steinmann [18] show that “... provided that the time integrals appearing in the [continuous Galerkin] time finite element formulation are calculated exactly, the resulting time-stepping scheme is exactly energy-conserving.”, where the words in the brackets have been added for clarity. An energy-conserving temporal finite element discretization is particularly interesting in case of a non-dissipative theory of type II. As shown in Section 4.2.2, Eq. (4.2.17), the internal entropy production  $\xi$  (and thus the dissipation) is determined via the free energy density  $\psi$ . Therefore, in this Chapter, the free energy density  $\psi$  is chosen to be independent of the thermal displacement  $\alpha$  in order to obtain an energy conserving theory of type II. In other words:  $\rho_0\theta\xi = -\rho_0\frac{\partial\psi}{\partial\alpha}\dot{\alpha} = 0$ . Thus, the total energy  $\mathcal{E}$ , i.e. the sum of the internal  $\epsilon = \psi + \theta\eta$  and the kinetic energy density  $k$ , is conserved:

$$\begin{aligned}\dot{\mathcal{E}} &:= \rho_0\dot{\epsilon} + \rho_0\dot{k} = 0 \\ \Rightarrow \rho_0\dot{\psi} + \rho_0\dot{\theta}\eta + \rho_0\theta\dot{\eta} - \mathbf{S} : \frac{1}{2}\dot{\mathbf{C}} &= 0.\end{aligned}\tag{6.5.1}$$

As mentioned above, the time integrals appearing in the finite element formulation have to be calculated exactly - a property which is rarely feasible with standard quadrature formulas. In order to derive an energy consistent algorithm for approximating the balance of linear momentum (3.2.6), the second Piola–Kirchhoff stress tensor  $\mathbf{S}$  is substituted by a modified stress tensor  $\mathbf{S}^{\text{alg}}$ , following the way of [57, 58, 111]. This step is necessary because standard quadrature rules do not conserve the internal energy, see e.g. [17]. However, this modified stress tensor  $\mathbf{S}^{\text{alg}}$  does not add any physical stress to the continuum formulation. In other words, it does not effect the physical stress. It only represents a non-standard quadrature rule ( e.g. instead of the Gaussian quadrature rule) for the approximation of the stress tensor  $\mathbf{S}$ . Consequently, the divergence term in Eq. (3.2.6) is expressed in terms of the second Piola–Kirchhoff stress tensor  $\mathbf{S}$  which reads

$$\begin{aligned}
 \int_{\mathcal{B}} \delta\varphi \cdot \text{Div} \mathbf{P} \, dV &= - \int_{\mathcal{B}} \nabla_{\mathbf{X}} \delta\varphi : \mathbf{P} \, dV + \int_{\partial\mathcal{B}} \delta\varphi \cdot \mathbf{P} \cdot \mathbf{N} \, dA \\
 &= - \int_{\mathcal{B}} \nabla_{\mathbf{X}} \delta\varphi : [\mathbf{F}^t \cdot \mathbf{S}^t] \, dV + \int_{\partial\mathcal{B}} \delta\varphi \cdot \mathbf{P} \cdot \mathbf{N} \, dA \\
 &= - \int_{\mathcal{B}} \frac{1}{2} [\mathbf{F}^t \cdot \nabla_{\mathbf{X}} \delta\varphi + \nabla_{\mathbf{X}} \delta\varphi^t \cdot \mathbf{F}] : \mathbf{S}^t \, dV + \int_{\partial\mathcal{B}} \delta\varphi \cdot \mathbf{P} \cdot \mathbf{N} \, dA \\
 &= - \int_{\mathcal{B}} \delta\mathbf{E} : \mathbf{S} \, dV + \int_{\partial\mathcal{B}} \delta\varphi \cdot \mathbf{P} \cdot \mathbf{N} \, dA
 \end{aligned} \tag{6.5.2}$$

Here, it is made use of the fact that the inner product of the symmetric tensor  $\mathbf{S}$  and the skew-symmetric part of  $\delta\mathbf{E}$  vanishes (cf. Appendix A.4).

In order to obtain an energy consistent stress approximation tensor  $\mathbf{S}^{\text{alg}}$ , it has to fulfill the constrained minimization problem

$$\mathcal{F}(\mathbf{S}^{\text{alg}}) := \frac{1}{2} \int_0^1 \|\mathbf{S}^{\text{alg}}(\tau) - \mathbf{S}(\tau)\|^2 \, d\tau \rightarrow \min, \tag{6.5.3}$$

with

$$\mathcal{E}(\mathbf{S}^{\text{alg}}) = \rho_0 \epsilon_1 - \rho_0 \epsilon_0 - \int_0^1 \mathbf{S}^{\text{alg}} : \frac{1}{2} D_{\tau} \mathbf{C} \, d\tau = 0 \tag{6.5.4}$$

being its constraint in each time step, as demanded by e.g. [57, 58, 111]. Here,  $D_{\tau}$  denotes the total derivative with respect to  $\tau$  and  $\epsilon_1 = \epsilon(\tau = 1)$  and  $\epsilon_0 = \epsilon(\tau = 0)$ , respectively. For brevity, the dependence of  $\epsilon$  and thus  $\mathcal{E}$ ,  $\mathcal{L}$ , ..., on the thermal displacement  $\alpha$ , the temperature  $T$  and the thermal displacement gradient  $\nabla_{\mathbf{X}} \alpha$  is taken into account but not explicitly mentioned. Thus, the difference between the modified stress tensor  $\mathbf{S}^{\text{alg}}$  and the original stress tensor  $\mathbf{S}$  is minimized with respect to the norm of the functional  $\mathcal{F}$ . The energy consistency, i.e. constraint (6.5.4), is taken into account with the help of a Lagrange multiplier  $\lambda$ . Thus, a minimization of the least-square Lagrange functional  $\mathcal{L}$

$$\begin{aligned}
 \mathcal{L}(\mathbf{S}^{\text{alg}}, \lambda) &:= \mathcal{F}(\mathbf{S}^{\text{alg}}) + \lambda \mathcal{E}(\mathbf{S}^{\text{alg}}) \\
 &= \frac{1}{2} \int_0^1 \|\mathbf{S}^{\text{alg}}(\tau) - \mathbf{S}(\tau)\|^2 \, d\tau + \lambda \left[ \rho_0 \epsilon_1 - \rho_0 \epsilon_0 - \int_0^1 \mathbf{S}^{\text{alg}} : \frac{1}{2} D_{\tau} \mathbf{C} \, d\tau \right]
 \end{aligned} \tag{6.5.5}$$

## 6. Theory of non-classical thermo-hyperelasticity

yields the following extremal conditions

$$\begin{aligned}\frac{\partial \mathcal{L}}{\partial \mathbf{S}^{\text{alg}}} &= \int_0^1 [\mathbf{S}^{\text{alg}} - \mathbf{S}] \, d\tau - \lambda \int_0^1 \frac{1}{2} \mathbf{D}_\tau \mathbf{C} \, d\tau = 0, \\ \frac{\partial \mathcal{L}}{\partial \lambda} &= \mathcal{E}(\mathbf{S}^{\text{alg}}) = 0.\end{aligned}\quad (6.5.6)$$

From Eq. (6.5.6)<sub>1</sub>, it follows locally

$$\mathbf{S}^{\text{alg}} = \mathbf{S} + \lambda \frac{1}{2} \mathbf{D}_\tau \mathbf{C}. \quad (6.5.7)$$

Inserting Eq. (6.5.7) into Eq. (6.5.4) leads to

$$\mathcal{E}(\mathbf{S}^{\text{alg}}) = \rho_0 \epsilon_1 - \rho_0 \epsilon_0 - \int_0^1 \mathbf{S} : \frac{1}{2} \mathbf{D}_\tau \mathbf{C} \, d\tau - \lambda \int_0^1 \frac{1}{4} \mathbf{D}_\tau \mathbf{C} : \mathbf{D}_\tau \mathbf{C} \, d\tau = 0. \quad (6.5.8)$$

As a result, it follows

$$\lambda = \frac{\mathcal{E}(\mathbf{S})}{\int_0^1 \frac{1}{4} \mathbf{D}_\tau \mathbf{C} : \mathbf{D}_\tau \mathbf{C} \, d\tau} \quad (6.5.9)$$

and consequently

$$\mathbf{S}^{\text{alg}}(\mathbf{S}) = \mathbf{S} + \frac{\mathcal{E}(\mathbf{S})}{\int_0^1 \frac{1}{2} \mathbf{D}_\tau \mathbf{C} : \mathbf{D}_\tau \mathbf{C} \, d\tau} \mathbf{D}_\tau \mathbf{C}. \quad (6.5.10)$$

Thus, Eq. (6.5.10) represents the general solution to the minimization problem (6.5.3) and therefore expresses the modified stress tensor  $\mathbf{S}^{\text{alg}}$ . The additional second term in Eq. (6.5.10) is a weighted time derivative of the right Cauchy–Green tensor  $\mathbf{C}$ .

In the following, an approximation of the stress integral  $\int_0^1 \mathbf{S} \, d\tau$  is given in case of a temporal cG-method (see Section 6.2.2 for information on the cG-method) as an algorithmic application of the modified stress tensor. For illustration, the simplest case, i.e.  $k = 1$ , is treated explicitly.

$$\mathbf{S}^{\text{alg}}(\mathbf{S}_{.5}) \approx \mathbf{S}_{.5} + \left[ \frac{2[\rho_0 \epsilon_1 - \rho_0 \epsilon_0] - \mathbf{S}_{.5} : [\mathbf{C}_1 - \mathbf{C}_0]}{\|\mathbf{C}_1 - \mathbf{C}_0\|^2} \right] [\mathbf{C}_1 - \mathbf{C}_0]$$

with

$$\mathbf{S}_{.5} = \mathbf{S}(\mathbf{C}(\tau = .5)) \quad (6.5.11)$$

$$= \mathbf{S}\left(\frac{\mathbf{C}_1 + \mathbf{C}_0}{2}\right). \quad (6.5.12)$$

Consequently, the resulting ecG(1)-approximation with Gauss point  $\tau = .5$  corresponds to the midpoint rule known from finite difference methods. Resorting to the terminology of [57], “ecG” refers to enhanced continuous Galerkin method meaning that the nonstandard energy consistent stress approximation introduced in Section 6.5.1 is applied to the stress integral.



It can easily be shown that for the ecG(1)-approximation Eq. (6.5.11) fulfills the local energy constraint, i.e. Eq. (6.5.4),

$$\begin{aligned}
 & \rho_0 \epsilon_1 - \rho_0 \epsilon_0 - \int_0^1 \mathbf{S} : \frac{1}{2} D_\tau \mathbf{C} \, d\tau \\
 = & \rho_0 \epsilon_1 - \rho_0 \epsilon_0 - \frac{1}{2} \int_0^1 \mathbf{S} \, d\tau : [\mathbf{C}_1 - \mathbf{C}_0] \\
 = & \rho_0 \epsilon_1 - \rho_0 \epsilon_0 - \frac{1}{2} \mathbf{S}^{\text{alg}} : [\mathbf{C}_1 - \mathbf{C}_0] \\
 = & \rho_0 \epsilon_1 - \rho_0 \epsilon_0 - \frac{1}{2} \left[ \mathbf{S}_{.5} + \left[ \frac{2 [\rho_0 \epsilon_1 - \rho_0 \epsilon_0] - \mathbf{S}_{.5} : [\mathbf{C}_1 - \mathbf{C}_0]}{\|\mathbf{C}_1 - \mathbf{C}_0\|^2} \right] [\mathbf{C}_1 - \mathbf{C}_0] \right] : [\mathbf{C}_1 - \mathbf{C}_0] \\
 = & \rho_0 \epsilon_1 - \rho_0 \epsilon_0 - \frac{1}{2} \left[ \frac{2 [\rho_0 \epsilon_1 - \rho_0 \epsilon_0]}{\|\mathbf{C}_1 - \mathbf{C}_0\|^2} [\mathbf{C}_1 - \mathbf{C}_0] \right] : [\mathbf{C}_1 - \mathbf{C}_0] \\
 = & 0.
 \end{aligned} \tag{6.5.13}$$

Thus, the energy is conserved and consequently,  $\mathcal{E}(\mathbf{S}^{\text{alg}}) \rightarrow 0$  and  $\mathbf{S}^{\text{alg}} \rightarrow \mathbf{S}$  for  $h_n \rightarrow 0$ . Conservation of energy is also shown independently of the applied polynomial degree for elasto-plasto dynamics in [111].

## 6.5.2. Numerical example

A free motion of a cannonball is modeled in two dimensions. The temperature inside the cannonball is set to 300 K. At the boundary, it is cooled by the air, thus the temperature is initiated at 290 K. An initial translational velocity of  $\mathbf{v}_{\text{trans}0} = 2\mathbf{e}_x + 2\mathbf{e}_y$  and an initial angular velocity  $\boldsymbol{\omega}_{\text{ang}0} = -0.5\mathbf{e}_z$  is assumed.

In space, 12 constant strain triangular and 84 bilinear quadrilateral elements are applied. A ecG(1)-approximation with 1000 linear elements is used for the temporal discretization. In the following, the results of the ecG(1)-approximation are shown. Figure 6.35 pictures the sequence of motion of the flying cannonball at times  $t = 0$  s,  $t = 12$  s,  $t = 24$  s,  $t = 36$  s and  $t = 48$  s. The disc's rotation is indicated by the red marker. The plot of the temperature distribution shows that the heat propagates as a thermal wave through the disc. Due to the lack of dissipation, it will propagate endlessly from the boundary to the center and vice versa.

In Figure 6.34, the total energy  $\mathcal{E}$  is plotted versus time. Figure 6.34 clearly shows that the energy is conserved with the ecG-method, whereas it is not in case of the cG-method.

6. Theory of non-classical thermo-hyperelasticity

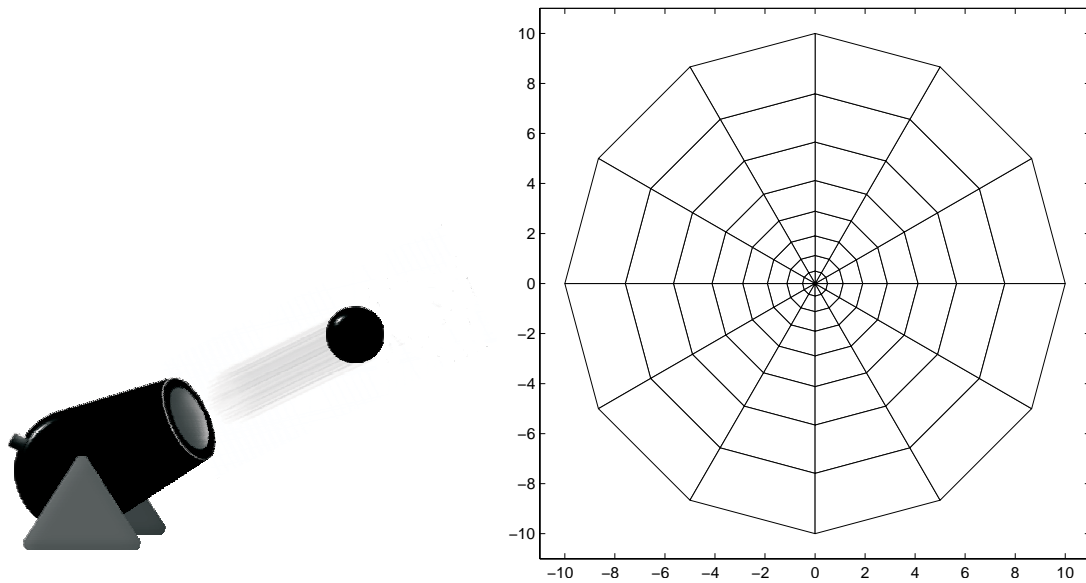


Figure 6.33.: Left: Cannonball fired from a gun barrel. Right: Spatial discretization of the cannonball: 12 constant strain triangular and 84 bilinear quadrilateral elements.

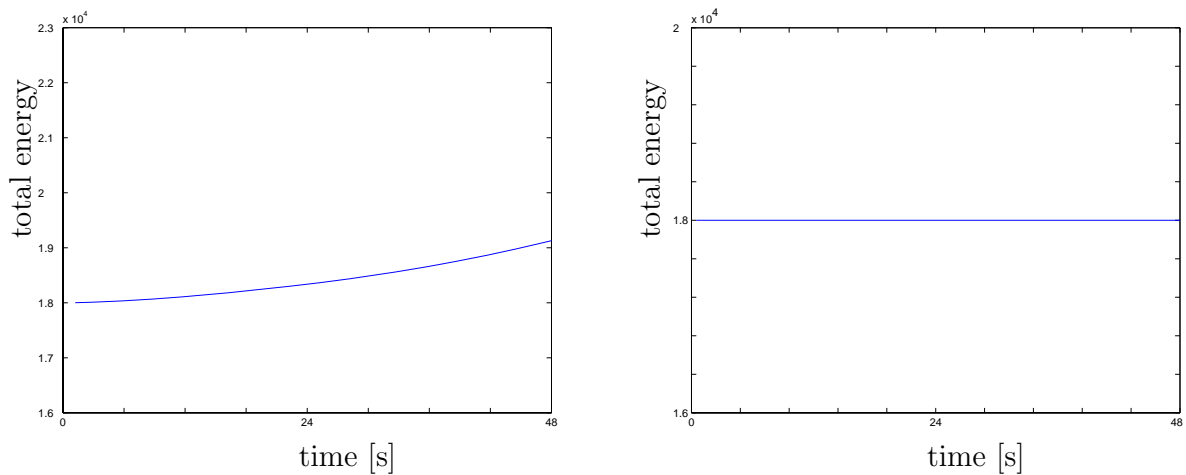


Figure 6.34.: On the left the total energy in case of a cG(1)-temporal finite element discretization is plotted. During the simulation the computed energy increases - this is physically unreasonable. On the right the total energy in case of a ecG(1)-discretization is depicted. Due to the fact that the thermoelastic theory of type II does not involve energy dissipation, the total energy is conserved during the simulation.

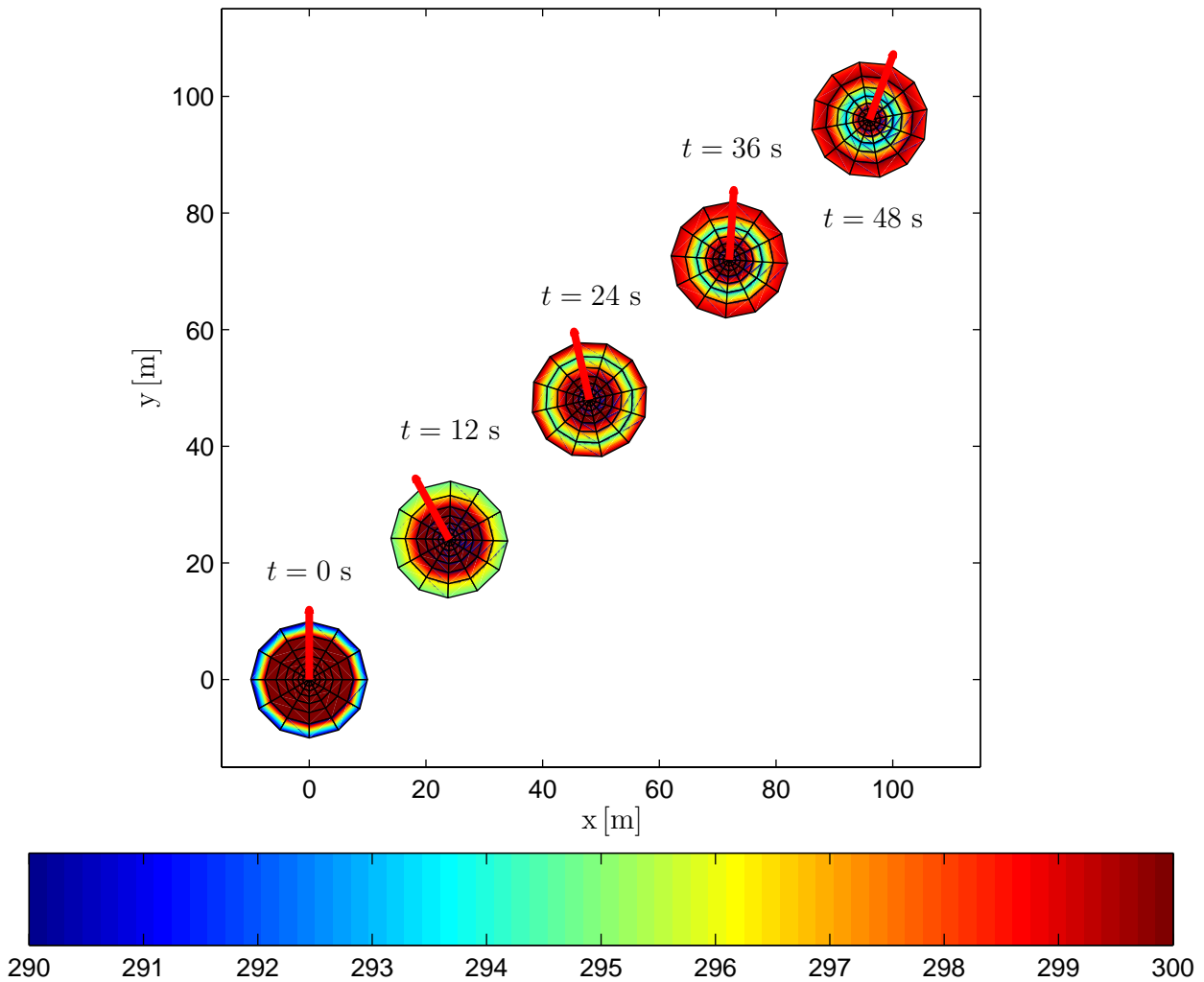


Figure 6.35.: Some snapshots of the motion of the flying cannonball at times  $t = 0$  s,  $t = 12$  s,  $t = 24$  s,  $t = 36$  s and  $t = 48$  s. The temperature distribution is also plotted. The heat slowly propagates as a thermal wave through the cannonball in the course of time.

6. *Theory of non-classical thermo-hyperelasticity*

## 7. Incremental variational formulation

This Chapter introduces a formulation of an variational principle describing coupled thermoelasticity of type I and II. The point of departure is the action functional  $I$  of which the variational formulation, i.e. the formulation of an extremum principle with respect to the motion  $\varphi$  and thermal displacement  $\alpha$ , leads to the Euler-Lagrange equations of thermoelasticity. In turn, the latter lead to the solutions of the unknown mechanical and thermal fields.

In this connection, the existence of a potential for the first Piola–Kirchhoff stress tensor  $\mathbf{P}$ , the entropy density  $\eta$  and the entropy flux vector  $\mathbf{H}$  is the key characteristic. A thermodynamic potential is a function from which state variables characterizing a thermodynamic state of the system are derived, cf. Holzapfel [66]. In case of the first Piola–Kirchhoff stress tensor  $\mathbf{P}$  and the entropy density  $\eta$ , the free energy density  $\psi$  forms a potential for type I, II and III and explicit expressions are well-known. Furthermore, the free energy density  $\psi$  is a potential for the entropy flux vector  $\mathbf{H}$  of type II (cf. Eq. (4.2.16)). Consequently, a variational setting can be derived which is shown by Maugin and Kalpakides [104, 105, 106]. Things are slightly more complicated in case of classical heat conduction. It is not possible to derive the classical theory of thermoelasticity from a variational principle, see e.g. [37]. At this point, the existence of a potential for the entropy flux vector  $\mathbf{H}$  in continuum mechanics is usually assumed, but it cannot be stated explicitly, cf. [146, 173]. Therefore, a derivation of an incremental entropy flux, following Fourier’s law by means of an incremental potential similar to the spirit of the theory of the non-dissipative Green–Naghdi-type II, is targeted. Motivated by the procedure of [93, 173], a variational formulation within the incremental framework for coupled thermoelasticity for type I mimicing type II is formulated. The results presented in this Chapter are published in the work of Bargmann and Steinmann [12].

### 7.1. Preliminaries

#### 7.1.1. Continuous setting

First, the Lagrange density function  $L$  is introduced

$$L(\dot{\alpha}, \nabla_{\mathbf{X}}\alpha, \varphi, \dot{\varphi}, \mathbf{C}; \mathbf{X}) := K - \rho\psi, \quad (7.1.1)$$

where  $K(\dot{\varphi}; \mathbf{X}) := \frac{1}{2}\rho\dot{\varphi} \cdot \dot{\varphi}$  denotes the kinetic energy. Furthermore, the analysis is restricted to conservative external loads. Therefore, the potential of the external mechanical and thermal

## 7. Incremental variational formulation

loads reads

$$P(\boldsymbol{\varphi}, \alpha) := \int_{\mathcal{B}_0} \boldsymbol{\varphi} \cdot \rho \mathbf{b} \, dV + \int_{\partial \mathcal{B}_P} \boldsymbol{\varphi} \cdot \bar{\mathbf{t}} \, dA + \int_{\mathcal{B}_0} \alpha \rho s \, dV, \quad (7.1.2)$$

where  $\bar{\mathbf{t}}$  denotes the traction vector. The Neumann boundary condition of the mechanical problem, i.e. the prescribed traction vector  $\bar{\mathbf{t}}$ , is defined on the surface  $\partial \mathcal{B}_P \subset \partial \mathcal{B}_0$ .

The corresponding action functional  $I$  is defined:

$$I(\boldsymbol{\varphi}, \alpha) := \int_t \left[ \int_{\mathcal{B}_0} L \, dV + P \right] dt = \int_t \int_{\mathcal{B}_0} L^* \, dV \, dt. \quad (7.1.3)$$

The variation with respect to the deformation map  $\boldsymbol{\varphi}$  and the thermal displacement  $\alpha$  and requiring an extremum for the action integral  $I$  leads to the Euler-Lagrange equations

$$\begin{aligned} \frac{\partial L^*}{\partial \alpha} - \frac{D}{DX_I} \left( \frac{\partial L^*}{\partial \alpha_{,I}} \right) - \frac{D}{Dt} \left( \frac{\partial L^*}{\partial \dot{\alpha}} \right) &= 0, \\ \frac{\partial L^*}{\partial \varphi_j} - \frac{D}{DX_I} \left( \frac{\partial L^*}{\partial \varphi_{j,I}} \right) - \frac{D}{Dt} \left( \frac{\partial L^*}{\partial \dot{\varphi}_j} \right) &= 0. \end{aligned} \quad (7.1.4)$$

At this point, the definition of an action functional  $I$  is of course only meaningful, if the underlying Lagrange function  $L^*$  describes the system at hand properly. More precisely, a potential structure is needed. In Section 7.1.2 an incremental potential formulation for thermoelastic solids of Green–Naghdi type I and II is constructed.

As mentioned above, one of the outstanding properties of the Green–Naghdi theory of type II is the fact the entropy flux vector  $\mathbf{H}$  is determined by the same potential, i.e. the energy density  $\psi$ , as the mechanical stress  $\mathbf{P}$  and the entropy density  $\eta$ , as stated in Eq. (4.2.16). This allows for deriving the governing equations of thermoelasticity of type II via a variational formulation [104, 105, 106]. Inserting the relations (4.2.14) - (4.2.15) and the constitutive assumptions (6.1.7) into the Euler-Lagrange equations (7.1.4) leads to the system of equations

$$\begin{aligned} \rho_0 \dot{\eta} &= -\text{Div} \mathbf{H} + \rho_0 s \\ \rho_0 \dot{\mathbf{v}} &= \text{Div} \mathbf{P} + \rho_0 \mathbf{b} \end{aligned} \quad (7.1.5)$$

governing non-classical thermoelasticity of type II. For reasons of transparency, the abbreviation  $\mathcal{Q}^{\text{mech}}$  is used for the thermomechanical coupling term in the following, i.e.  $\mathcal{Q}^{\text{mech}} = T \partial \mathbf{P} / \partial T : \dot{\mathbf{F}}$ . Remember, this term is responsible for the so-called Gough–Joule effect, i.e. when deformations lead to structural heating.

### 7.1.2. Incremental setting

As mentioned in Chapter 4.1, the Green–Naghdi theory is intrinsically based on three different state spaces for type I, II and III. In order to establish one consistent incremental variational formulation, it is resorted to one general state space  $\mathcal{S}_{\text{inc}} = \{\alpha, \dot{\alpha}, \nabla_{\mathbf{X}} \alpha, \mathbf{C}\}$  which only provides for first order gradients. In the continuous case, this state space corresponds to the one

of type II, see Definition (4.1.1). As in the following, the quantities' subscripts refer to the time step, the material mass density  $\rho_0$  is denoted by  $\rho_0 = \rho$ .

A potential formulation with an explicitly stated potential for the heat flux of type I cannot be derived in a continuous setting. Therefore, the arbitrary time interval  $[t_{n-1}; t_n]$  is considered in order to obtain an incremental formulation. For the reason of simplicity it is written  $\dot{\varphi}_n$  and  $\nabla_{\mathbf{X}}\alpha_n$  instead of  $(\dot{\varphi})_n$  resp.  $(\nabla_{\mathbf{X}}\alpha)_n$ .

The incremental internal working  $W_n$  is defined as

$$W_n(\mathbb{S}) := \int_{t_{n-1}}^{t_n} \rho \dot{\psi} + \rho \theta \xi \, dt \quad (7.1.6)$$

which consists of the storing part  $\rho \dot{\psi}$  and the dissipative part  $\rho \theta \xi$ . The latter consists only of the internal entropy production  $\rho \theta \xi$  due to the fact the only rate-independent material behavior is considered in this thesis. In order to account for the dissipative part, the incremental Lagrange density  $L_n$  reads

$$L_n(\dot{\alpha}_n, \nabla_{\mathbf{X}}\alpha_n, \varphi_n, \dot{\varphi}_n, \mathbf{C}_n; \mathbf{X}) := K_n - W_n. \quad (7.1.7)$$

$K_n(\dot{\varphi}_n; \mathbf{X}) := \frac{1}{2}\rho\dot{\varphi}_n \cdot \dot{\varphi}_n$  denotes the kinetic energy at time  $t = t_n$ .

The first term of the time integral (7.1.6) can be integrated exactly, whereas the midpoint rule is applied to the second term (of which the exact integral is unknown). This leads to

$$W_n = \rho\psi_n - \rho\psi_{n-1} + \frac{[\rho\theta_n\xi_n + \rho\theta_{n-1}\xi_{n-1}]\Delta t}{2} \quad (7.1.8)$$

which suffices for  $\Delta t \rightarrow 0$ . The differentiations with respect to time, i.e.  $D/Dt$  are approximated by the difference quotient. For example, the temperature  $T_n = \dot{\alpha}_n$  at time  $t_n$  yields

$$\dot{\alpha}_n = \frac{\alpha_n - \alpha_{n-1}}{\Delta t}. \quad (7.1.9)$$

Consequently, the following approximation of the temperature gradient  $\nabla_{\mathbf{X}}T_n$  at time  $t_n$  holds

$$\nabla_{\mathbf{X}}T_n = \nabla_{\mathbf{X}}\dot{\alpha}_n = \nabla_{\mathbf{X}}\left(\frac{\alpha_n - \alpha_{n-1}}{\Delta t}\right) = \frac{\nabla_{\mathbf{X}}\alpha_n - \nabla_{\mathbf{X}}\alpha_{n-1}}{\Delta t}. \quad (7.1.10)$$

The derivatives  $\partial\nabla_{\mathbf{X}}\dot{\alpha}_n/\partial\nabla_{\mathbf{X}}\alpha_n$  and  $\partial\nabla_{\mathbf{X}}\dot{\alpha}_n/\partial\dot{\alpha}_n$  fulfill:

$$\frac{\partial\nabla_{\mathbf{X}}\dot{\alpha}_n}{\partial\nabla_{\mathbf{X}}\alpha_n} = \frac{\partial\left(\frac{\nabla_{\mathbf{X}}\alpha_n - \nabla_{\mathbf{X}}\alpha_{n-1}}{\Delta t}\right)}{\partial\nabla_{\mathbf{X}}\alpha_n} = \frac{1}{\Delta t}\mathbf{I} \quad (7.1.11)$$

respectively

$$\frac{\partial\nabla_{\mathbf{X}}\dot{\alpha}_n}{\partial\dot{\alpha}_n} = \frac{D}{D\dot{\alpha}_n}\left(\frac{\partial\dot{\alpha}_n}{\partial X_I}\right) = \frac{D}{DX_I}\left(\frac{\partial\dot{\alpha}_n}{\partial\dot{\alpha}_n}\right) = \mathbf{0}. \quad (7.1.12)$$

This result is due to the different treatment of the time and the spatial derivative.

A similar time-discrete variational formulation is introduced by Simo in [146] who approximates the temperature by a generalized mid-point rule and the time rate of the temperature by a difference quotient.

## 7. Incremental variational formulation

### 7.1.2.1. Type I

In the incremental setting, the constitutive equations for the incremental free energy density  $\psi_n$  as well as for the incremental entropy flux vector  $\mathbf{H}_n$  are derived from those in the continuous setting, see Eqs. (6.1.2) and (6.1.3):

$$\begin{aligned}\rho\psi_n &:= \frac{\mu}{2} [\mathbf{C}_n - \mathbf{I}] : \mathbf{I} + \frac{\lambda}{2} \ln^2 J_n - \mu \ln J_n - 3wK [\theta_n - \theta_0] \frac{\ln J_n}{J_n} \\ &\quad + \rho c \left[ \theta_n - \theta_0 - \theta_n \ln \frac{\theta_n}{\theta_0} \right] - [\theta_n - \theta_0] S_0, \\ \mathbf{H}_n &:= -\frac{\kappa_1}{\theta_{n-1}} \nabla_{\mathbf{X}} \theta_n, \\ \theta_n &:= T_n.\end{aligned}\tag{7.1.13}$$

The relation between the incremental entropy flux vector  $\mathbf{H}_n$  and the incremental heat flux vector  $\mathbf{Q}_n$  originates from the continuous counterpart (Eq. (4.1.23)) and is defined as:

$$\mathbf{Q}_n := \theta_{n-1} \mathbf{H}_n.\tag{7.1.14}$$

Moreover, the incremental dissipation power  $\rho\theta_n\xi_n$  reads

$$\rho\theta_n\xi_n = -\mathbf{H}_n \cdot \nabla_{\mathbf{X}} \theta_n = \frac{\kappa_1}{\theta_{n-1}} \nabla_{\mathbf{X}} \theta_n \cdot \nabla_{\mathbf{X}} \theta_n.\tag{7.1.15}$$

The incremental first Piola-Kirchhoff stress  $\mathbf{P}_n$  and the incremental entropy density  $\eta_n$  are derived from the incremental free energy density  $\psi_n$ :

$$\mathbf{P}_n := \rho \frac{\partial \psi_n}{\partial \mathbf{F}_n}, \quad \eta_n := -\rho \frac{\partial \psi_n}{\partial \theta_n}.\tag{7.1.16}$$

Note that the constitutive equations and thermodynamic relations listed above all emerge from the continuous case (cf. Sections 4.2.1 and 6.1.1). Having now all the tools needed at hand, first the derivative  $\partial W_n / \partial \nabla_{\mathbf{X}} \alpha_n$  is calculated:

$$\begin{aligned}\frac{\partial W_n}{\partial \nabla_{\mathbf{X}} \alpha_n} &= \frac{\partial [\rho\psi_n - \rho\psi_{n-1} + [\rho\theta_n\xi_n + \rho\theta_{n-1}\xi_{n-1}] \Delta t / 2]}{\partial \nabla_{\mathbf{X}} \alpha_n} \\ &= \frac{\Delta t}{2} \frac{\partial [-\mathbf{H}_n \cdot \nabla_{\mathbf{X}} \theta_n]}{\partial \nabla_{\mathbf{X}} \alpha_n} \\ &= \frac{\Delta t}{2} \frac{\partial \left[ \frac{\kappa_1}{\theta_{n-1}} \frac{\nabla_{\mathbf{X}} \alpha_n - \nabla_{\mathbf{X}} \alpha_{n-1}}{\Delta t} \cdot \frac{\nabla_{\mathbf{X}} \alpha_n - \nabla_{\mathbf{X}} \alpha_{n-1}}{\Delta t} \right]}{\partial \nabla_{\mathbf{X}} \alpha_n} \\ &= \frac{\kappa_1}{\theta_{n-1}} \frac{\nabla_{\mathbf{X}} \alpha_n - \nabla_{\mathbf{X}} \alpha_{n-1}}{\Delta t} \\ &= -\mathbf{H}_n.\end{aligned}\tag{7.1.17}$$

Thus, the incremental internal working  $W_n$  inherits the role of a potential for the incremental entropy flux vector  $\mathbf{H}_n$ . Here, the approximation of the incremental internal working  $W_n$ , i.e.



Eq. (7.1.8), the calculation of the derivative  $\partial\nabla_{\mathbf{X}}\dot{\alpha}_n/\partial\nabla_{\mathbf{X}}\alpha_n$ , i.e. Eq. (7.1.11), the constitutive assumption (7.1.13) and relations (7.1.14) and (7.1.15) are inserted.

Inserting relation (7.1.17) into the incremental formulation of Euler-Lagrange equation (7.1.4)<sub>1</sub>

$$\begin{aligned} 0 &= \rho s_n - \frac{D}{DX_I}(H_{I\ n}) - \frac{D}{Dt} \left( \frac{\partial - [\rho\psi_n - \rho\psi_{n-1} + [\rho\theta_n\xi_n + \rho\theta_{n-1}\xi_{n-1}] \Delta t/2]}{\partial\dot{\alpha}_n} \right) \\ &= \rho s - \frac{D}{DX_I}(H_{I\ n}) - \frac{D}{Dt}(\rho\eta_n) \\ &= \rho s - \text{Div}(\mathbf{H}_n) - \rho\dot{\eta}_n \end{aligned} \quad (7.1.18)$$

leads to the incremental definition of the balance of entropy:

$$\rho\dot{\eta}_n = -\text{Div}\mathbf{H}_n + \rho s_n. \quad (7.1.19)$$

Thus, with the procedure suggested, an incremental balance of entropy of a similar format as type II for the classical theory obeying Fourier's law of heat conduction is derived.

Note that the entropy's time derivative is evaluated exactly because its time integral is evaluated exactly. Furthermore, the derivative  $\partial\nabla_{\mathbf{X}}\dot{\alpha}_n/\partial\dot{\alpha}_n$ , i.e. Eq. (7.1.12), and the relation  $\dot{\alpha} = T = \theta$  between the thermal displacement, the empirical and the absolute temperature have been used. Multiplying the incremental balance of entropy (7.1.19) with the temperature  $\theta_{n-1}$  and inserting the constitutive assumptions (7.1.13) leads to the incremental heat equation of type I

$$\begin{aligned} \rho c \frac{\theta_{n-1}}{\theta_n} \dot{\theta}_n &= -\text{Div}\mathbf{Q}_n + \nabla\theta_{n-1} \cdot \mathbf{H}_n + \rho \frac{\theta_{n-1}}{\theta_n} r_n + \frac{\theta_{n-1}}{\theta_n} \mathcal{Q}_n^{\text{mech}} \\ \Leftrightarrow \rho c \dot{\theta}_n &= -\theta_n \text{Div}\mathbf{H}_n + \rho r_n + \mathcal{Q}_n^{\text{mech}}. \end{aligned} \quad (7.1.20)$$

Here, the constant specific heat  $c$  is calculated via  $c := c_n = -\theta\partial^2\psi_n/\partial\theta_n^2$ . The structure of the incremental heat equation of type I mimics the structure of the dissipationfree heat equation of type II.

**Remark:** The incremental version differs from the algorithmic one of the continuous formulation

$$\rho c \dot{\theta}_n = -\text{Div}(\theta_n \mathbf{H}_n) + \rho r_n + \mathcal{Q}_n^{\text{mech}} \quad (7.1.21)$$

mainly via the extra term  $\nabla\theta_{n-1} \cdot \mathbf{H}_n$  due to the potential formulation. The "algorithmic heat equation" arises from continuous heat equation (6.1.6) which has been discretized in time as opposed to the "incremental heat equation" which is based on the incremental setting.

The incremental formulation of the second Euler-Lagrange equation (7.1.4)<sub>2</sub> yields

$$\begin{aligned} 0 &= \frac{\partial L_n^*}{\partial\varphi_j} - \frac{D}{DX_I} \left( \frac{\partial L_n^*}{\partial\varphi_{j,I}} \right) - \frac{D}{Dt} \left( \frac{\partial L_n^*}{\partial\dot{\varphi}_j} \right) \\ &= \rho \mathbf{b} - \frac{D}{DX_I} \left( \frac{\partial [K_n - W_n - P_n]}{\partial\varphi_{j,I}} \right) - \frac{D}{Dt} \left( \frac{\partial [K_n - W_n - P_n]}{\partial\dot{\varphi}_j} \right) \\ &= \rho \mathbf{b} - \frac{D}{DX_I} (-P_{Ij\ n}) - \frac{D}{Dt} (\rho \dot{x}_{j\ n}) \\ \Leftrightarrow \rho \ddot{\mathbf{x}}_n &= \text{Div}\mathbf{P}_n + \rho \mathbf{b}. \end{aligned} \quad (7.1.22)$$

## 7. Incremental variational formulation

Moreover, the prescribed traction vector  $\bar{\mathbf{t}}_n$  has to fulfill  $\bar{\mathbf{t}}_n = \mathbf{P}_n \cdot \mathbf{N}$  on the boundary  $\partial\mathcal{B}_P \subset \partial\mathcal{B}_0$ . For the sake of simplicity and consistency, the incremental balance of linear momentum (7.1.22) is discretized according to Eq. (7.1.9). However, better discretizations are possible, as suggested in e.g. Section 6.2.

Note that due to the potential structure, both the iteration submatrix of the mechanical and the thermal problem are symmetric.

### 7.1.2.2. Type II

Once more, the assumption for the free energy density  $\psi_n$  at time  $t_n$  emerges from the continuous counterpart (Eq. (6.1.7))

$$\begin{aligned} \rho\psi_n := & \frac{\mu}{2} [\mathbf{C}_n - \mathbf{I}] : \mathbf{I} + \frac{\lambda}{2} \ln^2 J_n - \mu \ln J_n - 3wK [\theta_n - \theta_0] \frac{\ln J_n}{J_n} \\ & + \rho c \left[ \theta_n - \theta_0 - \theta_n \ln \frac{\theta_n}{\theta_0} \right] - [\theta_n - \theta_0] S_0 + \frac{1}{2} \kappa_2 \nabla_{\mathbf{X}} \alpha_n \cdot \nabla_{\mathbf{X}} \alpha_n. \end{aligned} \quad (7.1.23)$$

Furthermore, the relation between the incremental heat flux  $\mathbf{Q}_n$  and the incremental entropy flux  $\mathbf{H}_n$  is set to

$$\mathbf{Q}_n = \theta_n \mathbf{H}_n. \quad (7.1.24)$$

Moreover, the incremental dissipation power  $\rho\theta_n \xi_n$  equals

$$\rho\theta_n \xi_n = -\rho \frac{\partial \psi_n|_{\dot{\alpha}, \nabla_{\mathbf{X}} \alpha, \mathbf{C}}}{\partial \alpha_n} = 0. \quad (7.1.25)$$

Like in the continuous setting, the free energy density  $\psi_n$  acts as an potential for the first Piola–Kirchhoff stress  $\mathbf{P}_n$ , the entropy density  $\eta_n$  and the incremental entropy flux vector  $\mathbf{H}_n$ :

$$\mathbf{P}_n = \rho \frac{\partial \psi_n}{\partial \mathbf{F}_n}, \quad \eta_n = -\frac{\partial \psi_n}{\partial \theta_n}, \quad \mathbf{H}_n = -\rho \frac{\partial \psi_n}{\partial \nabla_{\mathbf{X}} \alpha_n}. \quad (7.1.26)$$

Having a look at the derivative  $\partial W_n / \partial \nabla_{\mathbf{X}} \alpha_n$ , one obtains

$$\begin{aligned} \frac{\partial W_n}{\partial \nabla_{\mathbf{X}} \alpha_n} &= \frac{\partial [\rho\psi_n - \rho\psi_{n-1}]}{\partial \nabla_{\mathbf{X}} \alpha_n} \\ &= -\mathbf{H}_n. \end{aligned} \quad (7.1.27)$$

The incremental balance of entropy of type II is found by inserting relation (7.1.27) into the first Euler-Lagrange equation (7.1.4)<sub>1</sub>

$$\rho \dot{\eta}_n = -\text{Div} \mathbf{H}_n + \rho s_n. \quad (7.1.28)$$

Thus, the limit of the incremental balance of entropy will yield its continuous counterpart. Inserting the constitutive assumptions (7.1.23) into the incremental balance of entropy (7.1.28) leads to the incremental heat equation of type II

$$\rho c \dot{\theta}_n = -\theta_n \text{Div} \mathbf{H}_n + \rho r_n + \mathcal{Q}_n^{\text{mech}}. \quad (7.1.29)$$

Analogously to type I, the incremental balance of linear momentum follows from the incremental counterpart of the second Euler-Lagrange equation (7.1.4)<sub>2</sub>

$$\begin{aligned} 0 &= \frac{\partial L_n^*}{\partial \varphi_j} - \frac{D}{DX_I} \left( \frac{\partial L_n^*}{\partial \varphi_{j,I}} \right) - \frac{D}{Dt} \left( \frac{\partial L_n^*}{\partial \dot{\varphi}_j} \right) \\ \Leftrightarrow \rho \ddot{\mathbf{x}}_n &= \text{Div} \mathbf{P}_n + \rho \mathbf{b}, \end{aligned} \quad (7.1.30)$$

and the prescribed traction vector  $\bar{\mathbf{t}}_n$  has to fulfill  $\bar{\mathbf{t}}_n = \mathbf{P}_n \cdot \mathbf{N}$  on  $\partial \mathcal{B}_P$ .

**Remark:** In case of thermoelasticity of type II, the incremental version equals the algorithmic one of the continuous formulation:

$$\rho c \dot{\theta}_n = -\theta_n \text{Div} \mathbf{H}_n + \rho r_n + \mathcal{Q}_n^{\text{mech}}. \quad (\text{algorithmic heat equation}) \quad (7.1.31)$$

Analogously to type I, the “algorithmic heat equation” arises from continuous heat equation (6.1.10) which has been discretized in time.

### 7.1.3. Numerical example

Thermoelasticity in a thermoelastic solid is considered. In the following, bismuth is looked at. For further information on bismuth and the computational modeling of second sound in bismuth with the Green–Naghdi approach, the reader is referred to Section 5.3. At this point, only the material parameters are repeated.

A one-dimensional bar of 9 mm-length is fixed at both ends. Initially, it is set at equilibrium temperature 3 K. Then, at the left end a temperature perturbation of 1 K is added. The thermal displacement  $\alpha$  and the mechanical displacement  $\mathbf{u}$  are set to zero everywhere in the bar, i.e.  $\alpha_0 = 0$  and  $\mathbf{u}_0 = 0$ . The bar is observed for 10  $\mu\text{s}$ . At this cryogenic temperature, second sound occurs in Bi. The classical theory, i.e. type I, is only applicable for higher reference temperatures as shown in Section 5.3. Nevertheless, the same reference temperature is applied since the applicability of the discretization algorithm is in the center of interest. Thus, it is reasonable to compare both types of thermoelasticity for exactly the same model. A standard Bubnov–Galerkin finite element method as described in Section 6.2.1 is applied for the spatial discretization.

#### 7.1.3.1. Type I

The temperature solution of the incremental heat equation (7.1.20) is plotted in Figure 7.1. The initially perturbed temperature field equilibrates fast. Comparing the incremental solution with the algorithmic solution of the continuous problem, see Figure 7.2, shows that for a fine temporal discretization the general incremental temperature behavior is mapped correctly – despite the modified incremental heat equation (7.1.20). Thus, for small time steps  $h_n = t_n - t_{n-1}$ , the incremental thermoelastic problem description yields a satisfying solution. Figures 7.3–7.4 compare the solution of the incremental and the algorithmic problem also expressing that the formulation derived in the preceding chapter achieves good results.

## 7. Incremental variational formulation

Table 7.1.: Material parameters for coupled thermoelasticity in Bi

	Bi	
density $\rho$	9780	$\left[\frac{\text{kg}}{\text{m}^3}\right]$
specific heat $c$	0.052	$\left[\frac{\text{W}}{\text{kgK}}\right]$
thermal expansion coefficient $w$	$6.75 \cdot 10^{-6}$	$\left[\frac{1}{\text{K}}\right]$
thermal conductivity $\kappa_1$	20500	$\frac{\text{W}}{\text{mK}}$
thermal conductivity $\kappa_2$	309407875	$\left[\frac{\text{W}}{\text{s}^2\text{mK}}\right]$
Young's modulus $E$	$40 \cdot 10^9$	$\left[\frac{\text{N}}{\text{m}^2}\right]$
reference temperature $T_0$	3	[K]

As the incremental and the algorithmic heat equation differ via the extra term  $\nabla\theta_{n-1} \cdot \mathbf{H}_n$ , the incremental heat equation can never converge towards the algorithmic heat equation. Thereby, the error, i.e. the deviation of the incremental from the algorithmic formulation, will depend on the particular example. However, this incremental potential formulation is motivated by the potential structure of Green–Naghdi type II which was developed in order to model second sound, i.e. the example examined in this contribution. Since, in the first place, we are interested in the solution of the partial differential equations, i.e. the temperature  $T$  and the mechanical displacement  $\mathbf{u}$ , we calculated  $e = [ |T^{alg} - T^{inc}| + |u^{alg} - u^{inc}| ] / [ |T^{alg}| + |u^{alg}| ]$ . For a discretization as suggested above, the error in the solutions was smaller than 0.1 %, i.e.  $e < 0.001$ , if more than 100 time steps were chosen.

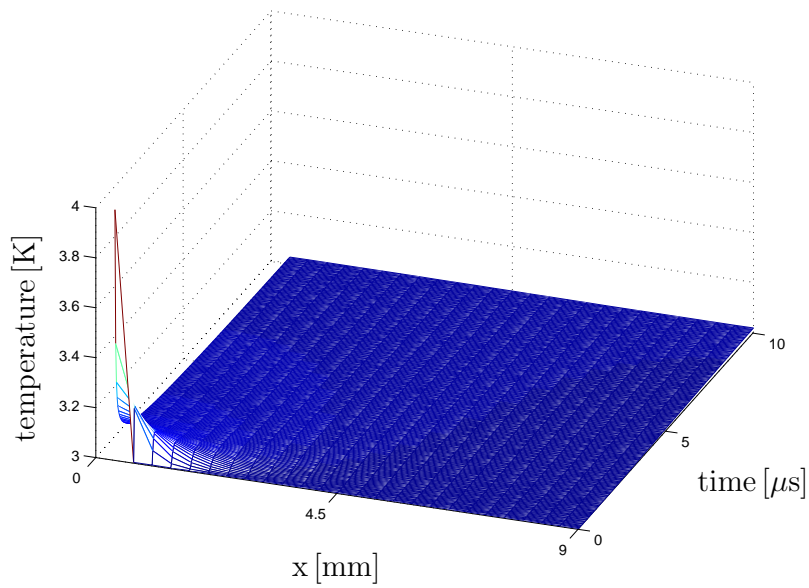


Figure 7.1.: Type I, incremental formulation. Eqs. (7.1.20) and (7.1.22) are solved monolithically. The temperature is plotted vs. space and time. 250 equidistant time steps and 25 spatial finite elements are applied.

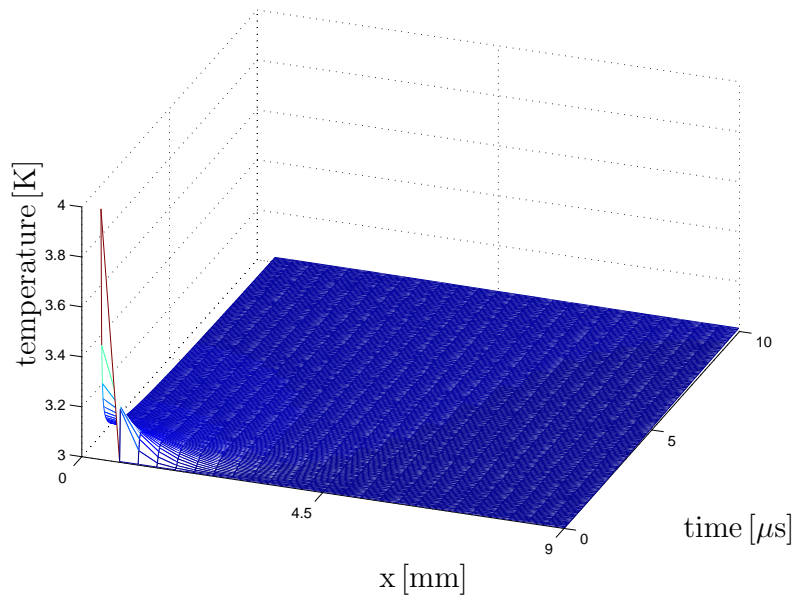


Figure 7.2.: Type I, algorithmic formulation. The temperature is plotted vs. space and time. The system of equations describing the algorithmic problem, i.e. Eq. (7.1.21) and (7.1.22), is solved monolithically. 250 temporal and 25 spatial finite elements are applied.

## 7. Incremental variational formulation

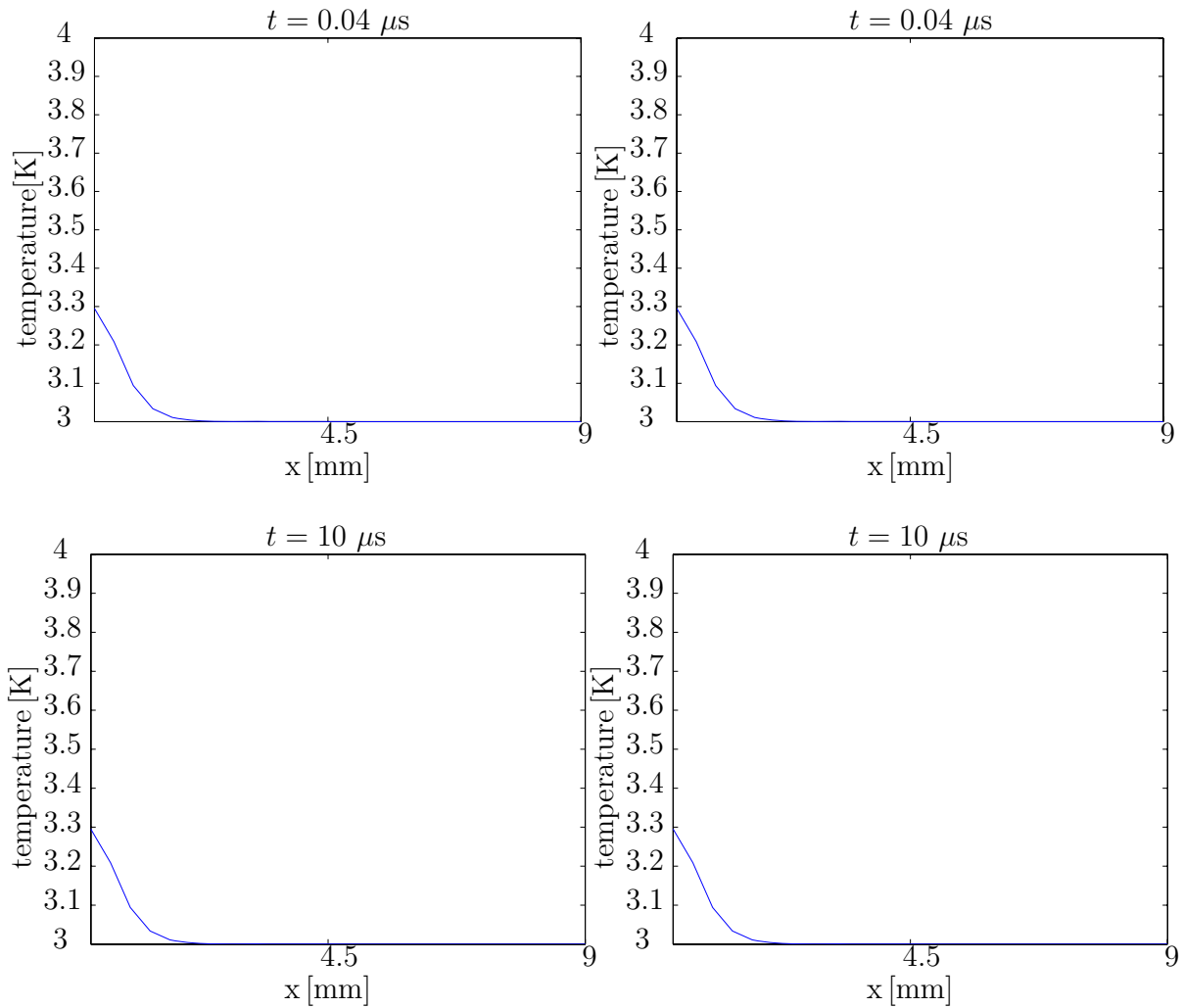


Figure 7.3.: Temperature solution according to type I at time  $t = 0.04 \mu s$  and at  $t = 10 \mu s$ . The solution of the incremental (left) and the algorithmic formulation (right) do not differ significantly. The system of partial differential equations describing the incremental formulation is given by Eqs. (7.1.20) and (7.1.22), whereas the algorithmic one is stated in Eqs. (7.1.21) and (7.1.22). In both cases a discretization of 250 temporal and 25 spatial elements is applied.

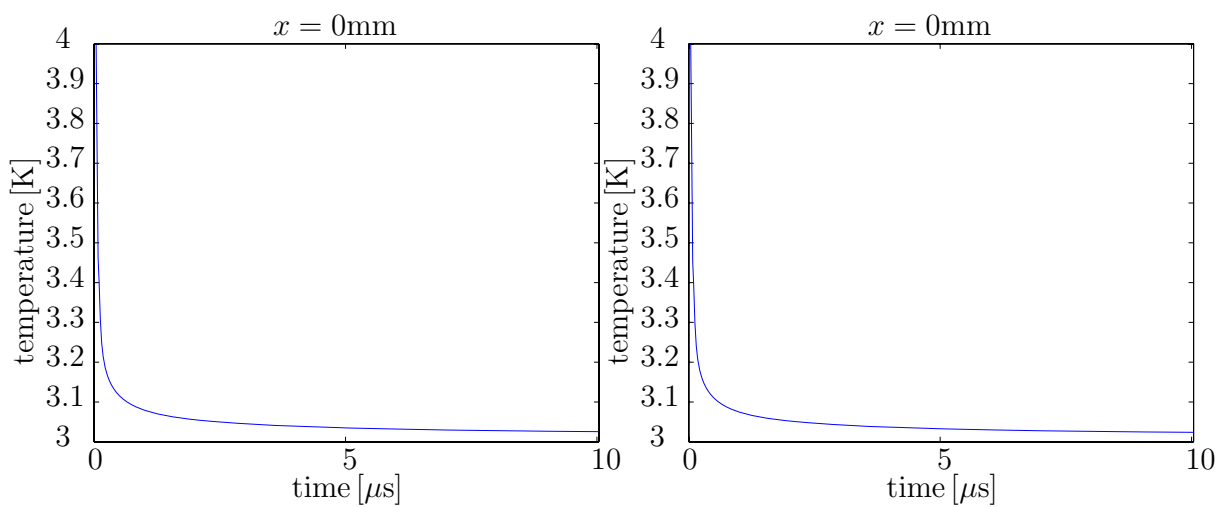


Figure 7.4.: Temperature solution according to type I at the left end of the bar, i.e.  $x = 0$ mm. The solution of the incremental (left) and the algorithmic formulation (right) closely resemble each other. The system of partial differential equations describing the incremental formulation is given by Eqs. (7.1.20) and (7.1.22), whereas the algorithmic one is stated in Eqs. (7.1.21) and (7.1.22). In both cases a discretization of 250 equidistant time steps and 25 spatial elements is applied.

## 7. Incremental variational formulation

### 7.1.3.2. Type II

The potential formulation of the entropy flux vector  $\mathbf{H}$  is naturally embedded in the continuous theory of type II. Thus, the limit of the incremental heat equation of type II (7.1.29) and the limit of the incremental balance of linear momentum (7.1.30) yield their continuous counterparts. As demonstrated in Figure 7.5, the incremental problem also models second sound. The speeds of the first and second sound waves are mapped correctly. However, due to the fact that the incremental scheme belongs to Euler Backward methods, numerical dissipation is artificially introduced into a problem which actually is non-dissipative. Clearly, by choosing a finer spatial finite element grid or smaller time steps  $h_n$ , the numerical dissipation can be decreased.

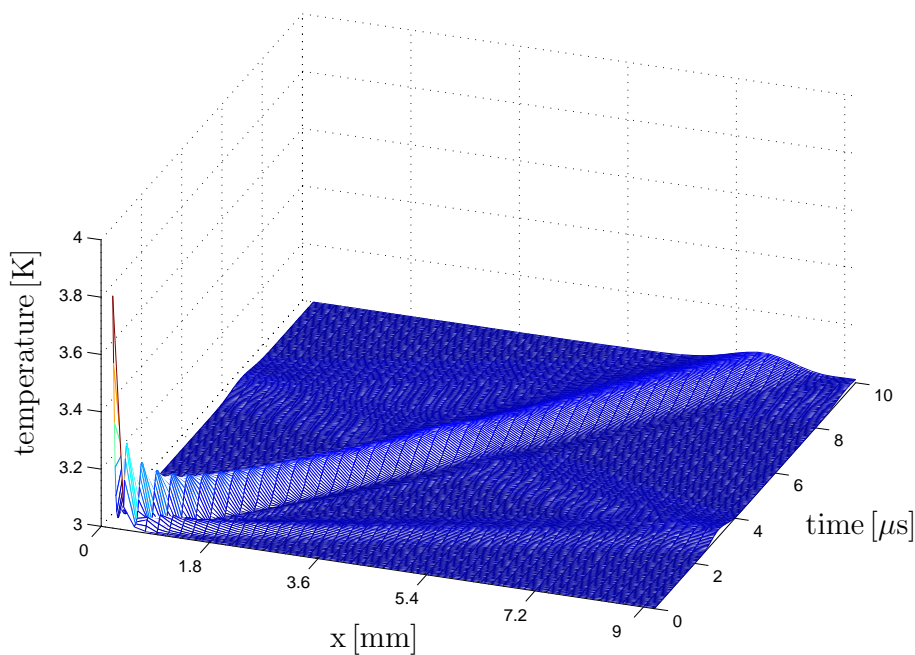


Figure 7.5.: Type II, incremental (and algorithmic) formulation. The temperature is plotted vs. space and time. The existence of two temperature waves can clearly be seen. The inertia term of the balance of linear momentum is fully considered, thus a smaller but faster first sound wave which is driven by the mechanical problem exists due to the two-folded coupling. The bigger but slower one is the second sound.



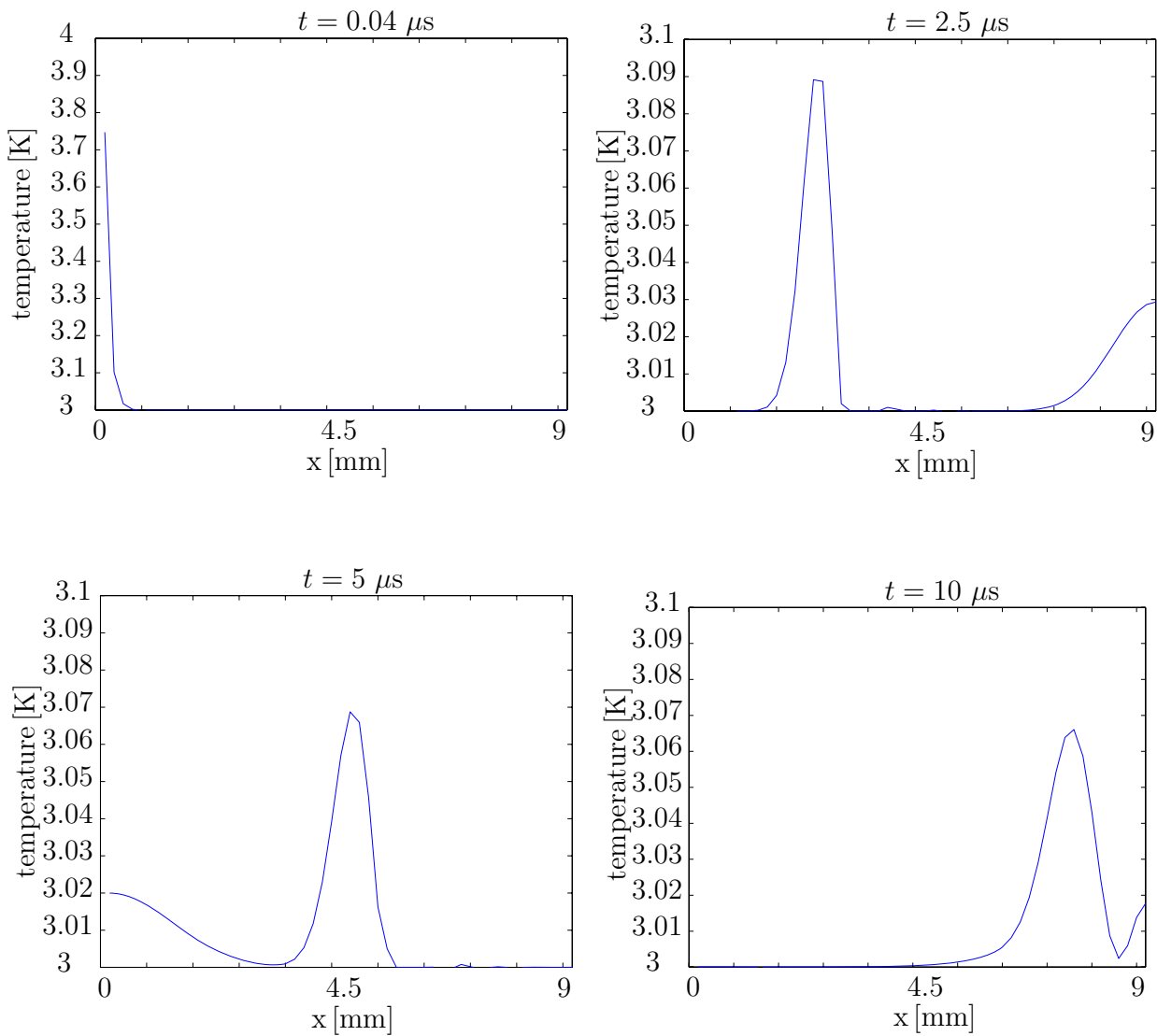


Figure 7.6.: Temperature solution according to type II at times  $t = 0.04 \mu s$ ,  $t = 2.5 \mu s$ ,  $t = 5 \mu s$  and at  $t = 10 \mu s$ . The second sound wave slowly propagates through the bar. At time  $t = 2.5 \mu s$  the first sound wave arrives at the bar's right end. Due to the reflection, it travels back to the left end as shown at time  $t = 5 \mu s$ . Because of the numerical dissipation, the both waves diffuse although the theory is inherently without energy dissipation. Both wave speeds are mapped correctly. Please note the different temperature scale in the first picture at  $t = 0.04 \mu s$  which was chosen in order to capture the entire wave amplitude.

## 7. Incremental variational formulation

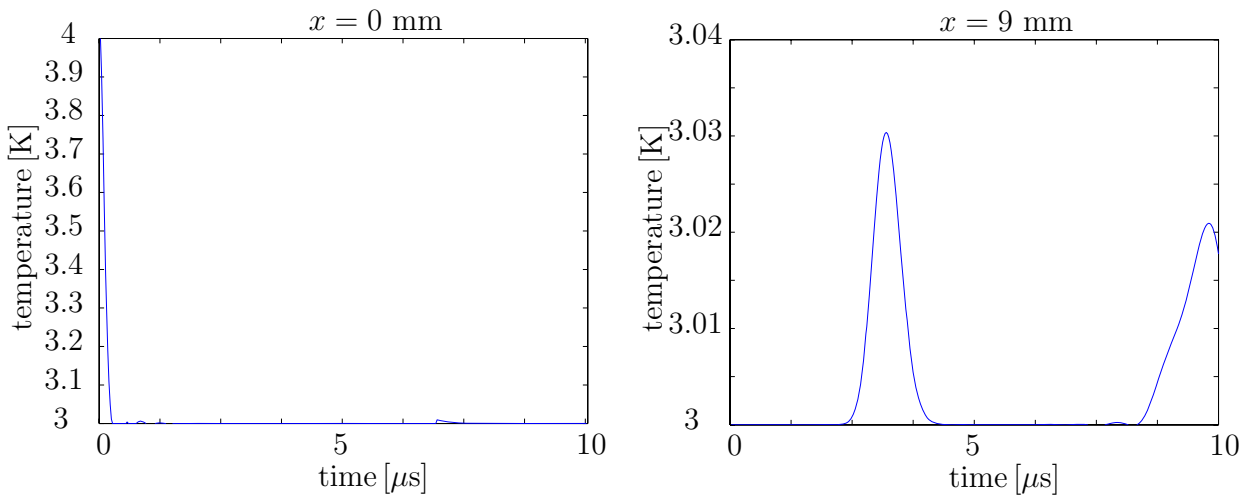


Figure 7.7.: Temperature solution according to type II at the left and at the right end of the bar, i.e.  $x = 0$  mm and  $x = 9$  mm.

Thus, motivated by the existence of a potential for the type II entropy flux  $\mathbf{H} = -\rho\partial\psi/\partial\nabla_{\mathbf{X}}\alpha$ , an incremental variational principle modeling classical dissipative and non-classical non-dissipative thermoelastic solids was introduced. Thereby, the incremental entropy flux following Fourier's classical law of heat conduction is determined by means of the incremental free energy function acting as a potential. Because of this potential structure, both the iteration submatrix of the mechanical and the thermal problem are symmetric, also for the theory of type I. A numerical example was presented in order to prove the applicability of the proposed algorithm. We showed that the solution of the incremental problem and the algorithmic problem do not deviate in any decisive manner. Thus, the resulting update algorithm is a convenient formulation of the underlying thermoelastic problem.

## 8. On wave speed in Green–Naghdi heat conduction

In this Chapter, some analytical findings concerning propagation speed in case of Green–Naghdi heat conduction are presented. First, the propagation speed of thermal waves in semi-infinite, one-dimensional, Green–Naghdi media is examined. In particular, the dynamic propagation of a Heaviside input signal is analyzed in order to show that the Green–Naghdi theory of type III predicts an infinite speed of heat conduction for  $\kappa_3 \neq 0$ . The results presented in the following have already been published by Bargmann et al. [13].

### 8.1. Mathematical formulation

As mentioned above, the classical heat equation obeying Fourier’s law of heat conduction, i.e. Eq. (5.1.3), implies that parts of an initial heat pulse will propagate with infinite speed (see e.g. Section 5.1.1). In the following, a closer look at the propagation speed in case of type-III-heat conduction on is made. More specifically, an example of infinite wave propagation speed in case of heat conduction type III is provided.

An initial boundary value problem with a Heaviside input signal in a semi-infinite body is considered. This problem models a thermal shock applied to the boundary  $x = 0$  of the half-space  $x > 0$ , which describes a thermal conductor obeying the Green–Naghdi type III theory. The analytical solution will be presented showing that the thermal wave propagation speed is finite in case of type II and infinite in case of type I and III. Since type I and II are special cases of type III, the initial boundary value problem is formulated for type III:

$$\begin{aligned} \rho c \ddot{T} &= \kappa_3 \operatorname{div} \nabla T + \kappa_4 \operatorname{div} \nabla \dot{T}, & (x, t) &\in [0, \infty) \times [0, \infty) \\ T(0, t) &= T_0 + T^\bullet H(t), & T(\infty, t) &= T_0, \quad (t > 0) \\ T(x, 0) &= T_0, & \dot{T}(x, 0) &= 0 \quad (x > 0). \end{aligned} \quad (8.1.1)$$

Only the thermal problem is considered, thus  $\mathbf{X} = \mathbf{x}$  and no distinction is made between the spatial and the material motion problem in this chapter. This implies  $\rho_0 = \rho_t =: \rho$  and  $\nabla_{\mathbf{x}} = \nabla_{\mathbf{X}} = \nabla$ .  $H$  is the Heaviside unit step function and the positive constants  $\rho$ ,  $c$ ,  $\kappa_3$  and  $\kappa_4$  again denote the material’s density, specific heat, and thermal conductivities, respectively, while  $T^\bullet > -T_0$  is a nonzero constant.

## 8. On wave speed in Green–Naghdi heat conduction

Following Green and Naghdi [52, p. 259], the empirical temperature is set to  $T = \theta + T_0$ . Next, the following nondimensional variables are introduced:

$$T = \theta/T^\bullet, \quad t = t(U/L), \quad x = x/L, \quad (8.1.2)$$

where the positive constants  $L$  and  $U$  respectively denote a characteristic length and speed, and recast the initial boundary value problem (8.1.1) in its dimensionless form

$$\begin{aligned} Ma^2 \operatorname{div} \nabla T - \ddot{T} + \chi \operatorname{div} \nabla \dot{T} &= 0, & (x, t) \in [0, \infty) \times [0, \infty) \\ T(0, t) = H(t), \quad T(\infty, t) &= 0, & (t > 0) \\ T(x, 0) = \dot{T}(x, 0) &= 0 & (x > 0) \end{aligned} \quad (8.1.3)$$

where the Mach number<sup>1</sup>  $Ma$  and the dimensionless thermal diffusivity  $\chi$  are given by

$$Ma = \frac{1}{U} \sqrt{\frac{\kappa_3}{\rho c}}, \quad \chi = \frac{\kappa_4}{\rho c U L}. \quad (8.1.4)$$

## 8.2. Analytical solutions

### 8.2.1. Type III

The dimensionless formulation of the initial boundary value problem (8.1.3) equals the initial boundary value problem stated by Jordan and Feuillade [79, Eq. (2.1)]. Jordan and Feuillade derive<sup>2</sup> the analytical solution [79, Eq. (3.14)]<sup>3</sup>

$$\begin{aligned} T(x, t) = H(t) &\left\{ 1 - \frac{2}{\pi} \int_0^{\xi^*} e^{-a_0(\xi)t} \left[ \cos(b_0(\xi)t) - \frac{a_0(\xi)}{b_0(\xi)} \sin(b_0(\xi)t) \right] \frac{\sin(\xi x)}{\xi} d\xi \right. \\ &\left. - \frac{2}{\pi} \int_{\xi^*}^{\infty} e^{-a_0(\xi)t} \left[ \cosh(b_0(\xi)t) - \frac{a_0(\xi)}{b_0(\xi)} \sinh(b_0(\xi)t) \right] \frac{\sin(\xi x)}{\xi} d\xi \right\}, \end{aligned} \quad (8.2.1)$$

where  $\xi^* = 2Ma/\chi$  is the integration breakpoint,

$$a_0(\xi) = \frac{1}{2}\chi\xi^2, \quad \text{and} \quad b_0(\xi) = \frac{1}{2}\chi\xi\sqrt{|\xi^2 - (\xi^*)^2|}. \quad (8.2.2)$$

<sup>1</sup>The Mach number  $Ma$  is a dimensionless measure of relative speed. It states the ratio of the velocity of an objective relative to a medium to the velocity of sound in the same medium.

<sup>2</sup>Omitting the details, but giving a short sketch of the rather lengthy derivation: Jordan and Feuillade solve the initial boundary value problem (8.1.3) by employing a dual (integral) transform approach. Specifically, they first apply the spatial sine transform, which reduces Eq. (8.1.3)<sub>1</sub> to an ordinary differential equation (ODE) with independent time variable  $t$  and then solve the resulting ordinary differential equation using the temporal Laplace transform.

<sup>3</sup>Note that the algebraic signs in front of the last three integrals appearing in the paper by Jordan and Feuillade [79, Eq. (3.14)] are incorrect; they should read:  $-$ ,  $+$ ,  $+$ , respectively.

Thus, in the theory of type III, the thermal shock applied to the boundary  $x = 0$  at time  $t = 0 + \varepsilon$ , with  $\varepsilon > 0$  being arbitrarily small, is felt instantly throughout the entire half-space. Unfortunately, the analytical solution (8.2.1) is complicated and difficult to analyze. Hence, simpler expressions that accurately capture the behavior of Eq. (8.2.1) are presented for more illustrative explanations. In particular, a closer look is taken at Eq. (8.2.1) for small and large  $t$ .

First, the small-time approximation is considered. It is returned to the dimensionless formulation of the initial boundary value problem and the temporal Laplace transform,  $\mathcal{L}[\cdot]$ , is applied both to Eq. (8.1.3)<sub>1</sub> and the boundary conditions given in Eq. (8.1.3)<sub>2</sub>. Subsequently, the initial conditions are employed and the resulting subsidiary equation is solved. The Laplace transform domain solution is thus given by

$$\bar{T}(x, s) = \frac{1}{s} \exp\left(\frac{-sx}{Ma\sqrt{1 + s\chi/Ma^2}}\right). \quad (8.2.3)$$

Here, the bar superposed over a quantity denotes the image of that quantity in the Laplace transform domain, i.e.,  $\bar{T}(x, s) = \mathcal{L}(T(x, t))$ , and  $s$  is the transform parameter. Now the behavior of the dimensionless temperature  $T$  for times immediately after the shock has been applied is examined. Looking at small times  $t$  corresponds to examining large transform parameters  $s$ . For large  $s$ ,  $\sqrt{1 + s\chi/Ma^2} \approx \sqrt{s\chi/Ma^2}$  is valid. Consequently, the argument of the exponential in Eq. (8.2.3) can be expanded for large  $s$ , which yields

$$\bar{T}(x, s) \approx \frac{1}{s} \exp\left(-\frac{x}{\sqrt{\chi}}\sqrt{s}\right) \left[1 + \frac{Ma^2x}{2\chi\sqrt{\chi}s} + \mathcal{O}(s^{-1})\right]. \quad (8.2.4)$$

Inverting term-by-term using a table of inverses, for dimensionless times  $t > 0$  sufficiently small, the dimensionless temperature  $T$  is approximately given by

$$T(x, t) \approx \operatorname{erfc}\left(\frac{x}{2\sqrt{\chi t}}\right) + \frac{Ma^2x}{2\chi\sqrt{\chi}} \left[2\sqrt{\frac{t}{\pi}} \exp\left(-\frac{x^2}{4\chi t}\right) - \frac{x}{\sqrt{\chi}} \operatorname{erfc}\left(\frac{x}{2\sqrt{\chi t}}\right)\right]. \quad (8.2.5)$$

The complementary error function, denoted by  $\operatorname{erfc}(\cdot)$ , is defined as

$$\operatorname{erfc}(x) = \frac{2}{\sqrt{\pi}} \int_x^\infty \exp(-y^2) dy \quad (8.2.6)$$

and its second derivative is given by

$$\frac{d^2\operatorname{erfc}(x)}{dx^2} = \frac{2}{\sqrt{\pi}} \exp(-x) > 0 \quad \forall x \in \mathbb{R}. \quad (8.2.7)$$

Thus, the complementary error function  $\operatorname{erfc}(\cdot)$  is strictly convex. Although

$$\lim_{x \rightarrow \infty} \operatorname{erfc}(x) = 0, \quad (8.2.8)$$

## 8. On wave speed in Green–Naghdi heat conduction

the complementary error function reaches the  $x$ -axis asymptotically due to its strict convexity. Returning to Eq. (8.2.5) and observing that  $x/2\sqrt{\chi t} \rightarrow \infty$  for  $t \rightarrow 0$ , this implies that instantly after the shock, i.e. even for very small  $t \neq 0$ ,

$$T(x, t) > 0 \quad \forall x \in \mathbb{R}. \quad (8.2.9)$$

Thus, Green–Naghdi-type III predicts infinite propagation speed.

In Figure 8.1 the exact (solid) and small-time (dashed) type III solutions are plotted, i.e., Eqs. (8.2.1) and (8.2.5), respectively. Here, the small-time expression is in very good agreement with the exact result for  $t < 0.04$  and the profile is strictly decaying, but always positive, i.e., there is no wavefront.

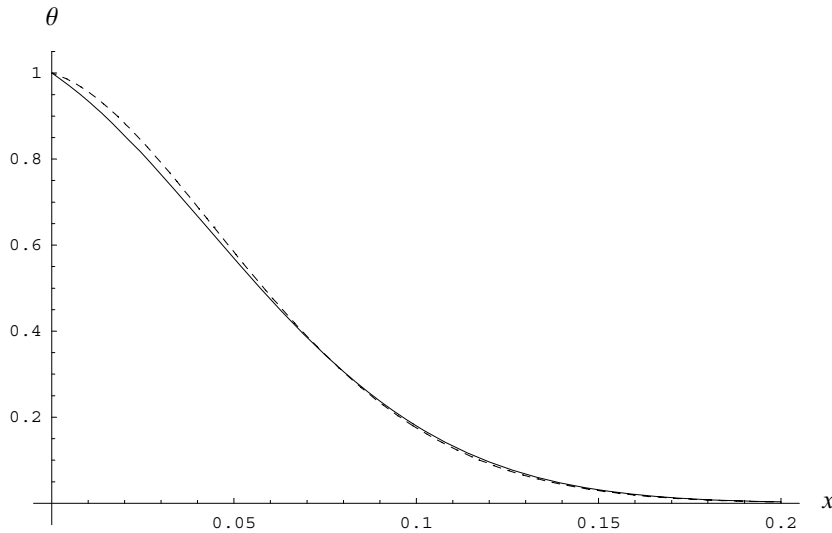


Figure 8.1.:  $T$  vs.  $x$  for type III is plotted at time  $t = 0.04$  with  $\chi = 0.05$  and  $Ma = 1.0$ . Solid: Eq. (8.2.1). Dashed: Eq. (8.2.5).

Second, the large-time approximation is looked at. From the last two frames of Figure 8.3, it can be seen that under Green–Naghdi type III, the temperature profile assumes the approximate shape of a Taylor shock as the dimensionless time  $t$  approaches infinity, i.e.  $t \rightarrow \infty$ . Based on the knowledge of actual Taylor shock solutions, the following *ad hoc* approximation for the type III case is constructed:

$$T(x, t) \approx \frac{1}{2} [1 - \tanh(2[x - Mat]/\ell)] \quad (t \rightarrow \infty). \quad (8.2.10)$$

Here, the “shock thickness”  $\ell$ , i.e. the length of the scale of the shock, is given by

$$\ell = \frac{1}{\left| \mathcal{L}^{-1} \left\{ \frac{-1}{Ma\sqrt{1+s\chi/Ma^2}} \exp\left(\frac{-sx}{Ma\sqrt{1+s\chi/Ma^2}}\right) \right\} \Big|_{x=Mat} \right|}, \quad (8.2.11)$$

where the expression inside the large  $\{ \}$  is just  $\partial\bar{T}/\partial x$ , with  $\bar{T}$  as given in Eq. (8.2.3).

In Figure 8.2, the exact (solid) and ad hoc (broken) solutions given in Eqs. (8.2.1) and (8.2.10), respectively, are plotted. Three different values of the dimensionless diffusivity  $\chi$  are chosen, where the Mach number  $Ma$  and the dimensionless time  $t$  have been fixed at  $Ma = 1.0$  and  $t = 10.0$ . While all three plots show very good/excellent agreement, it can be seen that the agreement improves as the dimensionless diffusivity  $\chi$  is reduced. Consequently, Eq. (8.2.10) is an especially accurate approximation of the type III solution profile provided the dimensionless time  $t$  is sufficiently large and the dimensionless diffusivity  $\chi$  is sufficiently small.

### 8.2.2. Type II

The heat equation of type II is stated in Eq. (5.1.6). Thus, the solution for the dimensionless problem (8.1.3) for this type can be obtained by letting the dimensionless diffusivity  $\chi$  approach zero,  $\chi \rightarrow 0$ , in Eq. (8.2.1). The solution of Eq. (8.1.3) is then is given by

$$T(x, t) = H\left(t - \frac{x}{Ma}\right). \quad (8.2.12)$$

Therefore, under Green–Naghdi type II, an undamped, undistorted, thermal wavefront propagates into the half-space (i.e., to the right) with speed  $Ma$ .

### 8.2.3. Type I

In order to obtain the heat equation according Green–Naghdi type I, i.e. Eq. (5.1.3), let  $Ma \rightarrow 0$  in Eq. (8.1.3)<sub>1</sub>. Then,  $\xi^* \rightarrow 0$  and  $b_0(\xi) \rightarrow a_0(\xi)$  (cf. Eq. (8.2.2)). Consequently, the Green–Naghdi type I, i.e. the one which corresponds to the classical Fourier theory of heat conduction, solution is found to be, as one would expect,

$$T(x, t) = \operatorname{erfc}\left(\frac{x}{2\sqrt{\chi t}}\right) \quad (t > 0), \quad (8.2.13)$$

where  $\operatorname{erfc}(\cdot)$  again denotes the complementary error function. Repeating the line of argumentation as applied after Eq. (8.2.5), Green–Naghdi type I predicts infinite propagation speed. Note that this result is already a well-known, see e.g. [63].

8. On wave speed in Green–Naghdi heat conduction

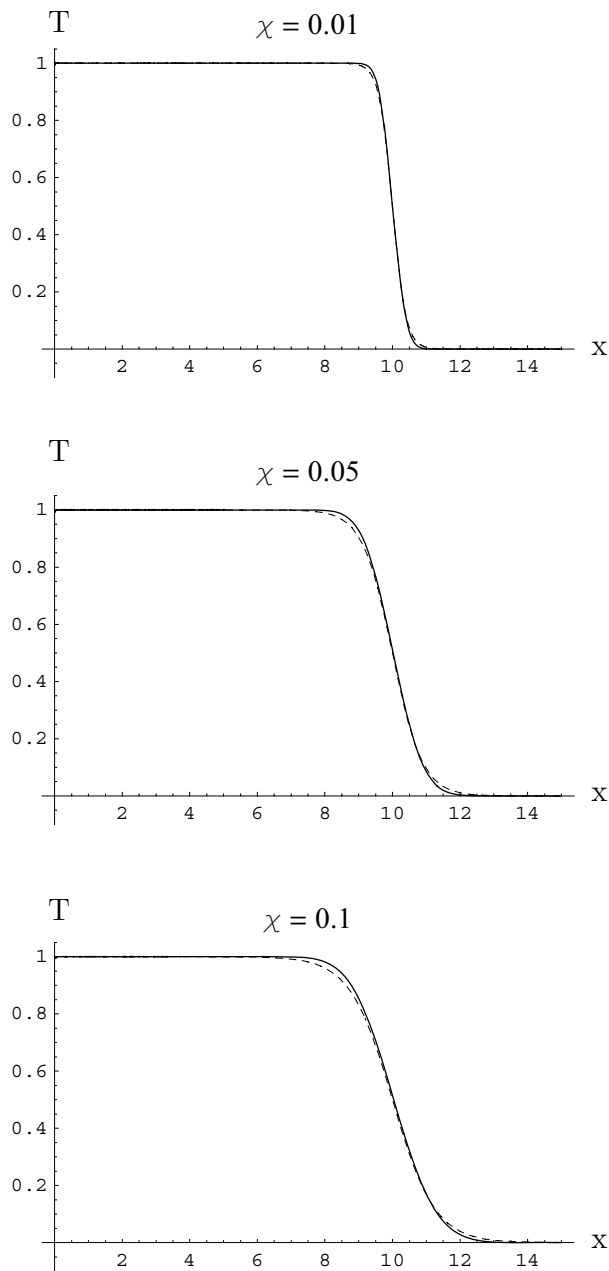


Figure 8.2.: Dimensionless temperature  $T$  vs. dimensionless position  $x$  for heat conduction of type III at time  $t = 10.0$ . The Mach number  $Ma = 1.0$  is constant and the dimensionless diffusivity  $\chi$  varies from  $\chi = 0.01, 0.05$  to  $0.1$ . Solid line: Exact solution (Eq. (8.2.1)). Dashed line: ad hoc approximation (Eq. (8.2.10)). In all three cases, the ad hoc approximation agrees with the exact solution very well. Thus, provided that  $T$  is sufficiently large and  $\chi$  sufficiently small, Eq. (8.2.10) presents an accurate approximation of the exact solution stated in Eq. (8.2.1).



### 8.3. Results

The sequence shown in Figure 8.3 illustrates the evolution of the solution profiles of the dimensionless temperature  $T$  corresponding to Green–Naghdi types I, II, and III. Therein, the different behavior of the three types of heat conduction can be seen. The dimensionless thermal diffusivity is set  $\chi = 0.05$  for type I and III (remember:  $\chi \rightarrow 0$  for type II). Furthermore,  $Ma = 1.0$  for type II and III, whereas  $Ma \rightarrow 0$  in case of the classical theory of type I.

The dashed line depicts the solution according to type I. The dimensionless temperature  $T$  reaches the  $x$ -axis asymptotically due to the infinite propagation speed. It is always positive, thus, there is no wavefront due to the infinite propagation speed. Contrary to that, in case of Green–Naghdi type II (bold solid line) the thermal shock leads to a thermal wavefront propagating with unit speed  $Ma = 1.0$  to the right. Due to the lack of dissipation, the wave front is undamped and undistorted. Under Green–Naghdi type III (thin solid line), the thermal shock applied to the boundary  $x = 0$  at time  $t = 0 + \varepsilon$  is felt instantly, but unequally, throughout the entire half-space, in much the same way as in the case of type I. In fact, for small values of time Eq. (8.2.1) behaves, to leading order, like the Green–Naghdi type I solution [see Eq. (8.2.13)]. As time passes, the solution of type III detaches from the one of type I. Also, the temperature changes from an exponential decay to approximately that of a Taylor shock with finite propagation speed of approximately  $Ma$ .

As mentioned above, the analytical solution (8.2.1) of the initial boundary value problem (8.1.3) implies infinite propagation speed under Green–Naghdi type III. Figure 8.4 depicts the solution of  $T$  at  $t = 0.01$ , thus shortly after a thermal shock is applied at the boundary  $x = 0$ . Near the boundary, the shock leads to a significant temperature rise. For points situated far from the boundary, the temperature rises only slightly. However, the perturbation is felt everywhere as the logarithmic scale in the right picture indicates.

8. On wave speed in Green–Naghdi heat conduction

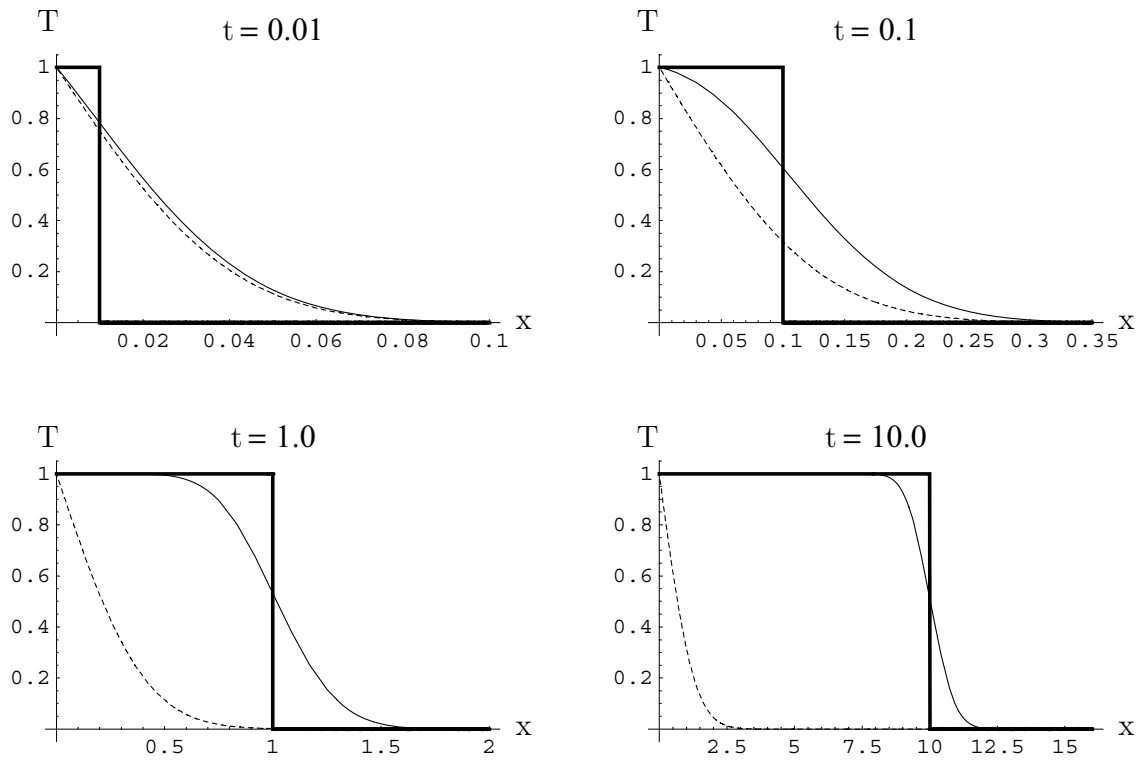


Figure 8.3.: Evolution of the temperature profiles. The dimensionless temperature  $T$  is plotted vs. the dimensionless position  $x$  for types I, II, and III. Dashed line: type I [Eq. (8.2.13)] with thermal diffusivity  $\chi = 0.05$ . Bold-solid: type II [Eq. (8.2.12)], with  $Ma = 1.0$ . Thin-solid: type III [Eq. (8.2.1)] with thermal diffusivity  $\chi = 0.05$  and  $Ma = 1.0$ .

Type I as well as type III predict an infinite propagation speed -  $T$  reaches the  $x$ -axis asymptotically. In case of type II, the thermal shock propagates as a thermal wavefront propagating undamped with constant speed  $Ma = 1.0$ .

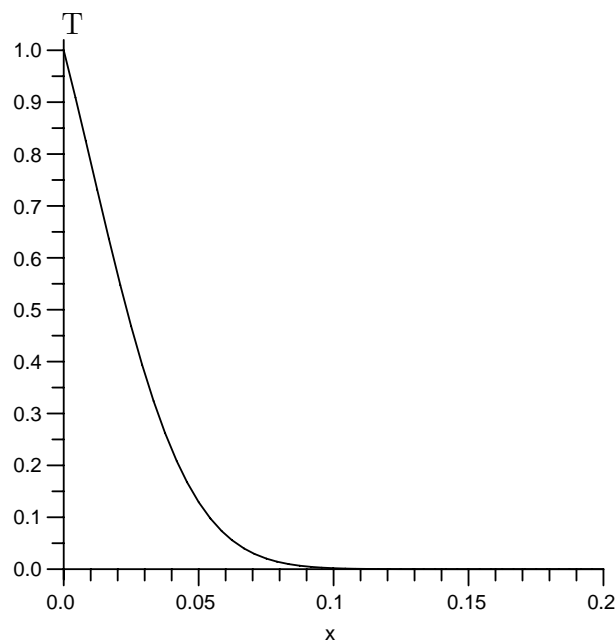


Figure 8.4.: Temperature solution for Green–Naghdi type III with thermal diffusivity  $\chi = 0.05$  and  $Ma = 1.0$ .  $T$  is plotted vs.  $x$  at time  $t = 0.01$ . A thermal shock was applied at  $x = 0$  at  $t = 0 + \varepsilon$ . The further a point is located from the boundary, the less the temperature rises. However, the temperature perturbation is instantly felt, see Eq. (8.2.9).

Summarizing, the theory of type III gives rise to infinite propagation speed, just like the classical theory based on Fourier’s law. However, for numerical simulations with values of  $\kappa_4 \ll \kappa_3$ , this effect is negligible. Moreover, agreeing with Green and Naghdi, type III is “perhaps a more natural candidate for its identification as thermoelasticity” because of its generality and the novelty of not necessarily involving energy dissipation.

8. *On wave speed in Green–Naghdi heat conduction*

## 9. Conclusion

In the present thesis a theory of non-classical thermoelasticity for cryogenic temperatures is presented. The thermal theory is based on the approach of Green and Naghdi [51]. It is coupled with the classical theory of elasticity. First, to set the basis, the general kinematic framework is introduced in Chapter 3. Subsequently, in Chapter 4, the Green–Naghdi theory in general is thermodynamically analyzed with the help of the entropy principle of Müller and Liu. The evaluation of the second law of thermodynamics yields thermodynamic relations between the free energy density on the one side and the entropy density, the entropy flux, the internal energy dissipation and the stresses on the other side.

The Green–Naghdi approach comprises three types of heat conduction, labeled type I, II and III. All three types are introduced and discussed in detail. Green and Naghdi include the classical Fourier theory fully into their approach (type I). However, this thesis concentrates on the non-classical part as Fourier’s theory leads to the unnatural property of infinite wave speed in case of temperature perturbations. Moreover, it is not capable of modeling second sound. The latter refers to the phenomenon where heat propagates as thermal waves. Thus, another approach is necessary in order to simulate second sound computationally. As a result of this thesis, it is shown that both, type II and III, are capable of modeling thermal waves. In contrast to most other thermal theories published so far, the Green–Naghdi theory of type II does not necessarily involve energy dissipation. Moreover, it possesses the outstanding property that the entropy flux vector is determined by the free energy acting as a potential. Type III also allows thermal wave propagation and usually energy is dissipated. Especially the theory of type III opens many (new) possibilities, as it is the most general one. It contains type I and II as limiting cases, thus type III is suitable for modeling classical as well as thermal wave propagation theories.

The theoretical part is accompanied by employing a suitable discretization method. A semi-discretization method was applied - first discretizing in space and subsequently in time. For the spatial discretization it was resorted to a standard Bubnov–Galerkin finite element method in space. Instead of finite differences, finite elements are also applied for the temporal discretization. Concerning the time integration, a discontinuous and a continuous Galerkin method are adopted. The classical theory of thermoelasticity, i.e. type I, is discretized with a mixture of a discontinuous and a continuous Galerkin method in order to take the coupling between the thermal and the mechanical problem fully into account and cope with the different mathematical structures of the governing equations. This discretization approach is referred to as mixed Galerkin finite element method in time, cf. Section 6.2.2.1. The temporal discretization of type II was done with a continuous Galerkin finite element approach due to the fact that the equation governing the thermal problem is hyperbolic. The same procedure is applied to all

## 9. Conclusion

numerical examples presented in this thesis which follow the theory of type III. In the case of fully coupled nonlinear thermoelasticity, the nonlinear system of equations is solved with a Newton–Raphson strategy. The performance of the proposed discretization methods is underlined by presenting various numerical examples. Among others, the second sound experiments in which the phenomenon was proven for the first times, are simulated.

The simultaneous introduction of the spatial as well as material formulation of the balance laws allowed for a natural incorporation of the material force method. It is discussed in the context of all three types of Green–Naghdi thermoelasticity.

Summarizing, this thesis provides a deeper insight into the very promising Green–Naghdi theory of thermoelasticity. Their elegant approach opens many new possibilities in the modeling of thermoelastic phenomena, especially at cryogenic temperatures. Theoretical and numerical aspects have been investigated and the applicability of the Green–Naghdi theory has been demonstrated. However, as mentioned above, there still exist some interesting open questions which are definitely worth having a look at in the future.

There are several problems which must be discussed in the future. For example, one important question which needs to be answered is whether or not modeling second sound involves energy dissipation. Unfortunately, the original second sound experiments do not address this question. However, second sound was also detected in superfluids - a state in which no energy is dissipated. Consequently, the theory of type II seems to be the better candidate for modeling second sound in solids.

Another field of ongoing research could be the transfer of the thermoelastic Green–Naghdi theory to fluids and gases. Green and Naghdi themselves picked up this task at the end of their lives, see [54]. But so far, only Quintanilla and Straughan [141] and Jordan and Straughan [78] started the analysis in this direction. Also, in this thesis the modeling was restricted to isotropic Neo–Hookean material behavior. An extension to more classes of materials can certainly be useful.

As shown in Appendix B, there exist several shortcomings of other fundamental laws, such as Fick’s law of diffusion or Darcy’s law for flow through porous media, for example. For those scenarios, the search for modifications of the classical law and their analyses are going on. For example, Jordan [77] applies the Maxwell–Cattaneo–Vernotte approach, which originally stems from modifying Fourier’s law, for modeling flow through porous media. To the author’s knowledge, Green and Naghdi’s theory has not yet been transferred in these contexts. Nevertheless, this definitely seems a direction worth heading for.

One numerical example, presented in this thesis, was the computational simulation of cryovolcanism on Saturn’s moon Enceladus. Especially in this field, a lot more research needs to be done. The phenomenon of cryovolcanism was only proven a few years ago during the fly-by of the spacecraft Cassini in 2005. Thus, scientists are still trying to figure out what exactly is happening during Enceladus’ volcanic eruptions. Here, computational simulations are a powerful tool, of course. Nevertheless, additional observational data is necessary in order to gain a better insight in this astonishing and interesting phenomenon. On the other hand, due to its outstanding properties, Enceladus is a very active research topic and new results are published just about every month.

# A. Mathematics

## A.1. Notation

Throughout this thesis, scalar quantities are indicated by non-bold symbols, e.g.  $a$ , whereas vectors and tensors are denoted by bold symbols, e.g.  $\mathbf{a}$ . As mentioned in Section 3.1, in order to distinguish spatial from material quantities, spatial quantities are denoted by lower case letters (e.g.  $q$ ) and material quantities by upper case letters (e.g.  $Q$ ). Furthermore, Einstein's summation convention is applied, i.e. it is summed over indices which appear twice. The following notation is used for the standard mathematical products: The simple contraction is denoted by " $\cdot$ ", e.g.  $\{\mathbf{A} \cdot \mathbf{B}\}_{ik} = A_{ij}B_{jk}$ , the double contraction by ":", e.g.  $\mathbf{A} : \mathbf{B} = A_{ij}B_{ij}$  and the triple contraction by ":", e.g.  $\{\mathbf{C} : \mathbf{D}\}_{lm} = C_{ijkl}D_{ijkm}$ . The standard dyadic product is indicated by " $\otimes$ ", e.g.  $\{\mathbf{A} \otimes \mathbf{B}\}_{ijkl} = A_{ij}B_{kl}$ . The transpose of  $\mathbf{A}$  is denoted by  $\mathbf{A}^t$ :  $(A_{ij})^t = A_{ji}$ .

Section 3.1 introduces the spatial and the material motion problem. Therein, it is distinguished between the spatial and the material operations: The spatial and the material gradient are denoted by  $\nabla_{\mathbf{x}}$  and  $\nabla_{\mathbf{X}}$ , respectively, whereas  $\text{div}$  and  $\text{Div}$  represent the corresponding divergences.

## A.2. Definitions

**classification of second-order partial differential equations:** A second-order partial differential equation in two independent variables  $\mathbf{x}$  and  $t$

$$a \frac{\partial^2 f(\mathbf{x}, t)}{\partial \mathbf{x}^2} + b \frac{\partial^2 f(\mathbf{x}, t)}{\partial \mathbf{x} \partial t} + c \frac{\partial^2 f(\mathbf{x}, t)}{\partial t^2} + d \frac{\partial f(\mathbf{x}, t)}{\partial \mathbf{x}} + e \frac{\partial f(\mathbf{x}, t)}{\partial t} + g(f, \mathbf{x}, t) = 0$$

is called **elliptic** if its discriminant  $ac - b^2/4$  is positive for all  $\mathbf{x}$  and all  $t$ ;  $a$ ,  $b$ ,  $c$ ,  $d$  and  $e$  being functions of  $\mathbf{x}$  and  $t$  as well. It is referred to as **parabolic**, if the discriminant equals zero. If the discriminant is negative, the second-order partial differential equation is called **hyperbolic**. The classification can also be made upon the signature of the eigenvalues of the coefficient matrix  $\begin{pmatrix} a & b/2 \\ b/2 & c \end{pmatrix}$ . The partial differential equation is called elliptic, if both

## A. Mathematics

eigenvalues are either positive or negative; parabolic, if one eigenvalue is zero and the other non-zero; hyperbolic, if there is one negative and one positive eigenvalue. Note that this definition can be position-dependent.

**closed system:** A closed system is defined as a fixed amount of mass in a region  $\Omega$ . It cannot exchange mass (only energy) with its surroundings.

**jump:** A jump of a physical quantity  $\{\bullet\}$  across a singular surface is the difference between its limiting values on either side of the singular surface and is denoted by  $[[\{\bullet\}]]$ .

**material singular surface:** A singular surface of order  $k \geq 1$  is an orientable smooth surface within a body on which a physical quantity (e.g. the motion  $\varphi$ ) and its spatial and temporal derivatives of order  $1, \dots, k-1$  are continuous and the derivatives of order  $k$  are almost everywhere discontinuous, i.e. the set of points where it is continuous is a set with measure zero. A singular surface is called material singular surface if its velocity is the same as the velocity of its particles.

**objective:** Let  $\mathbf{x}^*$  denote the position of a point  $\mathbf{x}$  after a change of the observer. A function  $\mathbf{f}$  is called objective if  $\mathbf{f}(\mathbf{x}^*, t) = \mathbf{Q}(t) \cdot \mathbf{f}(\mathbf{x}, t)$ , where  $\mathbf{Q}$  is an orthogonal tensor.  $\mathbf{Q}$  describes the observer's change, i.e.  $\mathbf{x}^* = \mathbf{Q} \cdot \mathbf{x}$ .

**one-form:** A one-form, also called a covector, is a linear functional which maps each vector in a vector space to a real number, such that the mapping is invariant with respect to coordinate transformations of the vector space.

**skew-symmetric tensor:** A second order tensor  $\mathbf{A}$  is called skew-symmetric, if  $\mathbf{A} = \mathbf{A}^{-t}$ .

**symmetric tensor:** A second order tensor  $\mathbf{A}$  is called symmetric, if  $\mathbf{A} = \mathbf{A}^t$ .

**thermodynamic equilibrium:** In classical thermoelasticity, a system is said to be in thermodynamic equilibrium, if its velocity and its temperature are constant in space and time [55, 66]. Throughout this thesis (dealing with non-classical thermoelasticity), a system is said to be in thermodynamic equilibrium, if its velocity, its thermal displacement and its temperature are constant and all production and supply terms vanish:

$$\begin{aligned} \mathbf{V}(\mathbf{X}, t) &= \mathbf{v}(\mathbf{x}, t) = \text{const.}, & \alpha(\mathbf{X}, t) &= \alpha(\mathbf{x}, t) = \text{const.}, \\ \mathbf{T}(\mathbf{X}, t) &= \mathbf{T}(\mathbf{x}, t) = \text{const.}, \\ \mathbf{b} &= \mathbf{0}, & r &= 0, & s &= 0. \end{aligned}$$

This implies that

$$\nabla_{\mathbf{X}} \mathbf{V} = \nabla_{\mathbf{x}} \mathbf{v} = \mathbf{0}, \quad \nabla_{\mathbf{X}} \alpha = \nabla_{\mathbf{x}} \alpha = \mathbf{0} \quad \text{and} \quad \nabla_{\mathbf{X}} T = \nabla_{\mathbf{x}} T = \mathbf{0}$$

hold in thermodynamic equilibrium. A system is said to be in non-equilibrium state if it is not in thermodynamic equilibrium.



### A.3. Jump conditions

The derivation of the local balance equations in Section 3.2 is based on the assumption that the fields under consideration are continuous and sufficiently smooth everywhere. However, the ideal-wall-argumentation in Section 4.1 assumes the existence of an ideal wall, thus a material singular surface, between the continuum under consideration and a second continuum.

In this thesis, the problem of material singular surfaces only occurs in the ideal-wall-argumentation and is not of central interest. Therefore, it is not dealt with in Chapter 3 and briefly listed in the spatial motion problem at this point. For details, the reader is referred to [55, 99].

The existence of a material singular surface in a body leads to so-called jump conditions for the balanced quantities linear momentum, energy and entropy on the singular surface:

$$\begin{aligned}
 \text{balance of linear momentum} & \quad [[\boldsymbol{\sigma} \cdot \mathbf{n}_s]] & = & \mathbf{0} \\
 \text{balance of energy} & \quad [[\mathbf{q} \cdot \mathbf{n}_s]] - [[\mathbf{v}_s] \cdot \boldsymbol{\sigma} \cdot \mathbf{n}_s] & = & 0 \\
 \text{balance of entropy} & \quad [[\mathbf{h} \cdot \mathbf{n}_s]] & = & 0,
 \end{aligned} \tag{A.3.1}$$

$\mathbf{n}_s$  and  $\mathbf{v}_s$  denote the normal unit vector and the velocity of the singular surface, respectively. The jump condition of the balance of mass is always fulfilled for a material singular surface and the jump condition of the balance of angular momentum does not lead to any further information if Boltzmann continua are considered [55], like in this thesis.

### A.4. Symmetry and skew-symmetry for two-point tensors

Every second order tensor  $\mathbf{A}$  can be uniquely decomposed into a symmetric and a skew-symmetric part,  $\text{sym}(\mathbf{A})$  and  $\text{skw}(\mathbf{A})$ , respectively,

$$\mathbf{A} = \frac{1}{2} [\mathbf{A} + \mathbf{A}^t] + \frac{1}{2} [\mathbf{A} - \mathbf{A}^t] = \text{sym}(\mathbf{A}) + \text{skw}(\mathbf{A}). \tag{A.4.1}$$

In addition, it holds

$$\text{sym}(\mathbf{A}) : \text{skw}(\mathbf{A}) = 0. \tag{A.4.2}$$

Let  $a : \mathcal{B} \times \mathbb{R} \rightarrow \mathbb{R}$  denote a scalar field which is at least twice differentiable. Then  $\nabla_{\mathbf{x}} \nabla_{\mathbf{x}} a := \nabla_{\mathbf{x}} (\nabla_{\mathbf{x}} a)$  is a symmetric tensor (Schwarz's theorem).

If  $\mathbf{C} \in \mathbb{R}^{3 \times 3}$  skew-symmetric, then there exists a unique vector  $\boldsymbol{\omega} \in \mathbb{R}^3$  such that

$$\mathbf{C} \cdot \mathbf{a} = \boldsymbol{\omega} \times \mathbf{a} \quad \forall \mathbf{a} \in \mathbb{R}^3. \tag{A.4.3}$$

$\mathbf{C}$  is related to  $\boldsymbol{\omega}$  via  $C_{ij}a_j = e_{ijk}\omega_k a_k$  for  $i, j, k = 1, 2, 3$ , where  $e$  is the permutation tensor.  $\boldsymbol{\omega}$  is called axial vector of  $\mathbf{C}$ . For example, in case of the vorticity tensor  $\mathbf{W}$ ,  $\boldsymbol{\omega} = \text{curl} \mathbf{v} / 2$ .

## A.5. Transformations

Let  $a : \mathcal{B} \times \mathbb{R} \rightarrow \mathbb{R}$  be a scalar field and  $\mathbf{u} : \mathcal{B} \times \mathbb{R} \rightarrow \mathbb{R}^3$  be a vector field. Then

$$\operatorname{div}(a\mathbf{u}) = a\operatorname{div}(\mathbf{u}) + \mathbf{u} \cdot \nabla_{\mathbf{x}} a \quad (\text{A.5.1})$$

holds. The well-known Gauss theorem relates a volume integral to a surface integral by

$$\int_{\mathcal{B}} \operatorname{div}(\mathbf{u}) \, dV = \int_{\partial\mathcal{B}} \mathbf{u} \cdot \mathbf{n} \, dA, \quad (\text{A.5.2})$$

$\mathbf{n}$  denoting the outward unit normal vector on the body's surface  $\partial\mathcal{B}$ .

Furthermore, let  $\mathbf{D}$  and  $\mathbf{W}$  be the rate of deformation tensor and the vorticity tensor. Then the following relation holds

$$(\nabla_{\mathbf{x}} a)' = \nabla_{\mathbf{x}} \dot{a} - \mathbf{D} \cdot \nabla_{\mathbf{x}} a + \mathbf{W} \cdot \nabla_{\mathbf{x}} a \quad (\text{A.5.3})$$

due to

$$\begin{aligned} (\nabla_{\mathbf{x}} a)'_i &= \frac{\partial}{\partial t} \left( \frac{\partial a}{\partial x_i} \right) + \frac{\partial}{\partial x_j} \left( \frac{\partial a}{\partial x_i} \right) v_j = \frac{\partial}{\partial x_i} \left( \frac{\partial a}{\partial t} + \frac{\partial a}{\partial x_j} v_j \right) - \frac{\partial a}{\partial x_j} \frac{\partial v_j}{\partial x_i} \\ &= (\nabla_{\mathbf{x}} \dot{a})_i - L_{ji} (\nabla_{\mathbf{x}} a)_j = (\nabla_{\mathbf{x}} \dot{a})_i - D_{ij} (\nabla_{\mathbf{x}} a)_j + W_{ij} (\nabla_{\mathbf{x}} a)_j. \end{aligned}$$

## A.6. Calculation of absolute entropy

The absolute entropy  $S_0$  is introduced in order to scale the entropy  $\rho\eta$ .  $S_0$  is a reference-temperature-dependent constant. Nernst' theorem, also known as the third law of thermodynamics, states that the entropy tends to zero as the absolute temperature goes to zero.

It is well-known that  $c = \theta \frac{\partial \rho\eta}{\partial \theta}$ . Consequently,

$$S(\theta) = \int_0^\theta \frac{c(\theta)}{\theta} \, d\theta.$$

Experiments have shown that the specific heat  $c$  is proportional to  $\theta^3$  at cryogenic temperatures, i.e.  $c = a\theta^3$  for some constant  $a$ .  $a$  can easily be calculated for given  $c$ . Thus, the absolute entropy at a small reference temperature  $T_0$  equals

$$S_0(T_0) = \int_0^{T_0} a\theta^2 \, d\theta.$$



Walther Nernst

## A.7. Cauchy's stress theorem

Cauchy's stress theorem is a special case of Cauchy's fundamental theorem (3.2.2) relating the true traction vectors to stress tensors. Let  $\mathbf{t}_C$  denote the true traction vector, i.e. the force measured per unit surface area in the spatial configuration  $\mathcal{B}_t$ , and  $\mathbf{T}_C$  the nominal traction vector, i.e. the force measured per unit surface area in the reference configuration  $\mathcal{B}_0$ . Let the Cauchy assumption

$$\mathbf{t}_C = \mathbf{t}_C(\mathbf{x}, t, \mathbf{n}), \quad \mathbf{T}_C = \mathbf{T}_C(\mathbf{X}, t, \mathbf{N})$$

hold, i.e. both vectors depend on the normals  $\mathbf{n}$  and  $\mathbf{N}$  at the surface. Then there exist unique second-order tensor fields, the Cauchy stress tensor  $\boldsymbol{\sigma}$  and the first Piola–Kirchhoff stress tensor  $\mathbf{P}$ , such that :

$$\mathbf{t}_C(\mathbf{x}, t, \mathbf{n}) = \boldsymbol{\sigma}^t(\mathbf{x}, t) \cdot \mathbf{n}, \quad \mathbf{T}_C(\mathbf{X}, t, \mathbf{N}) = \mathbf{P}(\mathbf{X}, t) \cdot \mathbf{N}.$$



Augustin Louis Cauchy

## A.8. Lemma on linear algebraic equations with an inequality constraint

The exploitation of the entropy principle of Müller and Liu is based on the following lemma stated by Liu [97]. The lemma provides necessary and sufficient conditions for solving a linear inequality being based on a given finite set of linear equations in a finite-dimensional space. Note that Liu's lemma is a special case of the classical result ascribed to Farkas and Minkowski, of which Liu was unaware of, as shown in the historical note [62]. Here Liu's lemma is given as he suggests it for the exploitation of Müller's entropy principle. Liu proves his version in [97], for further information on the lemma of Farkas and Minkowski - being of importance in mathematical optimization and linear programming - see [15].

**Lemma:** Let  $\mathbf{A} \cdot \mathbf{x} + \mathbf{b} = \mathbf{0}$  be a linear system of  $p$  equations and  $n$  unknowns, with  $\mathbf{A} \in \mathbb{R}^{p \times n}$ ,  $\mathbf{x} \in \mathbb{R}^n$  and  $\mathbf{b} \in \mathbb{R}^p$ . Let  $S$  be the corresponding non-empty solution set and  $\boldsymbol{\alpha} \in \mathbb{R}^n$ ,  $\boldsymbol{\alpha} \neq \mathbf{0}$ , and  $\beta \in \mathbb{R}$  be given. Then the following statements are equivalent:

- i.  $\boldsymbol{\alpha}^t \cdot \mathbf{x} + \beta \geq 0 \quad \forall \mathbf{x} \in S.$
- ii.  $\exists \boldsymbol{\lambda} \in \mathbb{R}^p$  with  $\boldsymbol{\lambda} \neq \mathbf{0}$  such that  $\boldsymbol{\alpha}^t \cdot \mathbf{x} + \beta - \boldsymbol{\lambda}^t \cdot [\mathbf{A} \cdot \mathbf{x} + \mathbf{b}] \geq 0 \quad \forall \mathbf{x} \in \mathbb{R}^n$
- iii.  $\exists \boldsymbol{\lambda} \in \mathbb{R}^p$  with  $\boldsymbol{\lambda} \neq \mathbf{0}$  such that  $\boldsymbol{\alpha} - \mathbf{A}^t \cdot \boldsymbol{\lambda} = \mathbf{0}$  and  $\beta - \boldsymbol{\lambda}^t \cdot \mathbf{b} \geq 0.$

$\boldsymbol{\lambda}$  is called Lagrange multiplier. Note that from the mathematical viewpoint, the prerequisite  $S$  not being empty is not necessary. However, in the spirit of thermodynamics an empty set  $S$  would imply that no thermodynamic process satisfies the underlying balance equations. In the

given context, the vector  $\boldsymbol{x}$  contains all those higher derivatives of the independent variables of the state space  $\mathbb{S}$  which are obtained by carrying out the differentiations in the Müller–Liu entropy inequality (4.1.1) according to the product rule. In that context,  $\boldsymbol{x}$  is referred to as the process direction [116].

## A.9. Analytical solutions

In case of the simple example introduced in Section 5.3 analytical solutions for the three heat equations (5.1.3), (5.1.6) and (5.1.10) can be determined. No boundary conditions are applied. Mathematically, the initial conditions can be expressed as

$$\begin{aligned} \alpha(x, 0) &= 0 & \forall x \in [0, L] \\ T(x, 0) = \dot{\alpha}(x, 0) &= \frac{e^{-nx^2} - e^{-nL^2}}{1 - e^{-nL^2}} & \forall x \in [0, L], \end{aligned} \quad (\text{A.9.1})$$

where  $n \in \mathbb{N}$ .

Then the Fourier series of the analytical solutions read

Type I

$$T(x, t) = A_0 + \sum_{j=1}^{\infty} A_j \cos\left(j\frac{\pi}{L}x\right) + B_j \sin\left(j\frac{\pi}{L}x\right) e^{-j^2 \frac{\kappa_1 \pi^2}{\rho c L^2} t} \quad (\text{A.9.2})$$

Type II

$$T(x, t) = A_0 + \sum_{j=1}^{\infty} \left[ A_j \cos\left(j\frac{\pi}{L}x\right) + B_j \sin\left(j\frac{\pi}{L}x\right) \right] \cos\left(j\sqrt{\frac{\kappa_2 \pi}{\rho c L}} t\right) \quad (\text{A.9.3})$$

Type III

$$T(x, t) = A_0 + \sum_{j=1}^{\infty} \left[ A_j \cos\left(j\frac{\pi}{L}x\right) + B_j \sin\left(j\frac{\pi}{L}x\right) \right] e^{at} \left[ \frac{a}{\omega} \sin(\omega t) + \cos(\omega t) \right] \quad (\text{A.9.4})$$

with  $a = -\frac{j^2 \kappa_4 \pi^2}{2L^2 \rho c}, \quad \omega = \sqrt{a^2 + \frac{j^2 \kappa_3 \pi^2}{L^2 \rho c} \left[ 1 + \frac{\kappa_4^2}{\kappa_3^2} a \right]}$

The Fourier coefficients are given by

$$\begin{aligned} A_0 &= \frac{1}{L} \int_0^L \dot{\alpha}(x, 0) \, dx, & A_j &= \frac{2}{L} \int_0^L \dot{\alpha}(x, 0) \cos\left(j\frac{\pi}{L}x\right) \, dx, \\ B_j &= \frac{2}{L} \int_0^L \dot{\alpha}(x, 0) \sin\left(j\frac{\pi}{L}x\right) \, dx. \end{aligned} \quad (\text{A.9.5})$$

## B. A glance at analogous fundamental laws

This thesis focuses on non-classical, i.e. non-Fourier heat conduction. From the mathematical point of view Fourier's law of heat conduction (5.1.1)<sub>2</sub> is structurally identical to Fick's law of diffusion, to Darcy's law for flow through porous media, similar to Hooke's law of elasticity and similar to the electric field's law in electromagnetics, all being valid for a wide range of physical, biological and engineering fields. Although these laws describe many applications fairly appropriate, there also exist various situations in which they have proven to be inadequate - as Fourier's heat conduction law. This section presents a brief introductory overview of the analogous laws and addresses to some of their limitations. It by no means claims to be complete.

### B.1. Fourier's law

The classical Fourier law of heat conduction states that the heat flux  $\mathbf{q}$  is proportional to the temperature gradient  $\nabla T$  (cf. Eq. (5.1.1)<sub>2</sub>)

$$\mathbf{q} = -\kappa_1 \nabla T$$

leading to the parabolic temperature equation Eq. (5.1.3)

$$\rho c \dot{T} = \operatorname{div}(\kappa_1 \nabla T) + \rho r,$$

see Section 5.1.1 for more detailed information. It is first expressed by Jean-Baptiste-Joseph Fourier in 1822 [46]. As mentioned in Chapter 2, Fourier's approach is not suitable to model the second sound phenomenon. Moreover, it has the drawback of allowing perturbations to propagate with infinite speed.



Jean-Baptiste-Joseph Fourier

## B.2. Fick's law

Fick's law of diffusion is formulated by Adolph Fick [45] in 1855 and relates the diffusion flux  $\mathbf{j}$  to the gradient of the mass concentration  $\mathcal{C}$ :

$$\mathbf{j} = -\mathfrak{D}\nabla\mathcal{C}. \quad (\text{B.2.1})$$

$\mathfrak{D}$  is referred to as the diffusion coefficient or diffusivity. Fick's law leads to the parabolic diffusion equation

$$\dot{\mathcal{C}} = \text{div}(\mathfrak{D}\nabla\mathcal{C}) + \mathfrak{s}, \quad (\text{B.2.2})$$

where  $\mathfrak{s}$  is a source term being independent of the concentration (cf. [121]).

Like Fourier's law, Fick's law is a phenomenological assumption. Both resulting equations (5.1.3) and (B.2.2) are parabolic and model diffusive processes. While the former models transport of energy, Fick's law describes the diffusion of matter.



Adolph Fick

Usually, Fick's law is applied to model transport processes in fluids, of polymers, in foods, pharmaceuticals, but also for modeling traffic flow or fiber spinning [77, 82, 100, 109]. Also, many biological phenomena are suitably described by the Fickian approach, e.g. pulse propagation in nerves, mass growth or dendritic growth [109].

Non-Fickian behavior is detected if the polymer swells due to a penetrator, if low molecular weight species permeate through thin polymeric membranes, if a polymer is put into contact with a solvent, or if a uniform polymer solution is sheared between two parallel rotating discs or in sorption experiments, for example [40, 82, 162].

Koch and Brady [88] as well as Kim and Kavvas [85] propose generalisations of Fick's law (B.2.1) in order to model transport of pollutants in a river. Kuhl and Schmid [91] simulate mineral exsolution, the phenomenon in which minerals segregate into discrete phases, and state that the process of phase separation cannot be modeled by the Fickian law (B.2.1) since nonuniform concentration profiles are needed. An akin approach is followed by Ubachs et al. [166] who model the microstructure evolution of tin-lead solder.

The paradox of infinite propagation speed also exists for the Fickian model. Jordan [77], who models traffic flow, Méndez and Camacho [109], who model growth of biological populations, and Jou et al. [82], who model diffusion in glassy polymers in the vicinity of the glass transition temperature, transfer the Maxwell–Cattaneo–Vernotte approach to Fick's law, i.e.

$$\mathbf{j} + \tau_r \dot{\mathbf{j}} = -\mathfrak{D}\nabla\mathcal{C}. \quad (\text{B.2.3})$$

The Maxwell–Cattaneo–Vernotte approach is the first approach to modify Fourier's law (5.1.1)<sub>2</sub> of heat conduction and is derived independently by Maxwell [107], Cattaneo [24] and Vernotte [168]. They introduce a relaxation time  $\tau_r$  in order to overcome the paradox of infinite propagation speed (cf. Chapter 2).

### B.3. Darcy's law



Henri Darcy

In 1856 Henri Darcy [36] investigates the flow of water through beds of sand and formulates the following law

$$\mathbf{v} = -\frac{ck}{m}\nabla p, \quad (\text{B.3.1})$$

describing the flow velocity  $\mathbf{v}$  of a single-phase fluid through porous media. Here,  $k$ ,  $c$ ,  $m$  and  $p$  denote the medium's permeability (also called hydraulic conductivity), its compressibility (also called porosity), its dynamic viscosity and the pressure. In theories of porous media one usually considers averaged quantities. Thus, Darcy's law is often stated in terms of the Darcy velocity  $\mathbf{V}$  which is the average of the fluid velocity and related to the usual velocity  $\mathbf{v}$  via  $\mathbf{V} = c\mathbf{v}$ .

Hubbert [86] shows that Darcy's law can be derived from the Navier–Stokes equations. Consequently, although it was originally formulated by using experimental observations, it has a theoretical foundation. Therefore, Darcy's law, as opposed to Fourier's law, cannot be regarded as a phenomenological equation, but rather as a result from the Navier–Stokes equations in case of quasi-stationary motion of fluids.

Inserting Darcy's law (B.3.1) and the relation for a fluid's compressibility (or in terms of porous media: the medium's porosity) for isothermal conditions  $c = -\frac{1}{v}\frac{dv}{dp} = \frac{1}{\rho}\frac{d\rho}{dp}$  (cf. e.g. [155]) into the mass balance Eq. (3.2.5) leads to the parabolic diffusion equation

$$\frac{\partial \rho}{\partial t} = \text{div} \left( \frac{k}{m} \nabla \rho \right). \quad (\text{B.3.2})$$

If Darcy's law is stated in terms of the hydraulic head  $h$ , i.e.  $\mathbf{v} = -k\nabla h$ , the so-called groundwater flow equation (cf. [100])

$$\frac{\partial h}{\partial t} = \text{div} (k\nabla h) \quad (\text{B.3.3})$$

is obtained. Both equations (B.3.2) and (B.3.3) are parabolic and structurally similar to the classical heat equation (5.1.3): the rate of the balanced quantity equals the divergence of the quantity's gradient.

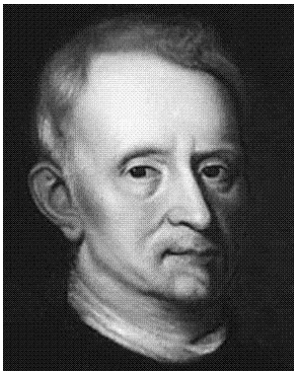
Darcy's law is generally applicable to fluid flow of low velocity in porous media. Engineering applications can be found in the fields of soil mechanics, biology (e.g. blood flow in tumors), chemical reactors, drying composite molding, hydrogeology (e.g. groundwater flow) and harbor engineering (e.g. prediction of wave-reflection by a impermeable, rock-filled breakwater) [32, 172], for example .

Darcy's law fails if the flow velocity is comparatively high, respectively above a critical Reynolds number [32, 121], for multi-phase fluids [172] or if viscous effects need to be included, which

## B. A glance at analogous fundamental laws

is discussed by e.g. [121] and [32]. Moreover, in the case of a moving porous medium, the inertial effects have to be considered by inserting the relative velocity between the fluid and the porous medium into Darcy's law [32].

### B.4. Hooke's law



Sir Robert Hooke

In elasticity, Hooke's law describes the linear relationship between the Cauchy stress  $\boldsymbol{\sigma}$  and the strains  $\boldsymbol{\varepsilon}$

$$\begin{aligned}\boldsymbol{\sigma} &= \mathbf{E} : \boldsymbol{\varepsilon} \\ &= \mathbf{E} : \text{sym}(\nabla \mathbf{u}),\end{aligned}\tag{B.4.1}$$

$\mathbf{E}$  denoting the fourth order elasticity tensor. It is first stated by Sir Robert Hooke in 1678. The symmetric part of the gradient of the displacement  $\mathbf{u}$  defines the strains:  $\boldsymbol{\varepsilon} := \text{sym}(\nabla \mathbf{u})$ . Hooke's law links two tensors of second order, whereas the other laws mentioned in this appendix link vectorial quantities.

In the one-dimensional case, inserting Hooke's law (B.4.1) into the balance of momentum (3.2.6) leads to the well-known hyperbolic wave equation

$$\rho_t \ddot{u} = \text{div}(E \nabla u) + \rho_t b,\tag{B.4.2}$$

where  $b$  is the one-dimensional volume force.

Contrary to Fourier's law, but in accordance with the thermal theory of type II, the elastic theory is governed by a hyperbolic equation.

The scope of Hooke's law is determined in tensile tests. If the material's stress is greater than the so-called yielding point, the material behavior changes from elastic to plastic and Hooke's law is no longer valid. Furthermore, if the material undergoes large strains, the relation between the stress and the strains often becomes nonlinear. Some materials already undergo large deformations near an equilibrium state, such as biological tissues or rubber-like polymers [66].

Numerous approaches exist in order to account for a geometrically nonlinear behavior, for example Neo-Hookean- (as presented in this thesis), Ogden-, Saint-Venant Kirchhoff- and Varga-model (cf. e.g. [66, 99]). The ideas of geometrically nonlinear behavior are well investigated and documented in various textbooks on continuum mechanics, e.g. [55, 66, 99], to which the reader is referred for further information.



## B.5. Maxwell's equations

Classical electromagnetic problems are described by the four Maxwell equations specifying the connections between the electric displacement  $\mathbf{D}$ , the electric field  $\mathbf{E}$ , the electromagnetic flux  $\mathbf{B}$ , the magnetic field  $\mathbf{H}$ , the charges  $\rho$  and the currents  $\mathbf{j}$  [74]:

$$\begin{aligned} \operatorname{div} \mathbf{D} &= \rho && \text{(charges generate electric displacements)} \\ \operatorname{curl} \mathbf{E} + \dot{\mathbf{B}} &= \mathbf{0} && \text{(rate of electromagnetic flux curl electric field)} \\ \operatorname{div} \mathbf{B} &= 0 && \text{(no magnetic monopoles)} \\ \operatorname{curl} \mathbf{H} - \mathbf{j} - \dot{\mathbf{D}} &= \mathbf{0} && \text{(currents curl the magnetic field)} \end{aligned} \quad (\text{B.5.1})$$



James C. Maxwell

The electric field  $\mathbf{E}$  can be written in terms of a scalar potential  $\phi$  and  $\mathbf{A}$ , the vector potential which defines the electromagnetic flux  $\mathbf{B}$  ( $\mathbf{B} = \operatorname{curl} \mathbf{A}$ ) [74]:

$$\mathbf{E} = -\nabla\phi - \frac{\partial \mathbf{A}}{\partial t}. \quad (\text{B.5.2})$$

$\phi$  is also referred to as electric potential and in electrostatics, where  $\mathbf{E} = -\nabla\phi$ , a potential difference  $\phi_a - \phi_b$  corresponds to the voltage  $\mathbb{V}$ .

The dynamic behavior of the two potentials  $\phi$  and  $\mathbf{A}$  is determined by the Maxwell equations (B.5.1)<sub>1</sub> and (B.5.1)<sub>4</sub> [74]. Restricting the considerations to the vacuum allows for linear constitutive relations between the electric displacement  $\mathbf{D}$  and the electric field  $\mathbf{E}$  and between the electromagnetic flux  $\mathbf{B}$  and the magnetic field  $\mathbf{H}$ :

$$\mathbf{D} = \epsilon \mathbf{E} \quad \text{and} \quad \mathbf{B} = \mu \mathbf{H}. \quad (\text{B.5.3})$$

$\epsilon$  and  $\mu$  denote the permittivity and the permeability, respectively. Applying the Lorenz gauge condition (cf. [74]) yields the decoupled inhomogeneous hyperbolic wave equations

$$\begin{aligned} \operatorname{div} \nabla \phi - \frac{1}{c^2} \frac{\partial^2 \phi}{\partial t^2} &= -\rho/\epsilon, \\ \operatorname{div} \nabla \mathbf{A} - \frac{1}{c^2} \frac{\partial^2 \mathbf{A}}{\partial t^2} &= \mu \mathbf{j}. \end{aligned} \quad (\text{B.5.4})$$

$c$  denotes the vacuum speed of light. Thus, Eqs. (B.5.4) can be seen as the electric analogues to the hyperbolic heat equation of type II (5.1.6).

The Maxwell equations in vacuum are also valid for electromagnetic simulations in air. Thus, they are applied to model microwave radio relay, television and radio broadcasting - the technology used for transmitting analog and digital signals. Further applications are transcontinental phone calls and cellular phone calls, for example.

## *B. A glance at analogous fundamental laws*

Maxwell's equations (B.5.1) lead to a more complicated version of Eq. (B.5.4) if the electromagnetic waves propagate through matter, thus if the medium is polarizable, for example. The right hand side of Eq. (B.5.4) may then depend on the potentials  $\phi$  and  $\mathbf{A}$  and consequently, one might lose hyperbolicity. Moreover, experimental research has shown that a more general approach is required to describe an electric current at high electric fields [120], for example.

## C. Albert E. Green and Paul M. Naghdi

Albert E. Green and Paul M. Naghdi met in 1955 when A.E. Green was on a lecture tour in the U.S.. P.M. Naghdi stated in his Timoshenko Medal acceptance speech in 1980: “[...] we hit it off rather well from the start. When we invited him to come to Berkeley as a visiting professor, he immediately accepted and, from my point of view, that visit led to a very exciting and profitable collaborative effort. [...]”. During their careers they published 68 reviewed journal papers together - of which the first one was published in 1965 and the last appeared in 1996. Some of them were cited more than 100 times by many different authors. All of their research activities were directed at theoretical mechanics. They contributed to the fields of classical continuum physics, generalized continua, mixtures, incompressible viscous fluid flow, thermoviscous fluids, water waves, electromagnetic effects, aspects of the 2nd law of thermodynamics in thermoelasticity and electromagnetics, fluid sheets, thermal effects, rods and of course thermoelasticity without energy dissipation.

### C.1. Albert E. Green

Albert Edward Green was born in London, England on November 11th, 1912 and died on August 12, 1999 at the age of 86. He spent his student years in the Department of Mathematics at Cambridge University, England. In 1934, A.E. Green received a First Class Honors in mathematics. Also in Cambridge, he did his research for his Ph.D. thesis under the supervision of Sir G.I. Taylor. A.E. Green earned his Ph.D. degree in 1937 for his work about gliding problems in seaplane theory as well as equilibrium and stability of thin twisted strips. After having held research positions at Cambridge and Durham University, he was appointed Professor of Applied Mathematic's at King's College, Newcastle-upon-Tyne, England in 1948. Back then, King's College was a division of Durham University, but later became part of the newly evolved University of Newcastle-upon-Tyne.



Albert Edward Green

picture taken from [118]

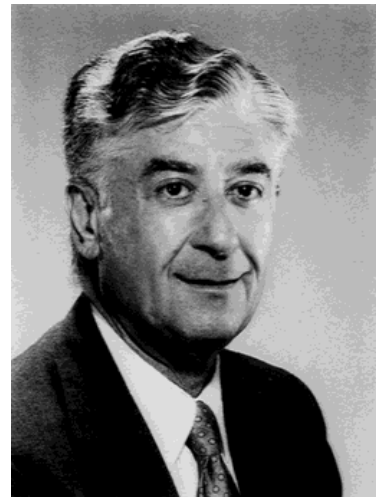
A.E. Green had spent 20 years in Newcastle-upon-Tyne before he moved to Oxford University where he became Sedleian Professor of Natural Philosophy in the department of mathematics

for 9 years. He stayed in Oxford until his death in 1999. During his career, he has been a visiting professor twice at Brown University in Providence, Rhode Island, USA and three times at the University of California, Berkley, USA. His stays in Berkley were certainly the basis for the fruitful and long-term collaboration with Paul M. Naghdi.

A.E. Green contributed to various fields of theoretical mechanics, such as linear and nonlinear elasticity, fluid mechanics and thermodynamics. His work was highly recognized. For example, he held honorary degrees from the Universities of Durham and Glasgow in 1970 and 1975, respectively. Moreover, he was elected a Fellow of the Royal Society of London in 1958 and was awarded the Timoshenko Medal by the American Society of Mechanical Engineers in 1974.

## **C.2. Paul M. Naghdi**

Paul Mansour Naghdi was born in Tehran, Iran, on March 29, 1924 and died on July 9, 1994 in Berkley, USA. After having finished his school education, he moved to the U.S.A. in 1943 and studied mechanical engineering at Cornell University, Ithaca, New York. He graduated in 1948. In the same year, he was granted U.S. citizenship. P.M. Naghdi went on to the University of Michigan, Ann Arbor, Michigan, USA where he earned his doctorate degree 1951 for his work on large deformations of elasto-plastic circular plates with polar symmetrical loading. Immediately afterwards, he was appointed assistant professor at University of Michigan and was promoted full professor only three years later. From 1958 onwards, he worked at the University of California at Berkley in the Division of Applied Mechanics in the Department of Mechanical Engineering.



Paul Mansour Naghdi

P.M. Naghdi's scientific work (of which there are more than 200 scientific journal papers) comprises publications on general continuum mechanics, linear and nonlinear elasticity, thermomechanics, plasticity, viscoelasticity, shells, fluid sheets and mixtures.

In recognition of his distinguished contributions, P.M. Naghdi obtained various awards. Among others, he was awarded the Timoshenko Medal by the American Society of Mechanical Engineers in 1980 and the Eringen Medal of the Society of Engineering Science in 1986. He earned honorary doctorates from the National University of Ireland (1987) and Université Catholique de Louvain (1992).

## References

- [1] Ackermann, C.C.; Bertram, B.; Fairbank, H.A.; Guyer, R.A. [1966] Second sound in solid Helium. *Physical Review* 16(18), 789–791
- [2] Ackermann, C.C.; Overton, W.C. [1969] Second sound in solid Helium-3. *Physical Review Letters* 22(15), 764–767
- [3] Allam, M.N.; Elsibai, K.A.; AbouElregal, A.E. [2002] Thermal stresses in a harmonic field for an infinite body with a circular cylindrical hole without energy dissipation. *Journal of Thermal Stresses* 25(1), 57–67
- [4] Amethyst Galleries, Inc.: Figure 5.7 is the property of Amethyst Galleries, Inc., and may not be copied for commercial purposes. Permission to copy descriptions and images is granted for personal and educational use only. All such copies must include this copyright notice and explicit references to the URL <http://mineral.galleries.com/>.
- [5] Askes, H.; Bargmann, S.; Kuhl, E.; Steinmann, P. [2005] Structural optimization by simultaneous equilibration of spatial and material forces. *Communications in Numerical Methods in Engineering* 21, 433–442
- [6] Bagri, A.; Taheri, H.; Eslami, M.R.; Fariborz, S. [2006] Generalized coupled thermoelasticity of a layer. *Journal of Thermal Stresses* 29, 359–370
- [7] Bargmann, S.; Steinmann, P. [2005] Finite element approaches to non-classical heat conduction in solids. *Computer Modeling in Engineering & Sciences* 9(2), 133–150
- [8] Bargmann, S.; Steinmann, P. [2006] Theoretical and computational aspects of non-classical thermoelasticity. *Computer Methods in Applied Mechanics and Engineering* 146(1-3), 516–527
- [9] Bargmann, S.; Steinmann, P. [2007] A classical result for a non-classical theory: Remarks on Green–Naghdi thermo-hyperelasticity. *Continuum Mechanics and Thermodynamics* 19 (1-2), 59–66
- [10] Bargmann, S.; Steinmann, P. [2008] Modeling of first and second sound. submitted
- [11] Bargmann, S.; Greve, R.; Steinmann, P. [2008] Simulation of cryovolcanism on Saturn’s moon Enceladus with the Green–Naghdi theory of thermoelasticity. submitted
- [12] Bargmann, S.; Steinmann, P. [2008] An incremental variational formulation of coupled thermoelasticity for dissipative and non-dissipative solids. *Heat and Mass Transfer*, accepted for publication
- [13] Bargmann, S.; Steinmann, P., Jordan, P.M. [2008] On the propagation of second-sound in linear and nonlinear media: Results from Green–Naghdi theory. *Physics Letters A*, accepted for publication. doi:10.1016/j.physleta.2008.04.010

## REFERENCES

- [14] Bauchau, O.A.; Theron, N.J. [1996] Energy decaying scheme for non-linear beam models. *Computer Methods in Applied Mechanics and Engineering* 134, 37–56
- [15] Bazaraa, M.S.; Sherali, H.D.; Shetty, C.M. [1993] *Nonlinear programming - theory and algorithms*. Wiley, New York
- [16] Bear, J. [1972] *Dynamics of fluids in porous media*. Elsevier, Amsterdam
- [17] Betsch, P.; Steinmann, P. [2000] Conservation properties of a time FE method. Part I: time-stepping schemes for N-body problems. *International Journal for Numerical Methods in Engineering* 49, 599–638
- [18] Betsch, P.; Steinmann, P. [2000] Inherently energy conserving time finite elements for classical mechanics. *Journal of Computational Physics* 160, 88–116
- [19] Betsch, P.; Steinmann, P. [2001] Conservation properties of a time FE method - Part II: time-stepping schemes for non-linear elastodynamics. *International Journal for Numerical Methods in Engineering* 50, 1931–1955
- [20] Betsch, P.; Steinmann, P. [2002] Conservation properties of a time FE method - Part III: Mechanical systems with holonomic constraints. *International Journal for Numerical Methods in Engineering* 53, 2271–2304
- [21] Bogy, D.B.; Naghdi, P.M. [1970] On heat conduction and wave propagation in rigid solids. *Journal of Mathematical Physics* 11(3), 917–923
- [22] Buratti, B.J.; Mosher, J.A. [1990] Albedo and color maps of the Saturnian satellites. *Icarus* 87, 339–357
- [23] Cahn, J.W.; Hilliard, J.E. [1958] Free energy of non-uniform system. I. Interfacial free energy. *Journal of Chemical Physics* 28, 258–267
- [24] Cattaneo, C. [1948] Sulla conduzione de calore. *Atti del Seminario Matematico e Fisico dell'Università di Modena* 3, 3
- [25] Chandrasekharaiah, D.S. [1996] A note on the uniqueness of solution in the linear theory of thermoelasticity without energy dissipation. *Journal of Elasticity* 43, 279–283
- [26] Chandrasekharaiah, D.S. [1996] One-dimensional wave propagation in the linear theory of thermoelasticity without energy dissipation. *Journal of Thermal Stresses* 19, 695–710
- [27] Chandrasekharaiah, D.S.; Srinath, K.S. [1997] Axisymmetric thermoelastic interactions without energy dissipation in an unbounded body with cylindrical cavity. *Journal of Elasticity* 46, 19–31
- [28] Chandrasekharaiah, D.S. [1997] Thermoelastic Rayleigh waves without energy dissipation. *Mechanics Research Communications* 24 (1), 99–101

- [29] Chandrasekharaiah, D.S. [1997] Complete solutions in the theory of thermoelasticity without energy dissipation. *Mechanics Research Communications* 24 (6), 625–630
- [30] Chandrasekharaiah, D.S. [1998] Hyperbolic thermoelasticity: A review of recent literature. *Applied Mechanics Reviews* 51(12), 705–729
- [31] Chandrasekharaiah, D.S.; Srinath, K.S. [2000] Thermoelastic waves without energy dissipation in an unbounded body with a spherical cavity. *International Journal of Mathematics and Mathematical Sciences* 23(8), 555–562
- [32] Chwang, A.T.; Chan, A.T. [1998] Interaction between porous media and wave motion. *Annual Review of Fluid Mechanics* 30, 53–84
- [33] Ciarletta, M. [1999] A theory of micropolar thermoelasticity without energy dissipation. *Journal of Thermal Stresses* 22 (6), 581–594
- [34] Cimmelli, V.A.; Kosiński, W. [1991] Nonequilibrium semi-empirical temperature in materials with thermal relaxation. *Archive of Mechanics* 43(6), 753–767
- [35] Coleman, B.D.; Noll, W. [1963] The thermodynamics of elastic materials with heat conduction and viscosity. *Archive for Rational Mechanics and Analysis* 13, 167–178
- [36] Darcy, H. [1856] *Les fontaines publiques de la ville de Dijon*. Victor Dalmont, Paris
- [37] Dascalu, C.; Maugin, G.A. [1995] The thermoelastic material-momentum equation. *Journal of Elasticity* 39, 201–212
- [38] Datta, N.; Jana, R.N. [1977] Hall effects on hydromagnetic flow and heat transfer in a rotating channel. *Journal of the Institute of Mathematics and its Applications* 19, 217–229
- [39] Dreyer, W.; Struchtrup, H. [1993] Heat pulse experiments revisited. *Continuum Mechanics and Thermodynamics* 5, 3–50
- [40] Elafif, A.; Grmela, M.; Lebon, G. [1999] Rheology and diffusion in simple and complex fluids. *Journal of Non-Newtonian Fluid Mechanics* 86, 253–275
- [41] Elafif, A.; Grmela, M. [2002] Non-Fickian mass transport in polymers. *Journal of Rheology* 46 (3), 591–628
- [42] Eriksson, K.; Estep, D.; Hansbo, P.; Johnson, C. [1996] *Computational differential equations*. Studentlitteratur
- [43] Eshelby, J.D. [1951] The force on an elastic singularity. *Philosophical transactions of the Royal Society of London A* 244, 87–112
- [44] Eshelby, J.D. [1975] The elastic energy-momentum tensor. *Journal of Elasticity* 5, 321–335

## REFERENCES

- [45] Fick, A. [1855] On liquid diffusion. *Philosophical Magazine* 10, 30–39
- [46] Fourier, J.-B.-J. [1822] *Théorie analytique de la chaleur*. Firmin Didot, Paris
- [47] Frischmuth, K.; Cimmelli, V.A. [1996] Hyperbolic heat conduction with variable relaxation time. *Journal of Theoretical and Applied Mechanics* 34(1), 58–65
- [48] Green, A.E.; Lindsay, K.A. [1972] Thermoelasticity. *Journal of Elasticity* 2(1), 1–7
- [49] Green, A.E.; Laws, N. [1972] On the entropy production inequality. *Archive for Rational Mechanics and Analysis* 45, 47–53
- [50] Green, A.E.; Naghdi, P.M. [1977] On thermodynamics and the nature of the second law. *Proceedings of the Royal Society of London A* 357, 253–270
- [51] Green, A.E.; Naghdi, P.M. [1991] A re-examination of the basic postulates of thermomechanics. *Proceedings of the Royal Society of London A* 432, 171–194
- [52] Green, A.E.; Naghdi, P.M. [1992] On undamped heat waves in an elastic solid. *Journal of Thermal Stresses* 15, 253–264
- [53] Green, A.E.; Naghdi, P.M. [1993] Thermoelasticity without energy dissipation. *Journal of Elasticity* 31, 189–208
- [54] Green, A.E.; Naghdi, P.M. [1995] A new thermoviscous theory for fluids. *Journal of Non-Newtonian Fluid Mechanics* 56, 289–306
- [55] Greve, R. [2003] *Kontinuumsmechanik*. Springer
- [56] Greve, R. [2006] Fluid dynamics of planetary ices. *GAMM-Mitteilungen* 29(1), 29–51
- [57] Gross, M. [2004] *Conserving time integrators for nonlinear dynamics*. TU Kaiserslautern, Ph.D. thesis
- [58] Gross, M.; Betsch, P.; Steinmann, P. [2005] Conservation properties of a time FE method - Part IV: Higher order energy and momentum conserving schemes. *International Journal for Numerical Methods in Engineering* 63, 1849–1897
- [59] Gross, M. [2006] An energy consistent hybrid space-time Galerkin method for nonlinear thermomechanical problems. *Proceedings in Applied Mathematics and Mechanics* 6, 443–444
- [60] Gurtin, M. E. [1999]. *Configurational forces as basic concepts of continuum physics*. Springer.
- [61] Hardy, R.J.; Jaswal, S.S. [1971] Velocity of second sound in NaF. *Physical Review B* 3(12), 4385–4387
- [62] Hauser, R.A.; Kirchner, N.P. [2002] A historical note on the entropy principle of Müller and Liu. *Continuum Mechanics and Thermodynamics* (14), 223–226



- [63] Herrera, L.; Pavón, D. [2002] Hyperbolic theories of dissipation: Why and when do we need them?. *Journal of Physics A* 307, 121–130
- [64] Hetnarski, R.B.; Ignaczak, J. [1996] Soliton-like waves in a low-temperature nonlinear thermoelastic solid. *International Journal of Engineering Science* 34(15), 1767–1787
- [65] Hetnarski, R.B.; Ignaczak, J. [2000] Nonclassical dynamical thermoelasticity. *International Journal of Solids and Structures* 37, 215–224
- [66] Holzapfel, G.A. [2000] *Nonlinear solid mechanics*. Wiley
- [67] Hughes, T. J. R. [2000] *The Finite Element Method*. Dover Publications
- [68] Hutter, K. [1977] The foundations of thermodynamics, its basic postulates and implications. A review of modern thermodynamics. *Acta Mechanica* 27, 1–54
- [69] Hutter, K.; Wang, Y. [2003] Phenomenological thermodynamics and entropy principles. In: *Entropy*. Eds.: Greven, A.; Keller, G.; Warnecke, G.. Princeton University Press, Princeton-Oxford
- [70] Iesan, D. [1998] On the theory of thermoelasticity without energy dissipation. *Journal of Thermal Stresses* 21, 295–307
- [71] Iesan, D.; Nappa, L. [2005] On the theory of heat for micromorphic bodies. *International Journal of Engineering Science* 43, 17–32
- [72] Jackson, H.E.; Walker, C.T.; McNelly, T.F. [1970] Second sound in NaF. *Physical Reviews* 25(1), 26–28
- [73] Jackson, H.E.; Walker, C.T. [1971] Thermal conductivity, second sound, and phonon-phonon interactions in NaF. *Physical Reviews B* 3(4), 1428–1439
- [74] Jackson, J.D. [1999] *Classical electrodynamics*. John Wiley & Sons, 3rd ed.
- [75] Jaisaardsuetrong, J.; Straughan, B. [2007] Thermal waves in a rigid heat conductor. *Physical Letters A* 366, 433–436.
- [76] Johnson, C. [1993] Discontinuous Galerkin finite element methods for second order hyperbolic problems. *Computer Methods in Applied Mechanics and Engineering* 107, 117–129
- [77] Jordan, P.M. [2005] Growth and decay of shock and acceleration waves in a traffic flow model with relaxation. *Physica D* 207, 220–229
- [78] Jordan, P.M.; Straughan, B. [2006] Acoustic acceleration waves in homentropic Green and Naghdi gases. *Proceedings of the Royal Society London A* 462(2076), 3601–3611
- [79] Jordan, P.M.; Feuillade, C. [2006] A note on Love's equation with damping. *Proceedings of the Royal Society of London A* 462, 2063–2076.

## REFERENCES

- [80] Joseph, D.D.; Preziosi, L. [1989] Heat waves. *Reviews of Modern Physics* 61(1), 41–73
- [81] Joseph, D.D.; Preziosi, L. [1990] Addendum to the paper “Heat waves”. *Reviews of Modern Physics* 62(2), 375–391
- [82] Jou, D.; Camacho, J.; Grmela, M. [1991] On the nonequilibrium thermodynamics of non-Fickian diffusion. *Macromolecules* 24, 3597–3602
- [83] Kalpadikes, V.K.; Dascalu, C. [2004] On the configurational force balance in thermo-mechanics. *Proceedings of the Royal Society of London A* 458, 3020–3039
- [84] Kalpadikes, V.K.; Maugin, G.A. [2004] Canonical formulation and conservation laws of thermoelasticity without energy dissipation. *Reports on Mathematical Physics* 53 (3), 371–391
- [85] Kim, S.; Kavvas, M.L. [2006] Generalized Fick’s law and fractional ADE for pollution transport in a river: detailed derivation. *Journal of Hydrologic Engineering*, 80–83
- [86] King Hubbert, M. [1956] Darcy’s law and the field equations of the flow of underground fluids. *Transactions of AIME* 207, 222–239
- [87] Kirchner, N. [2001] *Thermodynamics of structured granular materials*. Shaker, Aachen
- [88] Koch, D.L.; Brady, J.F. [1987] A non-local description of advection-diffusion with application to dispersion in porous media. *Journal of Fluid Mechanics* 180, 387–403
- [89] Kuhl, E.; Denzer, R.; Barth, F.J. ; Steinmann, P. [2004] Application of the material force method to thermo-hyperelasticity. *Computer Methods in Applied Mechanics and Engineering* 193, 3303–3325
- [90] Kuhl, E. [2004] *Theory and numerics of open system continuum thermodynamics - spatial and material settings-*. Habilitation thesis, University of Kaiserslautern
- [91] Kuhl, E.; Schmid, D.W. [2007] Computational modeling of mineral unmixing and growth - An application of the Cahn-Hilliard equation. *Computational Mechanics* 39(4), 439–451
- [92] Kumar, R.; Deswal, S. [2002] Surface wave propagation in a micropolar thermoelastic medium without energy dissipation. *Journal of Sound and Vibration* 256 (1), 173–178
- [93] Lambrecht, M. [2002] *Theorie und Numerik von Materialinstabilitäten elastoplastischer Festkörper auf der Grundlage inkrementeller Variationsformulierungen*, Ph.D. thesis, University of Stuttgart
- [94] Landau, L. [1941] Theory of the superfluidity of Helium II. *Physical Reviews* 60, 356–358
- [95] Leseduarte, M.C.; Quintanilla, R. [2006] Thermal stresses in type III thermo-elastic plates. *Journal of Thermal Stresses* 29, 485–503

- [96] Li, H.; Dhaliwal, R.S. [1996] Thermal shock problem in thermoelasticity without energy dissipation. *Indian Journal of Pure and Applied Mathematics* 27(1), 85–101
- [97] Liu, I-S. [1972] Method of Lagrange multipliers for exploitation of the entropy principle. *Archive for Rational Mechanics and Analysis* 46, 131–148
- [98] Liu, I-S. [1996] On the entropy flux - heat flux relation in thermodynamics with Lagrange multipliers. *Continuum Mechanics and Thermodynamics* 8, 247–256
- [99] Liu, I-S. [2002] *Continuum Mechanics*. Springer
- [100] Lu, N.; Likos, W.J. [2004] *Unsaturated soil mechanics*. John Wiley & Sons
- [101] Marcillac, P. de; Coron, N.; Dambier, G.; Leblanc, J.; Moalic, J.-P. [2003] Experimental detection of  $\alpha$ -particles from the radioactive decay of natural bismuth. *Nature* 422, 876–878
- [102] Maugin, G.A. [1993] *Material inhomogeneities in elasticity*. Chapman & Hall, London
- [103] Maugin, G.A. [1999] *Nonlinear waves in elastic crystals*. Oxford University Press
- [104] Maugin, G.A. [2000] Towards an analytical mechanics of dissipative materials. *Rend. Sem. Mat. Univ. Pol. Torino* 58(2)
- [105] Maugin, G.A.; Kalpadikes, V.K. [2002] A Hamiltonian formulation for elasticity and thermoelasticity. *Journal of Physics A: Math. Gen.* 35, 10775–10788
- [106] Maugin, G.A.; Kalpadikes, V.K. [2002] The slow march towards an analytical mechanics of dissipative materials. *Technische Mechanik* 22(2), 98–103
- [107] Maxwell, J.C. [1867] On the dynamical theory of gases. *Philosophical Transactions of the Royal Society of London* 157, 49
- [108] McNelly, T.F.; Rogers, S.J.; Channin, R.J.; Goubau, W.M.; Schmidt, G.E.; Krumhansl, J.A.; Pohl, R.O. [1970] Heat pulses in NaF: Onset of second sound. *Physical Reviews* 24(3), 100–102
- [109] Méndez, V.; Camacho, J. [1997] Dynamics and thermodynamics of delayed population growth. *Physical Review E* 55 (6), 6476–6482
- [110] Misra, J.C.; Chattopadhyay, N.C.; Chakravorty, A. [2000] Study of thermoelastic wave propagation in a half-space using GN theory. *Journal of Thermal Stresses* 23, 327–351
- [111] Mohr, R.; Menzel, A.; Steinmann, P. [2007] A consistent time FE-Method for large strain elasto-plasto-dynamics. submitted
- [112] Müller, I. [1971] Die Kältefunktion, eine universelle Funktion in der Thermodynamik viskoser wärmeleitender Flüssigkeiten (German). *Archive for Rational Mechanics and Analysis* 40, 1–36

## REFERENCES

- [113] Müller, I. [1974] On thermodynamics of a gas with vibrating molecules. *Annales de l'institute Henri Pointcaré* 21 (3), 245–258
- [114] Müller, I. [1985] *Thermodynamics*. Pitman
- [115] Mukhopadhyay, S. [2002] Thermoelastic interactions without energy dissipation in an unbounded medium with a spherical cavity due to a thermal shock at the boundary. *Journal of Thermal Stresses* 25, 877–887
- [116] Muschik, W.; Ehrentraut, H. [1996] An amendment to the second law. *Journal of Non-Equilibrium Thermodynamics* 21, 175–192
- [117] Nappa, L. [1998] Spatial decay estimates for the evolution equations of linear thermoelasticity without energy dissipation. *Journal Thermal Stresses* 21, 581–592
- [118] Naghdi, P.M.; Spencer, A.J.M.; England, A.H. (Eds.) *Nonlinear elasticity and theoretical mechanics - In honour of A.E. Green*. Oxford Science Publications
- [119] Narayanamurti, V.; Dynes, R.C. [1972] Observation of second sound in Bismuth. *Physical Reviews* 28, 1461–1464
- [120] Nathan, M.I. [1963] Anisotropy of the conductivity of n-type Germanium at high electric fields. *Physical Review* 130 (6), 2201–2204
- [121] Nield, D.A.; Bejan, A. [1999] *Convection in porous media*, 2nd edition. Springer
- [122] Nimmo, F.; Spencer, J.R.; Pappalardo, R.T.; Mullen, M.E. [2007] Shear heating as the origin of the plumes and heat flux on Enceladus. *Nature* 444, 289–291
- [123] Peshkov, V. [1944] *Journal of Physics USSR* 8, 381
- [124] Peshkov, V. [1946] *Inter. Conf. Fund. Particles and low temperatures: Report*, Cambridge, July 22-27
- [125] Pohl, D.W.; Irmiger, V. [1976] Observation of second sound in NaF by means of light scattering. *Physical Review Letters* 36(9), 480–483
- [126] Podio-Guidugli, P. [2006] *Models of phase segregation and diffusion of atomic species on a lattice*. *Ricerche die Matematica*, to appear.
- [127] Porco, C.C.; Helfenstein, P.; Thomas, P.C.; Ingersoll, A.P.; Wisdom, J. ; West, R.; Neukum, G.; Denk, T.; Wagner, R.; Roatsch, T.; Kieffer, S.; Turtle, E.; McEwen, A.; Johnson, T.V.; Rathbun, J.; Veverka, J.; Wilson, D.; Perry, J.; Spitale, J.; Brahic, A.; Burns, J.A.; DelGenio, A.D.; Dones, L.; Murray, C.D.; Squyres, S. [ 2006] Cassini observes the active south pole of Enceladus. *Science* 311, 1394–1401
- [128] Povstenko, Y.Z. [2005] Fractional heat conduction equation and associated thermal stresses. *Journal of Thermal Stresses* 28, 83–102

- [129] Powell, R.W. [1958] Preliminary measurements of the thermal conductivity and expansion of ice. *Proceedings of the Royal Society of London A* 247(1251), 464–466
- [130] Puri, P.; Jordan, P.M. [2004] On the propagation of plane waves in type-III thermoelastic media. *Proceedings of the Royal Society of London A* 460, 3203–3221
- [131] Quintanilla, R. [1999] On the spatial behavior of thermoelasticity without energy dissipation. *Journal of Thermal Stresses* 22(2), 213–224
- [132] Quintanilla, R.; Straughan, B. [2000] Growth and uniqueness in thermoelasticity. *Proceedings of the Royal Society of London A* 456, 1419–1429
- [133] Quintanilla, R. [2001] Structural stability and continuous dependence of solutions of thermoelasticity of type III. *Discrete and Continuous Dynamical Systems-Series B* 1(4), 463–470
- [134] Quintanilla, R. [2001] Instability and non-existence in the nonlinear theory of thermoelasticity without energy dissipation. *Continuum Mechanics and Thermodynamics* 13, 121–129
- [135] Quintanilla, R.; Racke, R. [2002] Stability for thermoelasticity of type III. *Konstanzer Schriften in Mathematik und Informatik* 180
- [136] Quintanilla, R.; Straughan, B. [2002] Explosive instabilities in heat transmission. *Proceedings of the Royal Society of London A* 458, 2833–2837
- [137] Quintanilla, R. [2002] Existence in thermoelasticity without energy dissipation. *Journal of Thermal Stresses* 25(2), 195–202
- [138] Quintanilla, R. [2002] Thermoelasticity without energy dissipation of materials with microstructure. *Applied Mathematical Modelling* 26, 1125–1137
- [139] Quintanilla, R. [2003] Thermoelasticity without energy dissipation of nonsimple materials. *Zeitschrift für Angewandte Mathematik und Mechanik* 83(3), 172–180
- [140] Quintanilla, R.; Straughan, B. [2004] A note on discontinuity waves in type III thermoelasticity. *Proceedings of the Royal Society of London A* 460, 1169–1175
- [141] Quintanilla, R.; Straughan, B. [2005] Bounds for some non-standard problems in porous flow and viscous Green-Naghdi fluids. *Proceedings of the Royal Society London A* 461, 3159–3168
- [142] Reissig, M.; Wang, Y.-G. [2005] Cauchy problems for linear thermoelastic systems of type III in one space variable. *Mathematical Models and Methods in Applied Sciences* 28, 1359–1381
- [143] Rogers, S.J. [1971] Transport of heat and approach to second sound in some isotopically pure Alkali-Halide crystals. *Physical Reviews B* 3(4), 1440–1457

## REFERENCES

- [144] Schröder, J.; Romanowski, H. [2005] A thermodynamically consistent mesoscopic model for transversely isotropic ferroelectric ceramics in a coordinate-invariant setting. *Archive of Applied Mechanics* 74, 863–877
- [145] Sharma, J.N.; Pathania, V. Generalized thermoelastic waves in anisotropic plates sandwiched between liquid layers. *Journal of Sound and Vibration* 278 (1–2), 383–411
- [146] Simo, J.C. [1991] Nonlinear stability of the time-discrete variational problem of evolution in nonlinear heat conduction, plasticity and viscoplasticity. *Computer Methods in Applied Mechanics and Engineering* 88, 111–131
- [147] Slack, G.A. [1980] Thermal conductivity of ice. *Physical Review B* 22(6), 3065–3071
- [148] Sloan, D.M. [1971] An unsteady MHD duct flow. *Applied Scientific Research* 25, 126–136
- [149] Song, Y.-Q.; Zhang, Y.-C. [2002] Reflection of magneto-thermoelastic waves under thermoelasticity without energy dissipation. *International Journal of Nonlinear Sciences and Numerical Simulation* 3, 703–706
- [150] Spencer, J. R.; Pearl, J. C.; Segura, M.; Flasar, F. M.; Mamoutkine, A.; Romani, P.; Buratti, B.J.; Hendrix, A.R.; Spilker, L.J.; Lopes, R.M.C. [2006] Cassini encounters Enceladus: Background and the discovery of a south polar hot spot. *Science* 311(5766), 1401–1405
- [151] Steinmann, P. [1999] A finite element formulation for strong discontinuities in fluid-saturated porous media. *Mechanics of cohesive-frictional materials* 4, 133–152
- [152] Steinmann, P. [2000] Application of material forces to hyperelastostatic fracture mechanics. I. continuum mechanical setting. *International Journal of Solids and Structures* 37, 7371–7391
- [153] Steinmann, P. [2002] On spatial and material settings of thermo-hyper-elastodynamics. *Journal of Elasticity* 66, 109–157
- [154] Steinmann, P. [2002] On spatial and material settings of hyperelastodynamics. *Acta Mechanica* 156, 193–218
- [155] Stephan, K.; Mayinger, F. [1986] *Thermodynamik*. Springer
- [156] Svanadze, M.; Tibullo, V.; Zampoli, V. [2006] Fundamental solution in the theory of micropolar thermoelasticity without energy dissipation. *Journal of Thermal Stresses* 29, 57–66
- [157] Svendsen, B. [1999] On the thermodynamics of thermoelastic materials with additional scalar degrees of freedom. *Continuum Mechanics and Thermodynamics* 11 (4), 247–262

- [158] Svendsen, B.; Hutter, K.; Laloui, L. [1999] Constitutive models for granular materials including quasi-static frictional behaviour: Toward a thermodynamic theory of plasticity. *Continuum Mechanics and Thermodynamics* 4, 263–274
- [159] Taheri, H.; Fariborz, S.; Eslami, M.R. [2004] Thermoelasticity solution of a layer using the Green-Naghdi model. *Journal of Thermal Stresses* 27, 795–809
- [160] Tamma, K.K.; Namburu, R.R. [1997] Computational approaches with applications to non-classical and classical thermomechanical problems. *Applied Mechanics Reviews* 60(9), 514–551
- [161] Tan, W.; Masuoka, T. [2005] Stokes' first problem for an Oldroyd-B fluid in a porous half space. *Physics of Fluids* 17, 023101
- [162] Thomas, N.L.; Windle, A.H. [1982] A theory of case II diffusion. *Polymer* 23, 529–542
- [163] Tisza, L. [1938] The thermal superconductivity of helium II and the statistics of Bose-Einstein. *Compt. rend.* 207, 1035–1037
- [164] Truesdell, C.; Noll, W. [1965] *The non-linear field theories of mechanics*. Springer
- [165] Tzou, D.Y. [1995] A unified field approach for heat conduction from macro- to micro-scales. *ASME Journal of Heat Transfer* 117, 8–16
- [166] Ubachs, R.L.J.M.; Schreurs, P.J.G.; Geers, M.G.D. [2004] A nonlocal diffuse interface model for microstructure evolution of tin-lead solder. *Journal of the Mechanics and Physics of Solids* 52, 1763–1792
- [167] Verma, K.L.; Hasebe, N. [2001] Dispersion of thermoelastic waves in a plate with and without energy dissipation. *International Journal of Thermophysics* 22 (3), 957–978
- [168] Vernotte, P [1958] Les paradoxes de la théorie continue de l'équation de la chaleur. *C. R. Acad. Sci.* 246, 3154–3155
- [169] Wall, W.A. [1999] *Fluid-Struktur-Interaktion mit stabilisierten Finiten Elementen*. University of Stuttgart, Ph.D. thesis
- [170] Ward, J.C.; Wilks, J. [1952] Second sound and the thermo-mechanical effect at very low temperatures. *Philosophical Magazine* 43, 48–51
- [171] Wilmański, K. [1998] *Thermodynamics of continua*. Springer
- [172] Yang, Z.L.; Dinh, T.N.; Nourgaliev, R.R.; Sehgal, B.R. [2000] Evaluation of the Darcy's law performance for two-fluid flow hydrodynamics in a particle debris bed using a lattice-Boltzmann model. *Heat and Mass Transfer* 36, 295–304
- [173] Yang, Q.; Stainier, L.; Ortiz, M. [2006] A variational formulation of the coupled thermo-mechanical boundary-value problem for general dissipative solids. *Journal of the Mechanics and Physics of Solids* 54, 401–424

## REFERENCES

- [174] Zhang, J.; Zuazua, E. [2003] Decay of solutions of the system of thermoelasticity of type III. *Communications in Contemporary Mathematics* 5(1), 1–59
- [175] Zienkiewicz, O.C.; Taylor, R.L. [2000] *The Finite Element Method, Vol. 1: The Basis*. Butterworth-Heinemann



# Curriculum Vitae

## Personal Data

Name: Swantje Bargmann  
Date of Birth: 21.05.1980 in Frankfurt/Main  
Nationality: German

## Profession

04/2004 onwards      Research Associate, University of Kaiserslautern  
Chair of Applied Mechanics  
(Prof. Dr.-Ing. habil. P. Steinmann)

## Education

10/1999 – 03/2004      Diploma studies in Mathematics, University of Kaiserslautern  
08/1990 – 06/1999      Gymnasium Heißen, Mülheim an der Ruhr